# Holistic Modeling and Evaluation of Material Recovery from Materially-Complex End-of-Life Vehicles

by

Karine Ip Kiun Chong

Sc.B., Brown University (2012)
S.M., Massachusetts Institute of Technology (2014)

Submitted to the Department of Mechanical Engineering
in partial fulfillment of the requirements for the degree of

Doctor of Philosophy in Mechanical Engineering

at the

MASSACHUSETTS INSTITUTE OF TECHNOLOGY

September 2019



Signature redacted

Signature of Author: _____
Department of Mechanical Engineering
July 10 2019

Signature redacted

Certified by: _____
Stephen C. Graves
Professor, Operations Management & Mechanical Engineering

Signature redacted

Accepted by: _____
Nicolas Hadjiconstantinou
Chairman, Departmental Committee on Graduate Theses

# Holistic Modeling and Evaluation of Material Recovery from Materially-Complex End-of-Life Vehicles

by

Karine Ip Kiun Chong

Submitted to the Department of Mechanical Engineering on
July 10, 2019, in partial fulfillment of the requirements for
the degree of
Doctor of Philosophy in Mechanical Engineering

## Abstract

Material recovery is a key lever to promote a sustainable materials recycling system. By capturing materials from end-of-life products and substituting primary with secondary material production, society can reduce the depletion of natural resources and prevent the accumulation of valuable materials in landfills. Material recovery from materially-complex products, such as vehicles, is becoming more challenging as the material mixture becomes more heterogeneous with new trends in lightweight materials and product designs. The goals of this thesis are to develop a holistic modeling framework for material recovery for end-of-life vehicles (ELVs) and to illustrate the application of this framework to evaluate the recovery performance for current ELVs and future lightweight ELVs, using an existing material recovery infrastructure.

The holistic framework encompasses an integrated series of material recovery models that span the recovery processes from grave to cradle: dismantling, hulk shredding, material separation, secondary metal production of steel and aluminum, and waste recovery from plastics. For each of these processes, we have developed an evaluative model using mass balance. The input into the recovery chain is the bill of materials of an ELV, including the assembly part hierarchies and assembly precedence constraints, as well as the material composition of all components and fasteners. The output from the recovery chain is an assessment of the value of the recovered scraps, based on the contribution of ferrous and aluminum scraps to secondary metal production, and of plastic residues to energy recovery. The intent of this holistic, grave-to-cradle framework is to allow one to rethink how the effectiveness of the recovery chain depends on the attributes of each of the end-of-life processes as well as on the vehicle product design.

For the first phase of the recovery chain, we model the dismantling process as an optimization problem to decide what valuable parts to remove, given the parts' hierarchies and assembly precedence relationships, and the parts' values and dismantling costs. After removing these parts, we are left with the ELV hulk. For the second phase, we develop a shredding model for the comminution of the ELV hulk, i.e. the transformation of the hulk into non-liberated (fasteners and

wires attached to parts' fragments) and liberated material particles of different sizes. For the third phase, we use a network flow model to model the sortation of the multi-material flow from the shredder through the network of sorting equipment, which performs separation based on material properties. Using this system of linear equations representing mass flow balance, we can solve for the material composition of the collected output scrap streams. From that, we can calculate the material quantity and quality losses due to inefficient separation. More importantly, this model is able to capture the metal contamination due to non-liberated particles ending up in the ferrous and aluminum scraps. For the fourth phase of the material recovery chain, we calculate the dilution losses incurred at secondary metal production for different scenarios of produced sink metal alloys. To tie together all losses from the material recovery chain, we propose the normalized contribution of scraps (NCS), an overall performance metric that improves upon the typical overall recovery rate (ORR) by accounting for the dilution losses. We illustrate the framework with a baseline ELV built from a family-car teardown data. In general, we observe the NCS to be significantly lower than the ORR (89%) for scenarios where the metal scraps are used to produce medium-quality alloys of the level of closed-loop recycling (NCS of 25% for 6061 Al alloy and rolled steel production), but not so much so when the metal scraps are down-cycled to low-quality alloys (NCS of 88 % for A380 Al alloy and steel bar production).

We conduct two case studies to explore the effects of variations to the profile of the baseline ELV on its material recovery performance. In the first case study, we run Monte-Carlo simulations to model the uncertainty in the profile of the ELV hulks. Using data on the resale of used parts, we create a sample of 1000 different hulks by randomly generating the parts that are disassembled for resale. For this sample we observe that 300 kg of materials are removed from an ELV on average; the ORR varies from 86% to 91%, while the best-case scenario NCS varies from 60% to 91%. The second case study investigates the material recovery performance of an aluminum-intensive lightweight vehicle. For this vehicle, in comparison to the baseline vehicle, there is not only a higher concentration of aluminum, but also more ferrous fasteners in the aluminum body. Our analysis of this case suggests a decrease in recovery performance compared to that of the baseline ELV case. In comparison to the baseline vehicle, the lightweight vehicle has less ferrous, which results in a greater concentration of copper contaminant in ferrous scrap; thus, the ferrous scrap is of lower grade and requires more dilution. However, the increase in aluminum input is high enough to counter the increase in aluminum-ferrous particle contamination in the aluminum scrap. While the performance results depend on the model parameters representing the material recovery infrastructure, these case studies highlight the need for a holistic material recovery model to capture unintended dilution loss consequences due to changes in vehicle designs.

Thesis Supervisor: Stephen C. Graves
Title: Abraham J. Siegel Professor of Management, Professor of Operations Management & Professor of Mechanical Engineering

# Acknowledgements

First, I would like to sincerely thank my advisor Professor Stephen Graves for giving me the opportunity to pursue my doctoral study under his patient guidance and generous support for the past four years. I am grateful for his approachability and wisdom in broad-ranging subjects. His high intellect, attention to details and dedication to promoting learning have been a great inspiration and will always inspire me personally and professionally throughout my future career.

I am grateful to my wonderful thesis committee. Besides Professor Graves, Professor Gutowski has provided great guidance on evaluating different research angles, with his engineer's knowledge on materials and recycling and his ability to see the big picture. Professor Olivetti provided insightful suggestions to frame my research questions and Dr. Kirchain gave thoughtful feedbacks on my research based on his expertise in material designs of vehicles and metal production. I would also like to acknowledge their dedication to furthering research on the important topic of environmental sustainability from their respective areas of expertise.

Funding from Ferrovial has been indispensable for me to join the research collaboration between Professor Graves and Professor Gutowksi. The Ferrovial project on household waste recycling in Spain has been the stepping stone to my PhD research, and I would thus like to acknowledge the Ferrovial team and my labmates Anne and Mapi, for the pleasure of working with them. A huge thanks to my other labmates who made my time in the EBM office enjoyable: Penny, Andi, Timo, Tobi. I would like to thank the MIT staff, including Karuna, Leslie and David for helping me with the administrative needs and making my journey at MIT smooth.

I am lucky for the support of other friends at MIT and in the Boston area: thank you for all the fun, for being there and reminding me to enjoy the small good things of life.

To Michel, my special person, his love and companionship have kept me going through the last few years.

And finally to my family, my parents and brother, without their unconditional love, encouragements and spiritual support 9000 miles away, I will not be where I am today.

# Contents

# List of Figures

# List of Tables

# Chapter 1 Background and literature

## 1.1 Motivation

Material recovery is a crucial aspect of sustainability. By capturing materials from products at their end-of-life phase and substituting them for primary production, society can reduce the depletion of natural resources. By circumventing the mining and processing of raw materials such as iron and aluminum ores, we can avoid the associated energy usage, greenhouse gas emissions, water and air pollution. The capture of materials also prevents disposal of useful resources which would otherwise end up in landfills, and would represent a lost opportunity. Material recovery is an area needing more research because products are becoming more materially-complex and thus making the capture process and the re-induction as a raw material challenging. The goal of this thesis is to maximize material recovery by modeling, analyzing and optimizing the system performances of a typical material recovery infrastructure, as well as to make informed decisions related to the product design, upstream of the end-of-life phase.

We choose vehicles as the product category of study because (i) there is already existing infrastructure for collecting, dismantling, shredding and recycling end-of-life vehicles (ELVs); (ii) while vehicles are becoming more materially complex, the existing material recovery infrastructure is not yet adapted to deal with these changes in material flow; (iii) ELVs in the U.S. represents more than 10 million tons of recyclable metals per year. About 75-80% by mass of a vehicle is recyclable metals (70-75% ferrous, 5% non-ferrous); the remaining 25% of the mass ends up as shredder residue (e.g., plastics), and eventually in landfills. In fact, the number of vehicles reaching end-of-life is only going to increase over the years: In the US, it is estimated that 12 million vehicles reach end-of-life per year, and there are around 240 million vehicles in current automobile ownership [1]. Moreover, the end-of-life treatment of vehicles is a global problem: in 2010, there were one billion vehicles in ownership, with 40 million reaching end-of-life; by 2050, it is estimated that we will reach 2.4 billion vehicles in ownership [1].

Material recovery from ELV is important because of the potential to displace the energy consumption and greenhouse gas emissions associated with primary material production. The primary material production is part of the cradle-to-gate phase in the life-cycle of a vehicle, during which materials are mined from their natural sources, transported and produced into raw material stocks. As seen from Figure 1.1, although the use-phase dominates the life cycle energy demand of a typical steel-intensive vehicle, the cradle-to-grave phase contributes on average 10 % as compiled by the LCA studies covered in [2]. We can see a similar trend in the GHG emissions, which correlates with the energy consumption. The energy consumed during secondary metal production, i.e. using recycled metals, is significantly smaller than that used during primary metal production. As seen from Figure 1.2, depending on the materials, there can be different savings in energy consumption during the material production if secondary metals were used as opposed to primary metals: while less than half of the primary production energy is used for secondary steel production, there is a seven-fold decrease in production energy needed for secondary aluminum production.

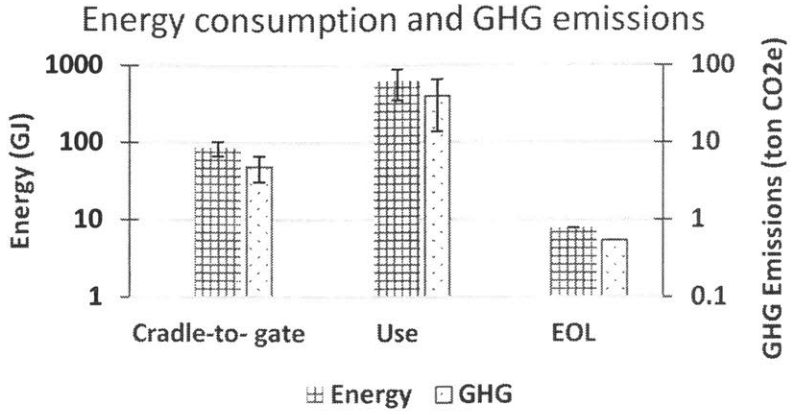


*Figure 1.1 Energy consumption and GHG emissions during a vehicle's life-cycle phases, adapted from data in [2]*

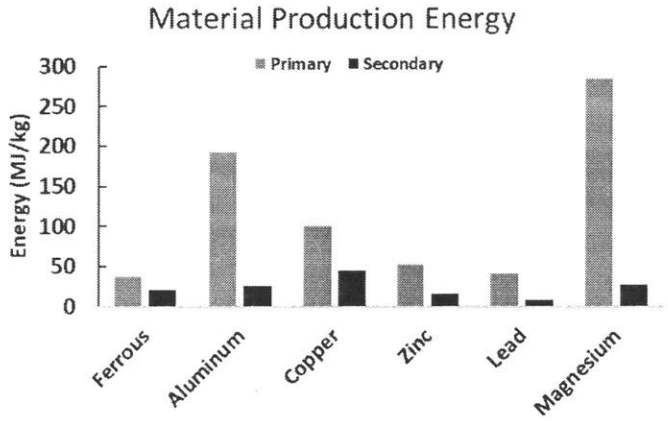


*Figure 1.2 Comparison of primary and secondary material production energies for some ELV metals, adapted from [3]*

Materially-complex products tend to have a higher recycling rate in the US, if they have a high recycled material value potential [4]. As seen from Figure 1.3, vehicles or automobiles have high material complexity and recycled material value, due to the big mass of a vehicle, and the wide range of materials used in vehicle components and systems. With technology advances, products are getting more materially-complex. Figure 1.4 shows a steady increase in material complexity in vehicle designs over the last five decades [4]. As a vehicle's median life-span is around 17 years [5], more materially-complex vehicles are now entering their end-of-life phase. Therefore, it is critical to research how the current recovery chain is dealing with this and how future vehicle design can enhance it.

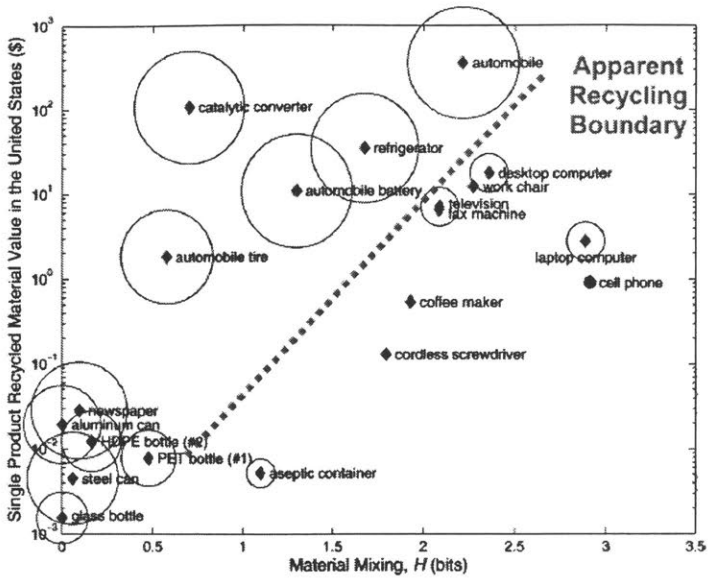


*Figure 1.3 Material complexity, recycled material value and recycling rate (size of circle) for different products [4]*

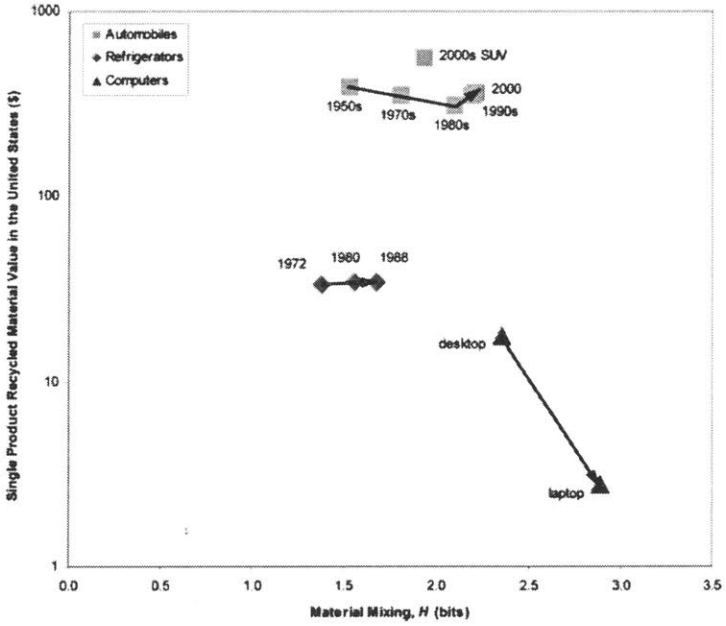


*Figure 1.4 Design trends in automobiles, refrigerators and computers [4]*

This research addresses the literature gap for a holistic model covering the whole material recovery chain. We seek to build a model with parameters defining different equipment configurations and system efficiencies, and which can take in as input different designs of ELVs. Thus, we are able to draw insights about overall material performance based on different aspects of the product design, in particular the material compositions and fasteners. While end-of-life is only one phase of the whole life-cycle of a vehicle (see red arrows in Figure 1.5), we need to make sure that the end-of-life material recovery processes are as efficient as possible to increase the quantity and quality of the scraps going into secondary material production.

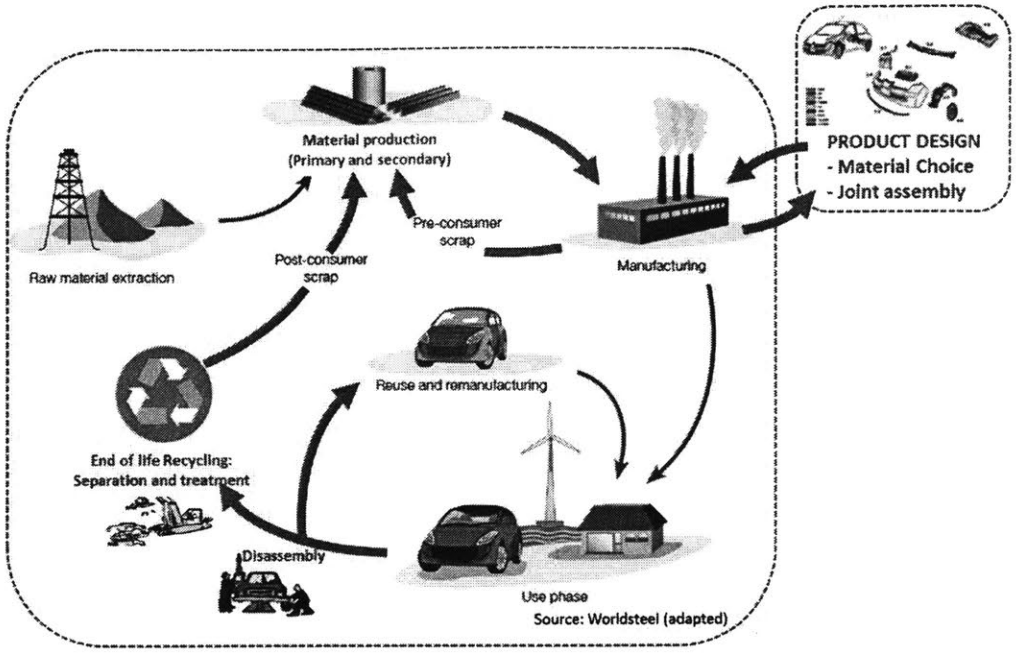


*Figure 1.5 How product design choices affects the overall recyclability throughout the different phases of a vehicle's life-cycle, adapted from [6]*

## 1.2 Research overview

This thesis will investigate how to model material flows throughout the recovery chain of ELVs. We define the scope of the recovery chain from grave to cradle. The recovery chain for an ELV starts with a dismantling process at which valuable components, as well as hazardous materials, are removed from the vehicle. After dismantling, the vehicle is input into a shredding process that converts the hulk into a stream of particles. This stream is then fed into a separation process that sorts the particles based on material properties, and produces scrap output streams of valuable targeted material such as ferrous, plastics and aluminum. These output streams may then require additional processing in order to capture the full value of the recovered material: for instance, the aluminum scrap stream is typically the feed input during aluminum secondary metal production process to produce final aluminum alloys.

This work describes the development of a holistic modeling framework, which is able to account for the material flows throughout all the above processes for a given material recovery infrastructure. To determine how to define the infrastructure, we first have a look at the literature in the rest of the Chapter 1: we investigate who are the stakeholders, how are the dismantling processes carried out, what are the existing shredding and separation technologies, what are the valuable and non-valuable output streams commonly generated and what are their fates as commodities or waste. Additionally, we look at how secondary metal processing is carried out in practice in industry.

**Chapter 2** This chapter focuses on the mathematical modeling of the disassembly process of a complex product, with multiple components connected together. We represent disassembly as an optimization

problem, to determine which valuable components can be cost-effectively removed without incurring a high labor cost, while ensuring that the removal sequence of the components remain feasible.

**Chapter 3** We explore the different aspects of shredding and separation system modeling from existing works of literature. Thus, we determine that the characterization of the material particle flow needs to be done by material type and size categories. We then explore the use of partition curves to estimate the separation efficiencies of particles of different material types and size at different sorting equipment. We also establish that non-liberated particles are formed when parts with attached fasteners become fragmented. When the parts' fragments and fasteners are of different materials, these particles are not efficiently separated, and they contribute to contamination of the output scrap streams.

**Chapter 4** Using the above insights, we define our mathematical representations of the shredding and separation processes. The shredding model we develop maps the transition of liberated material particles to smaller size categories, and models the breakage of non-liberated particles to liberated particles of different material types. Next, we propose a network flow model to model the sortation of the multi-material flow from the shredder through the network of sorting equipment, which separate based on material properties. We apply these two connected models on a small sample dataset of characterized input material flow, to illustrate how the material flow changes after shredding and separation, and how the output scrap composition can thus be calculated.

**Chapter 5** In this chapter, we determine a model representation for how metal scraps are used as feed material for secondary metal production of products of different grades. Depending on the concentration of the contaminants in the material composition of the scrap feed and on the requirements of the metal product, primary metal might be added. For aluminum, we develop a blending model to calculate how much alloying and dilution additions are needed to meet the element concentration specifications of the different possible aluminum alloys produced. For ferrous, we propose a simple equation to calculate the dilution costs, as we are only concerned with copper as a contaminant.

**Chapter 6** We first explore different performance metrics to evaluate the separation processes, namely grade, recovery rate and mixing entropy. Next, we propose new metrics to measure the actual value of scraps, by incorporating the dilution costs at secondary metal production: the effective scrap value and the scrap value index. With consideration to all scrap outputs, we propose the normalized contribution of scraps (NCS) as an alternative metric to the overall recovery rate (ORR). Finally, we illustrate how to calculate these performance metrics on an example set of the scraps' compositions.

**Chapter 7** This chapter introduces the baseline ELV built from literature teardown data. The ELV data is then applied to the models developed in chapters 4 to 6, from shredding to separation to secondary metal processing. We thus calculate the overall material recovery performance metrics of the baseline ELV.

**Chapter 8** We present a case study analyzing the effects of variations to the profile of the baseline ELV, caused by the different rates at which different resalable automotive components are removed during dismantling. We run Monte-Carlo simulations to create different resulting ELV hulks by randomly generating the parts that are disassembled for resale.

**Chapter 9** We present a second case study to investigate the material recovery performance of a lightweight aluminum-intensive vehicle (AIV). We first build its profile by modifying the automotive components that are seeing a shift from ferrous to aluminum, and by adding ferrous fasteners to the aluminum body structure.

**Chapter 10** This chapter summarizes the contributions and findings of this thesis.

## 1.3 ELV recovery chain in the US & EU

At the onset, it is necessary to distinguish between modeling for the US or for the EU context. The differences, which will lead to different model input and objectives are as follows:

- Recovery chain structure: this leads to different feed input to the shredder. The dismantling processes are slightly different: in the US, there are pick-and-pay system as well as small-scale and large-scale reuse facilities [7]. In the EU, the former is not present [8]. Additionally, US shredder facilities receive product systems other than ELVs (white goods, demolition waste) [7] while in the EU the facilities (Authorized Treatment Facilities, ATF) are dedicated to ELVs [9].
- ELV legislation: in the EU the current post-shredder practice is highly driven by the recycling targets set by the European Directive. As from January 2015, the new directive increased the new global recovery rate target for ELV to be at least 95%, of which 85% needs to be from reuse and recycling [10]. This has driven infrastructures for energy recovery from ASR [11], while in the US, ASR is usually landfilled or even used as landfill cover [12]. On the other hand, the ELV treatment is entirely profit-driven in the US.

Several stakeholders are involved in the recovery chain of ELVs: (i) Dismantlers who remove spare parts and valuable materials for resale/remanufacturing and hazardous materials per end-of-life vehicle regulations; (ii) shredding companies who grind and separate for valuable materials during post-shredding treatments. In the US and EU, the recovery supply chain practices differ slightly, even though the main stakeholders are the same: drivers in the US are mainly economic, while in the EU, legislations impose recovery targets to car manufacturers. Since January 2015, the European ELV Directive (2000/53/EC, enacted in 2000) enforces a 95% recycling, reuse of energy recovery target (on average per vehicle per year by weight), with up to 10% through energy recovery [13]. That said, different member states have slightly different economic approaches for ensuring compliance with the mandatory free take-back systems for cars at end-of-life. For instance, in the Netherlands and Sweden, vehicle importers and manufacturers fund the take-back systems through a waste disposal fee per vehicle, which funds premiums vehicle-dedicated dismantling facilities or post-shredder facilities; in Germany and UK, the manufacturers hold contracts with such recycling stakeholders [14], [15].

While the US does not have direct laws governing the treatment of ELVs, there are some related environmental laws at state and federal laws which guide the running of dismantling or shredding facilities, and Automotive Recyclers Association provides such information to them [1]. There are more than 6000 dismantlers who remove automotive components for reuse or as preparation of the vehicle for shredding, and 3000 of these companies are affiliates of the ARA [5]. Shredders accept flat bodies, also known as hulks which are commonly flattened by a car crusher to reduce transportation costs [7], from dismantlers and individuals. They also accept end-of-life white goods and industrial scraps. There are 212 shredders (less than 100 companies) in the US, under the organization of the non-profit trade association, Institute for Scrap Recycling Industries (ISRI) [5].

There are 3 business models for the dismantlers in the US [5], [7]: (i) no reuse but preparation for processing for shredders; (ii) reuse parts (customers do "U-Pull-It") and store in yards, till preparation for processing; (iii) vehicle brand-specific, with reuse and preparation. In the last business model, the dismantler is responsible for depolluting the vehicle (i.e. removing fluids, battery, fuel tank, catalytic converter, tires and mercury switches) and of removing and storing components with high resale value (e.g. engine,

transmission and radio) [5]. The dismantlers then sell their salvaged parts to wholesale (e.g. body shops) or retail customers [5]. The remaining hulk is sent to shredders after depollution. After shredding and separation into valuable scrap streams, the shredders sell to domestic or international customers for further separation or to smelters, steel mills and foundries. While dismantlers balances out the cost of the dismantling labor with the revenues from the components' resales, shredders need to choose the separation technologies used and the extent of the separation process based on the global scrap prices of different grades of scrap, and the contaminant requirements of mills [5].

## 1.4 Dismantling processes

The main limitation of dismantling is how labor-intensive it is relative to the value recovered. Moreover, due to different car make and models, it requires training for identification of the different car parts. Existing research has looked at dismantling from a cost analysis perspective [16]–[18], through case-studies to measure dismantling times for different car assemblies or parts.

Characterization of the dismantling processes is complex as the sequence is dictated by how accessible a part is, i.e. by the product design's geometrical constraints: contact on different axes, different connection means (e.g. adhesives, snap fits, screws etc [19]). While some literature has already looked at optimization of product disassembly sequence with respect to cost and potential revenues [20], none has looked at cases of complex products like end-of-life vehicles to optimize for recyclability. Moreover, there are additional sequence constraints as dismantlers must follow strict regulatory guidelines for removal of hazardous materials. It should be noted that in reality, dismantlers can also choose semi-destructive methods to access highly-valuable parts, sacrificing low value parts on the way [7].

For the dismantling process, we are concerned about the removal of parts and fluids from the end-of-life vehicle. This includes: what hazardous parts/fluids are removed during depollution, what parts are removed for resale/remanufacture or direct recycling, the sequence of removal.

### 1.4.1 End-of-life fates of parts/substances

Depollution, also known as the pre-treatment, involves the removal of fluids and parts/materials which are dangerous to the environment prior to sending the car hulk to shredders. If the shredders figure out that the car hulks they receive are not depolluted, the whole batch is rejected [5]. The removal of the hazardous fluids/parts is not necessarily prior to the dismantling, i.e. it can occur along with the disassembly sequence of parts [7], [21]. Fluids, which are recovered by most dismantlers for reuse (internally or sent to licensed waste haulers for off-site disposal), include: refrigerant, gasoline, engine oil, transmission oil, antifreeze, gear fluid, brake fluid, steering fluid, windshield washer fluid [7]. Hazardous parts/materials include: battery, airbags, gasoline tanks, tires, mercury switches. Batteries and tires are removed by all dismantlers, as they are unacceptable to shredders [7]. The table below shows the typical recycling or reuse rate (in kg/tonnes of ELVs processed) of fluids.

| Fluid | | Disposition of Recovered Fluids | |
|---|---|---|---|
| | | Recycling (kg/tonne ELVs processed) | Reuse (kg/tonne ELVs processed) |
| Lubricants | Engine Oil | 2.1 | 0.0 |
| | Transmission Oil | 3.1 | 0.0 |
| | Differential Fluid | 0.0 | 0.0 |
| | Brake-line Fluids | 0.0 | 0.0 |
| | Power Steering Fluid | 0.1 | 0.0 |
| Antifreeze | | 0.0 | 4.1 |
| Windshield Washer Fluid | | 0.0 | 0.9 |
| Gasoline | | 0.0 | 8.8 |
| Totals = | | 5.3 | 13.8 |

*Table 1.1 Mass of fluids recovered during depollution of ELVs at dismantling facilities in Sawyer-Beaulieu's study [7]*

Zamudio-Ramirez [22], Spicer [23], Sawyer-Beaulieu [7] and Duranceau [24] provide the most comprehensive published work on dismantling and provide a database of the parts typically taken out for reuse during dismantling. Zamudio-Ramirez's and Spicer's works stem from a 7-month 1995 project with the Vehicle Recycling Development Center (VRDC), during the course of which four cars (2 of each of 2 models of family-sized sedans) were fully dismantled, and the sequences of the dismantling steps and timing were recorded [22]. Sawyer-Beaulieu's & Duranceau's works provide a more macro perspective in terms of mass and part flow through several dismantling facilities. Sawyer-Beaulieu collected data from 7 dismantling facilities in Canada. In the context of the study by the Vehicle Recycling Partnership and the ARA/VRDC in 1997-1998, Duranceau collected data from the inventory of 48 dismantling facilities in the US [24], which involved : quantities of vehicles entering and types of parts sold.

Sawyer-Beaulieu identifies that 11.6% by weight of ELVs end up being reused (5.7%), remanufactured (0.1%) or recycled (3.9% for parts and 1.4% for fluids), while 88.4% go to shredders in the form of the remaining hulk [7]. One study by Santini et al. shows the different end-of-life fates for parts and fluids at dismantling facilities in Italy as follows: 21.5% recovered (8.9% reused, 9.6% recycled for parts, 3.0 % for fluids) and 87.5 % as hulk [25]. Some parts are removed for direct recycling separately as they are worth more thus: e.g. catalytic converters, brake calipers, engine accessories and brake rotors [7], [21]. Some parts are removed for remanufacturing, i.e. sold to part remanufacturers, when they are unsuitable for sale as a reusable parts but still have functional value. Parts which are typically remanufactured include: engines, starters, brake calipers, AC compressors, water pumps, carburetors, power steering pumps, carrier assemblies, alternators, transmissions, axle assemblies and transfer cases [7]. Many of the dismantlers in the US participate on car part exchange networks (e.g. Car-Part.com or Hollander), which are online inventories of used car parts [7]. In addition, there exists online resources which help dismantlers with the best practices for pre-treatment and dismantling, e.g. the International Dismantling Information System (https://www.idis2.com/) is an online platform put together by car manufacturers from Europe, USA, Japan South Korea and Malaysia which provides information about specific car brands and models.

Sawyer-Beaulieu documents the typical process flow used by the dismantlers in her study in the diagram below. She notes a slight process distinction made according to the received ELVs' age and condition: high-salvage (mainly late-model vehicles) and low-salvage ELVs (old and/or damaged vehicles). The HSELVs

incur maximum parts or materials recovery [7]. As summarized in the diagram below, the recovered parts can have 5 possible fates: (i) disposed, (ii) recycled (for hazardous parts or parts with high recycling values), (iii) remanufacturing, (iv) reused, (v) sent on with the ELV hulks to shredders. Note that the parts which are removed yet put back together with the hulks *are those which have to be removed first to make the desired parts accessible* [7]. From [7], it was not clear which parts were actually disposed, but it reported the weight proportions of parts that were remanufactured (Table 1.2), directly recycled (Table 1.3), or reused (Table 1.4) out of the total weight of vehicles processed by the dismantling facilities through a mass-balance analysis used in its study. Sawyer-Beaulieu also a comprehensive list of parts sold for reuse, according to the ELV category (HSELV and LSELV), and the parts' reuse rate per tonne of ELV processed: in HSELVs, the engine and transmission are among the most reused parts; in LSELVs, the battery and front seat are among the most reused parts [7]. However, it is unclear what masses of each part type were used as they were averaged over the different car brands and models received by the dismantling facilities. The study by Duranceau quantifies the reuse rate by vehicle parts on a count basis, see Figure 1.6.

| | Weight | | | |
|---|---|---|---|---|
| Part Type | kg per tonne HSELVs Processed | % Wgt. of HSELVs Processed | kg per tonne ELVs Processed | % Wgt. of ELVs Processed |
| AC Compressor | 0.844 | 0.084% | 0.112 | 0.011% |
| Alternator | 1.474 | 0.147% | 0.195 | 0.020% |
| L&R F Caliper | 1.550 | 0.155% | 0.205 | 0.021% |
| Steering Gear | 1.381 | 0.138% | 0.183 | 0.0183% |
| Steering Pump | 0.666 | 0.067% | 0.088 | 0.009% |
| Starter | 2.851 | 0.285% | 0.377 | 0.038% |
| Total | 8.766 | 0.877% | 1.160 | 0.116% |

*Table 1.2 Mass of parts recovered for remanufacturing from HSELVs at dismantling facilities in Sawyer-Beaulieu's study [7]*

| | Parts Recovered for Recycling | | | | | |
|---|---|---|---|---|---|---|
| | From LSELVs | | From HSELVs | | From LSELVs and HSELVs | |
| Part type | kg per tonne LSELVs processed | kg per tonne total ELVs processed | kg per tonne HSELVs processed | kg per tonne total ELVs processed | kg per tonne total ELVs processed | % Wgt of total ELVs processed |
| Tires, Regular | 23.5 | 20.4 | 21.9 | 2.9 | 23.3 | 2.33% |
| Tires, Spare | 3.0 | 2.6 | 2.8 | 0.4 | 2.9 | 0.29% |
| Batteries | 8.9 | 7.7 | 8.1 | 1.1 | 8.8 | 0.88% |
| Catalytic Convertors | 4.1 | 3.6 | 3.9 | 0.5 | 4.1 | 0.41% |
| Mercury Switches | | | | | 0.009 | 0.001% |

*Table 1.3. Mass of parts recovered for recycling from ELVs at dismantling facilities in Sawyer-Beaulieu's study [7]*

| | Weight | | | |
|---|---|---|---|---|
| | **kg per tonne HSELVs processed** | **% Wgt. Of HSELVs Processed** | **kg per tonne ELVs processed** | **% Wgt. Of ELVs processed** |
| **HSELV Parts sold for reuse** | 369.4 | 36.94% | 48.9 | 4.89% |
| **LSELV Parts sold for reuse** | 9.32 | 0.93% | 8.09 | 0.81% |

*Table 1.4. Mass of parts recovered for reuse from ELVs at dismantling facilities in Sawyer-Beaulieu's study [7]*

(i)

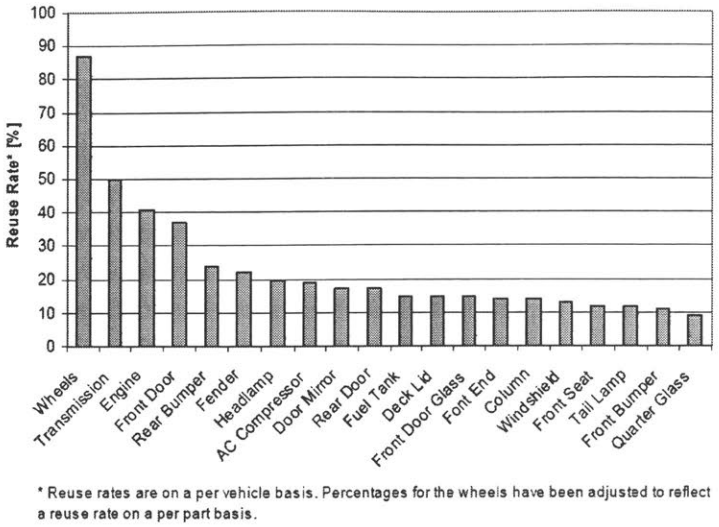


*Figure 1.6 Reuse rates of car parts in Duranceau's study [24]*

### 1.4.2 Disassembly sequences

Few studies have reported the typical dismantling steps for end-of-life vehicles. One reason might be that the vehicle structures differ a lot depending on the car brand and model. One study on Honda vehicles by Paul et al. gives a dismantling sequence (see Table 1.5) as performed by an experienced dismantler mechanic, but it is not clear (i) if this sequence if commonly used by commercial dismantlers; (ii) if the sequence in itself can be a several smaller sequences occurring independent of the other. Additionally, the process of removing can differ depending on the equipment available and state of the joints linking parts together. For instance, "Power tools, including a reciprocating saw, impact wrench, drill, die grinder, impact ratchet, air chisel, and angle grinder with cutoff wheel, were used by the dismantlers, in preference to manual hand tools wherever practical. On occasion, a torch was required to facilitate the removal of certain parts due to corroded fasteners." [7]. Note that in the Honda vehicles study, front clips and back clips were cut from ELVs, which were mostly less than seven years old, as they had huge resale value to collision repair shops and also saved on dismantling time [21]. In some Australian dismantling facilities, machines are used: a modified excavator manned by a single operator uses the mechanical force of a clamp arm and a wide jaw to separate materials, mainly metal parts which are baled together thereafter [26]. However, it is not clear before this process how many parts are disassembled manually by customers, in the same vein as the American u-pull-it model.

For complex end-of-life products like ELVs, which contain hundreds of parts joined to one another, two aspects need to be considered, which affect the disassembly sequences: (i) assemblies, (ii) precedence constraints. Few works in literature have accounted for these aspects, to the exception of the research works of Spicer and Zamudio-Ramirez [22], [23] , which were later adapted by Kirchain [27]. Their work looks at the disassembly of an ELV, with their parts' database lists 616 parts in total, including individual parts, subassemblies and assemblies. 117 of these parts are assemblies: e.g. right front door, left rear door, instrument panel, rear frame. In fact, the discrete parts are those parts which are considered removable separately and have a distinct material type. Note that this parts' database does not include fluids and gas tanks which have been removed already during the de-pollution phase. The parts' database includes each part's economic resale value, the removal time, weight and material type, as well as the immediate

predecessor part which provides information on the parts' precedence constraints necessary for determining feasible disassembly sequences. In total 450 precedence part constraints are listed. From the data, parts can have more than 1 predecessor part, which is the case if a part is connected to at least 2 parts which need to be removed to access it. From this predecessor connection data, we build a visual representation of the connections between the parts, as shown in Figure 1.7. This database provides comprehensive parts' information, including connection constraints and disassembly cost (part removal time), which will be the basis for this thesis work.

| | |
|---|---|
| 1. Wheel Bolts & Covers Removal | 28. Exhaust Pipe B & A and Catalytic Converter Removal |
| 2. Wheels & Tires Removal/Separation | 29. Transmission Fluid Removal |
| 3. Wheels | 30. Transmission Range Switch Harness Disassembly & Flywheel Bolts Removal |
| 4. Tires | 31. Fuel Tank Removal |
| 5. Front Suspension/Brakes Loosening | 32. Fuel Removal |
| 6. Front Brake Discs | 33. Brake & Fuel Lines Cut |
| 7. Front End Splash Shield Removal | 34. Engine Sub-Frame Bolts Removal (Includes Rubber Mounts) |
| 8. Front Quarter Fender Loosening | 35. Engine Mounts & Engine Drop (Removal) |
| 9. LF Door Mirror Removal<br>10. RF Door Mirror Removal | 36. Transmission Driveshaft Axles Removal |
| 11. LR Door Removal | 37. Alternator |
| 12. LF Door Removal | 38. A/C Compressor |
| 13. RF Door Removal | 39. Power Steering Pump |
| 14. RR Door Removal | 40. Starter |
| 15. RF Seat Removal | 41. Lower Control Arm & Spindle |
| 16. LF Seat Removal | 42.Power Steering Fluid |
| 17. Center Console Housing, Gear Shifter Assembly (Remains w/rear clip) | 43. Brake calipers |
| 18. Driver's Airbag Removal | 44. Brake Fluid |
| 19. Passenger Side Airbag Removal | 45. Power Steering Rack |
| 20. Air Bag Control Unit Removal | 46. Front End Clip Separation (By cutting vehicle) |
| 21. Radio Removal | 47. Rear End Clip (Results from cutting) |
| 22. A/C Refrigerant Removal | 48. Metal Scrap (Bolts, PFT Holder, Brackets) |
| 23. Front Windshield Removal | 49. Non-Metal Scrap (Plastic Trim, Rubber, Nylon) |
| 24. Coolant Removal | 50. RR Tail Light |
| 25. Battery Removal | 51. LR Tail Light |
| 26. Engine Assembly Disconnections - Disconnections include the following: Air Cleaner Case Removal, Motor Mounts, Throttle Cable, Cruise Control Cable, Under-Hood Fuse Box, Fuel Feed Hoses, Wiring Harness, Engine Brake Light, Engine Control Unit (ECU), Power Steering Rack | 52. Deck Lid |
| 27. Engine Oil Removal | 53. Rear Bumper |

*Table 1.5 Disassembly sequence used during dismantling in Honda study by Paul et al. [21]*


*Figure 1.7 Parts and assemblies arranged by connection constraints using data adapted from [27]*

## 1.5 Shredding and separation processes

### 1.5.1 Shredding process

The shredding process for ELV usually takes place at a shredding facility which also contains subsequent material separation processes which mechanically separate out the ferrous and non-ferrous metals [28]. Two types of shredder exists, those vertically or horizontally mounted motors, see Figure 1.8. In the first step at the shredding facility, the input feed are loaded to the shredder by a conveyor belt or a crane, after visual inspection and radiation detection for hazardous materials. Contrary to other countries, shredding facilities in America (U.S [5], [28] or Canada [7], the input feed contains a mixture of white goods (e.g. electrical appliances such as refrigerators, dish washer) and end-of-life vehicles, usually in a certain ratio

decided by expert knowledge and experience. Typical shredders have a throughput of around 30 tons of used vehicles per hour [29], and are driven by 3000-10000 hp motors at 450-600 rpm [5].

The shredder, also called hammermill, consists of a feed roller and a rotor equipped with many hammers, which reduces the input feed material into fist-size pieces. This process is called comminution, due to size reduction of particles, and helps further separation processing, i.e. helps increase separation efficiency downstream. Beyond comminution, shredding also helps in the liberation of joint materials. In experiments examining the shredding process, Tam et al. found that: (i) size distribution independent of material types; (ii) amount of liberation dependent on type and degree of fastening [30]. While they only tested with parts consisting of a combination of ABS and PVC plastic, Aboussouan et al. tested the shredding of steel-copper parts and also observed a size distribution in the fragments (liberated or non-liberated) [29]. Stagner et al. [31] and Bruyere et al. [32] showed that size distribution does not depend on shape but on cryogenic temperature. In [31], they tested that on automobile fascia and plastic headlights sent through a hammermill with output feed of <76mm size, while in [32], the shredding was investigated on ASR, with output feed of <4mm size reduction for possible digestion, with the input being pre-treated in liquid nitrogen. Note that the shredder output shredded particles' size depends on the clearance size of the grates through which the output feed needs to exit the shredder.

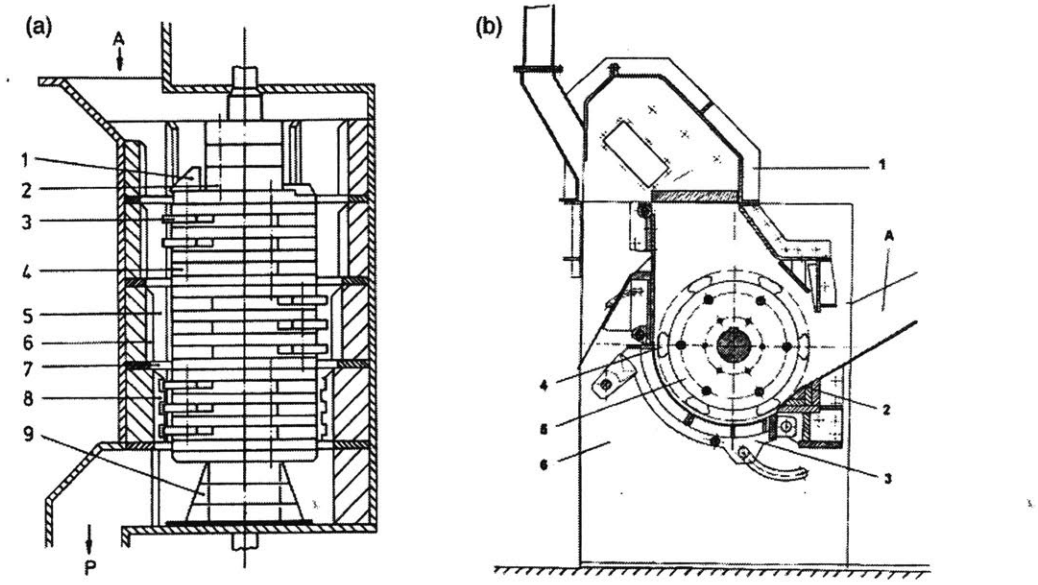


Fig. 1. (a) Small-scale shredder with vertically mounted rotor: (1) first comminution tool, (2) rotor, (3) hammer, (4) rotor unit, (5) baffle plate, (6) anvil, (7) retaining baffle, (8) comb-shaped anvil, (9) discharge, (A) feed, and (P) product. (b) Small-scale shredder with horizontally mounted rotor: (1) upper part of housing, (2) anvil, (3) swivelling mounted lower part of housing, (4) hammer, (5) rotor, (6) housing wall, and (A) feed.

*Figure 1.8 2 types of shredder: (a) vertically-mounted motor; (b) horizontally mounted rotor [33].*

The mechanical behaviors undergone by particles in a shredder are multiple: hardening, deformation and shearing (cutting), through bending, compression, tension and shear forces. It is too complex to simulate physically all the forces at work in a shredder, as the forces are imparted by the hammers at different points along the particles' surface and in different directions, and the moving particles dynamically interact with each other. Moreover, different residence times (inherently, the feed rate) and the design of the comminution chamber affect the intensity and degree of the shredding [33]. Additionally, ductile (such as plastics and copper) and brittle materials (e.g. iron) behave differently: ductile materials deform plastically

before fracturing such that the metal particles change shape without breaking, while brittle materials break down into smaller pieces more easily. Fracture happens when the particle undergoes stress high enough to exceed the fracture strength of the material. For ductile materials, shear force is more effective while for brittle materials, compressive force is more [34]. Another factor to keep in mind is the surface condition of the particles, since original defects and cracks can incite fracture [35].

In [35], an experiment to simulate fracture simplified the representation of shredding as an impacting tool (a rotating cantilever beam) striking a fixed piece of material. While numerical simulations of the whole shredding are rare in literature, numerous analyses have been done in literature to qualify the influence of size of input feed ([33], [34]) and process parameters such as rotation speed ([33], [36]), and hydraulic pressure [36] during shredding of metal sheets, electrical appliances and municipal solid waste. In [36], it was shown that increase in hydraulic pressure and increase in rotor speed for this particular shredder led to a decrease in specific energy (i.e. per mass of input) used by the shredder, as well as finer size distribution of the output particles. In [33], it was shown that less residence time is needed for the horizontally-mounted rotor shredder than for vertically-mounted one, while the feed sheets with a smaller thickness result in a smaller mean fragment size and fragment weight, but bigger apparent area (ratio of mass and thickness): "as the sheet thickness increases, the critical bending radius increases too. That means the crack formation and thus the failure occurs with a smaller scale of bending" [33] .

### 1.5.2 Separation technologies

The separation processes following shredding of ELV hulks vary by the shredding facilities, which typically also hold the equipment network performing material separation. The shredded particles are usually routed to the first separation unit directly from the shredder using a conveyor belt. Similarly, after each separation unit, the material flow is routed using conveyor belts to the next separation unit, to the collection unit or to waste streams.

Each separation equipment sorts based on the particles' specific properties (see Table 1.6). These separation properties can be physical or material, and represent target parameters by which the technologies equipment sort for a particular material. For instance, physical properties could be size, shape and mass; material properties could be material susceptibility, density, electrical conductivity.

| Material Type | Separation property | Separation equipment |
|---|---|---|
| Ferrous | Magnetic susceptibility | Magnet separator |
| Light fluff (plastics & polymers) | Density and mass | Air cyclone |
| Aluminum | Electrical conductivity to density ratio | Eddy-current induction separator |
| Fines | Size and shape | Trommels, screens |
| Plastics ( HDPE, PET, Tetrabrik, PP, Other Plastics) | Density<br>Surface hydrophobicity | Heavy media separation |

*Table 1.6 Mechanical separation technologies for ELVs, the physical properties and the target material properties*

Magnet

The magnet separator can consist of overhead magnet type or drum magnet type, which is the one typically used for ELVs. As shown in Figure 1.9, the magnetic poles inside the drum, exerts a strong magnetic field to collect magnetic materials onto the rotating drum shell, such that the target stream (mags) is separated into a different chute than the non-magnetic materials. The degree of the separation is a function of the magnetic field strength and of the particles' magnetic susceptibility. It should be noted that separation is not perfect as non-ferrous materials can remain attached to the ferrous materials. This is the case for copper wires from electric motors [5], which in some facilities are manually picked out downstream (see Figure 1.13, Figure 1.14).

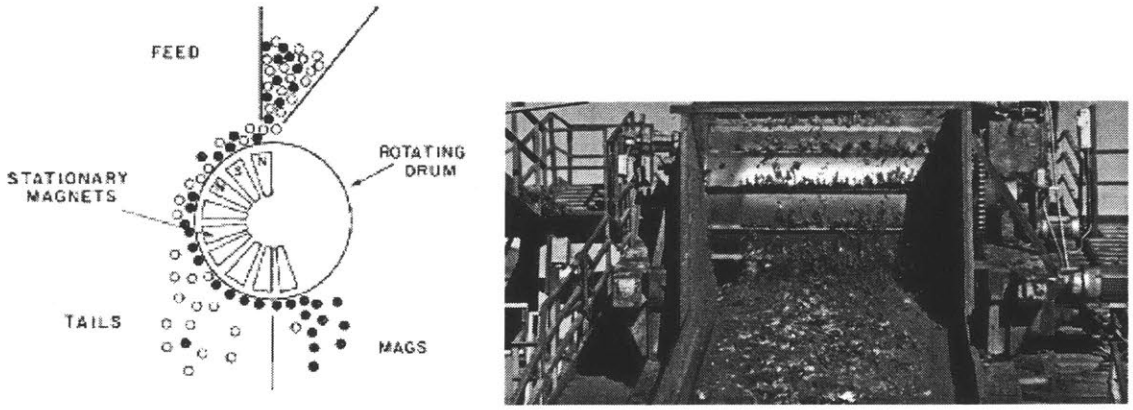


*Figure 1.9 Left: Illustration of a drum-type magnet separator [37], right: drum magnet separator in action [38]*

Eddy-current

An eddy-current separator in used to separate nonferrous metals based on their conductivities. It consists of a belt, with a magnetic rotor and splitter at the end. The splitter(s) separates the particles based on their deviation trajectory, as seen in Figure 1.10 below. While the particles bear gravitational ($F_g$), centrifugal forces ($F_c$) and other mechanical forces, the magnetic deflecting force ($F_d$) induced onto the particles is responsible for their selective deflection. This magnetic deflecting force can be given by [39], [40]:

$$F_d = KB^2 fm\frac{\rho}{\sigma}p$$

Where $K$ is the complex coefficient related to the magnetic roll system design, $B$ is the effective magnetic induction, $f$ is the oscillation frequency, $m$ is the mass of the conducting particle, $\rho$ is its mass density, $\sigma$ is its electrical conductivity, $p$ is the complex particle factor related to its dimension, shape and orientation in the magnetic field [39], [40].

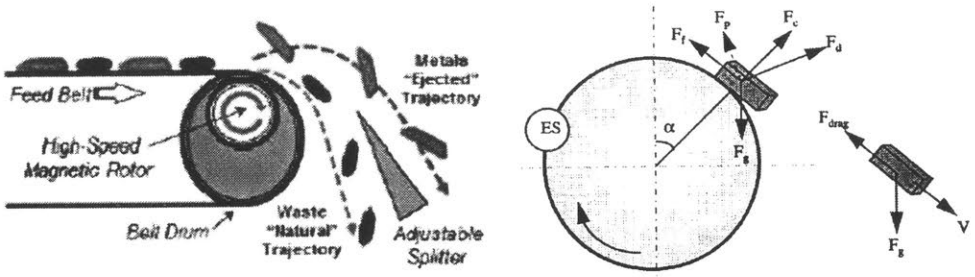


*Figure 1.10. Left: Illustration of a belt eddy-current separator [40], right: forces acting on particles at end of belt [39]*

Zhang et al. showed experimentally the different deviations undergone by particles of different materials: materials with higher ratio of magnetic conductivity to density ($\frac{\rho}{\sigma}$) have deflective force $F_d$, hence greater deflections. Additionally, at stronger rotational speeds, the oscillation frequency $f$ is stronger, leading greater deflection too [39].

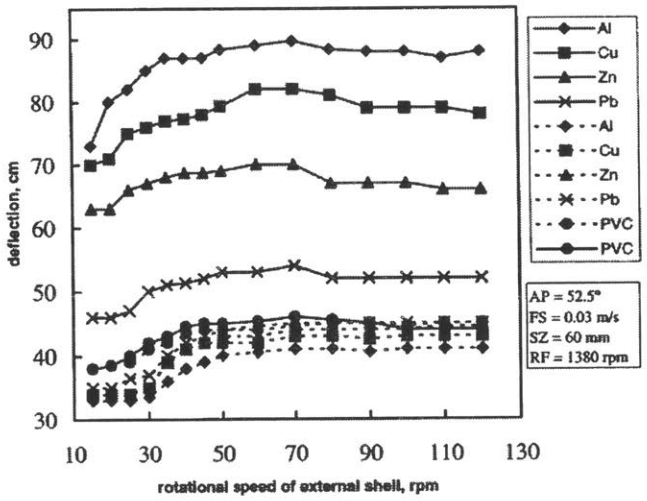


*Figure 1.11. Deflection as a function of the rotational speed of the belt shell for different particles [39]*

Heavy media separation

Heavy media separation (HMS) is used to separate high density metals from low density metals using a viscous medium [41]. The medium is used to float out desired or undesired materials of a smaller density. Typically, for automotive scraps, the heavy media separation process can include up to three HMS baths in series: the first bath is with water as the medium, of specific gravity of one, separates the non-metallic particles (e.g. plastics, foam); the second bath is with magnetite solution, of specific gravity 2.5, separates the magnesium and high density plastics; the third bath is with ferrosilicate solution, of specific gravity 3.5, separates the aluminum from the heavier metals (e.g. copper, zinc, lead) [42], [43].

Separation networks

Figure 1.12-Figure 1.14 show 5 different configurations of the separation process flows: Figure 1.12 shows a typical EU configuration [44], Figure 1.13 shows the configuration of the Schnitzer Steel Everett (MA) metal shredding facility as we perceived during a site visit, and Figure 1.14 shows those of 3 shredding facilities described in [5]. Generally, the shredding facilities consist of a magnet separator to recover ferrous material, an eddy-current separator to recover non-ferrous materials. The non-ferrous materials include mainly aluminum, as well as other non-ferrous metals (zinc, brass, copper and stainless steel). The non-ferrous materials as sometimes separated further by heavy media separation equipment, with aluminum separated from other denser non-ferrous metals. Additionally, some shredding facilities have induction sorting equipment which target stainless steel. We can also note the use of an air separation equipment which removes the light materials (in particular, plastics and other polymers) from the main material stream, and of a screening equipment (called trommel) to remove out the fines or divide the material flow into a smaller and bigger particle size flows. Depending on the separation network and equipment used, the output streams, i.e. the collected output scraps, vary from one shredding facility to another: in Figure 1.13, the valuable output scraps (in green) include ferrous, copper pickings, Zorba (a grade of aluminum scrap) and Zurik (a grade of stainless steel); in Figure 1.14, the valuable output scraps (in triangles) additionally include collected scraps fro zinc, brass and copper. Most shredding facilities can have a manual sorting unit stationed just before the output scrap collection, in order to visually identify and remove contaminating elements from the scrap.

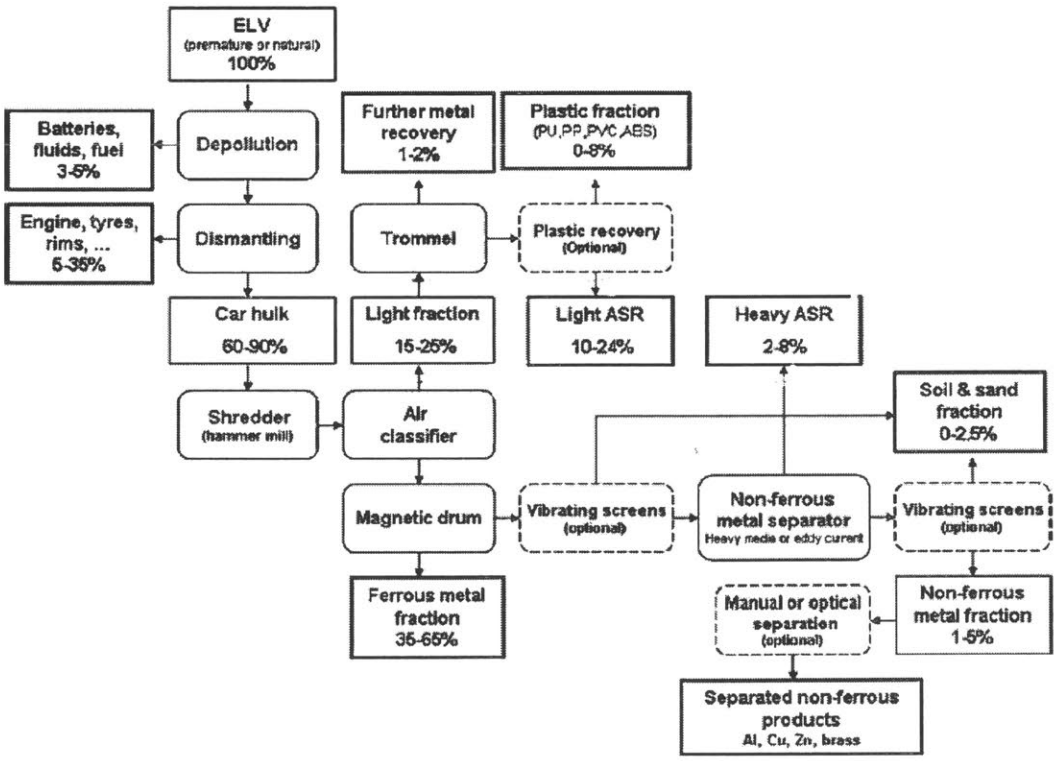


*Figure 1.12 Typical shredding and separation processes in the EU [44]*

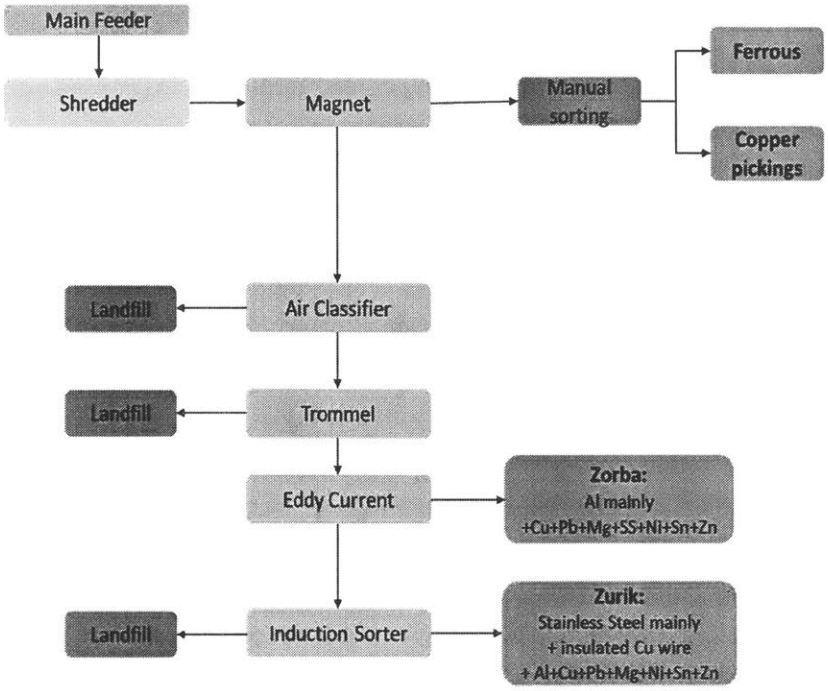


*Figure 1.13 Shredding and separation processes at the shredding facility of Schnitzer Steel, in Everett, MA*

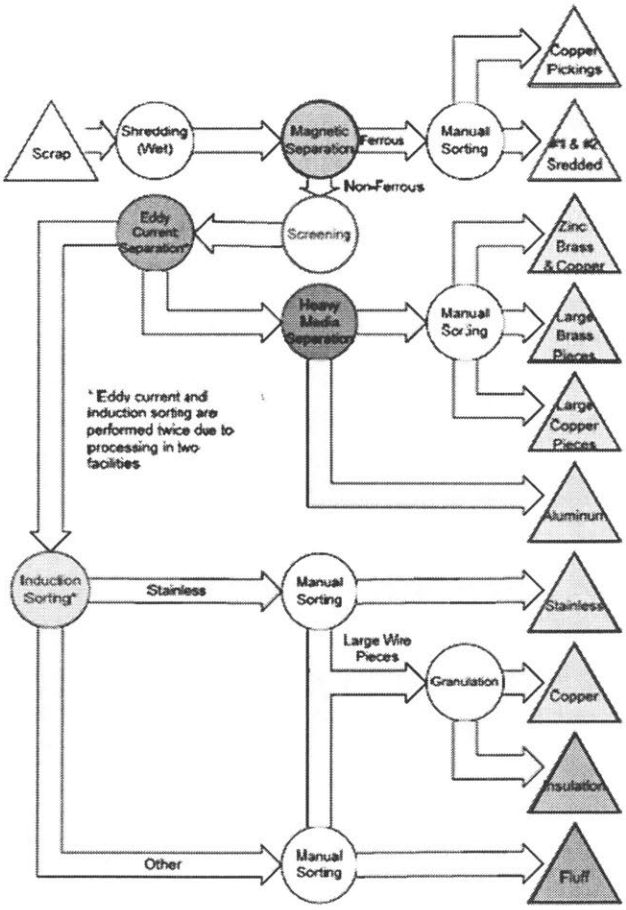


(i)

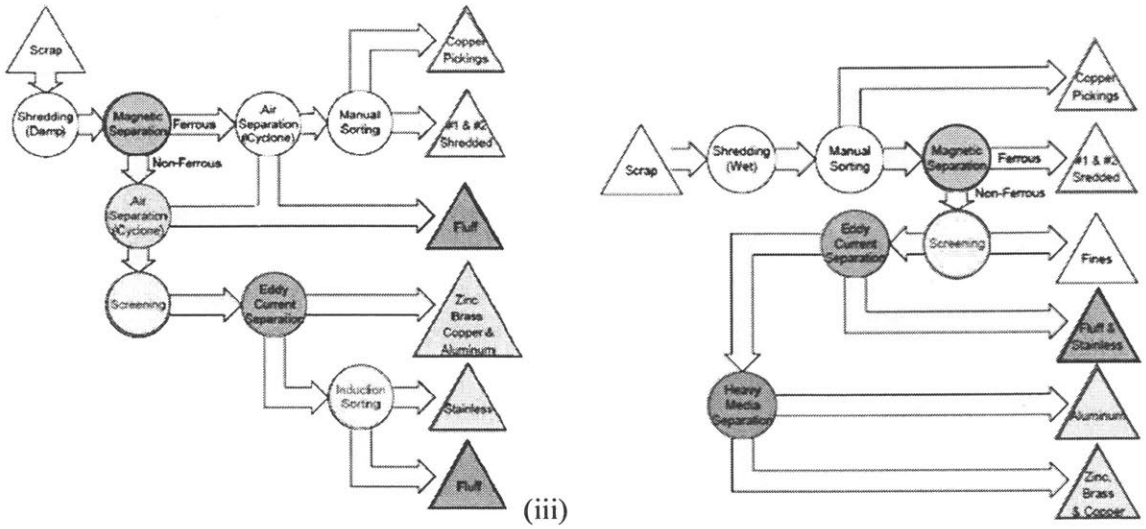


*Figure 1.14 Typical shredding and separation processes at 3 US shredding facilities (i) Omnisource, (ii) Ferrous Processing, (iii) Padnos, adapted from [5]*

## 1.6 Output scraps and ASR

As seen in the above section, different configurations used at shredding facilities give rise to different output valuable scraps. The waste streams from the facilities are generally termed as automotive shredder residues (ASR). ASR can further be divided in light and heavy fractions: the light fraction is derived from the air separation unit and contains mostly plastics; the heavy fraction is derived from the waste streams of the later separation units targeting metals.

### 1.6.1 Valuable scraps

The valuable scraps are either ferrous or non-ferrous. The shredding facilities usually fine-tune their network of sorting equipment such as to produce scraps of quality and content matching the general specifications of traded scrap on the local or global scrap market. Traded scrap metals can be classified according to several properties, namely: chemical composition of metals, level of impurity elements, physical size and shape, homogeneity or variation within the specifications [45].

While ISRI provides grade specifications for commercial scrap in their "Scrap Specification Circular", the percentage of each metal in the scrap is at the discretion of the buyer, as determined by the contract with the seller. Some scrap can be additionally specified with a number, for the estimated percentage of nonferrous metal content, e.g. Zorba 90. Alternatively, some scraps also include some specific size range description [46]. The table below shows the scrap of interest to us (i.e. from automotive industry) and their specifications.

| Main material type | Scrap name | Scrap specifications |
|---|---|---|

| | | |
|---|---|---|
| Aluminum | Zorba | Shredded non-ferrous scrap, a combination of the nonferrous metals: aluminum, copper, lead, magnesium, stainless steel, nickel, tin, and zinc, in elemental or alloyed (solid) form. |
| | Tweak | Fragmentizer aluminum scrap (after mechanical or hand separation). Composition limits: ≤4% free zinc, ≤ 1% free magnesium, ≤1.5% of iron, ≤5% non-metallics of which ≤1% rubber and plastics. |
| | Twitch | Floated fragmentizer aluminum scrap (after wet or dry media separation). Composition limits: ≤1% free zinc, ≤ 1% free magnesium, ≤1% of iron, ≤2% non-metallics of which ≤1% rubber and plastics. |
| Stainless steel | Zurik | Shredded non-ferrous sensor-sorted scrap. Made up of nonferrous metals: stainless steel, insulated copper wire, aluminum, copper, lead, magnesium, nickel, tin, and zinc, in elemental or alloyed (solid) form |
| | Sabot | Clean 18-8 type stainless steel clips and solids. Composition limits: ≥ 7% nickel, ≥16% chrome, ≤.50% molybdenum, ≤.50% copper, ≤.045% phosphorous, ≤ .03% sulfur |

*Table 1.15 ISRI's scrap grade guidelines for Aluminum and stainless steel scrap [46]*

| **Main material type** | **Scrap name** | **Scrap specifications** |
|---|---|---|
| Aluminum | Tally | Aluminum automobile radiators. All contaminants including iron, plastic, and foam not to exceed 1% of weight. |
| | Tense | Mixed aluminum castings, including auto and airplane castings but no ingots, and to be free of iron, brass, dirt and other non-metallic items. Oil and grease not to total more than 2%. |
| | Troma | Aluminum auto or truck wheels. Shall consist of clean, single piece, unplated aluminum wheels of a single specified alloy, free of all inserts, steel, wheel weights, valve stems, tires, grease and oil and other non-metallic items. |
| | Trump | Aluminum castings. Clean automobile aluminum castings of sufficient size to be readily identified and to be free from iron, dirt, brass, bushings, and non-metallic items. Oil and grease not to total more than 2%. |
| Zinc | Scoot | Zinc die cast automotive grilles. Clean, old or used zinc base die cast automotive grilles, free from soldered material. |
| | Scribe | Crushed sorted fragmentizer zinc die cast scrap. To be clean, free of dirt, oil, glass, rubber, and trash. To contain a maximum of 5% unmeltables such as free iron, copper, aluminum and other metals. |
| | Scroll | Unsorted fragmentizer zince die cast scrap.<br>Material to contain about 55% zinc-bearing scrap. Other nonferrous metals such as aluminum, stainless steel, red metal, etc., to be about 40%. Insulated copper wire about 1%. Trash, dirt, glass, rubber, oil, iron, not to exceed 5%. |
| Lead | Rink | Scrap wet whole intact lead batteries<br>Consisting of SLI (starting, lighting & ignition), automotive, truck, 8-D and commercial golf cart and marine-type batteries. Cases to be either plastic or rubber and to be complete. |
| Red metals | Elder | Babbitt-lined brass bushings. Shall consist of red brass bushings and bearings from automobiles and other machinery, shall contain not less than 12% high tin-base babbitt, and shall be free of iron-backed bearings. |
| | Ocean | Mixed unsweated auto radiatiors. Shall consist of mixed automobile radiators, to be free of aluminum radiators, and iron-finned radiators. |
| Plastics | Bumper | Post-Consumer TPO Plastic Automotive Bumper Covers generated by collision or refurbishment centers or automobile dismantlers. |

| | | |
|---|---|---|
| | | The following parts must be removed from the bumper cover: head lamps, tail lamps, grills, emblems, rub strips, reflectors, and any other components attached to the bumper. Everything attached to the bumper cover should be removed before baling. Contamination should be limited to small metal parts such as clips, bolts, and screws. |
| Ferrous | HMS mix and shredded scrap* | 204: No. 2 heavy melting steel. Wrought iron and steel scrap, black and galvanized, maximum size 36 x 18 inches.<br>205: No. 2 heavy melting steel 3 feet x 18 inches. Wrought iron and steel scrap, black and galvanized, maximum size 36 x 18 inches. Free of sheet iron or thin gauged material.<br>206: No. 2 heavy melting steel 5 feet x 18 inches. Wrought iron and steel scrap, black and galvanized, maximum size 60 x 18 inches. Free of sheet iron or thin gauged material.<br>210: Shredded scrap. Homogeneous iron and steel scrap, magnetically separated, originating from automobiles, unprepared No. 1 and No. 2 steel, miscellaneous baling and sheet scrap. Average density 50 pounds per cubic foot.<br>211: Shredded scrap. Homogeneous iron and steel scrap magnetically separated, originating from automobiles, unprepared No. 1 and No. 2 steel, miscellaneous baling and sheet scrap. Average density 70 pounds per cubic foot.<br>218 Bundled No. 2 steel. Wrought iron or steel scrap, black or galvanized, 1/8 inch and over in thickness, compressed to charging box size and weighing not less than 75 pounds per cubic foot. Auto body and fender stock, burnt or hand stripped, may constitute a maximum of 60 percent by weight. (This percent based on makeup of auto body, chassis, driveshafts, and bumpers.)<br>224: Auto slabs. Clean automobile slabs, cut 3 feet x 18 inches and under.<br>225: Auto slabs. Clean automobile slabs, cut 2 feet x 18 inches and under.<br>244: Springs and crankshafts. Clean automotive springs and crankshafts, either new or used.<br>248: Hard steel cut 30 inches and under. Automotive steel consisting of rear ends, crankshafts, driveshafts, front axles, springs, and gears prepared 30 inches and under. May not include miscellaneous small shoveling steel or any pieces too bulky for gray iron foundry use. |
| Ferrous (cast) | Cast iron grade** | 252: Cupola cast. Clean cast iron scrap such as columns, pipes, plates, and castings of a miscellaneous nature, including automobile blocks and cast iron parts of agricultural and other machinery. Free from stove plate, burnt iron, brake shoes or foreign material. Cupola size, not over 24 inches x 30 inches, and no piece over 150 pounds in weight.<br>259: Clean auto cast. Clean auto blocks; free of all steel parts except camshafts, valves, valve springs, and studs. Free of nonferrous and non-metallic parts.<br>260: Unstripped motor blocks. Automobile or truck motors from which steel and nonferrous fittings may or may not have been removed. Free from driveshafts and all parts of frames.<br>262: Clean auto cast, broken, not degreased. Clean auto blocks, free of all steel parts except camshafts, valves, valve springs and studs. Free of nonferrous and non-metallic parts, and must be broken to cupola size, 150 pounds or less.<br>263: Clean auto cast, degreased. Free of all steel parts except camshafts, valves, valve springs, and studs. Free of nonferrous and non-metallic parts, and must be broken into cupola size, 150 pounds or less. |

| | | |
|---|---|---|
| | | 264: Malleable. Malleable parts of automobiles, railroad cars, locomotives, or miscellaneous malleable iron castings. Free from cast iron and steel parts and other foreign material. |

*Table 1.7 ISRI's scrap grade guidelines for scrap that can completely or partially source from automobiles [46]*

*Ferrous scrap sell as different mixtures on scrap markets: e.g. scrap from Northern Europe of US ship to Turkey as ISRI 200-206 scrap, and scrap shipped to India as 210-212 [47]. Ferrous scrap 200-206 as per ISRI specifications are heavy melting scrap (HMS) categories for recyclable steel and wrought iron of various dimensions. On scrap markets, shredded scraps 200-206 are sold as HMS 1& 2 in different ratios (e.g. 80:20 or 75:25 mix), where HMS 2 only contains galvanized and blackened steel [46].

**These are specifically prepared to meet with the steel mill or foundry requirements [46].

As seen above, there can be different scraps for the same material types. They differ based on quality, content or source. For example, aluminum scraps include: Zorba, Tweak, Twitch coming from automobile specifically. Detailed characterizations of Zorba and Twitch samples have been carried out by S. Kelly in [43]: The cast alloys identified in the mixture were 319, 356, 380, 390, and 413, and the wrought alloy distribution was clustered by series from 2000 to 7000. Zorba has average aluminum alloy content of 62%, while that of twitch is 95%.

Note that the prices of the traded scraps of a given main material type do not necessarily correlate with the quality of the scrap. As seen in Figure 1.16, the price of Zorba is not far off from that of Twitch, even though Twitch is of a higher aluminum grade. This can be attributed to the fluctuating market prices of other metals also contained in Zorba (for e.g. nickel, copper). Zorba is usually exported abroad to China, India, Vietnam or other countries, where the scrap is separated further (typically manually) for these non-ferrous metals, which are valuable enough to offset the foreign labor costs.

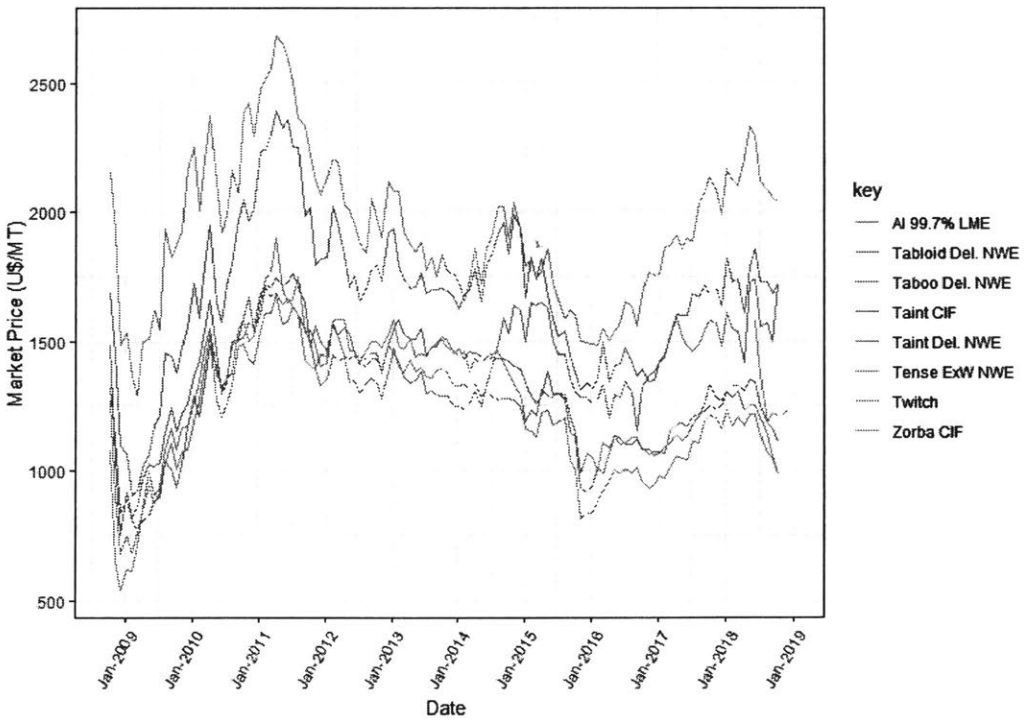


*Figure 1.16 Variation in market price of different Aluminum scraps (data source: LME exchange)*

### 1.6.2 Automotive shredder residue (ASR)

Automotive shredder residue (ASR) is one output stream from the material separation processes, consisting of light materials, primarily plastic and other polymers. Table 1.8 below lists the typical composition of ASR. ASR contains 20-25 % by weight of a typical vehicle, but this percentage is predicted to increase due to the increased use of light materials, including polymers and aluminum [11].

| Material | (%) |
|---|---|
| Textiles and foam | 27–27.2 |
| Plastics | 19–20.2 |
| Metal | 1–4.6 |
| Rubber | 2.8–7 |
| Cellulose | 0.2–1 |
| Fines | 45 |

*Table 1.8. Typical composition in weight percentage of ASR [11]*

Plastics in the ASR are difficult to recycle because of the heterogeneous nature of the mixture, with contaminating materials attached with fasteners [12]. There could be many types of plastics used in different automotive parts which end up in the ASR: for the car data in [22], [27], there were at least 10 types of plastics. Moreover, certain plastics, such as thermoset plastics, cannot be recycled due to their permanent cross-link structure [12]. The literature has reported some research being done on material recovery from ASR [11], [48]: chemical leaching to remove the small amounts of metals; mechanical separation using air, magnetic and eddy-current separation to remove the non-plastics; mechanical separation using float/sink or froth floatation techniques to separate the different plastics.

However, these separation methods for further recycling of the ASR are not economically feasible at the moment. In the US, the ASR typically ends up in landfills, with a small portion used as landfill cover or incinerated [48]. With the new EU directive for ELV treatment, landfilling in the EU is not longer an option. Another option being pursued is energy recovery through pyrolysis or incineration. ASR can be transformed to or used as fuel as it contains combustible materials (plastic, rubber, foam and textiles), with its Lower Heating Value of about 15-30 MJ/kg depending on composition [11]. Pyrolysis is the thermal decomposition of organic materials in an oxygen-deficient environment to produce a synthetic coal/fuel product [12], [48]. However, pyrolysis of ASR is troublesome with plastics during processing, and is not cost-effective compared to landfilling options and the lower costs of other fuels [48]. In Japan, the end-of-life fate of ASR is energy recovery through incineration: Nissan and Toyota have dedicated energy recovery plants where ASR is used in their furnaces [5]. Comparatively, Europe is pursuing energy recovery in the presence of other waste streams (e.g. municipal solid waste) or as an alternative fuel in the foundry and cement industries [11].

The maximum energy content of an ASR of a given composition can be calculated from the properties of the specific plastics or polymers, e.g. using their high heating values or chemical exergies [49].

## 1.7 Secondary metal processing (refining, alloying and dilution)

### 1.7.1 Secondary metal production processes

Metal scrap, due to heterogeneous mixing with other metals after shedding and separation of end-of-life complex products, can contain many minor chemical elements. These minor elements depending on their role in the process metallurgy and wanted mechanical properties of the final metal, can be either [50]:

(i) alloy elements: with positive effect on the mechanical properties or following metal processing steps;

(ii) impurity elements: with negative effect on the mechanical properties or following metal processing steps;

(iii) Tramp elements: which cannot be easily removed by any known metallurgical refining process, and pose long-term problem due to accumulation in metal scraps

(iv) Trace elements: with negligible effect on the mechanical properties or following metal processing steps.

The metal scrap can contain too high level of some contaminants, which can be alloying elements or tramp elements, depending on the end-use aluminum alloy. Some elements can be removed by refining processes (called impurity elements), others that cannot are called tramp elements. In case of excess contaminants, dilution with primary material can be used to decrease their concentration which has exceeded the maximum target concentration limit for a particular metal alloy production. Also possible, is blending with other alloys, while making sure to determine the ratio of the blending alloys which ensure that the concentration of the limiting contaminant does not exceed the threshold.

Aluminum

Primary aluminum production is an energy intensive process, as it comes from bauxite ore from which is extracted an aluminum oxide compound, which is electrolytically reduced to aluminum (source: www.aluminum.org) . On the other hand, secondary aluminum production circumvents the need for the energy-intensive reduction process. It occurs in furnaces where smelting and refining take place. Figure 1.17 illustrates typical processing steps for secondary aluminum processing. Note that aluminum scrap is often pre-treated before the smelting/refining processes, however the extent of pre-treatment operations done varies from one facility to another. Often 'new' or industrial scrap as well as 'old' or end-of-life scrap are both used as feedstock. Pre-treatment operations can include [41]:

- mechanical comminution& separation:
  - hammer mills & ring rushers for comminution,
  - magnet, screens or air classifiers for separation),
- pyrometallurgical cleaning, called 'drying' in industry:
  - techniques include roasting and sweating, which uses heat to temperatures below aluminum melting point to vaporize or carbonize organic contaminates),
  - Catalytical technique is used to clean aluminum dross, with a salt/cryolite mixture.
- hydrometallurgical cleaning:
  - leaching is used to recover aluminum from dross, furnace skimmings and slag,

- heavy media separation processes separates high density metal from low density metal using a viscous medium. This technique is used to concentrate aluminum recovered from shredded cars.

Smelting and refining take place in the melting and holding furnace. Steps include [41]:

- charging & melting: feeding the scrap into a melted aluminum pool maintained in the melting furnace
- fluxing: flux materials trap impurities and float to the surface providing a barrier preventing oxidation of melted aluminum
- demagging: As noted by [51], magnesium can be removed by an oxidation process in rotary furnace with addition of oxygen gas during a metallurgical process called demagging"". and can also be removed by chlorine or fluorine gas [41], [52].
- Degassing: high-pressure inert gases mixing the melt brings entrained gases to the surface.
- **Alloying:** In the holding furnace, alloying elements (e.g. zinc, copper, manganese, magnesium and silicon) are added and the resulting alloy is analyszd iteratively, until the correct chemical composition is reached.
- skimming & pouring: the semisolid fluxes containing contaminants are removed from the surface of the melt. Then the melt is allowed to cool before pouring into molds or casting machines

The smelting /refining process can also take place in a small crucible for 500kg or less of scrap. It can also take place in an electric induction furnace, to provide increased strength and hardness with hardening elements like manganese and silicon [41].

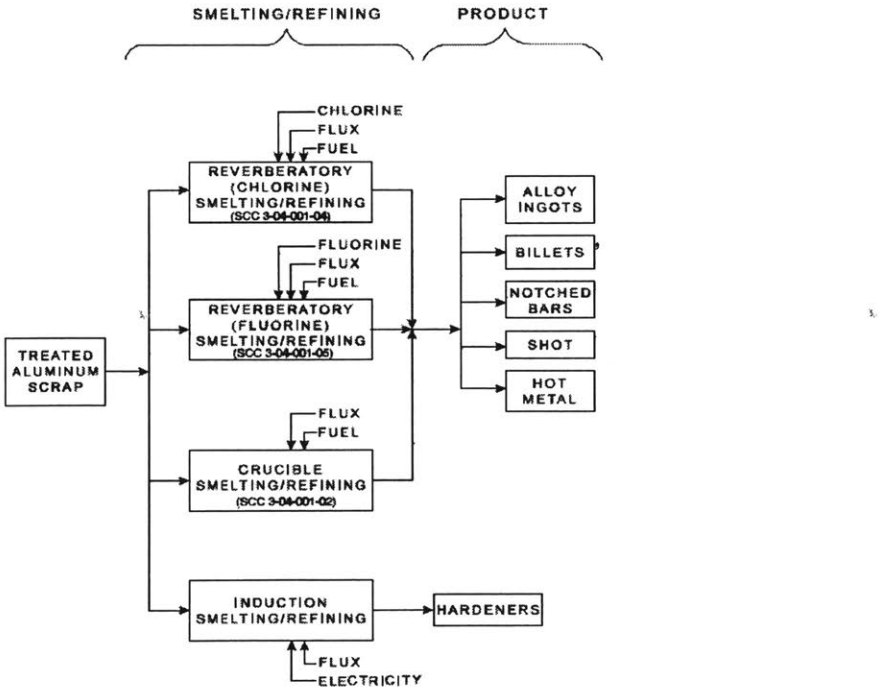


*Figure 1.17 Typical process diagram for secondary aluminum processing industry [41]*

Ferrous, steel and alloys

The remelting of secondary ferrous materials to crude steel takes place in a basic oxygen furnace (BOF) or an electric arc furnace (EAF). There are 2 emission intensive processes in the BOF: (i) the reduction step where iron ore (iron oxide compounds) is melted with coke; (ii) oxygen is blown through to reduce the carbon content in the metal [50]. During this largely exothermic oxidation step, some cooling agent is often needed, which can include pig iron, iron ore. Additionally, industrial ferrous scrap, which is of better quality than EOL scrap, can be used as cooling agent in the BOF. The next step is ladle metallurgy where alloying and refining take place, with stirring for uniform distribution [50].

On the other hand, secondary steel production using end-of-life product scrap can only be used in an EAF. EOL scrap, or old scrap, nevertheless, represents a large part of the global crude steel production: 40% globally [53] and 30% in Japan as shown in Table 1.9 [54].

| | Scrap types | | |
|---|---|---|---|
| | New scrap | Old scrap | Pig iron |
| Input ($10^9$ kg) | 24.0 | 23.2 | 84.4 |
| (a) Direct use (initial destination) | | | |
| Crude ordinary steel (BOF) | 0.351 | 0.000 | 0.777 |
| Crude special steel (BOF) | 0.085 | 0.000 | 0.005 |
| Crude ordinary steel (EAF) | 0.241 | 0.733 | 0.192 |
| Crude special steel (EAF) | 0.175 | 0.153 | 0.004 |
| Cast iron materials | 0.096 | 0.074 | 0.014 |
| Forged iron materials | 0.052 | 0.040 | 0.008 |

*Table 1.9 Comparison of industrial (new) scrap, EOL (old) scrap, and primary (pig iron) ferrous material for steel/iron production in Japan [54]*

In the EAF, an electric current is passed through graphite electrodes and forms an arc, which generates heat melting the scrap [55]. In additional to a general classification system for steel scrap of different qualities and sources [46], the EAF plant also has an internal classification system that further divides the scrap types based on origin, supplier chemical content and size distribution: there can be around 20 such subtypes of steel as well as 100 for stainless steel [50]. Different steelmaking plants have different scrap-mix optimization schemes to produce a target steel alloy: (i) based on standard scrap recipes of different scrap mixes, (ii) scrap recipes based on energy consumption and metallic yield, (iii) dynamic scrap recipes with parameters updated based on melting tests.

For both BOF and EAF, they are followed by refining and alloying processes [55]. Refining includes injection of desulfurizing agents, and addition of silicon and aluminum for deoxidation, and fluxing out through the slag. The alloying process includes mixing of the alloying element into the melt with degassing, i.e. inert gas bubbling.

Note that if the produced steel is stainless steel (lower carbon content than steel or other alloy steel), the stainless steel-making process has an important additional refining step after melting in the EAF: the melt is moved into an argon-oxygen decarburization (AOD) converter where the carbon is removed to meet the produced stainless steel quality requirement [53].

### 1.7.2 Refining processes during secondary metal production

Oxidation is the typical method used to remove metal contaminants from metal scraps. Nakajima et al. investigated the removability of elements during the aluminum remelting process by looking at the thermodynamics of their oxidation and evaporation, whereby the elements are distributed among the solvent metal (Al), oxide slag and gas phases. They looked at various elements denoted by $M$, and its oxidation: $mM + \frac{n}{2}O_2 \rightarrow M_mO_n$

$L$", the distribution ratio of $M$ between the metal and gas phases was given by [56], with a bigger $L$"giving easier removal of $M$ by evaporation :

$$L" = \frac{p_M}{p_{Al}} = \frac{p^o \gamma_M x_M}{p_{Al}}$$

$L'$, the distribution ratio of M between the metal phase and slag phase, with a smaller $L'$ giving an easier removal of $M$ by oxidation [56]:

$$L' = \frac{x_M}{x_{M_mO_n}} = \frac{\gamma_{M_mO_n}}{K'\gamma_M^m x_M^{m-1} p_{O_2}^{n/2}}$$

Where $p$ refers to partial pressure of the vapor, $p_M^o$ is the partial pressure of the pure element M, $\gamma_M$ is the activity coefficient of M, $x_M$ is the mole fraction of M in the solvent, $\gamma_{M_mO_n}$ is the activity coefficient of $M_mO_n$, $K'$is the equilibrium constant of the oxidation reaction.

From these equations, Nakajima et al. built a graph showing the predicted distribution of various elements among the gas, slag and metal phases for aluminum remelting, see Figure 1.18. It can be observed that: Cu, Fe, Si, and Mn remained in the aluminum metal but Mg can be removed through the slag; Zn can be removed by evaporation if at high concentration [56].

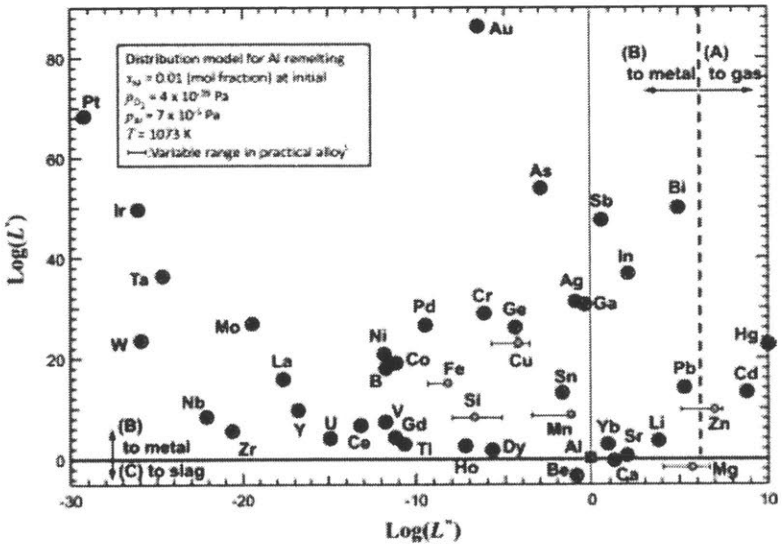


*Figure 1.18 Distribution of elements among gas, slag and metal phases for simulated aluminum remelting [56]*

Nakajima et al. also extended the analysis to the remelting of steel, Cu, Pb, and Zn, with the results shown in the element radar chart to illustrate the ease of removal of impurities in the figure below. The radian direction (inward to slag phase) shows ease for oxidation, whereas the arc direction (clockwise to gas phase) shows ease for evaporation. This element radar chart is an improvement on the Metal Wheel proposed by Castro et al. [57], where the relationships between the different metals are based off their extraction and primary production processes.

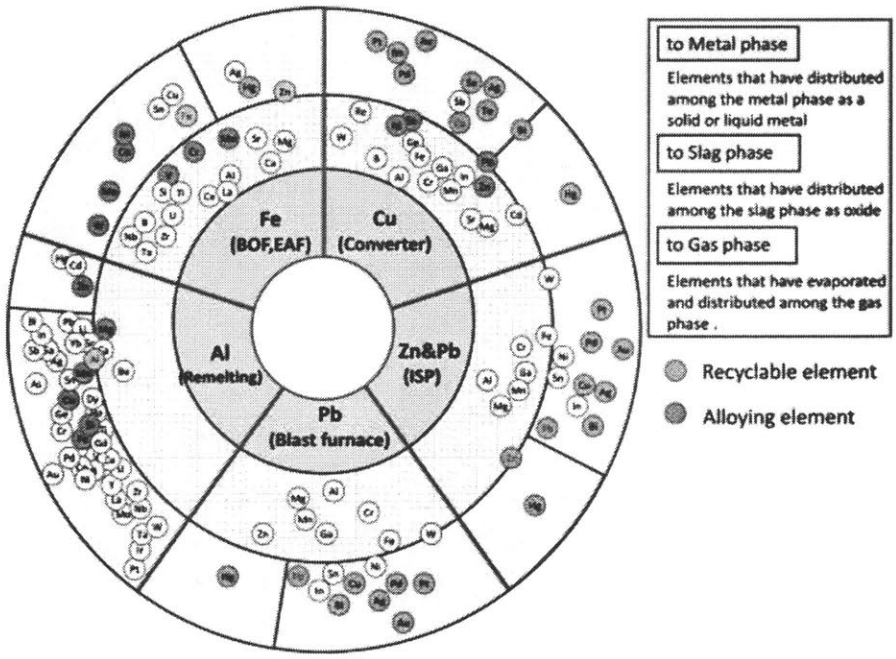


*Figure 1.19 Element radar chart for the metallurgical process of base metal, with various impurity metals dissolved [56]*

The element radar chart is useful to identify which material will constitute tramp elements in the remelting of the specific target metal stream. For example, in the Aluminum target stream, Fe will constitute tramp elements for the production of Al alloys without Fe; in the Ferrous target stream, Cu and Sn will constitute tramp element for the production of steel.

### 1.7.3 Aluminum alloys and constituent requirements

Most aluminum is used in the form of alloys rather than pure metal, and require the addition of alloying elements (Cu, Fe, Mn, Mg, Si, Zn, Cr, Ni, Ti) for specific chemical and physical properties. As a result, there exists several series of Aluminum, depending on the purity level of the aluminum alloy. For instance, 1000 series alloys are 99.9% aluminum and produced from primary aluminum. On the other hand, cast aluminum (300 series) contains high levels of alloying elements, about 27%, and can increase to 40% [58]. Table 1.10 shows common aluminum alloys and their alloying elements with minimum and maximum levels, as well as the associated properties.

In Figure 1.20 below, Modaresi et al. looked at the potential blending paths for scrap aluminum alloy, where the denoted maximum recycled content is the ratio of the upper limit of the limiting element in the produced alloy to its nominal concentration in the source alloy [52].

To summarize, depending on the contaminating elements present in aluminum scrap, scrap can only be recycled to certain series of aluminum alloys, after refining and/or dilution or blending. However, with its impurity due to the heterogeneous mixture resulting from imperfect comminution and separation, aluminum scrap is usually down-cycled to cast aluminum which can tolerate the highest level of contaminants. However, Modaresi et al. foresees a need for change as the current aluminum scrap supply will exceed the demand for cast alloys soon [52]. The performance output (recovery rate and grade, and material breakdown) from our recovery model can be used to evaluate which blending/dilution path is more efficient for a particular end-of-life product input composition to the recovery chain.

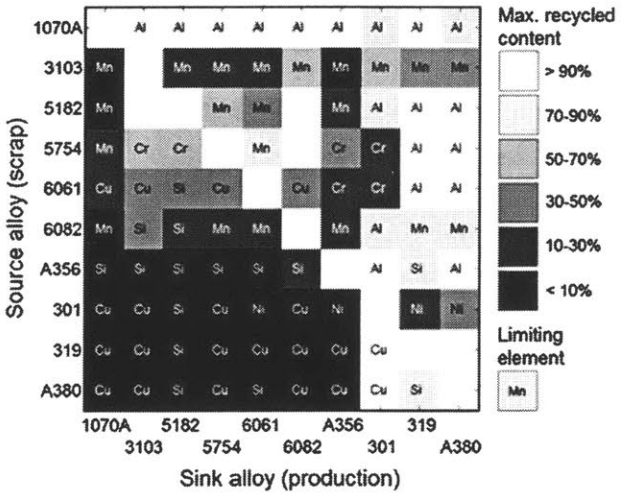


*Figure 1.20 Source-sink diagram: recycling paths for aluminum alloys from scrap (source) to different potential alloys at secondary production [52]*

| | **Properties** | **Si** | **Fe** | **Cu** | **Mn** | **Mg** | **Cr** | **Ni** | **Zn** | **Ti** |
|---|---|---|---|---|---|---|---|---|---|---|
| **P0506A** | Others: 0.02% max each | 0-0.05 | 0-0.06 | 0-0.02 | 0-0.02 | 0-0.02 | 0-0.02 | 0-0.02 | 0-0.03 | 0-0.02 |
| **P1020A** | Others: 0.03% max each | 0-0.10 | 0-0.20 | 0-0.03 | 0-0.03 | 0-0.03 | 0-0.03 | 0-0.03 | 0-0.03 | 0-0.03 |
| **1070A** | Formability, good corrosion resistance, high heat conductivity | 0-0.2 | 0-0.25 | 0-0.03 | 0-0.03 | 0-0.03 | 0-0.03 | 0-0.03 | 0-0.07 | 0-0.03 |
| **3103** | High formability, corrosion resistance, medium strength | 0-0.5 | 0-0.7 | 0-0.1 | 0.9-1.5 | 0-0.3 | 0-0.1 | 0-0.05 | 0-0.2 | 0-0.1 |
| ***5182*** | *Excellent corrosion resistance, toughness and weldability, can be strain hardened. Used in sheet form.* | *0-0.2* | *0-0.35* | *0-0.15* | *0.2-0.5* | *4.0-5.0* | *0-0.1* | *0-0.05* | *0-0.25* | *0-0.1* |
| **5754** | | 0-0.4 | 0-0.4 | 0-0.1 | 0-0.5 | 2.6-3.6 | 0-0.3 | 0-0.05 | 0-0.2 | 0-0.15 |

| | | | | | | | | | | |
|---|---|---|---|---|---|---|---|---|---|---|
| **6061** | Can be strengthened by heat treatment, for higher strength requirement. Used in sheet and extruded form. | 0.4-0.8 | 0-0.7 | 0.15-0.4 | 0-0.15 | 0.8-1.2 | 0.04-0.35 | 0-0.05 | 0-0.25 | 0-0.15 |
| **6082** | | 0.7-1.3 | 0-0.5 | 0-0.1 | 0.4-1.0 | 0.6-1.2 | 0-0.25 | 0-0.05 | 0-0.2 | 0-0.1 |
| **6022** | | 0.8-1.5 | 0.05-0.2 | 0.01-0.11 | 0.02-0.1 | 0.45-0.7 | 0-0.1 | | 0-0.25 | 0-0.15 |
| **6111** | | 0.7-1.1 | 0-0.4 | 0.5-0.9 | 0.15-0.45 | 0.5-1 | 0-0.1 | | 0-0.15 | 0-0.1 |
| **A356** | High Si content and other alloying elements used as Cast alloys | 6.5-7.5 | 0-0.2 | 0-0.2 | 0-0.1 | 0.25-0.45 | 0-0.05 | 0-0.05 | 0-0.1 | 0-0.2 |
| **301** | | 9.5-10.5 | 0.8-1.5 | 3-3.5 | 0.5-0.8 | 0.25-0.5 | 0-0.03 | 1.0-1.5 | 0-0.05 | 0-0.2 |
| **319** | | 5.5-6.5 | 0-1.0 | 3.0-4.0 | 0-0.5 | 0-0.1 | 0-0.5 | 0-0.35 | 0-1.0 | 0-0.25 |
| **A380** | | 7.5-9.5 | 0-1.3 | 3.0-4.0 | 0-0.5 | 0-0.1 | 0-0.5 | 0-0.5 | 0-3.0 | 0-0.5 |

*Table 1.10 Composition limits for aluminum alloys and their properties, adapted from [51], [52] from ASTM International*

### 1.7.4 Steel alloys and constituent requirements

Steels and cast irons are alloys of iron and various alloying elements, of which carbon is the principal. Unlike a cast iron, a steel has carbon content of less than 2%. The alloying elements are mainly carbon, manganese and silicon, but can include nickel (Ni), chromium (Cr), molybdenum (Mo), vanadium (V), columbium/niobium (Nb), copper (Cu), aluminum (Al), titanium (Ti), tungsten (W), cobalt (Co) and Silicon (Si). Apart from iron as its main constituent, steel has as main alloying elements: manganese (Mn), nickel (Ni) and molybdenum (Mo) and chromium (Cr) [59].

There are thousands of different steel compositions manufactured around the world, for which there are several classification systems which differ by country and/or type: composition, microstructure, application or specification [60]. There are several classification systems: the American Iron and Steel Institute (AISI) and Society of Automotive Engineers (SAE), i.e. AISI/SAE steel classification based on chemical composition; systems based on application e.g. ASTM system and Japanese Industrial Standards (JIS) system as used in these references [54], [59].

According to the AISI/SAE classification system, steels can be categorized as follows [60]:

(i) carbon and low-alloy steels (<8% total alloying elements)
   a. carbon steels (main other element is carbon, at <2%)
   b. alloy steels
   c. high-strength low-alloy steels (HSLA)
   d. other low-alloy steels:
      i. With high-temperature properties;
      ii. With improved corrosion resistance;
      iii. With formability;
      iv. Bake-hardenable;
      v. Dual-phase.

(ii) High-alloy steels (>8% total alloying elements
   a. Corrosion-resistant steels (stainless steels)
   b. Heat-resistant steels (tool steels)
   c. Wear-resistant steels (tool steels)

Automotive steels can be of the following types [6]:

- Low-strength steels;
- Conventional high-strength steels (e.g. bake-hardenable and HSLA);
- Advanced high-strength steels (AHSS).

While typically car structures have been dominated by conventional high-strength steel, there is an increased use of AHSS in the body structure for light-weighting. AHSS requires different chemical and processing (heating and cooling) combinations, which give the materials microstructures providing strengthening mechanisms. The AHSS family includes Dual Phase (DP), Complex-Phase (CP), Ferritic-Bainitic (FB), Martensitic (MS), Transformation-Induced Plasticity (TRIP), Hot-Formed (HF), and Twinning-Induced Plasticity (TWIP). AHSS are able to provide for structure requirements of vehicles: For example, DP and TRIP steels are excellent in the crashzones of the car for their high energy absorption. For

structural elements of the passenger compartment, extremely high-strength steels, such as Martensitic and boron-based Press Hardened Steels (PHS) result in improved safety performance. [6].
Stainless steel is a steel alloy with a minimum of 11.5 wt% chromium (Cr) content, and thus corrosion resistant unlike carbon steel.

The target concentrations of these alloying elements are shown in the table below for some stainless steel alloys of (700 series).

| Product | Element concentrations (%) | | | |
|---|---|---|---|---|
| | Mn | Cr | Ni | Mo |
| 710–2 | 1–1.4 | 16.5–16.9 | 6.35–6.55 | 0.65–0.8 |
| 720–1 | 1.6–1.8 | 18–18.4 | 8.5–8.65 | 0–0.4 |
| 720–4 | 1.4–1.6 | 18–18.4 | 10–10.2 | 0–0.4 |
| 731–1 | 1.6–1.8 | 17–17.4 | 9–9.15 | 0–0.4 |
| 750–1 | 1.4–1.6 | 16.7–17.1 | 11–11.15 | 2–2.2 |
| 757–2 | 1.5–1.8 | 16.6–17 | 10.5–10.7 | 2.5–2.7 |

*Table 1.11 Stainless steel products considered for steel secondary production in study by [53]*

The following tables list the vehicle car parts and their corresponding Aluminum or AHSS alloys. This would be useful to establish the ratio of different alloys that end up in the end metal scraps.

| **Vehicle Parts** | **Aluminum alloys used** |
|---|---|
| Engine castings | 38X, 319, 356 |
| Wheels | A356, 5754 |
| Closure sheet | 6111,6016, 6022 |
| Structural sheet | 5182,5754, 2036 |
| Extrusion | 6082, 6061, 6063 |
| Bumper extrusions | 7003, 7129 |
| Radiators | 4xxx, 3003, 1X00 |

*Table 1.12 Vehicle parts using Aluminum alloys [61]*

| **AHSS steel alloys used** | **Vehicle Parts** |
|---|---|
| DP 300/500 | Roof outer, door outer, body side outer, package tray, floor panel |
| DP 350/600 | DP 350/600 Floor panel, hood outer, body side outer, cowl, fender, floor reinforcements |
| DP 500/800 | DP 500/800 Body side inner, quarter panel inner, rear rails, rear shock reinforcements |
| DP 600/980 | DP 600/980 Safety cage components (B-pillar, floor panel tunnel, engine cradle, front sub-frame package tray, shotgun, seat), |
| DP 700/1000 | Roof rails |
| DP 800/1180 | B-pillar upper |
| TRIP 350/600 | Frame rails, rail reinforcements |
| TRIP 400/700 | Side rail, crash box |
| TRIP 450/800 | Dash panel, roof rails |
| TRIP 600/980 | B-pillar upper, roof rail, engine cradle, front and rear rails, seat frame |
| CP 600/900 | Frame rails, B-pillar reinforcements |
| CP 680/780 | Frame rails, chassis components, transverse beams |

| | |
|---|---|
| CP 750/900 | B-pillar reinforcements, tunnel stiffener |
| CP 800/1000 | Rear suspension brackets, fender beam |
| CP1000/1200 | Rear frame rail reinforcements, rocker outer |
| CP1050/1470 | Rocker panels, bumper beams |
| MS 950/1200 | Cross-members, side intrusion beams, bumper beams, bumper reinforcements |
| MS 1150/1400 | Rocker outer, side intrusion beams, bumper beams, bumper reinforcements |
| MS 1250/1500 | Side intrusion beams, bumper beams, bumper reinforcements |
| FB 330/450 | Rim, brake pedal arm, seat cross member, suspension arm |
| FB 450/600 | Lower control arm, rim, bumper beam, chassis parts, rear twist beam |
| TWIP 500/900 | TWIP 500/900 A-Pillar, wheelhouse, front side member |
| TWIP 500/980 | TWIP 500/980 Wheel, lower control arm, front and rear bumper beams, B-pillar, wheel rim |
| TWIP 600/900 | TWIP 600/900 Floor cross-member, wheelhouse |
| TWIP 750/1000 | TWIP 750/1000 Door impact beam |
| TWIP 950/1200 | TWIP 950/1200 Door impact beam |

*Table 1.13 Vehicle parts using advanced high-strength steels [6]*

# Chapter 2 Modeling the disassembly process

In this chapter, we will review the literature on modeling the disassembly process, and will present our model and solution procedure for the decision problem to decide what parts to remove. A vehicle is a complex multi-component product. In this section, we will refer to a part as any component of the product, which can be a single indivisible piece of material or an assembly of sub-components of one or more materials that can be disassembled from each other.

During disassembly, we assume that the removal of a part by the disassembly workers requires some amount of effort and resource (e.g. tools), depending upon how the parts have been integrated into the vehicle assembly. Disassembly is often quite labor intensive as the car parts are structurally well-joined together for safety reasons. These actions require differing amounts of time depending on the difficulty of the specific disassembly tasks, and thus come with different labor costs. Modeling the disassembly process entails the identification of for feasible sequences for part removal, as well as the balancing of the economic resale values from these discrete parts with the labor costs required to remove the parts. As seen in Section 1.4.2, the industry practice for the dismantling sequence is typically based on expert knowledge of what is a feasible sequence, and what parts are worthwhile to remove.

When modeling the disassembly process, there are several considerations:

- Destructive or non-destructive disassembly

  Destructive disassembly is when one of more components are destructively removed from an assembly of the ELV: by destroying fasteners, cracking housings and shearing valuable parts (e.g. using blow-torches). For simplification, we shall not consider destructive actions which can sometimes be used to cut through a car body to get access to a valuable part. This would present difficulty for modeling as destructive actions are hard to specify; they can be done haphazardly, irrespective of precedence constraints among parts. Moreover, destructive actions necessarily will damage some parts in the process, which also can present modeling difficulties. For reference, we cite the literature on destructive disassembly in [62], [63]and semi-destructive disassembly in [64], [65]. We note that semi-destructive disassembly means that some components can be destroyed while others are dismantled depending on their respective economic/material values.

- Partial or complete disassembly

  Electronic appliances are commonly disassembled completely due to the small number of parts and tasks. In contrast, the dismantling process of end-of-life vehicles is never a complete disassembly due to the large number of parts, and thousands of disassembly tasks which would be required [66]. Currently in the automobile industry, the dismantling process is guided by expert knowledge of what is valuable enough for removal, of what is hazardous and requires removal, and the rest of the vehicle (known as the car hulk), is sent to the shredder. Hence, the model and optimization formulation should allow for partial disassembly.

- Modeling fasteners as a part itself

Several disassembly models in literature treat fasteners (such as screws/bolts) as parts, which need to be removed to access and remove other parts [67], [68]. While this is true for vehicles too, there is a high number of fasteners of small mass compared to that of the parts themselves. Therefore, a reasonable simplification is to not consider fasteners as a part for the disassembly model, but rather to still capture the precedence constraints between the parts which the fasteners bring together.

- Geometrical constraints

While modeling the disassembly sequence, it is important to capture the geometrical constraints of the problem. Product parts can only be removed, if the disassembly sequence is physically feasible. This feasibility can de deduced from the parts' connectivity and precedence constraints:

  - Consider a first outer accessible part *A* which is removed. The next part to be removed could be another outside accessible part, or part(s) which were previously attached to part *A*. In product design terms, we need to satisfy the mating constraints of the product parts. In the disassembly literature, this is often represented by a liaison graph [69], also called a connectivity graph [67]. These are un-directed graphs, with nodes representing the parts and arcs representing the connections between pairs of parts. The connection, could be a loose connection such as point, line or surface contact. Alternatively, the connection could be qualified as a tight connection if it results from a joining technique (such as screws, bolts, adhesives, welding) [69].
  - In addition to the connectivity information, the precedence relationships among parts also help define feasibility of a disassembly sequence. The precedence constraints take into consideration the spatial relationships between components by describing the interferences between a component and other components during its removal. Often, this is described along a particular axis of extraction [67], with up to 6 possible axes in the positive and negative x, y, z directions. These spatial relationships are captured in a interference/precedence graph. This is a directed graph, where the node represents the parts and the arc direction connecting two parts signifies the precedence relationship between the parts

- Distinguishing between parts and assemblies

An end-of-life vehicle contains many parts and assemblies, of different functions, materials and costs. Because of the large number of total individual parts, it is important to distinguish between removing a part from its assembly versus removing a part with its assembly. Additionally, the resale value of an individual part is not the same as that of the assembly that contains the part. For this reason, it is necessary to keep track of whether an assembly is fully, partially or not disassembled; as well as whether a part is removed individually, or as part of its assembly.

For example, from data in [22], [23], a door is an assembly, as it consists of sub-components such as a panel and a mirror. A panel itself is also an assembly consisting of the handle, light, speaker cover, top cover and a base. A mirror is an assembly too, consisting of a housing, lens, and electrical component. Depending on the value (or cost) each individual part or assembly, it is possible that the value (or cost) of the assembly is higher than the sum of the value (or cost) of its sub-components, or vice-versa.

## 2.1 Literature on disassembly modeling

There is a growing literature in the field of disassembly, which can be divided into the topics of disassembly sequencing/planning and scheduling, as well as various applications of those topics. Lambert provides a thorough breakdown of research on disassembly. As shown in Figure 2.1, it can range from the detailed level relating component geometry, to the sequence level relating to product structure, to the task planning level relating to disassembly line, to the reverse-logistic level relating to the reuse/recycle chain [70]. The plan of this section is to identify the disassembly models developed in literature, that can inform our research and can apply to our case-study of end-of-life vehicle disassembly. Beyond obtaining feasible disassembly sequences, the goal is to link the sequence level to the reverse-logistic level, i.e. use such output to cascade into recycle chain, and feedback to the disassembly model to optimize the disassembly plan for better recycling performance.

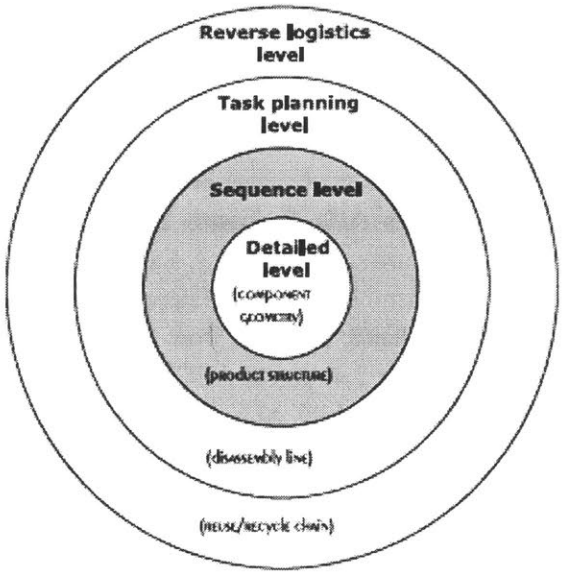


*Figure 2.1 Different levels of abstractions of disassembly in disassembly literature [70]*

Line balancing & disassembly sequencing

The research for disassembly task planning is related to and builds upon the research done in assembly task planning in the field of operation research. Lambert highlights differences to consider in [70], with the major differences being that disassembly is a "divergent" flow process ( a single product broken down into several assemblies and parts), and that there is a greater uncertainty in the product quality and manual disassembly task times. The assembly/disassembly line consists of several workstations connected in series by a material handling system, where each workstation successively adds or removes parts to or from an assembly. Assembly line balancing is an aspect of assembly planning which is well-researched in academic literature. Introduced in 1955 by Salveson [71], it gained importance because of the investment costs of automated assembly lines in production systems. Line balancing involves efficiently deciding on the system capacity (cycle time, number of workstations, and equipment) and assigning assembly (or disassembly) tasks to the workstations, given a set of production (assembly or disassembly times and directions, demand

levels, hazardous material handling) and product design (geometrically based precedence relationships between parts) constraints [72]. In [72], Boysen et al. does a thorough literature review of the different optimization problems on assembly line balancing.

Line balancing was first introduced for disassembly by Gungor and Gupta [73]–[75] to solve for the number of workstations needed to disassemble a sample product completely using an algorithmic approach. Since then, disassembly line balancing literature has expanded to include partial disassembly, hazardous materials and uncertainties associated with task constraints (e.g. disassembly times, product conditions), with various mathematical programming formulations. These works are described in Riggs et al. [76] and Bentaha et al. [68].

The disassembly sequencing problem is to find the best sequence of disassembly tasks from all possible disassembly sequences for a given product [70]. Disassembly sequencing requires a certain representation of the successive stages of the disassembly process, which respects the connections and precedence relations among the product parts. This can be derived from the CAD file or from expert knowledge, i.e. a set of questions with yes/no answers, set to an expert.

The representation itself can be of two forms: (i) state representation; (ii) AND/OR graph representation. The state representation defines either the connective states present or the assembly states present. For example, for the product consisting of parts A-D in Figure 2.2, the disassembly graphs based on connectivity states and assembly states are shown in Figure 2.3. Each node represents a complete state of the product which is either partially disassembled or completely disassembled towards the end. The AND/OR graph representation on the other hand, branches from a parent state to one of more pairs of feasible children states. For example, in Figure 2.4, parent ABC links to child A AND child BC, OR to child B AND child AC, OR to child C AND child AC, all feasible subassemblies. AND/OR graph representation is widely used as it has been extensively used in robotic science since 1983 [70].

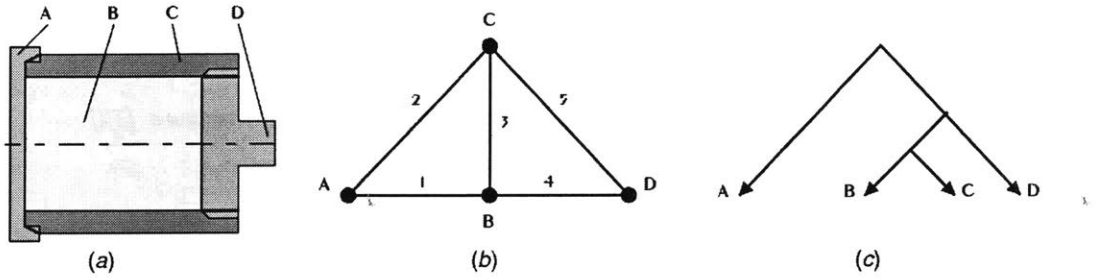


*Figure 2.2 Connection diagram (b) and disassembly tree (c) for example assembly drawing in (a) [70]*

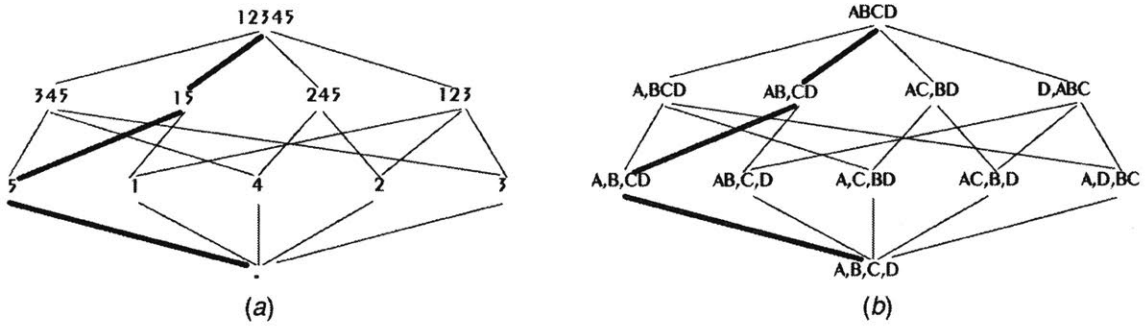


*Figure 2.3 Disassembly graph based on (a) connectivity states and (b) corresponding assembly states [70]*

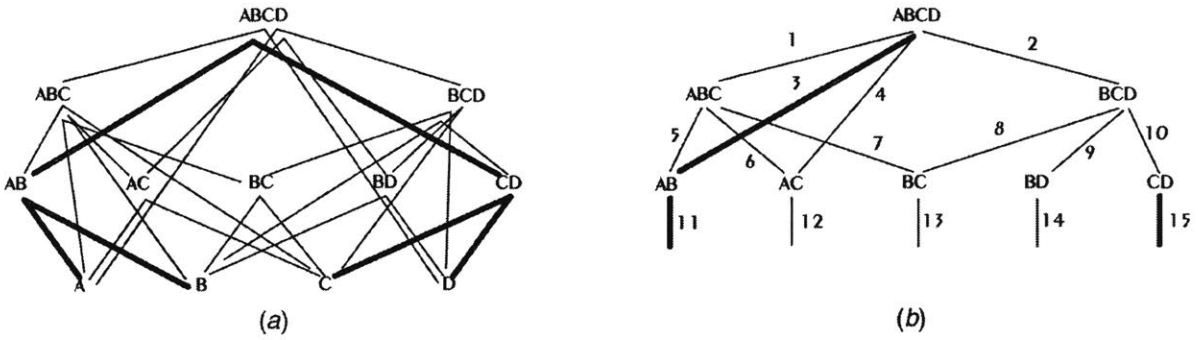


*Figure 2.4 (a) AND/OR graph , (b) reduced AND/OR graph with arc for only 1 of the 2 children of each parent shown, and numbers indicating disassembly actions [70]*

While disassembly graphs and AND/OR graphs provide good visual representation of the disassembly problem, they need to be translated to mathematical representations in order to be used in optimization formulations. The disassembly precedence matrix (DPM) has also been used extensively by Moore et al. [73], [77], Gupta and Gungor [74], [75] to represent AND and OR precedence relationships between parts of an assembly. Transition matrix has also been used to represent AND/OR graphs mathematically in [67], [69], [70], [78]–[80] . Instead of indexing by parts, the transition matrix has the rows and columns correspond to sub-assemblies and disassembly tasks respectively. Petri nets are another mathematical technique using a discrete event approach to represent disassembly with uncertainty in part conditions and resource constraints [73], [77], [81], [82].

Applications of disassembly models and optimization methods used

Various optimization methods have been applied to disassembly models [69]. The objectives are linked to the applications of the disassembly models. While all papers start with the generation of feasible disassembly sequences, their objectives could be of two types depending on whether the problem is approached from a task planning level or recovery level.

For disassembly line balancing problems of task planning, the objective is to assign the disassembly tasks to specific workstations in sequence and/or parallel so as to minimize operation costs [68], [73]–[75]. Additionally, constraints are added so that disassembly tasks do not exceed the workstations' specific cycle time. Furthermore, in [73]–[75], costs associated with idle times of workstations are included. In [76], the authors seek to minimize the maximum difference in total workstation time for a given number of workstations. In [68], a "recourse cost" is also included in the minimization objective to incorporate the effect to task time uncertainties, where the "recourse cost" is defined as the line stoppage costs caused by the task processing time uncertainties.

The other application of disassembly models is of interest to us: an economic evaluation of the disassembly process to be able to choose the best disassembly operations for recycling, remanufacturing and/or reuse, while balancing revenues for valuable parts, and the costs associated with disassembly tasks. Now there is more and more interest in the applications of disassembly sequencing to environmental performances, in the form of product design for disassembly and material recovery optimization. Early research includes [83]–[85], which looked at the disassembly of a headlamp, and that of a weight scale respectively, while later research applies disassembly models to mobile phones and hard disk drives [69], [80].

Various works have used mathematical programming formulations applied to their disassembly models, including linear programming, integer programming. In [83], Chandra formulated his disassembly problem as a traveling salesman problem, and hence required complete disassembly. In [85], Johnson and Wang defined their problem as a mixed integer programming problem, solved with the branch and bound algorithm in a linear programming software. They reduced the search space by clustering by material compatibility, disposal affinity and disassembly operations affinity. In [69], Cong et al. used a simple linear programming model, while in [80], Behdad et al. also used mixed integer programming formulation, but applied it to optimize shared disassembly operations for different product types.

More recently, artificial intelligence approaches have been used to find feasible disassembly sequences. While not all such sequences are covered, these approaches are computationally more tractable.

In [86], Hui et al. used genetic algorithm, while in [87], Huang et al. used artificial neural network for disassembly sequence generation. In [88], Meng et al. used co-evolutionary algorithm to search for the optimal end-of-life solution. In [82], Guo et al used scatter search to look for optimum disassembly sequences from the product petri net. Scatter search is a bit different from genetic algorithm as it incorporates systematic designs and methods for creating new solutions rather than simple randomization.

Few works have looked at the disassembly of end-of-life vehicles, as they have mostly focused on small-scale products with reproducible disassembly operations. However, some pioneering work has been done by Spicer and Zamudio-Ramirez on ELV disassembly modeling, together with data-gathering about the parts. This section will examine their work more closely. In [22], [23], Spicer and Zamudio-Ramirez worked on a disassembly model which analyzes and optimizes the profit-optimizing disassembly plan of cars. Their model takes physical information about the car parts as well as economic information about the disassembly costs (labor, landfilling) weighed against possible values through resale or recycling. The disassembly plan decides whether a part is removed or not. The list is then checked for feasibility with respect to precedence constraints, i.e. whether a part can only be removed after another. The possible fates of the parts modeled include four material recovery options: reuse, remanufacturing, recycling and disposal. The disassembly model is solved with an integer programming formulation, where the objective was to minimize the cost of the disassembly plan depending on which parts are removed or not.

## 2.2 Disassembly optimization: linear programming model formulation

We will now propose our own integer programming (IP) formulation to tackle the disassembly optimization problem. We decouple the problem by using two sets of decision variables: (i) one set determines if a particular part is removed; (ii) the other set determines if a particular disassembly job is chosen. We define a disassembly job as a feasible combination of parts to be removed. A combination is feasible if the parts removed satisfy their precedence constraints. In the formulation, we assume that the set of feasible disassembly jobs is known. The feasible jobs can be obtained either through expert knowledge or through search algorithms over the list of part precedence constraints for a given product.

Assume for an assembly (vehicle), we can identify parts, indexed by $j= 1,2...J$; we assume that all parts are by default candidates for removal or disassembly. For each part, we identify the value of the part when

removed (i.e. the resale or direct recycling value), calling it $v_j$; we assume we can somehow determine the value of the part if it is not removed (i.e. the shredders' recycling value), calling it $u_j$. These values can be positive or negative, where a negative value is a cost.

We are not concerned with details such as the optimal sequence of disassembly. Our only concern is whether a set of parts to be removed is feasible. As such, we define jobs instead of paths, where a job is a combination of parts that can be removed.

Disassembly job formulation

We assume that we can identify a set of possible complete and feasible disassembly jobs, $k = 1,2...K$, where $K$ denotes the number of possible jobs, and where each job removes either one part, or some set of parts. We denote the total disassembly cost for job $k$ by $c_k$. One possibility for computing this cost is cumulating the costs to remove the joints associated with the removal of each part of the job $k$. We specify each feasible job $k$ by a set of parts: $\left(i_1, i_2 ... i_k\right)$. We capture this information in a job-listing matrix: $\{a_{jk}\}$ where $a_{jk} = 0,1$ to denote whether or not part $j$ is removed through job $k$. We note that again, we observe that this does not convey the sequence in which parts are to be removed. We leave the complexity of generating feasible jobs and the associated costs outside of the optimization problem, by taking these as given from a pre-processing procedure.

The following guidelines are used to define possible distinct jobs:

- There can be more than one way to remove a set of parts, with different total cost of removal. For instance, we might have two jobs: $k_1 = \{P, Q\}$ and $k_2 = \{R, S\}$; the two jobs together remove the parts $A, B, C, D$. We might also have a third job $k_3 = \{P, Q, R, S\}$ that removes the same set of parts, but has a lower cost that the sum of the costs of job $k_1$and job $k_2$. This can happen if the removal is done in different ways, i.e. with removal of different geometric constraints, e.g. by extracting along different spatial axes.
- A job can be a subset of another bigger job, and is considered a different complete job with its own smaller cost. Such a job can contain the first few parts ($k_4 = \{A, B\}$) of the bigger job ($k_1 = \{A, B, C\}$), in the Figure 2.5 below.
- A job is considered complete if either:
    - (i) The job by itself is feasible, i.e. all related precedence constraints are met. The job includes an outer part, with no predecessors and the predecessors for every other part in the job are within the job; e.g. $\{A, B, C\}$ is a complete job.
    - (ii) The feasibility of the job depends on the selection of other complete jobs. This dependence can be captured in an "arc-node incidence" matrix, where the nodes correspond to the jobs, and the arcs correspond to precedence relationships between jobs. In the example below, job $k_5$ or job $k_6$ is feasible if we choose job $k_2$, which is itself feasible only if we choose job $k_1$. Hence, $k_1$ precedes $k_2$ and $k_3$, and $k_2$ precedes $k_5$ and $k_6$.

We define the job precedence square matrix as $\{s_{kl}\}$ where $s_{k_2k_1} = 1$ if $k_1$ preceding $k_2$, else $s_{k_2k_1} = 0$. Let set $\zeta$ denote the arc set, i.e. the set of existing precedence relationships among jobs.

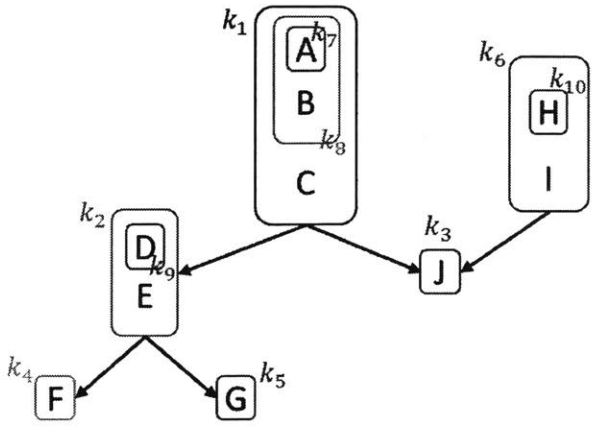


*Figure 2.5 Example of a product with 10 parts (A, B, C, D, E, F, G, H, I, J), 10 possible disassembly jobs ($k_1$ to $k_{10}$), and the arrows representing the job precedence relationships*

We can now represent our disassembly process as an optimization problem, with the following decision variables:

$x_j = 0,1$ denotes whether or not part $j$ is disassembled.

$y_k = 0,1$ denotes whether or not job $k$ is chosen.

The objective is to maximize the total values of removing each part or not, net of the costs. Thus, we define the objective function as follows:

$$Max \sum_{j=1}^{J} (v_j x_j + u_j (1 - x_j)) - \sum_{k=1}^{K} c_k y_k$$

The sets of constraints are as follows:

$$x_j = \sum_{k=1}^{K} a_{jk} y_k, \forall j$$

$$a_{jk} y_k \le x_j, \forall j, k$$

$$y_k \le \sum_{l=1}^{K} s_{kl} y_l, \forall k$$

$$x_j = 0,1, \forall j$$

$$y_k = 0,1, \forall k$$

The three sets of constraints achieve the following:

- The first set of constraints says that if we remove part $j$, then we can choose *only one* disassembly job which contains it. This constraint set is quite reasonable as we would not want to choose jobs that overlap in the parts that are removed. But in order to get the best solution with this constraint we need to formulate the problem with a complete set of all possible jobs.
- The second set forces us to remove part $j$, if we choose a job $k$ that includes part $j$. Note that for the second set of constraints, we only need to include the constraint if $a_{jk} = 1$.
- The third set of constraints represents the precedence relationships among the jobs: for example, if job $k_3$ is preceded by either job $k_1$ or job $k_6$, the constraint is represented as $y_{k_3} \leq y_{k_1} + y_{k_6}$. Thus, if we choose job $k_3$, then we need to choose job $k_1$ or job $k_6$ or possibly both. The precedence relationships are contained in the matrix $S$ where element $s_{kl} = 1$, when job $k$ is preceded by job $l$, and $s_{kl} = 0$ when otherwise.
- We note that as formulated we are modeling OR precedence relationships, such as illustrated in the prior bullet. If we have AND precedence relationships, then we need a forcing constraint for each such relationship. For instance, if job $k_3$ is preceded by both job $k_1$ and job $k_6$, then we need two constraints: $y_{k_3} \leq y_{k_1}$ and $y_{k_3} \leq y_{k_6}$.

This optimization problem is a large IP problem, with order $J^2$ constraints and variables. But the structure lends itself to being relatively solvable, at least in terms of finding very good solutions quickly. There are at least two big challenges. One is to enumerate the feasible candidate disassembly jobs that contain removable valuable parts. However, this has been studied extensively in the literature (e.g. search algorithms). The second challenge is estimating the values for removal ($v_j$) or non removal ($u_j$). The value of removal, $v_j$, should not be difficult to obtain: it is the reuse value or direct recycling value of the part. The value of non-removal is less straightforward, because in practice only the ELV hulk left after disassembly has a value, i.e. the price paid by shredder facilities for the ELV hulk per weight. However, the hulk consists of all the parts that have not been removed. As an approximation, we might estimate the non-removal value of a particular part with respect to its weight.

One of the goals of this thesis is to be able to capture the effect of contaminants in the output scraps after processing further downstream of the disassembly process. However, the decisions made at the disassembly stage can certainly determine if there would be contamination. For instance, consider a part that contains material that can be potential source of contamination: e.g. ferrous fasteners in an aluminum part. If this part remains in the hulk, then it can end up in the aluminum scrap stream and cause contamination. Until now we have been thinking of the value of the parts in economic terms; with the disassembly model we can also think of a part value in terms of its effect on material recovery performance. In such case, we need some way to estimate the impact from contamination of leaving such a part in the hulk. A possible solution is to use our model of shredder and separation to estimate $u_j$: we could do this by determining the difference in value from shredding the vehicle with or without part $j$.

Toy example

To illustrate our IP formulation, we apply the above optimization formulation to the 10-part example of Figure 2.5, with the jobs $k_1$ to $k_{10}$ as described in the figure. This gives the following job listing matrix ($a_{jk}$) and precedence matrix ($s_{kl}$):

$$a_{jk} = \begin{bmatrix} 1 & 0 & 0 & 0 & 0 & 0 & 1 & 1 & 0 & 0 \\ 1 & 0 & 0 & 0 & 0 & 0 & 0 & 1 & 0 & 0 \\ 1 & 0 & 0 & 0 & 0 & 0 & 0 & 0 & 0 & 0 \\ 0 & 0 & 1 & 0 & 0 & 0 & 0 & 0 & 0 & 0 \\ 0 & 1 & 0 & 0 & 0 & 0 & 0 & 0 & 1 & 0 \\ 0 & 1 & 0 & 0 & 0 & 0 & 0 & 0 & 0 & 0 \\ 0 & 0 & 0 & 1 & 0 & 0 & 0 & 0 & 0 & 0 \\ 0 & 0 & 0 & 0 & 1 & 0 & 0 & 0 & 0 & 0 \\ 0 & 0 & 0 & 0 & 0 & 1 & 0 & 0 & 0 & 1 \\ 0 & 0 & 0 & 0 & 0 & 1 & 0 & 0 & 0 & 0 \end{bmatrix} \begin{matrix} j = 1\,(A) \\ j = 2(B) \\ j = 3(C) \\ j = 4(J) \\ j = 5(D) \\ j = 6(E) \\ j = 7(F) \\ j = 8(G) \\ j = 9(H) \\ j = 10(I) \end{matrix}$$

$$k = \begin{matrix} 1 & 2 & 3 & 4 & 5 & 6 & 7 & 8 & 9 & 10 \end{matrix}$$

$$s_{kl} = \begin{bmatrix} 0 & 0 & 0 & 0 & 0 & 0 & 0 & 0 & 0 & 0 \\ 1 & 0 & 0 & 0 & 0 & 0 & 0 & 0 & 0 & 0 \\ 1 & 0 & 0 & 0 & 0 & 1 & 0 & 0 & 0 & 0 \\ 0 & 1 & 0 & 0 & 0 & 0 & 0 & 0 & 0 & 0 \\ 0 & 1 & 0 & 0 & 0 & 0 & 0 & 0 & 0 & 0 \\ 0 & 0 & 0 & 0 & 0 & 0 & 0 & 0 & 0 & 0 \\ 0 & 0 & 0 & 0 & 0 & 0 & 0 & 0 & 0 & 0 \\ 0 & 0 & 0 & 0 & 0 & 0 & 0 & 0 & 0 & 0 \\ 0 & 0 & 0 & 0 & 0 & 0 & 0 & 0 & 0 & 0 \\ 0 & 0 & 0 & 0 & 0 & 0 & 0 & 0 & 0 & 0 \end{bmatrix}$$

We use the following cost vectors for the disassembly job costs ($c_k$), and for the parts' removal value ($v_j$)and non-removal value ($u_j$):

$$c_k = 0.1 * [4 \quad 5 \quad 9 \quad 5 \quad 7 \quad 3 \quad 2 \quad 3 \quad 3 \quad 1]; \quad v_j = \begin{bmatrix} 1 \\ 2 \\ 3 \\ 4 \\ 3 \\ 6 \\ 9 \\ 9 \\ 2 \\ 3 \end{bmatrix}; \quad u_j = \begin{bmatrix} 1 \\ 1 \\ 1 \\ 1 \\ 1 \\ 1 \\ 1 \\ 1 \\ 1 \\ 1 \end{bmatrix}$$

As expected with such a negligible cost, this leads to all parts being removed, through the following solution:

Maximum objective: $42 + 0 - 3.3 = 38.7$

$x_j = [1 \quad 1 \quad 1 \quad 1 \quad 1 \quad 1 \quad 1 \quad 1 \quad 1 \quad 1]'$

$y_k = [1 \quad 1 \quad 1 \quad 1 \quad 1 \quad 1 \quad 0 \quad 0 \quad 0 \quad 0]$

### 2.2.1 Model with assemblies and their subassembly components

In the prior model, we only consider and value the removal of individual parts. In a complex product, the parts can have a hierarchical structure, where a small part can be part of a bigger component or assembly.

For instance, a wheel is an assembly consists of the following subassembly components: the rim, cover and rubber tire. On the other hand, we also have parts which can be stand-alone: e.g. the rear view mirror is a part in itself, and does not have any sub-components that could be removed for resale separately. To accommodate for a product's complex hierarchy, we can modify the above disassembly model to distinguish between assemblies, their subassembly components and standalone parts. We add new variables to help us decide for each assembly whether we should remove it altogether or not; or whether we should remove one or more of its subassembly components as separate parts. Note that an assembly can have costs or values different from the sum of those of its subassembly parts. Hence, while this will increase the dimensions of the problem, introducing subassembly components and assemblies can account for this difference in costs/values.

To formulate this problem we now combine the set of parts and assemblies, indexed as $j = 1,2...J, J+1,...J+S$ where $j = 1,2...J$ denotes the parts (as above), and $j = J+1,...J+S$ denotes the assemblies that can be removed as a whole. Additionally, we specify possible disassembly jobs $k = 1,2...K_j$ for each assembly $j = J+1,...J+S$. Again, for each such job we assume we have a cost $c_k$ and matrix $a$ with element $a_{jk}$ denoting whether part or assembly $j$ is removed on job $k$.
In addition, for each assembly $j = J+1,...J+S$, we define the index set $E_j = \{i\}$ such that $i \in E_j$ if and only if part $i$ is part of assembly $j$. And we define $E = \bigcup_{j=J+1}^{J+S} E_j$ to be the index set of parts that are part of an assembly. We now extend the IP formulation to reflect these new choices relating to using an assembly-part hierarchy within the optimization. The new formulation is modified to the following:

$$Max \sum_{j=1}^{J+S} v_j x_j + \sum_{j=1}^{J} u_j z_j - \sum_{k=1}^{K} c_k y_k$$

The sets of constraints are now:

$$x_j = \sum_{k=1}^{K} a_{jk} y_k, \forall j = 1,2...J+S$$

$$a_{jk} y_k - x_j \le 0, \forall j = 1,2...J+S; k = 1,2...K$$

$$y_k \le \sum_{l=1}^{K} s_{kl} y_l, \forall k = 1,2...K$$

$$x_i + z_i = 1, \forall i = 1,2...J, i \notin E$$

$$x_i + z_i + x_j = 1, \forall j = J+1,...J+S, \forall i \in E_j$$

$$x_j = 0,1, \forall j = 1,2...J+S$$

$$y_k = 0,1, \forall k = 1,2...K$$

$$z_j = 0,1, \forall j = 1,2...J$$

In this new formulation, the first three sets of constraints are the same as for the earlier formulation, but now extended to include the assemblies. Moreover, we need to introduce a new decision variable: $z_i$ to denote that a part (a standalone part or a sub-assembly part) is not removed. Thus, we have added 2 new

sets of constraints: (i) $x_i + z_i = 1$; (ii) $x_i + z_i + x_j = 1$. The first constraint set says that a part is either removed or not removed; this set of constraint applied to the standalone parts. The second constraint set says that: a subassembly part is either removed individually ($x_i = 1$), or within the assembly to which it belongs ($x_j = 1$), or the part is not removed in either way ($z_i = 1$). The decision variable: $z_i$ is used as an indicator (0 or 1 by default) making sure that a subassembly part's non-removal value ($u_j$) is not double-counted when it is not removed in either way. Hence, $u_j z_j$ is used to define the non-removal values of part/subassembly $j$ in the objective function.

Note that in the above formulation, we assume that the product hierarchy has at most two levels, i.e. an assembly is not itself part of a larger assembly. If this were not the case, the formulation will need additional indicator variables similar to $z_i$.

Toy Example

Building on the example used in the previous section, we now define parts $\{E, F, G\}$ as a assembly called $\pi$, which is indexed as $j = 11$. This also gives rise to an additional feasible job, $k = 11$, which contains the removal of part $D$ and assembly $\pi$.

We now modify the matrices (job listing matrix $a_{jk}$ and precedence matrix $s_{kl}$) and vectors (the disassembly job costs $c_k$, parts' removal value $v_j$ and non-removal value $u_j$ as follows, with the modification marked in red:

$$a_{jk} = \begin{bmatrix} 1 & 0 & 0 & 0 & 0 & 0 & 1 & 1 & 0 & 0 & 0 \\ 1 & 0 & 0 & 0 & 0 & 0 & 0 & 1 & 0 & 0 & 0 \\ 1 & 0 & 0 & 0 & 0 & 0 & 0 & 0 & 0 & 0 & 0 \\ 0 & 0 & 1 & 0 & 0 & 0 & 0 & 0 & 0 & 0 & 0 \\ 0 & 1 & 0 & 0 & 0 & 0 & 0 & 0 & 1 & 0 & 1 \\ 0 & 1 & 0 & 0 & 0 & 0 & 0 & 0 & 0 & 0 & 0 \\ 0 & 0 & 0 & 1 & 0 & 0 & 0 & 0 & 0 & 0 & 0 \\ 0 & 0 & 0 & 0 & 1 & 0 & 0 & 0 & 0 & 0 & 0 \\ 0 & 0 & 0 & 0 & 0 & 1 & 0 & 0 & 0 & 1 & 0 \\ 0 & 0 & 0 & 0 & 0 & 1 & 0 & 0 & 0 & 0 & 0 \\ 0 & 0 & 0 & 0 & 0 & 0 & 0 & 0 & 0 & 0 & 1 \end{bmatrix} \begin{matrix} j = 1\,(A) \\ j = 2(B) \\ j = 3(C) \\ j = 4(J) \\ j = 5(D) \\ j = 6(E) \\ j = 7(F) \\ j = 8(G) \\ j = 9(H) \\ j = 10(I) \\ j = 11(\pi) \end{matrix}$$

$$s_{kl} = \begin{matrix} k = 1 & 2 & 3 & 4 & 5 & 6 & 7 & 8 & 9 & 10 & 11 \end{matrix}$$

$$\begin{bmatrix} 0 & 0 & 0 & 0 & 0 & 0 & 0 & 0 & 0 & 0 & 0 \\ 1 & 0 & 0 & 0 & 0 & 0 & 0 & 0 & 0 & 0 & 0 \\ 1 & 0 & 0 & 0 & 0 & 1 & 0 & 0 & 0 & 0 & 0 \\ 0 & 1 & 0 & 0 & 0 & 0 & 0 & 0 & 0 & 0 & 0 \\ 0 & 1 & 0 & 0 & 0 & 0 & 0 & 0 & 0 & 0 & 0 \\ 0 & 0 & 0 & 0 & 0 & 0 & 0 & 0 & 0 & 0 & 0 \\ 0 & 0 & 0 & 0 & 0 & 0 & 0 & 0 & 0 & 0 & 0 \\ 0 & 0 & 0 & 0 & 0 & 0 & 0 & 0 & 0 & 0 & 0 \\ 0 & 0 & 0 & 0 & 0 & 0 & 0 & 0 & 0 & 0 & 0 \\ 0 & 0 & 0 & 0 & 0 & 0 & 0 & 0 & 0 & 0 & 0 \\ 1 & 0 & 0 & 0 & 0 & 0 & 0 & 0 & 0 & 0 & 0 \end{bmatrix} \begin{matrix} k = 1 \\ k = 2 \\ k = 3 \\ k = 4 \\ k = 5 \\ k = 6 \\ k = 7 \\ k = 8 \\ k = 9 \\ k = 10 \\ k = 11 \end{matrix}$$

$$c_k = 0.1 * [4 \quad 5 \quad 9 \quad 5 \quad 7 \quad 3 \quad 2 \quad 3 \quad 3 \quad 3 \quad 3]; v_j = \begin{bmatrix} 1 \\ 2 \\ 3 \\ 4 \\ 3 \\ 6 \\ 9 \\ 9 \\ 2 \\ 3 \\ 30 \end{bmatrix}; u_j = \begin{bmatrix} 1 \\ 1 \\ 1 \\ 1 \\ 1 \\ 1 \\ 1 \\ 1 \\ 1 \\ 1 \\ 3 \end{bmatrix} \begin{matrix} j = 1\,(A) \\ j = 2(B) \\ j = 3(C) \\ j = 4(J) \\ j = 5(D) \\ j = 6(E) \\ j = 7(F) \\ j = 8(G) \\ j = 9(H) \\ j = 10(I) \\ j = 11(\pi) \end{matrix}$$

With assembly $\pi$ having resale value $v_{11} = 30$ (6 more than the sum of the resale values of the individual parts) this leads to assembly $\pi$ being removed, i.e. none of parts $E$, $F$ or $G$ are removed individually, with revenue of 48 and cost of 1.9.

$$x_j = [1 \quad 1 \quad 1 \quad 1 \quad 1 \quad 0 \quad 0 \quad 0 \quad 1 \quad 1 \quad 1]'$$
$$y_k = [1 \quad 0 \quad 1 \quad 0 \quad 0 \quad 1 \quad 0 \quad 0 \quad 0 \quad 0 \quad 1]$$

If we modify the assembly resale value to $v_{11} = 20$ (4 less than the sum of the resale values of the individual parts) the solution changes, to the removal of $E$, $F$ and $G$, but not of assembly $\pi$ as a whole. The revenue is 42 and cost is 3.3.

$$x_j = [1 \quad 1 \quad 1 \quad 1 \quad 1 \quad 1 \quad 1 \quad 1 \quad 1 \quad 1 \quad 0]'$$
$$y_k = [1 \quad 1 \quad 1 \quad 1 \quad 1 \quad 1 \quad 0 \quad 0 \quad 0 \quad 0 \quad 0]$$

In this chapter, we have determined the integer programming (IP) formulation to use to tackle the disassembly optimization problem for a complex product such as an ELV, having stand-alone parts as well as assemblies and sub-assembly parts. In Section 7.3, we will apply this IP formulation to a case study of a complete ELV.

# Chapter 3 Recovery modeling in literature

Different papers in literature have different ways of modeling the recovery of materials from end-of-life vehicles (ELVs) at ELV treatment facilities. While several different models exist for the separation phase, the literature for the shredding phase is not as in-depth. The models differ in terms of the description of the input material and the characterization of the material flow throughout the shredding and separation steps. These models can account for three physical processes that occur during shredding or separation: comminution, liberation and separation/mixing. Comminution and liberation both occur during shredding of materially-complex products such as ELVs, while separation and possibly mixing occur during sequences of separation processes. Due to the nature of these processes, we need to characterize the material flow at least by material type, size, and the state of liberation. Other characterization bases can include shape and product design details such as joint specification. This review will largely draw from the works of Schaik and colleagues [89]–[91], and Coates and Rahimifard [16] which are among the most comprehensive ones on modeling of recycling of vehicles.
In the next sections, we will review and present models of shredding and separation from literature, as they might apply to end-of-life recycling.

## 3.1 Shredding modeling

The shredding process of materially-complex products involves comminution as well as liberation. Comminution of ELVs occurs because the giant hammers of the shredder crush and fragment the input feed, and the shredded output then leave through grates. Unlike end-of-life treatment for municipal solid waste, the shredder is an important step, as it reduces size for easier further processing but also helps in liberation of joint materials [30].

Liberation is a term typically used in the mineral processing research community to denote a grade change: a particle is defined as liberated if it consists of a single compound [92, p. 5], i.e. liberation is the process during which "the mineral composition distribution in particles changes due to breakage" [93]. However, Castro et al. point to differences for liberation of EOL products, due to "large dimensions and a coarse mineralogical structure...different materials non-isotropically dispersed along any section..."[90]. For our purpose, we will use liberation as the "reduction of the amount of material physically joined to other materials" [30].

Mineral processing models

The central ideas for modeling shredding come from the breakage modeling used in the field of mineral processing. Note that this field refers to the *input* feed of a comminution process as *parent* particles, and the *output* stream as *progeny* particles. The breakage process of minerals results from fracture of brittle mineral ore particles, and it can be modeled through breakage functions. Selection functions are sometimes used to account for the parent particles that do not undergo breakage.

Nevertheless, mineral processing models are not directly applicable for modeling the shredding of ELVs; materials found in ELVs are a non-homogeneous mixture of many materials, which are mostly metals that are ductile and undergo plastic deformation. In addition to ductility, other properties which distinguish ELVs from natural mineral ores are large particle size, variation in size, variation in size and complex material composition [90]. These properties make the breakage phenomenon of ELVs particles even more complex than in mineral processing. We will now briefly look at some mineral processing models before examining the few comminution models used on ELV hulk in literature.

Breakage Functions, Selection Functions and Breakage Theory

Breakage Functions have been developed in the mineral fields for the modeling of comminution of coal since a long time ago [30], [94], [95]. A breakage function predicts the resulting size distribution. For instance, there is the Broadbent and Calcott equation developed in 1956 [30], [95]:

$$Y = \frac{1-e^{-\frac{d}{d'}}}{1-e^{-1}}$$

Where $Y$ is the cumulative weight fraction smaller than size $d$, $d'$ is the feed particle size before comminution.

Selection Functions determine what fraction of the feed/parent particles will or will not undergo breakage. In [96], the selection function is set to depend on the particle's brittleness, which can be determined from physical kinetic models. Selection ($\boldsymbol{S}$) and breakage ($\boldsymbol{B}$) functions can be combined together through the Pi Breakage Theory proposed by Broadbent and Calcott [95]:

In matrix equation form [95],

$$P = BS\,F + (I - S)F$$

In linear equation form [95],

$$p_n = b_{n1}s_1f_1 + b_{n2}s_2f_2 + b_{n3}s_3f_3 + \cdots + b_{nn}s_nf_n + (1 - s_n)f_n$$

Where $F$ is the vector of feed fractions over all $n$ size classes, $P$ is the vector of product fractions, and I is an identity matrix. B is a matrix with elements $b_{nm}$ equal to the fraction of particles in class $m$ breaking into particles of class $n$, with index $m$ smaller or equal to $n$. $S$ is a diagonal matrix with diagonal elements $s_n$ equal to the fraction of particles of size class $n$ selected to be broken.

As the above linear equations do not have a unique solution set for $s$, the Pi Breakage Theory assumes that the breakage function is known and the selection function is set to a constant [95]:

$$s_1 = s_2 = \cdots = s_n = \pi \text{ such that } P = B\Pi F + (I - \Pi)F$$

Where $\Pi$ is a diagonal matrix with elements $\pi$ on the diagonal. One can estimate $\pi$ by calibration using known $P$ and $F$ vectors. Selection and breakage functions have been applied by Tam et al. to investigate the prediction of comminution of plastic waste, using ABS and PVC typically found in automotive components. Their selection function was based on the feed size class.

Colledani (2013) acknowledges the use of selection and breakage functions, determined experimentally, to model the transition from one particle class to another (with particle classes categorized by size, liberation and shape classes) during comminution of electronic waste, in particular power inductors [94]. This process is modeled by a transition matrix, which corresponds to $B$.

Population balance methods

Another model used in the minerals processing field is the Population Balance Method [94], [96]. The fundamental population balance equation represents any comminution process dynamically in time [96] through differential equations. Colledani & Tolio applied this method to simulate the evolution of the mass of materials per particle class over time. Besides selection and breakage functions for transition among particle classes, additionally they assumed a discharge function based on the comminution grate size [94]. Note that the selection, breakage and discharge functions need to be statistically determined for the type of feed and equipment they use.

Kernel functions

In [93], Gay uses kernel functions to probabilistically map the input feed $f$ of each particle class $i$ to an output product $y$ of particle class $j$. As opposed to transition matrix mapping one particle class to another, the kernel method allows numerous class particles to be expressed while being computationally efficient, once the kernel function is estimated.

Gay defines $p_{i,j,k}$ as the joint frequency distribution of progeny particles of particle type $j$ in size-class $k$ that came from parent particles of type $i$, $f_i$ as the frequency of the parent particles of type $i$, $s_k$ is the frequency (by volume) of particles in size-class $k$. $g_{j,k}$ is the frequency of the progeny particles of type $j$ in the size-class $k$, $c_{j,k,m}$ is the composition of the $m$th mineral in progeny particles of type $j$ and size-class $k$, $C_{i,m}$ is that for the parent particle. A particle type regroups particles with very similar compositions. Gay proposes the following constraint equations [93]:

$$\sum_k p_{i,j,k} = f_i s_k \text{ for each } i \text{ and } k$$

$$\sum_i p_{i,j,k} = s_k\, g_{j,k} \text{ for each } j \text{ and } k$$

$$\sum_{j,k} p_{i,j,k}\left(c_{j,k,m} - C_{i,m}\right) = 0 \text{ for each } i \text{ and } m$$

Using maximization of the probability entropy constrained by the above equations, gives the following equation of which the parameters can be numerically estimated more efficiently with Markov-Chain Monte Carlo methods using known measurement datasets of volumes of parent and progeny particles [93]:

$$p_{i,j,k} = A_i B_{j,k} exp(\lambda_{i,k,m}(c_{j,k,m} - C_{i,m}))$$

$p_{i,j,k}$ is thus the kernel which provides a parent particle type to progeny particle type mapping, and can be estimated as above. $A_i, B_{j,k}$ and $\lambda_{i,k,m}$ are the kernel parameters that are adjusted to meet the above constraint equations. In the above formulation, Gay assumes that for non-preferential breakage, each size-class can be solved separately. For preferential breakage, i.e. breakage occurs dependent on the mineral composition of the particles, the constraints need to be modified.

We note that the definition of the particle class types was left very general, and Gay suggests grouping particles by similar composition such as grouping by all liberated particles. Hence, this modeling method can be adapted for multi-material particles, with different liberation and size classes.

Coates model

In the Coates' post-fragmentation model for ELVs [97], Coates et al. accounts for the shredding process using a Monte-Carlo analysis with Lattice Hypercube Sampling to generate the particle-size distribution for each material type, which results from the shredding step. We note that Coates et al. only use size characterization as a separation parameter in the separation curve for the trommel and air-cyclone separation steps. Moreover, liberation is decoupled from size-reduction: Coates et al. assume that a particle does not change liberation class (inexistent) during comminution. In fact, the effects of non-liberation are only accounted for during subsequent separation steps: (i) the associated contaminant materials modify the separation efficiency of the main material; (ii) in the target material stream, the liberated materials are sorted with the original separation efficiency, while the non-liberated materials are sorted with the modified separation efficiency.

Schaik Model

The Schaik model operates at a mineral basis, i.e. the material flow of each mineral can each be analyzed separately. For instance, in [89] and [90], they define mineral $m$ from the 5 elements of the set $\{Al_{wrought}, Al_{cast}, Steel, Copper, rest\}$. In [98], they define 12 minerals, A to L for each element in the following set, respectively: *{Al cast, Al wrought, Cu, glass, Mg, Organic Non-Plastic, Plastics (PP), Plastics Chloride (PVC), Rest (all other materials), rubber, steel and zinc}*. The particles of mineral can be liberated or non-liberated, and will typically consists of the major element, e.g. $steel$, and in its non-liberated form, will also contain contaminating elements other than steel, e.g. copper, Al cast, Al wrought . This leads to the definition of liberation classes $l$, which categorize different levels of contamination by minor elements. The elemental composition of a specific liberation class of a mineral is defined with the composition matrix $C$, with elements $c_{m,l,k}$ , i.e. the mass fraction of element $k$ in mineral $m$ with liberation class $l$. An example of a composition matrix is shown below.

| **Mineral A** | **Al wrought** | Al cast | Fe | Cu | Rest |
|---|---|---|---|---|---|
| Lib. class 1 | 0.5 | 0.2 | 0.2 | 0.05 | 0.05 |
| Lib. class 2 | 0.65 | 0.15 | 0.15 | 0.03 | 0.02 |
| Lib. class 3 | 0.75 | 0.1 | 0.1 | 0.03 | 0.02 |
| Lib. class 4 | 0.87 | 0.05 | 0.05 | 0.02 | 0.01 |
| Lib. class 5 | 1 | 0 | 0 | 0 | 0 |

*Figure 3.1 Example of definition of the elemental composition of each liberation class in a mineral in[99]*

Additionally, the material flow is further characterized by the particle size $s$, with the size classes divided into 5 categories: $\{< 10\text{mm}, 10-20\text{mm}, 20-28\text{mm}, 28-37.5\text{mm}, 37.5-50\text{mm}, > 50\text{mm}\}$.Thus, the material flow rate for mineral $m$ is defined by $f_{m,s}$. Furthermore, a liberation matrix $\bar{\bar{L}}$ per particle size $s$ and and liberation class $l$ basis is defined and needs be estimated to characterize the shredder product flow. Each element of $\bar{\bar{L}}$ represents the fraction of the particles of size $s$ and that are of liberation class $l$. For example, the liberation matrix of flow before and after shredding is shown in the Figure 3.2 below.

The above model requires prior measurement estimates for the values of elements of the shredding transformation matrix, and a good definition of the liberation classes. It is however not clear how the range categories were selected for these classes.

| | | Total mass | | Lib. class 1 | Lib. class 2 | Lib. class 3 | Lib. class 4 | Lib. class 5 |
|---|---|---|---|---|---|---|---|---|
| *Panel A scenario 1* | | | | | | | | |
| Input | | | | | | | | |
| A in ELV | Particle size class 1 | 15.000 | $\vec{f}$ | 0.158 | 0.442 | 0.000 | 0.381 | 0.020 |
| A in ELV | Particle size class 2 | 0.000 | | 1.000 | 0.000 | 0.000 | 0.000 | 0.000 |
| A in ELV | Particle size class 3 | 0.000 | | 1.000 | 0.000 | 0.000 | 0.000 | 0.000 |
| A in ELV | Particle size class 4 | 0.000 | | 1.000 | 0.000 | 0.000 | 0.000 | 0.000 |
| A in ELV | Particle size class 5 | 0.000 | | 1.000 | 0.000 | 0.000 | 0.000 | 0.000 |
| Output | | | | | | | | |
| A in shredded | Particle size class 1 | 3.000 | | 0.632 | 0.367 | 0.000 | 0.000 | 0.000 |
| A in shredded | Particle size class 2 | 4.500 | | 0.000 | 0.999 | 0.000 | 0.000 | 0.000 |
| A in shredded | Particle size class 3 | 4.500 | | 0.000 | 0.000 | 1.001 | 0.000 | 0.000 |
| A in shredded | Particle size class 4 | 1.500 | | 0.000 | 0.000 | 0.000 | 0.999 | 0.000 |
| A in shredded | Particle size class 5 | 1.500 | $\vec{f}'$ | 0.000 | 0.000 | 0.000 | 0.000 | 0.999 |

$\bar{\bar{L}}$ $\bar{\bar{L}}'$

*Figure 3.2 Example of liberation matrix of feed and product flow of a shredder [99]*

Using these characterization basis, the prediction of the size distribution and liberation class of the comminuted particles is based on a shredder transformation matrix and mass conservation per element $k$. Neglecting the indices for mineral $m$, the equations for each mineral for the shredder model in [89] have been simplified to:

$$\vec{f}' = \bar{\bar{S}}\vec{f}$$

$$\sum_i s_{i,j} = 1 \text{ for all } j$$

Where $\bar{\bar{S}}$ is the shredder transformation matrix with element $s_{i,j}$ which maps the probability of a feed particle of size $j$ of shredding to output size $i$, $\vec{f}'$ is the shredder output vector i.e. mass flow rate for each size class $s$, $\vec{f}$ is the feed vector

While the above equation represents comminution or size reduction, inherent in the shredding process is liberation. Hence, there must be a change of liberation class, while mass of each element $k$ remains balanced after shredding.

$$\bar{\bar{L}}'\ \bar{\bar{C}}\ \vec{f}' - \bar{\bar{L}}\ \bar{\bar{C}}\ \vec{f} = 0$$

$$\sum_j l'_{i,j} = 1$$

Where $\bar{\bar{L}}'$ is the liberation matrix for flow after shredding, $\bar{\bar{L}}\iota$ is the liberation for flow before shredding, $\bar{\bar{C}}$ is the composition matrix mapping the mass fraction from a liberation class $l$-basis to a element $k$-basis. For each mineral $m$, if 5 size classes and 5 liberation classes are used for 5 material elements , this gives a set of 5 mass balance equations with 25 unknowns, i.e. the shredder output elements of the liberation matrix $\bar{\bar{L}}\iota$ in each liberation class and each size class. Additionally, there are 5 constraint equations, one for each summation of fractions over the 5 output liberation classes. The system of linear equations being underconstrained, the unknowns need to be solved through optimization.

Castro Model

In addition to ductility, other properties which distinguish ELVs from natural mineral ores are large particle size, variation in size, and complex material composition [90]. These make the breakage phenomenon even more complex. Castro et al. sought to reconcile these differences using a statistical approach, i.e. using probability distribution to predict joint survival.

The Castro model builds on the Schaik model by additionally incorporating product design information, which conditions the probability of non-liberated particles staying so during the shredding process. The model couples the comminution and liberation processes, i.e. particles can undergo liberation class change as well as size change during shredding.

Castro et al. further assume the following for their model:

- Non-liberation occurs in joint particles only;
- Input representation of the ELV:
  - The ELV is partitioned into cubes of dimension corresponding to the largest mesh size of the sieve for shredded particles;
  - Joint particles are randomly distributed throughout these partition cubes, with not more than one joint possible in a partition cube.
- Particle representation in the ELV:
  - Mineral classes: can be liberated (of the set $\{Al_{wrought}, Al_{cast}, Steel, Copper, rest\}$) or non-liberated, binary combinations as commonly found in joint particles (of the set $\{Al_w - Al_c, Al_c - Cu, Al_c - Fe, Al_c - Rest, Al_w - Cu,\ Al_w - Fe, Al_w - Rest, Cu - Fe, Cu - Rest, Fe - Rest\}$)
  - Liberation classes: the non-liberated mineral classes are further each divided into 10 liberation classes with different ratio composition
  - Size classes: divided into 5 categories: {<10, 10-20, 20-35, 35-50, >50mm}
- Characterization of joints:
  - Binary combinations, i.e. 2 materials considered only (reasonable because (i) sample analyses show so, (ii) usually only 2 conflicting materials considered during recycling)
  - Material particles of the partition cubes can be of 4 types of joint classes (see Figure 3.3):
    - *Z* class: no joints, i.e. all liberated materials, particles consists of only one material,
    - *P* class: point joints where a mechanical joining element is used to connect components at specific points (e.g. bolts and rivets), characterized in terms of quantity,
    - *L* class: line joints where 2 materials are joined along a continuous line (e.g. welding, adhesive joinings), characterized in terms of length and thickness ratio,
    - *S* class: surface joints where 2 whole surfaces of 2 materials are joined (e.g. coated materials and laminate composites), characterized in terms of area and thickness ratio.

Castro's modeling consists of 2 stages :

(a) EOL product characterization: the car hulk is modeled as of a single mineral class and using joint data, its liberation level can be calculated;

(b) Shredding process: the coupled comminution-liberation phenomena are modeled by determining the fate of the joints. Possible outcome states depend on the types of joints.

- The possible outcome states of the joint particles include (see Figure 3.4):
  - state A, unchanged, i.e. not comminuted and not liberated (joint P, L and S particles);
  - state B, comminuted and partially liberated (joint P and L particles);
  - State C, no survival, i.e. all liberated with comminution (joint P particles);
  - State D, comminuted but no liberation (joint S particles).

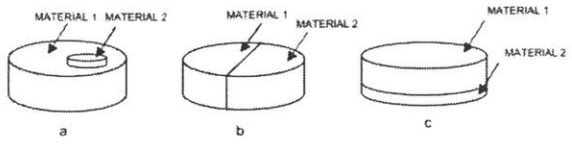


*Figure 3.3 Joint types: (a) P joint particles, (b) L joint particles, (c) S joint particles [90]*

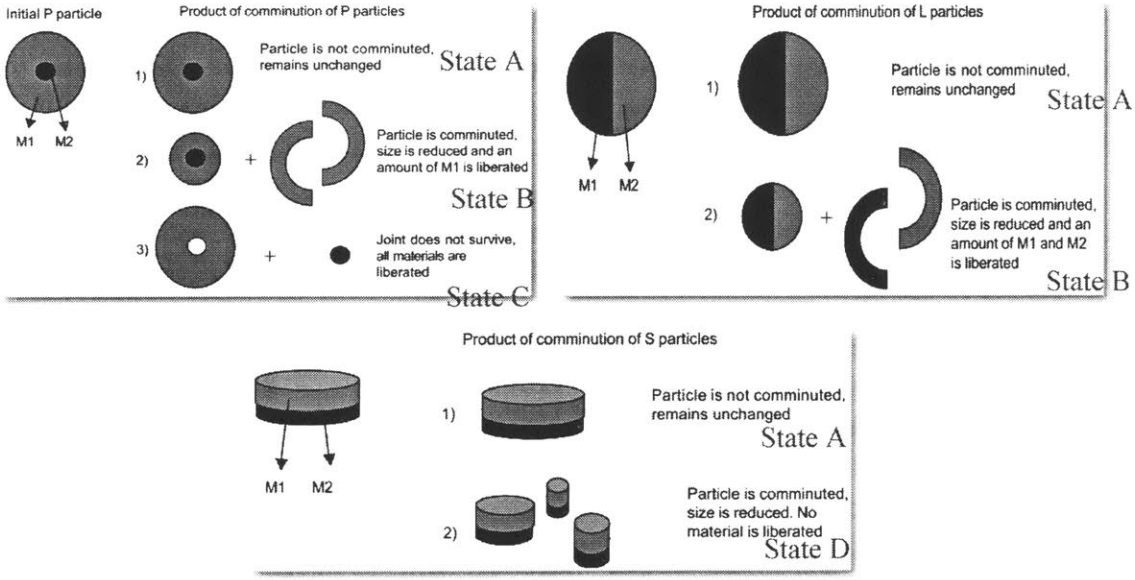


*Figure 3.4 Comminution and liberation of the joint particles [90]*

- To model the coupled comminution-liberation phenomena, Castro et al. uses a size distribution matrix and a survival matrix in the same mass balance equations:
  - The size distribution matrix gives the mass fraction of an initial material particle transitioning from one size class to another
  - The survival matrix gives the "statistical distribution describing probability of survival of a joint-containing particle in the progeny size class". [90]

While the Castro model brings novelty with the survival modeling of joints, the input representation of the ELVs and the mass balance equations seem overly complicated and unclear. Our shredder model will seek to present a more streamlined input representation which incorporates joint information with "survival" probability as well.

## 3.2 Separation system modeling

After shredding, the shredded feed goes through a series of sorting equipment, where the separation technologies sort by physical or material properties. These properties are target parameters by which the technologies equipment sort for a particular material. While configurations of separation equipment might differ from one treatment facility to another, the main separation processes involve most of the following separation processes: air separation (by density), magnetic separation (by magnetic properties), eddy-current (by conductivity properties), trommel screening (by particle size), stainless steel sorting (by induction). These equipment sort on a material-type basis, with the exception of the trommel. Please refer to Section 1.5.2 for examples of separation networks.

The following sections will look at existing separation models discussed in literature.

Network flow model

In [100], [101] and [102], a network flow model was developed, introduced and applied to the material flow in material separation systems used in recycling of municipal solid waste. A network flow model represents each unit a separation system as a node. The set of mass balance equations formed at each node can be solved to determine estimates for all material flow throughout the separation system. While Wolf uses unit-level equations for all materials, Testa and Ip use a set of system-level equations for each material, which allows formulation in matrix form.

The network flow model can be used for any network of separation units, each of which sorts a mixture of $M$ materials into $K$ output streams. For each material $m$, we define a mass flow rate of $f_i^m$ to be the input stream (e.g., ton per hour) to unit $i$. The sorting unit will separate this material input into $K$ output streams; each output stream will either go next to another separation unit or will be collected. The mass flow in the output stream $k$ is $q_{i,k}^m f_i^m$, where $q_{i,k}^m$ is the fraction of the input stream of material $m$ that is sorted into output stream $k$ by unit $i$. $q_{i,k}^m$ is called the separation parameter. Consequently we have for each sorting unit $i$ and each material $\sum_{k=1}^{K} q_{i,k}^m = 1$. Figure 3.5 shows the most common case when there are only $K$=2 output streams: if unit $i$ sorts for target material type ($m$=T), it diverts a fraction of its flow, denoted by $q_{i,j}^{\mathrm{T}}$, to target stream $j$, and diverts $q_{i,k}^{N}$ of the flow of non-target material type(s) ($m$=N) to non-target stream $k$. $q_{i,j}^{\mathrm{T}}$ and $q_{i,k}^{\mathrm{N}}$ are expected to be greater than 0.5. We note that the imperfect separations for the target and non-target materials represent two forms of errors: (i) Type I error where the non-target material is incorrectly sorted into the target stream causing a false positive; (ii) Type II error where the target material is incorrectly sorted into the non-target stream causing a false negative. Type I and type II errors respectively contribute to a lower grade and a lower recovery rate at the target collection output stream.

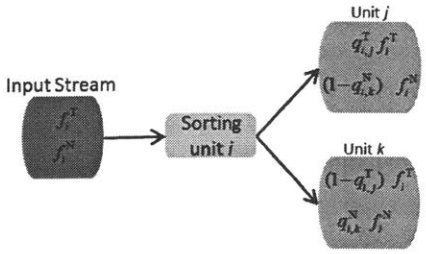


*Figure 3.5 Material flow: unit sorting an input mixture of target and non-target materials into 2 streams*

We can write the mass-balance equation for the flow of each material through each sorting and output unit $j$ as follows:

$$f_j^m = \mu_j^m + \sum_i q_{i,j}^m f_i^m \qquad \textit{Equation 3.1}$$

with $f_i^m, q_{i,j}^m$ defined previously and $\mu_j^m$ being the external input rate of material $m$ to unit $j$. We note that $q_{i,j}^m = 0$ if there is not a direct connection between unit $i$ and $j$; and we have $\mu_j^m \neq 0$ only if there is an input unit that directly feeds sorting unit $j$. For each material $m$, we can write Equation 3.1 as a system of linear equations [103]:

$$\bar{f}^m = \bar{\mu}^m + \left(Q^m\right)^T \bar{f}^m \qquad \textit{Equation 3.2}$$

$\bar{f}^m$ is the flow vector ($N$x1) for material $m$, with elements $f_i^m$. $\bar{\mu}^m$ is the input vector ($N$x1) for material $m$, with elements $\mu_i^m$, $Q^m$ is the sorting matrix ($N$x$N$) for material $m$, with elements $q_{i,j}^m$ . $N$ is the number of sorting units plus output units.

We can solve the system of linear equations (Equation 3.2) to obtain the steady-state flow rates for each material at each unit:

$$\bar{f}^m = \left(I - \left(Q^m\right)^T\right)^{-1} \bar{\mu}^m \qquad \textit{Equation 3.3}$$

Linear Circuit Analysis

Linear circuit analysis has been used extensively in the minerals engineering research community [104]–[106]. Because their goal is to concentrate dilute mining products, they use a multi-unit separation circuit to concentrate the valuable material through multiple stages of liberation and separation. However, the difference between the minerals engineering context and scrap recycling is that in the former the focus is on recovery of a single material.

A linear circuit analysis assumes, similar to our network flow model, a probability P that a particle going through a separation unit goes out to the correct output stream. The analysis then traces the concentrate grade of the target material in the flow through the units using mass balance equations. As shown in the figure below, Koermer applied the linear circuit analysis to a sequence of units producing a Zorba (Al-heavy) output stream: a "rougher" unit for initial sorting of the target from non-target particles, a "cleaner" unit to eliminate non-target particles from the resulting output stream by recycling it upstream, a "scavenger" unit to recover any target particles and recycling it upstream [40]. As illustration, if we assume

the same separation probability for all units, it is easy to calculate an analytical solution for the recovery rate of the target materials at the output stream:

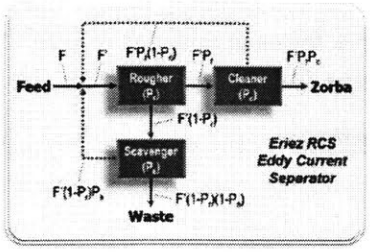


$$\textit{Metals in Zorba}: \quad \frac{C}{F} = \frac{P^2}{1-2P+2P^2} = \frac{0.9^2}{1-2(0.9)+2(0.9^2)}$$

$$\textit{Waste in Zorba}: \quad \frac{C}{F} = \frac{P^2}{1-2P+2P^2} = \frac{0.1^2}{1-2(0.1)+2(0.1^2)}$$

*Figure 3.6 (Left) Material flow for a 3-stage eddy-current separator, (right) recovery rate calculations of target and non-target materials in the Zorba output stream [40]*

In the minerals engineering context, a separation network can contain up to hundreds of separating units. Consequently, a matrix reduction algorithm, similar to that of our network flow model is used to solve for the mass flows efficiently. However, in [106] they solve for flows through each stream instead of through each unit and this results in a higher dimension if there are many recirculation streams.

Coates model

The separation technologies commonly used during ELV material recovery processes in shredder facilities have been described in Section 1.5.2. Separation technologies do not perfectly sort for their target materials: separation inefficiencies occur due to equipment error and imperfect liberation. While most case-studies in literature have only focused on giving empirical separation efficiencies based on averaged measurements, Coates et al. have developed a modelling approach which incorporates material sizing, inefficiencies of separation as well as material entanglement [97]. Material entanglement occurs when particles of different materials get crushed together and thus 'interact" with each other, remaining entangled. Their post-fragmentation modeling approach is described in the schematic in Figure 3.7.

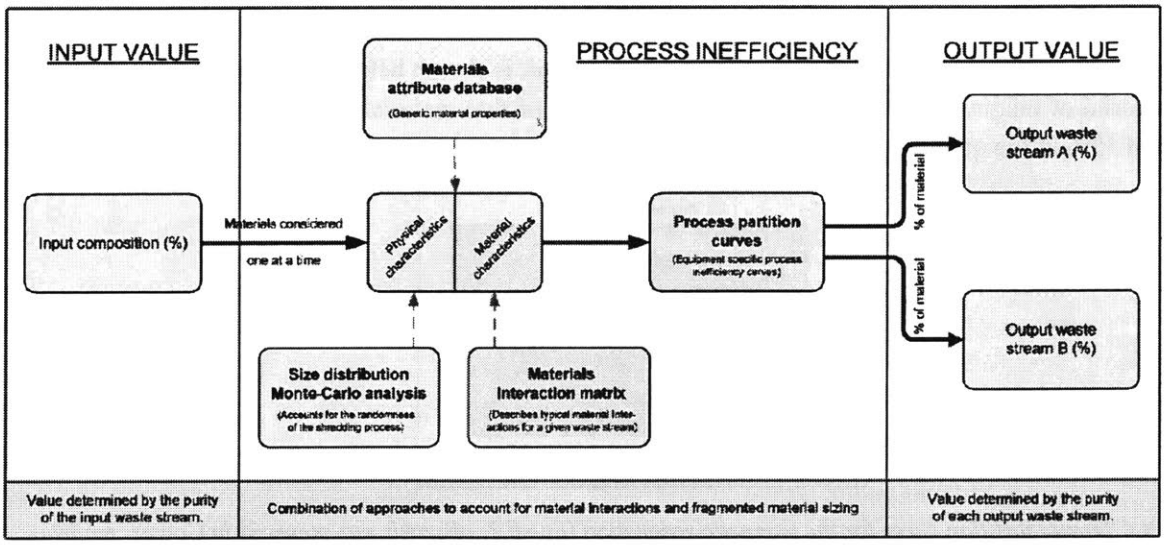


*Figure 3.7 Coates' post-fragmentation modeling approach [97]*

Coates' modelling approach has been made available in an excel and VBA file at [107]. The ELV input waste stream is turned into fist-sized fragments as it first goes into the shredder (usually a rotary hammer-mill) fragmentation. To account for the comminution process and resulting particle size variation, Coates et al. propose using random sampling of a fitted beta-curve for each material type $m$. The beta function parameters $(\alpha, \beta)$ are determined from the average, minimum and maximum particle size as follows [107]:

$$meanVal_m = \frac{minVal_m + 4 * avgVal_m + maxVal_m}{6} \quad \textit{Equation 3.4}$$

$$\alpha = \frac{6(meanVal_m - minVal_m)}{(maxVal_m - minVal_m)} \quad \textit{Equation 3.5}$$

$$\beta = \frac{6(maxVal_m - meanVal_m)}{(maxVal_m - minVal_m)} \quad \textit{Equation 3.6}$$

Using Lattice Hypercube Sampling (with 100 samples and 30 bands), particle size distributions were generated for each material present in the waste flow. Note that the size distribution only impacts the separation efficiency of the trommel and air cyclone, if these separation technologies are used downstream.

To account for the variation in the separation efficiency with the target material property, Coates et al. suggest the use of the Tromp/partition curve, which is generally well used in the minerals processing industry. This curve works with separation units having only two output streams. To determine the shape of this partition curve, 3 parameters are required [108]: the cut-point ($f_{cutPoint}$), the probable error of separation ($E_p$), and the cut-point offset ($f_{offset}$). The cut-point is described as the value of the material property at which 50% will go to one output stream; $E_p$ is the value of the material property at which 75% of the waste will go to the wrong output stream, and 25% to the correct one [97]. For a given value $f'$ of the material property of material $m$, the partition coefficient ($P_c$), equal to the probability of being sorted into the target stream, is determined by the following equation [108]:

$$P_c = \frac{1}{1 + exp\left(1.099 * \frac{f_{cutPoint} + f_{offset} - f'}{E_p}\right)} \quad \textit{Equation 3.7}$$

For instance, the partition curve for the magnetic separation unit is shown below. For instance, if a particle is of a material of magnetic susceptibility 3.5, 85% by mass of that material ends up in the target output stream, and 15% in the other stream. The separation efficiency for that target material is 0.85.

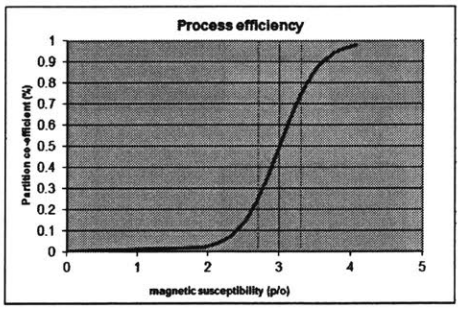


*Figure 3.8 Tromp/partition curve for the magnetic separation (Ep=0.3, offset=0, cut-point=3) in Coates' model [107]*

For the trommel and air cyclone which sort by size and mass respectively, for each feed size $s$ with a corresponding fraction $S_s^m$ of input stream of material $m$, the fraction ending in the target stream is denoted

by $P_C(m,s)$. Coates et al. thus model the material flow outputs from the separation unit as a sum over all particle sizes of material $m$ as follows [107]:

$$f_m^{target\ stream} = \frac{f_m^{input}}{100} * \sum_s S_s^m * P_C(m,s) \qquad \textit{Equation 3.8}$$

$$f_m^{non-target\ stream} = \frac{f_m^{input}}{100} * \sum_s S_s^m * (1 - P_C(m,s)) \qquad \textit{Equation 3.9}$$

The output flows for each material type $m$ of a unit are used as the input flows for connected units downstream, if any.

We note that Coates et al. argue the need to account for material entanglement, which while not relevant to the mineral processing industry, occurs in end-of-life shredding output. This could be because of incomplete liberation or post-fragmentation entanglement [97]. To account for its negative effect on efficiencies of the separation technology units, Coates et al. define an material interaction matrix, where the fractions of entangled particle of a certain material type interacting with other material types are tabulated, using measurement data to get these values. They then use the equation for the partition curve in Equation 3.7 to calculate the new separation efficiency of these non-liberated entangled particles, by calculating the average material property by mass-weighting the respective property of each of the material type found in the entangled particles.

Schaik Model

Schaik et al.'s separation model follows along the same line as their shredding model. While Coates et al define the separation efficiency of each sorting unit on a size and material/mineral basis, Schaik et al. extend this to include the liberation class [89].

# Chapter 4 Proposed recovery model and application example

In this chapter, we synthesize our findings from the literature review on material recovery modeling carried out in Chapter 3. We propose a material recovery model to characterize the material flows as they undergo comminution in the shredder, followed by separation sequences in the network of separation equipment. Compared to previous literature papers, the proposed material recovery model uses a very simple mass balance representation of particle flows at the comminution stage and each separation step, with the flows connected from one step to another by a system of linear equations. The end goal of the model is to predict the material compositions of the output streams of the separation processes. We characterize the material flow according to the mass of particles in different categories of: material type, state of liberation and size.

The next section explains how we characterize a given input material flow into these different categories. We then propose our mathematical models for the shredder and separation processes, where we represent the flow through the shredding and separation processes by a system of linear equations representing mass balance for all particle categories. Finally, we apply these two connected models on a small sample dataset of characterized input material flow, to illustrate how the material flow changes after shredding and separation, and how the output scrap composition can thus be calculated.

## 4.1 Input feed characterization

The input feed to the shredder needs to be characterized according to the material and joint types making up its particles. We will use the following nomenclature to characterize the material flow.

Nomenclature:

$L$: the set of liberated materials, $L = \{1, \dots, l\}$.

$N$: the set of non-liberated materials, $N = \{1, \dots, n\}$.

$M$: the set of all materials, $M = L \cup N = \{1, \dots, l, \dots, l+n\}$.

$S$: the set of all size classes, S= $\{1, \dots, s\}$.

$J$: the set of all joint classes, $J = \{1, \dots, j\}$.

$Z$: the set of all particle classes, $Z = \{1, \dots, (l + jn)s\}$, if we assume that each non-liberated material can be categorized into each joint type.

$Z^{input}$: the set of all particle classes in the input feed, with $Z^{input} \subset Z$

Materials

The Schaik model uses the term mineral to describe the particle type, in contrast we will use the term *material*, which can be described as either *liberated* or *non-liberated*. When characterizing the material flow, we assume that:

- a particle can consist of more than one material types when non-liberated, and of one material type when liberated.
- non-liberation occurs mainly due to physical or chemical joints [90]. We can further specify non-liberated materials in terms of the type of joint: for instance, joints of dissimilar materials (e.g. Al-steel clinching joints), or a mechanical fastener that is of different material type from the automotive part fragments attached (e.g. Steel bolts & Al).
- We neglect non-liberation that occur when particles commingle, i.e. a fragment gets intertwined or stuck into another fragment of different material type.
- The shredding process may or may not break a non-liberated particle, depending on the shredding model parameters.

For illustration here in this Section 4.1, we will use car-door recycling data in [109], where Soo et al. used doors of different car models as input feeds to a shredder-separation facility in Australia. In our example, we will use measurement data for doors of Ford Fiesta and Mazda 2 cars with manufacturing years ranging from 2007-2013.

For this input feed, there is a set of 15 material types, i.e. set *L={ Steel or ferrous (Fe), plastic/plastic composites (Pl), glass, rubber, aluminum (Al), cardboard, dirt, synthetic leather, foam, wire, stainless steel, zinc alloy, brass, fabric, copper}*. The set *N* contains the material combinations in non-liberated particles, which we assume to come from joints only. From the car-door recycling data, we can identify the material combinations in terms of pairs of parts of different materials that are joined with a fastener: set *N = { Fe part- plastic part -plastic rivet, Fe part-plastic part - adhesive, Fe part – rubber part - adhesive, Fe part - Al/wire - steel screw/bolt, Al part – plastic part - steel screw/bolt, Al part –plastic part - steel rivet, Zinc part –Fe part - Steel screw/bolt, Plastic part –Plastic part - steel screw/bolt, Fe part - foam/leather part - steel screw/bolt, Fe/Al part - Plastic part - plastic rivet, Fe/Al part - Plastic part - steel screw/bolt }*.

Joints

The joint classes include the types of joining techniques or fasteners used. In the case of Soo et al.'s car-door recycling data, the set *J* contains the following joints: set *J = {plastic rivet, adhesive, steel screw/bolt, steel rivet}*. Table 4.1 summarizes the joint data that is obtained when characterizing the input feed. The joint data classifies the joint non-liberated particles according to material combinations as well as joint type. Additionally, the joints are quantified in terms of units for point joints (e.g. rivets, screw/bolt) and in terms of length for line joints (e.g. adhesive).

| | **Plastic rivet (unit)** | **Adhesive (m)** | **Steel screw/bolt (unit)** | **Steel rivet (unit)** |
|---|---|---|---|---|
| **Fe-plastic** | 251 units | 14.2m | None | None |
| **Fe-rubber** | None | 1.4m | None | None |
| **Fe-Al/wire** | None | None | 14 units | None |

| | | | | |
|---|---|---|---|---|
| **Al-plastic** | None | None | 112 units | 35 units |
| **Zn-Fe** | None | None | 7 units | None |
| **Plastic-plastic** | None | None | 376 units | None |
| **Fe-foam/leather** | None | None | 21 units | None |
| **Fe/Al-Plastic** | None | None | 351 units | None |

*Table 4.1 Joint data for 22 recycled car-doors (Bale 3: Ford fiesta and Mazda 2), adapted from [109]*

## 4.2 Shredding model

After characterizing the input feed into a set of predefined particle classes (categorized according to liberated and non-liberated minerals, size classes and joint types), we need to compute the mass of particles falling into each particle class. To do this, we need to make some simplifying assumptions about the partitioning of input mass and the mass distribution with non-liberated joint particles:

(i) While car hulks or car parts enter the shredder as a large bulk product, we will assume that the input product can be partitioned into particles of the biggest size class, as done in [90], see Figure 4.1 below. We can set this size class to be the size of the output grate of the shredder, as the particles' size of the shredder output can only be of comparable size of smaller if they are to get out.

(ii) While it is easy to compute the mass of liberated particles material type from the bill of materials, some assumptions are needed for non-liberated particles formed from joints: (a) *each* joint forms *one* non-liberated particle of a particular non-liberated material class, e.g. an Al-steel non-liberated joint particle (formed from a fragment of an automotive part of aluminum, with a steel screw attached) contributed to the Al-steel material class; (b) we assume that the volume of the part material is proportional to that of the fastener material; (c) using the material density, we calculate the masses of the materials in the part fragment and in the fastener, and the overall mass of the joint particle; (d) using the *quantity of a joint* in the input stream, we calculate the *overall mass* of particles in the corresponding non-liberated material class.

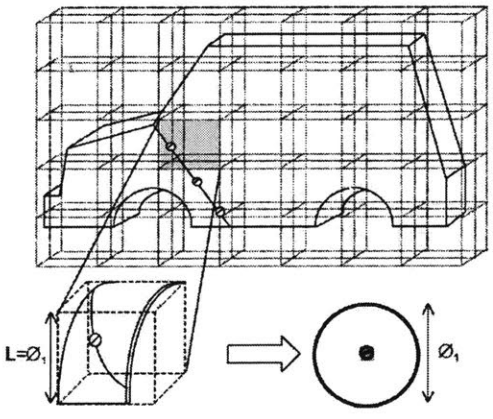


*Figure 4.1 Partitioning of the shredder input product in particles of the largest shredder output dimension [90]*

During shredding each particle can undergo comminution (size change) and/or liberation, in the case of non-liberated joint particles. The following shredding equation is used to trace what happens to particles in all classes on a mass basis:

$$p_i = \sum_j b_{ij}(1 - \pi_j)f_j + \pi_i f_i \qquad \textit{Equation 4.1}$$

Where $i \in Z$, set of all possible particle classes; $p_i$ and $f_i$, mass of particles of class $i$ after and before shredding; $b_{ij}$ is the probability of transition from particle class $j$ to $i$; $\pi_i$ is the survival probability of a non-liberated particle of class $i$, i.e. is the probability that it remains unchanged and stays in the same non-liberated particle class. If a non-liberated particle does not survive, it undergoes comminution to smaller particle size classes; the size and material class transitions are determined by the values of $b_{ij}$. A particle that is originally already liberated has by default a value of 0 for its survival probability.

In matrix form:

$$\vec{p} = \bar{\bar{B}}\left((\vec{1} - \vec{\pi}) \circ \vec{f}\right) + \vec{\pi} \circ \vec{f} \qquad \textit{Equation 4.2}$$

Where $\circ$ denotes element-wise multiplication, and $\vec{1}$ is a vector of ones.

While the vector $\vec{f}$ is obtained from the shredder input characterization and partitioning, the matrix $\bar{\bar{B}}$ and vector $\vec{\pi}$ are function of material type and joint type. The $\bar{\bar{B}}$ matrix is sparse, with non-zero entries at indexes defined by the material and joint types undergoing comminution and/or liberation, with their value determining what mass fraction of the particle classes transitions to a smaller size class and/or an non-liberated material class, if the particle class is initially non-liberated. Vector $\vec{\pi}$ only has non-zero entries at indices for non-liberated particles. Their non-zero value indicates what mass fraction of their particle classes end up surviving shredding, i.e. are neither comminuted nor liberated.

Ideally these non-zero entries are to be estimated using experimental data from characterization of a shredder. Another possible approach is to run Monte-Carlo simulations around finite-element analysis of breakage of particles of different material types and material combinations (for non-liberated joint particles) to determine a probabilistic distribution of the size of the resulting broken product, over a range of force applied. Some regression and dimensional analysis can then be run to determine the transition probabilities based on material properties.

Additionally, some heuristic rules can help determine the values of the transition and survival probabilities:

(i) Because shredding is a sequence of breaking processes, the transition probabilities of a liberated particle to smaller size classes could be viewed as the outcome from a geometric process.

(ii) For non-liberated joint particles, the survival probabilities can be qualitatively compared for different joint types, based on known comparison of joint strengths.

(iii) For non-liberated joint particles, upon liberation, the transition probabilities to the liberated material classes are a function of the mass of each material in the joint particles. As described above, transition probabilities to the individual material types should be in the ratio of their material densities in the non-liberated particle.

## 4.3 Separation model

In the separation model, we will use material class (also defined by liberated and non-liberated) and size class, as a continuation of the categorization used in the shredding modeling. This differs from Schaik et al. who introduced liberation classes, where a liberation class has a main material with several other materials found in much smaller proportions. We view this level of detail as being unreasonable for separation as it requires the additional discretization of separation efficiencies into many more dimensions. As described by Soo et al. and Castro et al., non-liberation is primarily due to joint particles not breaking down during the comminution process of shredding, and these joint particles are mainly a combination of two main elements, which we can capture within a material class of non-liberated type.

Our separation model is an expansion of the network flow model (described in Section 3.2), with the addition of size as another basis for separation. One key assumption of our separation model is that no further liberation happens during separation stages. Hence, we only need to account for mass balance across the different separation units for each pair of a material class and size class. We assume a separation network with a total of $U$ sorting and output units; then our separation model can be expressed as a linear system of equations for each material class $m$ and size class $s$:

$$\mathrm{f}^{\mathrm{m,s}} = \mu^{\mathrm{m,s}} + (\mathrm{Q}^{\mathrm{m,s}})^{\mathrm{T}}\mathrm{f}^{\mathrm{m,s}} \qquad \textit{Equation 4.3}$$

Where $f^{m,s}$ is the flow vector ($U$x1) , $\mu^{m,s}$ is the input vector ($U$x1), $Q^{m,s}$ is the sorting matrix ($U$x$U$) for material class $m$ and size class $s$. The elements of the matrix $q_{i,j}^{m,s}$ denote the fraction or probability of the output from unit $i$ that is separated to go next to unit $j$.

Note that we can include a simplifying assumption to deal with the sorting matrix. Since a sorting unit $i$ sorts by either material property or by size (trommel),we can assume that the separation probabilities are the same across the different size classes or across the different material classes.

$q_{i,j}^{m,s} = q_{i,j}^{m}$ if unit $i$ separates according to material property

$q_{i,j}^{m,s} = q_{i,j}^{s}$ if unit $i$ separates according to particle size.

Another simplifying assumption concerns the separation probabilities for non-liberated particles. For separation within units sorting by material properties, one can make use of partition curve used by Coates, and assume a weighted average of separation probabilities matching their material properties, e.g. steel and aluminum have different conductivity properties and a steel-Al particle would require a weighted separation probability when going through an eddy-current.

For material class $m$ and size class $s$, we can solve the above system of linear equations (to obtain the steady-state flow rates for each particle class at each unit, for a given input feed:

$$\mathrm{f}^{\mathrm{m,s}} = \left(\mathrm{I} - (\mathrm{Q}^{\mathrm{m,s}})^{\mathrm{T}}\right)^{-1}\mu^{\mathrm{m,s}} \qquad \textit{Equation 4.4}$$

## 4.4 Toy example for the recovery model

The dimensions of the shredding matrix scale up with the number of materials, class sizes and joint material combinations. Therefore, we consider a simple toy example to illustrate our recovery model.

Particle characterization

We start with characterizing the input stream to the shredder as:

- liberated particles of Fe (60kg) , Al (15kg), and plastic (5kg),
- non-liberated particles of Fe-Al screwbolt joints (10kg), and of Fe-plastic adhesives (10kg).

$L$: the set of liberated materials, $L = \{Fe,\ Al,\ plastic\}$.

$N$: the set of non-liberated materials, $N = \{Fe - Al, Fe - plastic\}$.

$M$: the set of all materials, $M = L \cup N = \{Fe,\ Al,\ plastic, Fe - Al, Fe - plastic\}$.

$J$: the set of all joint classes, $J = \{'screwbolt', 'adhesive'\}$.

$S$: the set of all size classes, S= $\{'big: > 100mm', 'medium: 50 - 100mm',\ 'small: < 50mm'\}$.

$Z$: the set of all particle classes,

$$Z = \{Fe_{big},\ Al_{big},\ plastic_{big}, Fe - Al_{big}^{j=screwbolt}, Fe - plastic_{big}^{j=adhesive},$$
$$Fe_{medium},\ Al_{medium},\ plastic_{medium}, Fe - Al_{medium}^{j=screwbolt}, Fe - plastic_{big_{medium}}^{j=adhesive},$$
$$Fe_{small},\ Al_{small},\ plastic_{small}, Fe - Al_{small}^{j=screwbolt}, Fe - plastic_{small}^{j=adhesive}\}.$$

We assume that the particles in the input stream are all from the largest size class, prior to repeated shredding. Typically, this is the size of the grate of the shredder, since outflow from the shredder can only be of this size or less. Hence, our input mass flow vector $\vec{f}$ has dimension length of 15, with each entry defining the mass for each particle of class $\in Z$ , in the order of the elements of the set $Z$; but only five of the entries in the input mass flow vector $\vec{f}$ are non-zero.

Shredding

For our toy example, breakage-transition matrix $\bar{\bar{B}}$, and survival vector $\vec{\pi}$ are as follows:

$$\bar{\bar{B}} = \begin{bmatrix} 0.3 & 0 & 0 & 0 & 0 & 0 & 0 & 0 & 0 & 0 & 0 & 0 & 0 & 0 & 0 \\ 0 & 0.2 & 0 & 0 & 0 & 0 & 0 & 0 & 0 & 0 & 0 & 0 & 0 & 0 & 0 \\ 0 & 0 & 0.1 & 0 & 0 & 0 & 0 & 0 & 0 & 0 & 0 & 0 & 0 & 0 & 0 \\ 0 & 0 & 0 & 0 & 0 & 0 & 0 & 0 & 0 & 0 & 0 & 0 & 0 & 0 & 0 \\ 0 & 0 & 0 & 0 & 0 & 0 & 0 & 0 & 0 & 0 & 0 & 0 & 0 & 0 & 0 \\ 0.5 & 0 & 0 & 0.3 & 0.1 & 0 & 0 & 0 & 0 & 0 & 0 & 0 & 0 & 0 & 0 \\ 0 & 0.6 & 0 & 0.3 & 0 & 0 & 0 & 0 & 0 & 0 & 0 & 0 & 0 & 0 & 0 \\ 0 & 0 & 0.1 & 0 & 0.1 & 0 & 0 & 0 & 0 & 0 & 0 & 0 & 0 & 0 & 0 \\ 0 & 0 & 0 & 0 & 0 & 0 & 0 & 0 & 0 & 0 & 0 & 0 & 0 & 0 & 0 \\ 0 & 0 & 0 & 0 & 0 & 0 & 0 & 0 & 0 & 0 & 0 & 0 & 0 & 0 & 0 \\ 0.2 & 0 & 0 & 0 & 0 & 0 & 0 & 0 & 0 & 0 & 0 & 0 & 0 & 0 & 0 \\ 0 & 0.2 & 0 & 0 & 0 & 0 & 0 & 0 & 0 & 0 & 0 & 0 & 0 & 0 & 0 \\ 0 & 0 & 0.8 & 0 & 0 & 0 & 0 & 0 & 0 & 0 & 0 & 0 & 0 & 0 & 0 \\ 0 & 0 & 0 & 0.4 & 0 & 0 & 0 & 0 & 0 & 0 & 0 & 0 & 0 & 0 & 0 \\ 0 & 0 & 0 & 0 & 0.8 & 0 & 0 & 0 & 0 & 0 & 0 & 0 & 0 & 0 & 0 \end{bmatrix}; \vec{\pi} = \begin{bmatrix} 0 \\ 0 \\ 0 \\ 0.7 \\ 0.5 \\ 0 \\ 0 \\ 0 \\ 0 \\ 0 \\ 0 \\ 0 \\ 0 \\ 0 \\ 0 \end{bmatrix}$$

Each element of the matrix, $b_{ij}$, maps the mass fraction of input particles transitioning from their initial class $j$ to class $i$ by the end of the shredding process, such that elements along each column $j$ sum to 1. Transitioning can be due to comminution and/or liberation. The transition and survival parameters for each of the input particle class are non-zero entries in the above transition matrix and survival vector. For instance:

- Column 1: $Fe_{big}$ particles (class $j$=1) comminute into smaller size particles: 0.5 of their initial mass becomes $Fe_{medium}$ (class $i$=6) and 0.2 becomes $Fe_{small}$(class $i$=11), 0.3 of the particles stays in the same class;
- Column 4: $Fe - Al_{big}^{j=screwbolt}$ particles (class $j$=4) is partially liberated: 0.3 of their initial mass becomes $Fe_{medium}$ particles (class $i$=6), 0.3 becomes , $Al_{medium}$ particles (class $i$=7), 0.4 becomes comminuted to $Fe - Al_{small}^{j=screwbolt}$particles.

With regard to the survival vector $\vec{\pi}$, the non-zero entry corresponds to the survival fraction for particle s of class $Fe - Al_{big}^{j=screwbolt}$ and $Fe - plastic_{big}^{j=adhesive}$. Hence 70% of the input screwbolt joints survives the shredding process, i.e. are neither comminuted nor liberated. Using the shredder equation $\vec{p} = \bar{\bar{B}}\left((\vec{1} - \vec{\pi}) \circ \vec{f}\right) + \vec{\pi} \circ \vec{f}$ , our input mass flow vector $\vec{f}$ gives the following shredder output mass flow vector $\vec{p}$:

$$\vec{f} = \begin{bmatrix} 60 \\ 15 \\ 5 \\ 10 \\ 10 \\ 0 \\ 0 \\ 0 \\ 0 \\ 0 \\ 0 \\ 0 \\ 0 \\ 0 \\ 0 \end{bmatrix}; \vec{p} = \begin{bmatrix} 18 \\ 3 \\ 0.5 \\ 7 \\ 5 \\ 31.4 \\ 9.9 \\ 1 \\ 0 \\ 0 \\ 12 \\ 3 \\ 4 \\ 1.2 \\ 4 \end{bmatrix}$$

For illustration, the mass distribution of the particles of the 5 material classes and 3 size classes at the shredder input and output is shown below.

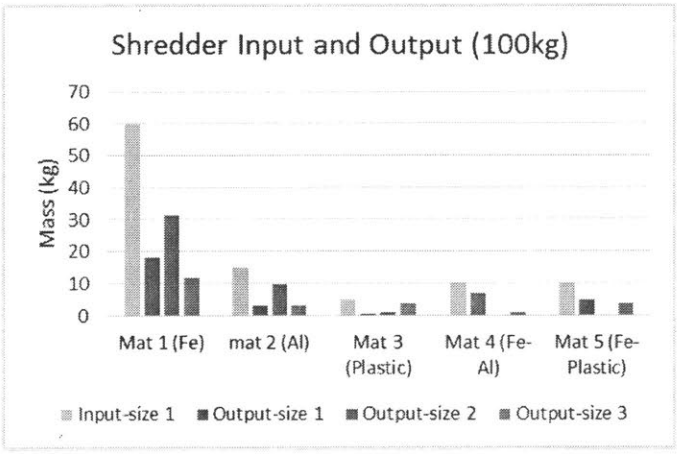


*Figure 4.2 Mass composition of shredder input and output by material and size classes, for toy example*

Separation processes

Following the shredding process, the output mass flow vector $\vec{p}$ is fed into the separation model. We assume a simple separation network targeting the ferrous and Al particles, with magnet and eddy-current separators, as well as a trommel, see Figure 4.3. This simple network of 8 units (counting both separation and output units) is a subset of that used in the case-study of Soo et al [109]. We recall that we have a set of mass balance equations for each material class and size class, for a total of 3 x 5= 15 sets of linear equations; each set of equations has mass balance at each of the units, so each set of equations is of dimension 8. That is, for each particle class of set $Z$, i.e. each material $m \in set\ M$ and for each size $s \in set\ S$, we have a separation matrix equation, with the indices corresponding to units 1-8 as shown in Figure 4.3. We have the input vector $\mu^{m,s}$ defined as $\mu^{m,s} = \begin{bmatrix} p(m,s) \\ 0 \\ 0 \\ 0 \\ 0 \\ 0 \\ 0 \\ 0 \end{bmatrix}$,

where the first entry $p(m,s)$ denotes the mass flow from the shredder output of material $m$ and size $s$, which is input at unit $i$=1 of our separation network, the magnet.

Our sorting matrix $Q^{m,s}$ represents the flow structure within the network of separating units such that $q_{i,j}^{m,s}$ is the fraction of the input stream of material $m$ and size $s$ that is sorted into unit $j$ (column) by unit $i$ (row). For Fe particles ($m = 1$) of size 'big'($s = 1$), the following sorting matrix ($Q^{m=1,s=1}$) dictates their flow among the units. For example, in the magnet (unit $i = 1$), 10% of the Fe input goes to the next trommel (unit $i = 2$), and 90% goes to the Fe output stream (unit $j = 5$); for the Fe particles that reach the eddy-current on the right (unit $i = 4$), 10% goes to non-ferrous output stream 1 (unit $j = 7$), and 90% goes to landfill (unit $j = 8$).

$$Q^{m=1,s=1} = \begin{bmatrix} 0 & 0.1 & 0 & 0 & 0.9 & 0 & 0 & 0 \\ 0 & 0 & 0.2 & 0.8 & 0 & 0 & 0 & 0 \\ 0 & 0 & 0 & 0 & 0 & 0.1 & 0 & 0.9 \\ 0 & 0 & 0 & 0 & 0 & 0 & 0.1 & 0.9 \\ 0 & 0 & 0 & 0 & 0 & 0 & 0 & 0 \\ 0 & 0 & 0 & 0 & 0 & 0 & 0 & 0 \\ 0 & 0 & 0 & 0 & 0 & 0 & 0 & 0 \\ 0 & 0 & 0 & 0 & 0 & 0 & 0 & 0 \end{bmatrix}$$

Table 4.2 below shows the sorting matrices used for all the materials ($m$=1 to 5) and sizes ($s$=1 to 3). Note that only the first 4 rows are shown, as the other rows are all zero entries. As the trommel (unit $i = 2$) is the only unit sorting according to particle size, its separation efficiency is different across the different sizes (see the red, blue and green color in Table 4.2) but the same across the different materials, i.e.

$$q_{i=2,j}^{m=1,s} = q_{i=2,j}^{m=2,s} = \ldots = q_{i=2,j}^{m=5,s}$$

On the other hand, for the other units that sort mainly by material properties, we assume that the separation efficiency is the same across the different particle sizes, i.e.:

$$q_{i,j}^{m,s=1} = q_{i,j}^{m,s=2} = q_{i,j}^{m,s=3} \; \forall \, i = \{1,3,4,5\}$$

| Material | Size s=1 (biggest) | Size s=2 | Size s=3 (smallest) |
|---|---|---|---|
| $m$=1 (Fe) | $\begin{bmatrix} 0 & 0.1 & 0 & 0 & 0.9 & 0 & 0 & 0 \\ 0 & 0 & 0.2 & 0.8 & 0 & 0 & 0 & 0 \\ 0 & 0 & 0 & 0 & 0 & 0.1 & 0 & 0.9 \\ 0 & 0 & 0 & 0 & 0 & 0 & 0.1 & 0.9 \end{bmatrix}$ | $\begin{bmatrix} 0 & 0.1 & 0 & 0 & 0.9 & 0 & 0 & 0 \\ 0 & 0 & 0.4 & 0.6 & 0 & 0 & 0 & 0 \\ 0 & 0 & 0 & 0 & 0 & 0.1 & 0 & 0.9 \\ 0 & 0 & 0 & 0 & 0 & 0 & 0.1 & 0.9 \end{bmatrix}$ | $\begin{bmatrix} 0 & 0.1 & 0 & 0 & 0.9 & 0 & 0 & 0 \\ 0 & 0 & 0.8 & 0.2 & 0 & 0 & 0 & 0 \\ 0 & 0 & 0 & 0 & 0 & 0.1 & 0 & 0.9 \\ 0 & 0 & 0 & 0 & 0 & 0 & 0.1 & 0.9 \end{bmatrix}$ |
| $m$=2 (Al) | $\begin{bmatrix} 0 & 0.9 & 0 & 0 & 0.1 & 0 & 0 & 0 \\ 0 & 0 & 0.2 & 0.8 & 0 & 0 & 0 & 0 \\ 0 & 0 & 0 & 0 & 0 & 0.9 & 0 & 0.1 \\ 0 & 0 & 0 & 0 & 0 & 0 & 0.9 & 0.1 \end{bmatrix}$ | $\begin{bmatrix} 0 & 0.9 & 0 & 0 & 0.1 & 0 & 0 & 0 \\ 0 & 0 & 0.4 & 0.6 & 0 & 0 & 0 & 0 \\ 0 & 0 & 0 & 0 & 0 & 0.9 & 0 & 0.1 \\ 0 & 0 & 0 & 0 & 0 & 0 & 0.9 & 0.1 \end{bmatrix}$ | $\begin{bmatrix} 0 & 0.9 & 0 & 0 & 0.1 & 0 & 0 & 0 \\ 0 & 0 & 0.8 & 0.2 & 0 & 0 & 0 & 0 \\ 0 & 0 & 0 & 0 & 0 & 0.9 & 0 & 0.1 \\ 0 & 0 & 0 & 0 & 0 & 0 & 0.9 & 0.1 \end{bmatrix}$ |
| $m$=3 (Plastic) | $\begin{bmatrix} 0 & 0.9 & 0 & 0 & 0.1 & 0 & 0 & 0 \\ 0 & 0 & 0.2 & 0.8 & 0 & 0 & 0 & 0 \\ 0 & 0 & 0 & 0 & 0 & 0.1 & 0 & 0.9 \\ 0 & 0 & 0 & 0 & 0 & 0 & 0.1 & 0.9 \end{bmatrix}$ | $\begin{bmatrix} 0 & 0.9 & 0 & 0 & 0.1 & 0 & 0 & 0 \\ 0 & 0 & 0.4 & 0.6 & 0 & 0 & 0 & 0 \\ 0 & 0 & 0 & 0 & 0 & 0.1 & 0 & 0.9 \\ 0 & 0 & 0 & 0 & 0 & 0 & 0.1 & 0.9 \end{bmatrix}$ | $\begin{bmatrix} 0 & 0.9 & 0 & 0 & 0.1 & 0 & 0 & 0 \\ 0 & 0 & 0.8 & 0.2 & 0 & 0 & 0 & 0 \\ 0 & 0 & 0 & 0 & 0 & 0.1 & 0 & 0.9 \\ 0 & 0 & 0 & 0 & 0 & 0 & 0.1 & 0.9 \end{bmatrix}$ |
| $m$=4 (Fe-Al) | $\begin{bmatrix} 0 & 0.7 & 0 & 0 & 0.3 & 0 & 0 & 0 \\ 0 & 0 & 0.2 & 0.8 & 0 & 0 & 0 & 0 \\ 0 & 0 & 0 & 0 & 0 & 0.7 & 0 & 0.3 \\ 0 & 0 & 0 & 0 & 0 & 0 & 0.7 & 0.3 \end{bmatrix}$ | $\begin{bmatrix} 0 & 0.7 & 0 & 0 & 0.3 & 0 & 0 & 0 \\ 0 & 0 & 0.4 & 0.6 & 0 & 0 & 0 & 0 \\ 0 & 0 & 0 & 0 & 0 & 0.7 & 0 & 0.3 \\ 0 & 0 & 0 & 0 & 0 & 0 & 0.7 & 0.3 \end{bmatrix}$ | $\begin{bmatrix} 0 & 0.7 & 0 & 0 & 0.3 & 0 & 0 & 0 \\ 0 & 0 & 0.8 & 0.2 & 0 & 0 & 0 & 0 \\ 0 & 0 & 0 & 0 & 0 & 0.7 & 0 & 0.3 \\ 0 & 0 & 0 & 0 & 0 & 0 & 0.7 & 0.3 \end{bmatrix}$ |
| $m$=5 (Fe-Plastic) | $\begin{bmatrix} 0 & 0.7 & 0 & 0 & 0.3 & 0 & 0 & 0 \\ 0 & 0 & 0.2 & 0.8 & 0 & 0 & 0 & 0 \\ 0 & 0 & 0 & 0 & 0 & 0.3 & 0 & 0.7 \\ 0 & 0 & 0 & 0 & 0 & 0 & 0.3 & 0.7 \end{bmatrix}$ | $\begin{bmatrix} 0 & 0.7 & 0 & 0 & 0.3 & 0 & 0 & 0 \\ 0 & 0 & 0.4 & 0.6 & 0 & 0 & 0 & 0 \\ 0 & 0 & 0 & 0 & 0 & 0.3 & 0 & 0.7 \\ 0 & 0 & 0 & 0 & 0 & 0 & 0.3 & 0.7 \end{bmatrix}$ | $\begin{bmatrix} 0 & 0.7 & 0 & 0 & 0.3 & 0 & 0 & 0 \\ 0 & 0 & 0.8 & 0.2 & 0 & 0 & 0 & 0 \\ 0 & 0 & 0 & 0 & 0 & 0.3 & 0 & 0.7 \\ 0 & 0 & 0 & 0 & 0 & 0 & 0.3 & 0.7 \end{bmatrix}$ |

*Table 4.2 Sorting matrix on a material and size basis over the separation network of the toy example*

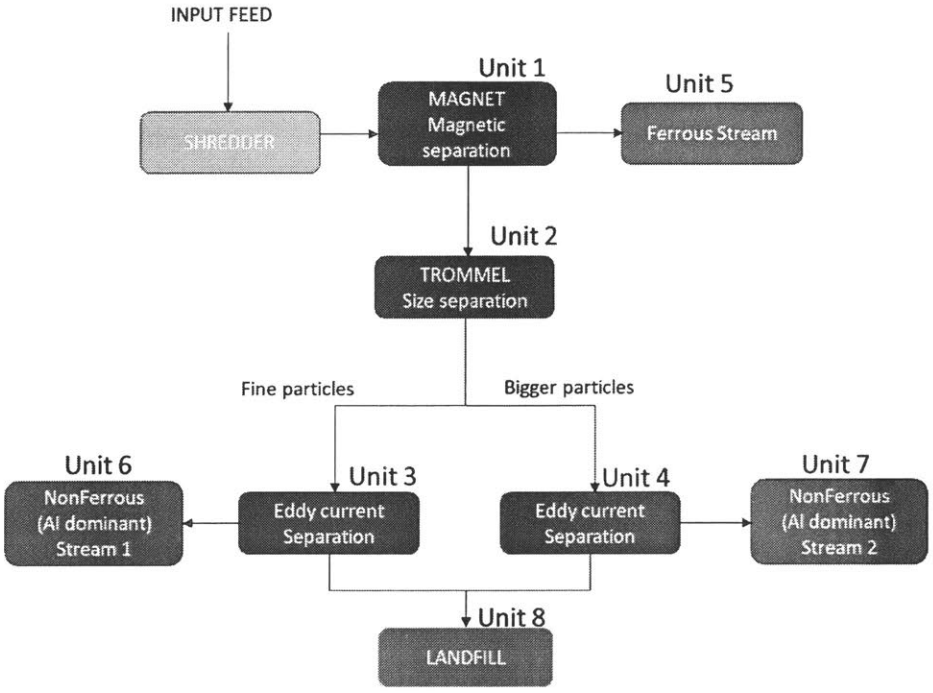


*Figure 4.3 Simple separation network for toy example*

Output streams

We use the linear model $f^{m,s} = \mu^{m,s} + (Q^{m,s})^T f^{m,s}$ with the input vector and the sorting matrices described above, to calculate the mass composition of the output streams for all particle classes, i.e. over all material and size classes. We can thus calculate the grade of the output stream. The figure below illustrates the mass composition at each output stream.

Note that for the calculation of grade, we have to assume how the mass of the two material types in non-liberated particles is distributed. For example, in the Fe output stream, we have 1.4kg of Fe-Al particles in the size 1('big') category and 0.36kg in the size 3 ('small') category. If we assume that the volume of Fe and Al in the non-liberated particles are of similar order, the ratio of the mass would be in ratio of their respective mass densities. Hence, we get an additional mass of Fe within non-liberated Fe-Al particles, of $\frac{7870\,(\frac{\mathrm{kg}}{\mathrm{m}^3})}{7870+2698(\frac{\mathrm{kg}}{\mathrm{m}^3})} * (1.4 + 0.36)\mathrm{kg} = 1.3\mathrm{kg}$. Similar calculations can be done to obtain the mass of Fe within non-liberated Fe-plastic particles in the Fe output stream.

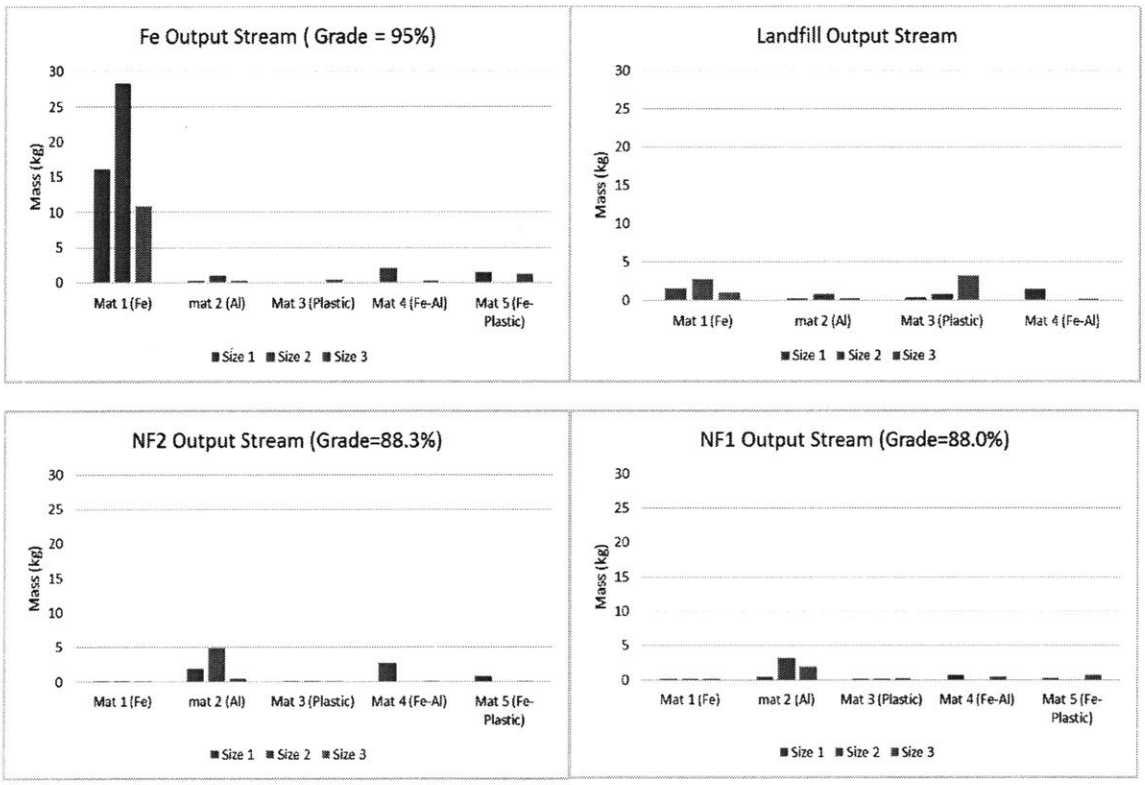


*Figure 4.4 Output streams' mass composition by material and size classes, for toy example*

# Chapter 5 Modeling secondary metal processing

Secondary metal processing is the last stage of the material recovery process of materially-complex products. For the case of end-of-life vehicles (ELVs), the main material streams that we will consider are Aluminum and Ferrous/Steel. As shown in the schematic in Figure 5.1, the secondary metal processing stage comes after disassembly, comminution and material separation. At the end of these stages, we have material scrap streams.

The material recovery model (MRM), developed in Chapter 4, takes as input data, the characterization of an end-of-life product (in terms of components, material breakdown and joint description). The model parameters quantify the comminution, separation and liberation inefficiencies. The MRM is thus able to estimate the metal scrap composition that leaves stage III, the separation stage. Thence, we assume that no further mechanical/chemical separation takes place at the secondary metal processing plant, as the plant expects a certain composition relative to the quality of scrap purchased. The following section details how we model the secondary metal processing part in order to estimate the value of a metal scrap. For material recovery from end-of-life vehicles, the typical metal scraps processed are ferrous scrap an Aluminum scrap.

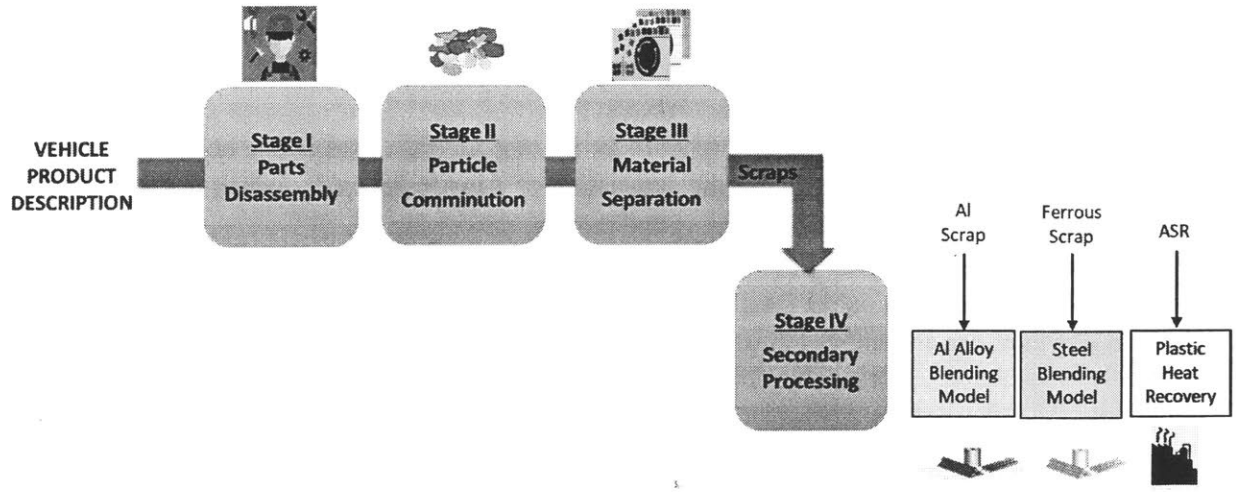


*Figure 5.1 Schematic of the four stages of material recovery processes*

Metal processing steps

Different scrap metals can undergo different metal processing depending on the scrap grade and the metal processing plant. The scrap can be new (from industrial processes) or old (from end-of-life products). The processing sequences at the plants can also differ: if there is a dedicated secondary metal smelter, or if the smelter integrates some amount of secondary raw material to the normal primary production. For instance, this is done for WEEE recycling in primary copper production to recover noble metals [110]. For our modeling, we will assume we are dealing with old scrap and dedicated secondary metal processing plants.

During metal processing, the feedstock undergoes smelting, refining and alloying, as described in Section 1.7. During refining, the thermodynamics of the different scrap tramp elements with respect to the target

metal dictates the metallurgical processes undergone to remove them. For instance, noble metals dissolve in the copper slime, and can be recovered through electrolyte purification [110]. On the other hand, for aluminum processing, *oxidation* can remove unwanted metals, .e.g. Mg and Zn are removed thus when in high concentration [51], [52], [56]. Based on their different distribution among the gas, slag and metal phases, Mg can be removed through the slag, Zn can be removed by evaporation if at high concentration, but Cu, Fe, Si, and Mn remain in the metal [56]. If the tramp elements cannot be removed partially or totally, *dilution* with the primary metal is needed. Afterwards, alloying is done if a certain final metal alloy is wanted for production: In the holding furnace, *alloying* elements (e.g. zinc, copper, manganese, magnesium and silicon) are added and the resulting alloy is analyzed iteratively, until the correct chemical composition is reached [41].

For our modeling, we will account for the oxidation, dilution and alloying processes. We will use the following assumptions:

(i) Oxidation: Removal of unwanted metals through oxidation as done in industry when possible thermodynamically. For Aluminum, Zn and Mg are assumed removable, such that any amount found in the scrap is neglected.

(ii) Dilution: We assume dilution with primary metal, .e.g for Al 99.7% for aluminum

(iii) Alloying: Unless we have the specific standard specifications, we assume that alloying elements have a metal content of *95%*, the average of processed data observed in [111]. We neglect the possible metal content in the remaining 5%.

(iv) The metals found in the scrap are not in oxide form.

(v) Process inefficiencies: We do not account for process inefficiencies which occur during the metal production, e.g. we ignore the production of Aluminum oxide, which is collaterally produced during the remelting, refining and salt slag processing [111].

(vi) pyrometallurgical cleaning/pre-processing: Any non-metal material in the metal scrap feedstock is neglected in the final product mass, as it is assumed that non-metal materials such as polymers can be removed through vaporization during pyrometallurgical cleaning[41].

## 5.1 Dilution and blending formulations

In this section, we will consider how to calculate the required dilution to produce a final alloy $j$ from recovered metal scrap at the secondary metal production stage. The dilution is needed to bring the metal tramp elements lie to within their respective concentration specification constraints.

We suppose that $X$ kg of metal scrap contains $x_i$kg of tramp element $i$, and then we denote the concentration of the contaminant $i$ by $f_i = \frac{x_i}{X}$. With a given maximum concentration threshold $f_{ij}^*$ in the final output as per the metal alloy $j$'s requirement, the dilution amount $y_{ij}$ kg with primary pure metal is given by, assuming that the concentration of tramp element in the recovered metal scrap exceeds that of the final alloy requirement ($f_i > f_{ij}^{max}$):

$$y_{ij} = X\left(\frac{f_i}{f_{ij}^{max}} - 1\right) \qquad \textit{Equation 5.1}$$

If instead of dilution with primary metal, dilution is done with an alloy $z$, i.e. *blending* feedstock with a concentration of the tramp element $i$ of $f_i^z$ and $f_i^z > f_{ij}^{max}$, the amount of dilution needed is now given by:

$$y_{ij}^z = \frac{X\left(\frac{f_i}{f_{ij}^{max}} - 1\right)}{\left(1 - \frac{f_i^z}{f_{ij}^{max}}\right)} \qquad \textit{Equation 5.2}$$

We note that in the case of there being more than one tramp element $i$ in excess of the maximum threshold (e.g. Sn and Cu are both tramp elements in ferrous/steel production) we have the final dilution amount given by the maximum over $i$, i.e. $\max_i y_{ij}^z$.

Above, we have only considered the case where we have excessive tramp elements. On the other hand, if the concentration of alloying element in the recovered metal scrap is less than that of the final alloy requirement $\left(f_i < f_{ij}^{min}\right)$, we need to account for the addition of alloying element(s). To solve simultaneously for the amount of primary metal needed for dilution against tramp element as well as the amount of alloying element(s) needed, we can use an optimization formulation. We will use a deterministic optimization to find the best recipe (i.e. what amounts of alloying elements and primary metal to add) based on costs of these raw materials, for a given input scrap composition.

Optimization formulation

We can formulate the optimization problem as a linear programming problem where the decision variables are the amounts of alloying elements and primary metal to add, for each possible target alloy $j$ that we might consider producing.

Decision variables:

$y_j$ is the decision variable for the mass of primary metal added for dilution,

$z_{ij}$ is the decision variable for the mass of alloying raw material $i$ added for alloying

Inputs:

X is amount of scrap (kg),

$x_i$ is amount of tramp or alloying element $i$ found in the scrap (kg),

$f_{ij}^{\min}, f_{ij}^{\max}$ are respectively minimum and maximum concentration of element $i$ in alloy $j$,

$f_i^k$ represents the concentration of element $i$ in the alloying raw material $k$,

$f_i^p$ represents the concentration of element $i$ in the primary metal raw material,

$c_i, c_p$ represent the raw material cost in \$/kg for respectively the alloying raw material $i$, and the primary metal used for dilution.

The optimization formulation is as follows, with the first line representing the total costs of dilution and alloying raw materials to minimize, and the second and third line representing the mass balance for element $i$ such that its concentration is within the alloy $j$'s concentration limits:

$$\min \sum_i c_i z_{ij} + c_p y_j$$

$$s.t.$$

$$x_i + \sum_k f_i^k z_{kj} + f_i^p y_j \leq f_{ij}^{\max}\left(X + \sum_i z_{ij} + y_j\right), \forall i$$

$$x_i + \sum_k f_i^k z_{kj} + f_i^p y_j \geq f_{ij}^{\min}\left(X + \sum_i z_{ij} + y_j\right), \forall i$$

$$z_{ij}, y_j \geq 0, \forall i$$

In industry, heuristics or recipes for blending schedules exist for different grades of scrap feedstock used. Some researchers have explored the deterministic and stochastic optimization of steel scrap [53], [112] to minimize scrap purchase costs by selecting the best scrap types and suppliers for a target inventory and by selecting the best scrap mix for each steel grade produced. [113] also incorporates stochastic optimization using fuzzy sets to deal with scrap composition uncertainty in order to optimize batch planning at an aluminum smelter.

For this research's purpose, we are only focusing on determining the optimal value of the input metal scrap, for a given input composition and sink metal alloy to be produced, based on the calculated dilution and alloying raw materials needed to meet the alloy concentration limits. For instance, a high-purity aluminum wrought alloy (e.g. P1020A) requires a lot of primary aluminum added for dilution due to the low concentration limits of contaminant elements (e.g. Cu, Fe). Thus, aluminum scrap used to produce high-purity Al wrought alloys will have low effective scrap value, while the same scrap used to produce lower-purity Al cast alloys will have comparatively high effective scrap value. Section 6 will go in depth on the different performance metrics to evaluate the value of the scrap. In this section, we will provide an illustration using *the effective value of scrap* (described in details in Section 6.2.1). With the effective value of the scrap, we want to capture the displaced costs of raw materials due the secondary scrap, while accounting for costs for dilution and additional alloying needed. To calculate it, we compare the raw material costs during the secondary metal production (for the calculated addition as solved by the optimization formulation) to that incurred for the primary metal production of a final alloy of similar composition and mass, normalized over the mass of alloy $j$ produced:

$$Scrap\ value_j = \frac{Primary\ cost_j - Secondary\ cost_j}{mass\ produced_j}$$

$$Scrap\ value_j = \frac{\left(\sum_i c_i(z_{ij}^* + x_i) + c_y(y_j^* + x_{Al})\right) - \left(\sum_i c_i z_{ij}^* + c_y y_j^* + c_x X\right)}{\sum_i z_{ij}^* + y_j^* + \sum_i x_i}$$

$$Scrap\ value_j = \frac{\left(\sum_i c_i x_i + c_y x_{Al}\right) - c_x X}{\sum_i z_{ij}^* + y_j^* + \sum_i x_i}$$

Where $c_x$ is the cost/kg of the metal scrap, $y$ and $x_{Al}$ are the amount of dilution aluminum and aluminum contained in the scrap respectively. We note that the mass of scrap that forms part of the final alloy may be less than the original mass of the scrap, i.e. $\sum_i x_i \leq X$, if some metal elements are removed from the scrap feedstock by oxidation or if non-metal elements are removed by pyrometallurgical cleaning, i.e. burning them off.

The following schematic shows the algorithm flow for the secondary metal processing modeling.

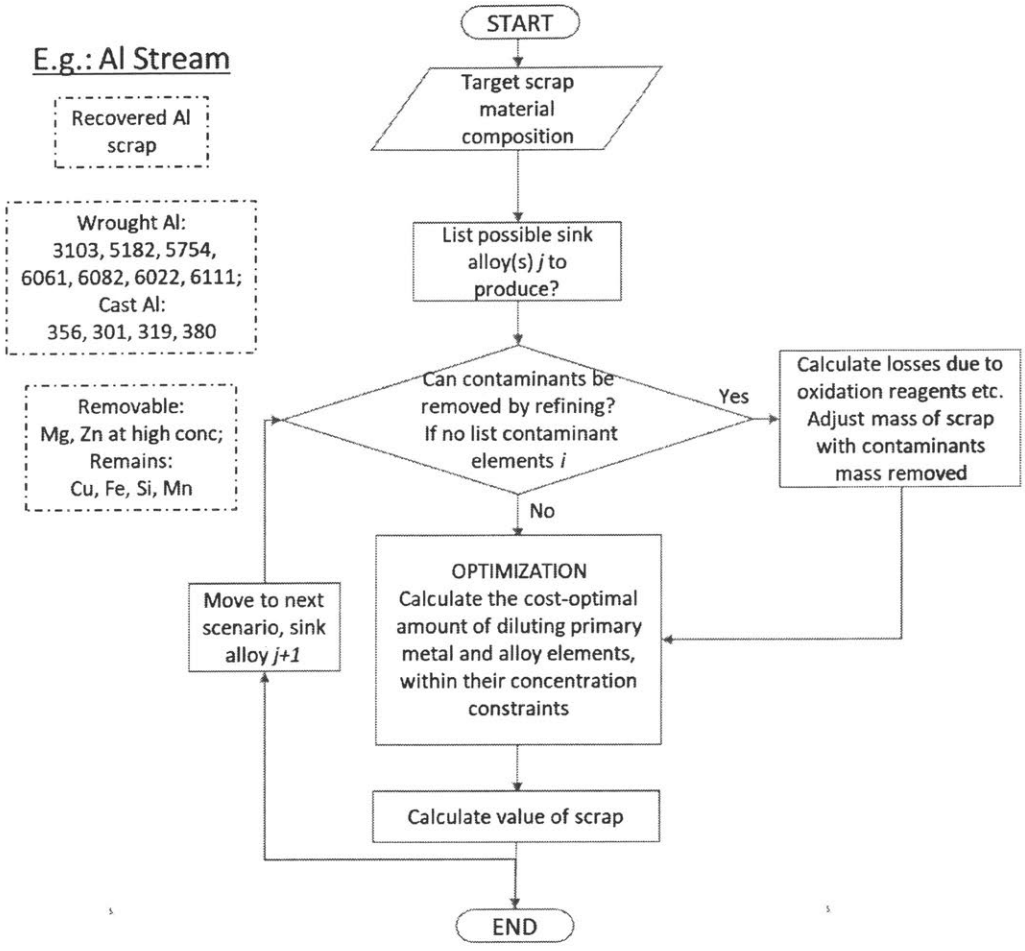


*Figure 5.2 Algorithm flow for secondary metal processing modeling, with example for aluminum*

## 5.2 Example blending calculations for aluminum scrap

In this section, we will look at an example calculation for the aluminum scrap.

The model's inputs are listed in Table 5.1 to Table 5.4 for: (i) aluminum scrap composition; (ii) raw material composition; (iii) alloys' element concentration limits; (iv) raw material pricing; (v) oxidation assumptions.

(i) Aluminum scrap composition:

We set $X$ and $x_i$ based on the inputs in Table 5.1, which are representative of the typical Aluminum scrap output from ELVs. The aluminum-heavy scrap is contaminated with some elements, Fi, Mg, Zn. The "rest" are materials that will somehow be removed during the pyrometallurgical processes e.g. polymers. Hence, for our study, $\sum_i x_i = 105.9 - 0.3 = 105.6kg$.

| Scrap Composition | Si | Fe | Cu | Mn | Mg | Cr | Ni | Zn | Ti | Al_c | Al_w | Rest | Total |
|---|---|---|---|---|---|---|---|---|---|---|---|---|---|
| **Mass (kg)** | 0 | 1.6 | 0 | 0 | 0.1 | 0 | 0 | 0.1 | 0 | 9.1 | 94.7 | 0.3 | 105.9 |
| **Conc (%)** | 0.0 | 1.5 | 0.0 | 0.0 | 0.1 | 0.0 | 0.0 | 0.1 | 0.0 | 8.6 | 89.4 | 0.3 | 100.0 |

*Table 5.1 Example scrap composition, adapted from [114]*

(ii) Raw material composition:

In Table 5.2, we define the elemental compositions of the raw materials that can be added for dilution ($f_i^p$) or alloying ($f_i^k$). The table provides conservative estimates of these compositions, in that it lists the maximum or minimum amounts of the elements as found in their raw materials, as defined by the chemical requirements in their ASTM standards.

| Element | Si | Fe | Cu | Mn | Mg | Cr | Ni | Zn | Ti | Primary Al |
|---|---|---|---|---|---|---|---|---|---|---|
| **Primary Al** | 0.1 | 0.2 | 0 | 0 | 0 | 0 | 0 | 0 | 0 | 99.7 |
| **Alloying Si** | 98 | 0 | 0 | 0 | 0 | 0 | 0 | 0 | 0 | 0 |
| **Alloying Fe** | max 1.5 | max 92 | 0 | max 0.05 | 0 | 0 | 0 | 0 | 0 | 0 |
| **Alloying Cu** | | max 0.001 | min 99.95 | 0 | 0 | 0 | max 0.001 | 0 | 0 | 0 |
| **Alloying Mn** | 0 | 0 | 0 | min 99.9 | 0 | 0 | 0 | 0 | 0 | 0 |
| **Alloying Mg** | max 0.005 | max 0.04 | max 0.01 | max 0.004 | min 99.9 | max 0.01 | max 0.01 | max 0.01 | 0 | 0.003 |
| **Alloying Cr** | max 0.15 | max 0.35 | max 0.01 | max 0.01 | 0 | min 99.0 | 0 | max 0.005 | max 0.050 | 0.30 |
| **Alloying Ni** | max 0.005 | max 0.02 | max 0.02 | max 0.005 | 0 | 0 | min 99.8 | max 0.005 | 0 | 0 |
| **Alloying Zn** | 0 | max 0.002 | max 0.001 | 0 | 0 | 0 | 0 | min 99.995 | 0 | 0.001 |
| **Alloying Ti** | 0 | max 0.20 | 0 | 0 | 0 | 0 | 0 | 0 | min 99.5 | 0 |

*Table 5.2 Material specification for raw materials for primary Aluminum, Al 99.7 LME brand and alloying elements (source: Fastmarkets Metal-Bulletin and ASTM standards)*

(iii) Element concentration limits:

In Table 5.3, we give the production specifications of each alloy $j$ ($f_{ij}^{min}$ and $f_{ij}^{max}$) for each element $i$, as each element enhances the alloy with different physical properties. Each row corresponds to the concentration limit specifications of an aluminum alloy that might be produced from the scrap input.

| Al Alloy | Si (%) | Fe (%) | Cu (%) | Mn (%) | Mg (%) | Cr (%) | Ni (%) | Zn (%) | Ti (%) |
|---|---|---|---|---|---|---|---|---|---|
| **P0506A** | 0-0.05 | 0-0.06 | 0-0.02 | 0-0.02 | 0-0.02 | 0-0.02 | 0-0.02 | 0-0.03 | 0-0.02 |
| **P1020A** | 0-0.10 | 0-0.20 | 0-0.03 | 0-0.03 | 0-0.03 | 0-0.03 | 0-0.03 | 0-0.03 | 0-0.03 |
| **1070A** | 0-0.2 | 0-0.25 | 0-0.03 | 0-0.03 | 0-0.03 | 0-0.03 | 0-0.03 | 0-0.07 | 0-0.03 |

| | | | | | | | | | |
|---|---|---|---|---|---|---|---|---|---|
| **3103** | 0-0.5 | 0-0.7 | 0-0.1 | 0.9-1.5 | 0-0.3 | 0-0.1 | 0-0.05 | 0-0.2 | 0-0.1 |
| ***5182*** | *0-0.2* | *0-0.35* | *0-0.15* | *0.2-0.5* | *4.0-5.0* | *0-0.1* | *0-0.05* | *0-0.25* | *0-0.1* |
| **5754** | 0-0.4 | 0-0.4 | 0-0.1 | 0-0.5 | 2.6-3.6 | 0-0.3 | 0-0.05 | 0-0.2 | 0-0.15 |
| **6061** | 0.4-0.8 | 0-0.7 | 0.15-0.4 | 0-0.15 | 0.8-1.2 | 0.04-0.35 | 0-0.05 | 0-0.25 | 0-0.15 |
| **6082** | 0.7-1.3 | 0-0.5 | 0-0.1 | 0.4-1.0 | 0.6-1.2 | 0-0.25 | 0-0.05 | 0-0.2 | 0-0.1 |
| ***A356*** | *6.5-7.5* | *0-0.2* | *0-0.2* | *0-0.1* | *0.25-0.45* | *0-0.05* | *0-0.05* | *0-0.1* | *0-0.2* |
| ***301*** | *9.5-10.5* | *0.8-1.5* | *3-3.5* | *0.5-0.8* | *0.25-0.5* | *0-0.03* | *1.0-1.5* | *0-0.05* | *0-0.2* |
| ***319*** | *5.5-6.5* | *0-1.0* | *3.0-4.0* | *0-0.5* | *0-0.1* | *0-0.5* | *0-0.35* | *0-1.0* | *0-0.25* |
| **A380** | 7.5-9.5 | 0-1.3 | 3.0-4.0 | 0-0.5 | 0-0.1 | 0-0.5 | 0-0.5 | 0-3.0 | 0-0.5 |

*Table 5.3 Minimum and maximum concentration limits of alloying elements in different Aluminum alloys, adapted from [51], [52] from ASTM International*

(iv) Raw material pricing:

The costs of the primary material, alloying raw materials and scrap are defined here ($c_p, c_i, c_x$).

| **Raw Material** | **Si** | **Fe** | **Cu** | **Mn** | **Mg** | **Cr** | **Ni** | **Zn** | **Ti** | **Primary Al** |
|---|---|---|---|---|---|---|---|---|---|---|
| Price ($/MT) | 2634.5 | 345 | 6251 | 2200 | 2525 | 10350 | 10735 | 2557.5 | 4880 | 2040 |

*Table 5.4 Alloying elements' prices as of Nov 2018 (source: metalbulletin.com and LME data)*

We estimate the price point of this composition of Al scrap is estimated to be that of Twitch, which has specifications of: not more than 4% maximum free zinc, 1% maximum free magnesium, and 1.5% maximum of analytical iron [46]. We take the price point to be 1414 $/ton from [115].

(v) Oxidation:

Based on the thermodynamics of the remelting of Aluminum, we note that any Mg and Zn at high concentration are removable, if they are in high enough concentration to constitute as tramp elements [56].

Optimization results

Because of the range of concentration limits in which the alloying elements can exist, there can be multiple associated amounts of Aluminum needed for dilution and total raw materials costs. As an example, we show in Figure 5.3 below the cost for various amounts of Al, Fe and Si that are combined with the Al scrap to produce the final aluminum alloy, Al356. We see that there exists a minimum cost for a certain combination of alloying elements and diluting Aluminum added. The optimization formulation can determine this minimum. The table below gives the result of the optimization runs for various |j|=14 sink alloys. The optimization was done in Julia/JuMP with Gurobi solver.

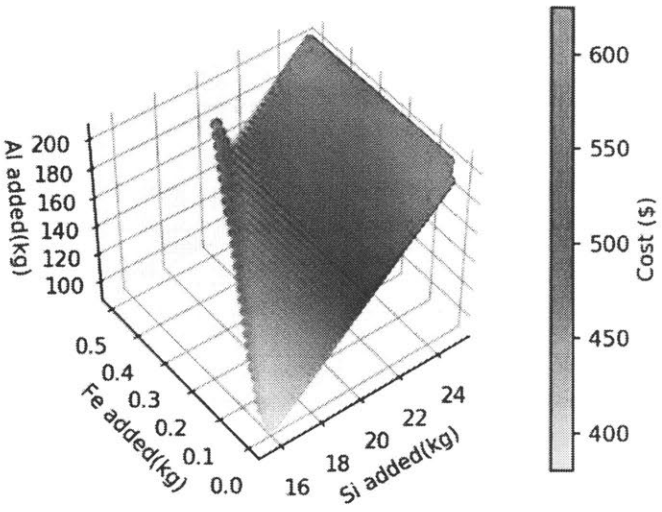


*Figure 5.3 Example range of resulting Al needed for dilution and raw material costs if amounts of Fe and Si alloyed are varied, with Al 356 as the produced sink alloy*

We did optimization runs for the following scenarios:

A. Using first 100% grade diluting and alloying raw materials (not the elemental compositions defined in Table 5.2),

B. Using raw materials with their respective elemental composition as defined in Table 5.2 above (baseline),

C. Using the Aluminum content in the input scrap as wrought or cast, i.e. not 100% Al. Wrought Al used in automotive components is mainly from the 6xxx series, the alloys are high in magnesium and silicon. On the other hand, cast Al is from the 3xx series. Using Al6061 and Al380 as reference wrought and cast aluminum, we calculate the effective metal element composition, $x_i'$, from the known ratio $r$ of cast to wrought Aluminum in the scrap:

$$x_i' = x_i + r * f^S_{i,j=Al380} + (1-r) * f^S_{i,j=Al6061}$$

$$x'_{Al} = x_{Al} - \sum_i r * f^S_{i,j=Al380} + (1-r) * f^S_{i,j=Al6061}$$

Where $f^S_{i,j=Al380}$, the concentration of element $i$ in alloy $j = Al380$, is taken to be the average of the allowed range of concentration (see Table 5.3). For example, $f^S_{i=Si,j=Al380} = 8.5\%$.

D. Using oxidation to remove Mg and/or Zn for the production alloy $j$ for which Mg/Zn is a tramp element, according to the following pseudocode:

*for each production alloy j*:

*for each element α that is removable by oxidation*:

$$if \frac{x_\alpha}{X} > f^{max}_{\alpha j}:$$

$$put\ x_\alpha = 0$$

This scenario (D) allows the possibility of a constituent element in the scrap being considered as either a tramp element, removable by oxidation if thermodynamically possible, or an alloying element, i.e. a

valuable element. For example, for the alloys considered in Table 5.3, both Mg and Zn are in excess of the alloying limits for $j$ =1:3, and Zn only in $j$=8.

Table 5.5 to Table 5.8 list the results of the optimization for the four scenarios. Compared to the baseline scenario in Table 5.6, we can observe the following:

- In the scenarios (B-D) where the raw materials used for dilution and alloying are not taken as 100% pure elements, we can see that there are infeasible solutions for the purest alloy P0506A, whereby the concentration limit constraints for the particular production alloy j cannot be met, as dilution is not with 100% pure elements.
- In all scenarios, while the scrap value stays the same over all possible production alloys j, the scrap value normalized by output weight changes. Generally, producing the alloy that has less stringent concentration limit for the tramp elements (Fe), has a larger normalized scrap value, as less Aluminum needs to be added for dilution.

To summarize, for a given input scrap composition, the blending optimization will generate a range of effective scrap values, showing the scrap potential over a range of different produced alloys. For instance, under scenario D and for the scrap composition of Table 5.1, the effective scrap value range is 0.0004-1.61 $/kg.

| Produced Alloy | Si added (kg) | Fe added (kg) | Cu added (kg) | Mn added (kg) | Mg added (kg) | Cr added (kg) | Ni added (kg) | Zn added (kg) | Ti added (kg) | Al added (kg) | 2ndary Cost ($) | 1ary cost ($) | Scrap Value ($) | Total Mass (kg) | Effective Scrap Value ($/kg) |
|---|---|---|---|---|---|---|---|---|---|---|---|---|---|---|---|
| P0506A | 0.00 | 0.00 | 0.00 | 0.00 | 0.00 | 0.00 | 0.00 | 0.00 | 0.00 | 2561.07 | 5033.67 | 5083.03 | 49.37 | 2666.67 | 0.07 |
| P1020A | 0.00 | 0.00 | 0.00 | 0.00 | 0.00 | 0.00 | 0.00 | 0.00 | 0.00 | 694.40 | 1473.93 | 1523.30 | 49.37 | 800.00 | 0.25 |
| 1070A | 0.00 | 0.00 | 0.00 | 0.00 | 0.00 | 0.00 | 0.00 | 0.00 | 0.00 | 534.40 | 1168.81 | 1218.18 | 49.37 | 640.00 | 0.31 |
| 3103 | 0.00 | 0.00 | 0.00 | 2.06 | 0.00 | 0.00 | 0.00 | 0.00 | 0.00 | 120.91 | 384.82 | 434.19 | 49.37 | 228.57 | 0.87 |
| 5182 | 0.00 | 0.00 | 0.00 | 0.91 | 18.19 | 0.00 | 0.00 | 0.00 | 0.00 | 332.44 | 836.16 | 885.53 | 49.37 | 457.14 | 0.44 |
| 5754 | 0.00 | 0.00 | 0.00 | 0.00 | 10.30 | 0.00 | 0.00 | 0.00 | 0.00 | 284.10 | 720.07 | 769.44 | 49.37 | 400.00 | 0.50 |
| 6061 | 0.91 | 0.00 | 0.34 | 0.00 | 1.73 | 0.09 | 0.00 | 0.00 | 0.00 | 119.89 | 388.60 | 437.96 | 49.37 | 228.57 | 0.87 |
| 6082 | 2.24 | 0.00 | 0.00 | 1.28 | 1.82 | 0.00 | 0.00 | 0.00 | 0.00 | 209.06 | 562.16 | 611.53 | 49.37 | 320.00 | 0.62 |
| A356 | 52.00 | 0.00 | 0.00 | 0.00 | 1.90 | 0.00 | 0.00 | 0.00 | 0.00 | 640.50 | 1513.41 | 1562.78 | 49.37 | 800.00 | 0.25 |
| 301 | 19.00 | 1.40 | 6.00 | 1.00 | 0.40 | 0.00 | 2.00 | 0.00 | 0.00 | 64.60 | 384.89 | 434.25 | 49.37 | 200.00 | 1.00 |
| 319 | 8.80 | 0.00 | 4.80 | 0.00 | 0.00 | 0.00 | 0.00 | 0.00 | 0.00 | 40.80 | 280.00 | 329.37 | 49.37 | 160.00 | 1.24 |
| A380 | 9.23 | 0.00 | 3.69 | 0.00 | 0.00 | 0.00 | 0.00 | 0.00 | 0.00 | 4.55 | 205.25 | 254.62 | 49.37 | 123.08 | 1.62 |

*Table 5.5 Sample blending optimization results for dilution and alloying for different Al sink alloy j, assuming 100% raw materials (scenario A)*

| Produced Alloy | Si added (kg) | Fe added (kg) | Cu added (kg) | Mn added (kg) | Mg added (kg) | Cr added (kg) | Ni added (kg) | Zn added (kg) | Ti added (kg) | Al added (kg) | 2ndary Cost ($) | 1ary cost ($) | Scrap Value ($) | Total Mass (kg) | Effective Scrap Value ($/kg) |
|---|---|---|---|---|---|---|---|---|---|---|---|---|---|---|---|
| P0506A | NaN | NaN | NaN | NaN | NaN | NaN | NaN | NaN | NaN | NaN | NaN | NaN | NaN | NaN | NaN |
| P1020A | 0.8 | 0.0 | 148.0 | 148.1 | 148.0 | 0.0 | 148.3 | 147.8 | 0.0 | 492358.3 | 942688.7 | 942738.1 | 49.4 | 493205.0 | 0.0004 |
| 1070A | 2.9 | 0.0 | 0.8 | 0.8 | 0.7 | 0.0 | 0.0 | 1.8 | 0.0 | 2637.1 | 5199.8 | 5249.2 | 49.4 | 2749.8 | 0.0724 |
| 3103 | 1.2 | 0.0 | 0.0 | 4.1 | 0.0 | 0.0 | 0.0 | 0.5 | 0.0 | 164.0 | 476.0 | 525.4 | 49.4 | 275.4 | 0.7228 |
| 5182 | 1.0 | 0.0 | 0.0 | 4.4 | 43.4 | 0.0 | 0.0 | 2.1 | 0.0 | 713.1 | 1647.8 | 1697.1 | 49.4 | 869.6 | 0.2289 |
| 5754 | 2.2 | 0.0 | 0.0 | 3.3 | 24.0 | 0.0 | 0.0 | 1.2 | 0.0 | 532.1 | 1247.3 | 1296.6 | 49.4 | 668.5 | 0.2978 |

| | | | | | | | | | | | | | | | |
|---|---|---|---|---|---|---|---|---|---|---|---|---|---|---|---|
| **6061** | 2.1 | 0.0 | 0.4 | 0.4 | 2.1 | 0.1 | 0.0 | 0.6 | 0.0 | 164.4 | 480.7 | 530.0 | 49.4 | 275.7 | 0.7220 |
| **A356** | 627.9 | 0.0 | 16.6 | 8.3 | 37.3 | 0.0 | 4.2 | 8.2 | 0.0 | 7495.9 | 16387.3 | 16436.7 | 49.4 | 8303.9 | 0.0240 |
| **301** | 19.3 | 1.4 | 6.0 | 1.0 | 0.4 | 0.0 | 2.0 | 0.0 | 0.0 | 64.5 | 385.8 | 435.2 | 49.4 | 200.3 | 0.9940 |
| **319** | 9.5 | 0.0 | 5.1 | 0.8 | 0.0 | 0.0 | 0.0 | 0.0 | 0.0 | 48.7 | 300.6 | 349.9 | 49.4 | 169.8 | 1.1728 |
| **A380** | 9.5 | 0.0 | 3.7 | 0.6 | 0.0 | 0.0 | 0.0 | 0.0 | 0.0 | 4.3 | 207.0 | 256.3 | 49.4 | 123.7 | 1.6087 |

*Table 5.6 Blending optimization results for scenario B - with impure raw materials (baseline scenario)*

| **Produced Alloy** | **Si added (kg)** | **Fe added (kg)** | **Cu added (kg)** | **Mn added (kg)** | **Mg added (kg)** | **Cr added (kg)** | **Ni added (kg)** | **Zn added (kg)** | **Ti added (kg)** | **Al added (kg)** | **2ndary Cost ($)** | **1ary cost ($)** | **Scrap Value ($)** | **Total Mass (kg)** | **Effective Scrap Value ($/kg)** |
|---|---|---|---|---|---|---|---|---|---|---|---|---|---|---|---|
| **P0506A** | NaN | NaN | NaN | NaN | NaN | NaN | NaN | NaN | NaN | NaN | NaN | NaN | NaN | NaN | NaN |
| **P1020A** | 0.0 | 0.0 | 309.1 | 309.9 | 308.9 | 0.0 | 310.3 | 309.2 | 0.0 | 103108.8 | 2.0E+06 | 2.0E+06 | 5.8E+01 | 1.0E+06 | 2.0E-04 |
| **1070A** | 2.9 | 0.0 | 0.6 | 1.1 | 0.0 | 0.0 | 0.0 | 2.4 | 0.0 | 4199.7 | 8.2E+03 | 8.2E+03 | 5.8E+01 | 4.3E+03 | 4.8E-02 |
| **3103** | 0.0 | 1.7 | 0.0 | 6.5 | 0.0 | 0.0 | 0.0 | 0.0 | 0.0 | 629.0 | 1.4E+03 | 1.4E+03 | 5.8E+01 | 7.4E+02 | 2.8E-01 |
| **5182** | 0.0 | 0.0 | 0.0 | 7.0 | 70.8 | 0.0 | 0.0 | 3.0 | 0.0 | 1252.9 | 2.8E+03 | 2.8E+03 | 5.8E+01 | 1.4E+03 | 1.4E-01 |
| **5754** | 1.7 | 0.0 | 0.0 | 5.1 | 36.5 | 0.0 | 0.0 | 1.5 | 0.0 | 897.2 | 2.0E+03 | 2.0E+03 | 5.8E+01 | 1.0E+03 | 2.0E-01 |
| **6061** | 1.5 | 0.0 | 0.0 | 0.5 | 2.2 | 0.0 | 0.0 | 0.5 | 0.0 | 322.0 | 7.8E+02 | 8.3E+02 | 5.8E+01 | 4.3E+02 | 4.8E-01 |
| **6082** | 3.0 | 0.1 | 0.0 | 2.8 | 3.2 | 0.0 | 0.0 | 0.0 | 0.0 | 628.4 | 1.4E+03 | 1.4E+03 | 5.8E+01 | 7.4E+02 | 2.8E-01 |
| **A356** | 983.0 | 0.0 | 25.3 | 12.8 | 57.4 | 0.0 | 6.4 | 12.4 | 0.0 | 11820.4 | 2.6E+04 | 2.6E+04 | 5.8E+01 | 1.3E+04 | 1.6E-02 |
| **301** | 119.0 | 15.8 | 37.0 | 6.1 | 1.9 | 0.0 | 12.5 | 0.0 | 0.0 | 959.2 | 2.7E+03 | 2.7E+03 | 5.8E+01 | 1.3E+03 | 1.7E-01 |
| **319** | 67.1 | 8.7 | 36.6 | 0.0 | 0.0 | 0.0 | 0.0 | 0.0 | 0.0 | 1027.5 | 2.5E+03 | 2.6E+03 | 5.8E+01 | 1.2E+03 | 1.7E-01 |
| **A380** | 92.4 | 12.8 | 36.6 | 0.0 | 0.0 | 0.0 | 0.0 | 0.0 | 0.0 | 998.0 | 2.5E+03 | 2.6E+03 | 5.8E+01 | 1.2E+03 | 1.7E-01 |

*Table 5.7 Optimization results for scenario C - where cast and wrought Aluminum are distinguished in the scrap for scrap composition calculation*

| **Produced Alloy** | **Si added (kg)** | **Fe added (kg)** | **Cu added (kg)** | **Mn added (kg)** | **Mg added (kg)** | **Cr added (kg)** | **Ni added (kg)** | **Zn added (kg)** | **Ti added (kg)** | **Al added (kg)** | **2ndary Cost ($)** | **1ary cost ($)** | **Scrap Value ($)** | **Total Mass (kg)** | **Effective Scrap Value ($/kg)** |
|---|---|---|---|---|---|---|---|---|---|---|---|---|---|---|---|
| **P0506A** | NaN | NaN | NaN | NaN | NaN | NaN | NaN | NaN | NaN | NaN | NaN | NaN | NaN | NaN | NaN |
| **P1020A** | 0.0 | 0.0 | 309.1 | 309.9 | 310.1 | 0.0 | 310.4 | 309.8 | 0.0 | 103112.5 | 2.0E+06 | 2.0E+06 | 5.8E+01 | 1.0E+06 | 5.7E-05 |
| **1070A** | 2.9 | 0.0 | 0.6 | 1.1 | 1.3 | 0.0 | 0.0 | 3.0 | 0.0 | 4200.7 | 8.2E+03 | 8.2E+03 | 5.8E+01 | 4.3E+03 | 1.4E-02 |
| **3103** | 0.0 | 1.7 | 0.0 | 6.5 | 0.0 | 0.0 | 0.0 | 0.0 | 0.0 | 630.9 | 1.4E+03 | 1.4E+03 | 5.8E+01 | 7.4E+02 | 7.8E-02 |
| **5182** | 0.0 | 0.0 | 0.0 | 7.0 | 70.8 | 0.0 | 0.0 | 3.6 | 0.0 | 1252.9 | 2.8E+03 | 2.8E+03 | 5.8E+01 | 1.4E+03 | 4.1E-02 |
| **5754** | 1.7 | 0.0 | 0.0 | 5.1 | 36.5 | 0.0 | 0.0 | 2.1 | 0.0 | 897.2 | 2.0E+03 | 2.0E+03 | 5.8E+01 | 1.0E+03 | 5.6E-02 |
| **6061** | 1.5 | 0.0 | 0.0 | 0.5 | 2.2 | 0.0 | 0.0 | 1.1 | 0.0 | 322.0 | 7.8E+02 | 8.4E+02 | 5.8E+01 | 4.3E+02 | 1.3E-01 |
| **6082** | 3.0 | 0.1 | 0.0 | 2.8 | 3.2 | 0.0 | 0.0 | 0.0 | 0.0 | 629.0 | 1.4E+03 | 1.4E+03 | 5.8E+01 | 7.4E+02 | 7.8E-02 |
| **A356** | 983.2 | 0.0 | 25.3 | 12.8 | 58.7 | 0.0 | 6.4 | 13.0 | 0.0 | 11823.2 | 2.6E+04 | 2.6E+04 | 5.8E+01 | 1.3E+04 | 4.5E-03 |
| **301** | 119.0 | 15.8 | 37.0 | 6.1 | 3.1 | 0.0 | 12.5 | 0.0 | 0.0 | 960.2 | 2.7E+03 | 2.7E+03 | 5.8E+01 | 1.3E+03 | 4.6E-02 |
| **319** | 13.1 | 0.0 | 7.2 | 1.1 | 0.0 | 0.0 | 0.0 | 0.0 | 0.0 | 140.3 | 5.0E+02 | 5.6E+02 | 5.8E+01 | 2.7E+02 | 2.2E-01 |
| **A380** | 13.1 | 0.0 | 5.1 | 0.8 | 0.0 | 0.0 | 0.0 | 0.0 | 0.0 | 70.7 | 3.5E+02 | 4.1E+02 | 5.8E+01 | 2.0E+02 | 3.0E-01 |

*Table 5.8. Optimization results for scenario D - where oxidation removes the tramp Zn and Mg content in the input scrap, before any dilution and alloying*

## 5.3 Example dilution calculations for Ferrous scrap

In this section, we will look at an example calculation for the ferrous scrap.

As described in section 1.7.4, there are thousands of steel and cast iron alloys of different element compositions. From the literature, it is not clear what are the typical final produced alloys in secondary steel production. This is because of the different classification systems which exist throughout the world, based on not only composition, but microstructure, application or specification [60]. For our model, we will use a simplified classification of steel product types, proposed by Nakamura et al. in [54], which have different tolerance levels for contaminant elements of copper (Cu) and tin (Sn), see Table 1.1: Steel sheets for deep drawing, hot and cold rolled steel, sections, steel bars.

For simplification, we will only focus on copper as a contaminant or tramp element in steel secondary production. Based on the thermodynamics of the remelting of steel (referring to the element radar chart in [56], copper (Cu) and tin (Sn) are not removable. Additionally, other elements which serve as alloying elements in certain steel alloys, albeit in trace amounts, are also not removable: nickel (Ni), cobalt (Co), molybdenum (Mo) and tungsten (W) [56]. We do not have granular ELV data to the level of steel alloys used in ferrous automotive parts. But we do know the amount of copper in a vehicle (as an automotive part or as wires), and thus, we will focus only on the contamination brought by copper in the ferrous scrap.

For the ferrous blending model, the input data used is as follows:

(i) Scrap composition

For our example, we will refer to the ELV ferrous scrap composition used by Nakamura et al. in [54].

| **Scrap Composition** | **Fe** | **Cu** | **Zn** | **Al** | **Total** |
|---|---|---|---|---|---|
| **Mass (kg)** | 681.5 | 3.6 | 3.6 | 29.4 | 718.1 |
| **Conc (%)** | 94.9 | 0.5 | 0.5 | 4.1 | 100 |

*Table 5.9 Example Ferrous scrap composition, adapted from [54]*

(ii) Raw material composition

We assume pig iron to be the raw material used for dilution. Note that unlike for the aluminum blending model, we are only considering one tramp element, copper (Cu). In our calculation, we assume pig iron to have an average of 0.01% of copper, as in [54].

(iii) Tramp element concentration limit

For the four final steel product types considered, we assume the following concentration limits for copper as in [54]:

| **Steel product type** | **Cu (%)** |
|---|---|
| **Steel sheets for deep drawing** | 0-0.06 |
| **Hot & cold rolled steel** | 0-0.10 |
| **Sections** | 0-0.30 |
| **Steel bars** | 0-0.4 |

*Table 5.10 Element concentration limits in 4 different produced steel stocks from [54]*

(iv) Material pricing:

For the costs, we are concerned with the price of the ferrous scrap, and primary pig iron. From LME data, we take the costs to be \$312.50/ton and \$375/ton for Ferrous scrap and pig iron respectively.

Dilution calculations for Fe scrap

Unlike the blending model for aluminum, we are not looking at several elements and their concentration constraints. Hence, we do not need an optimization model to determine the dilution needed due to copper as a single contaminant. From Equation 5.2, we can calculate $y_{Cu,j}^{pig\ Iron}$, the amount of pig iron needed for dilution as for each of the possible produced steel product $j$:

$$y_{Cu,j}^{\text{pig Iron}} = \frac{X\left(\frac{f_{Cu}}{f_{Cu,j}^{max}} - 1\right)}{\left(1 - \frac{f_{Cu}^{\text{pig Iron}}}{f_{Cu,j}^{max}}\right)} \qquad \textit{Equation 5.3}$$

Here, the net mass of Fe scrap ($X$) is the sum of the ferrous and copper content, assuming that the other metals are removable by oxidation and that the non-metals are removed due to the high temperature in the pyro-metallurgical processes. In Table 5.11 below, we show the dilution amounts for the four final alloy scenarios ($j = 1, \ldots, 4$), and the corresponding effective scrap values. As was the case for the aluminum blending model, we can observe that as the maximum copper concentration limit of the product increases, less dilution is needed, and the effective scrap value conversely increases.

| **Produced Steel Product ($j$)** | **Dilution, pig iron added (kg)** | **Effective Scrap Value (\$/kg)** |
|---|---|---|
| **Steel sheets for deep drawing** | *6.69E+03* | 4.21E-03 |
| **Hot & cold rolled steel** | *3.39E+03* | 6.21E-02 |
| **Sections** | *5.58E+02* | 2.00E-01 |
| **Steel bars** | *2.31E+02* | 2.69E-01 |

*Table 5.11 Calculated dilution added to Fe scrap for different produced steel products, and corresponding effective scrap values*

# Chapter 6 Performance metrics

The development of the Material Recovery Model has as end-goal the ability to estimate material flows throughout the recovery processes with high granularity. Depending on the system boundaries set for our analysis or depending on the focus, there are different possible performance metrics that can be used to evaluate the recovery performance. In this section, we first discuss the different types of metrics used in the literature: material performance metrics, economic metrics, thermodynamic metrics, environmental metrics. Then, we propose and define the performance metrics that we use to capture and quantify the real end-of-life vehicles' recyclability.

The schematic in Figure 6.1 displays the flow model that is considered for this study within the scope of the material recovery chain of end-of-life vehicles. While prior literature has focused on the inner system boundaries 1 and 2, we seek to expand to boundary 3 to capture the downstream processes of secondary metal processing or energy recovery. As discussed in Chapter 5, these downstream processes are affected by the metal composition in the input scrap feed, and thus dilute the actual recyclability of the collected target metal.

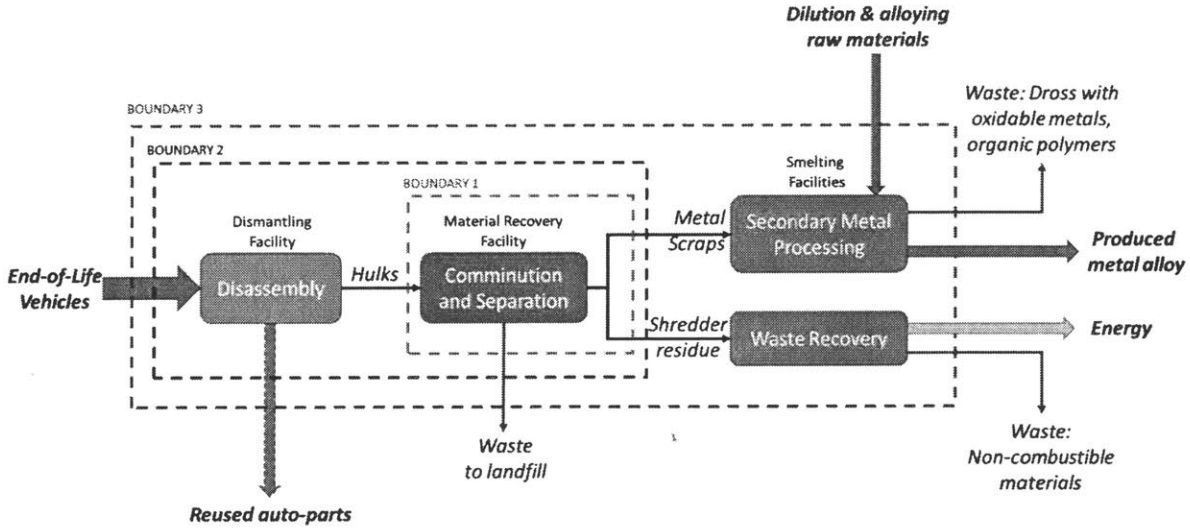


*Figure 6.1 System boundaries for material recovery processes from ELVs, from cradle-to-gate*

## 6.1 Material performance metrics

### 6.1.1 Grade and recovery rate

The typical performance metrics used to evaluate material recovery from material recovery facilities are grade and recovery rate. Whether for general waste streams such as household waste or for complex products such as end-of-life vehicles, the separation process aims at recovering one or more valuable

target materials from a heterogeneous mixture of materials. Recovery rate and grade are basic performance metrics that have been used for a long time in the mineral processing industry [105], [116] . In [101], [116], [117], grade and recovery rate have been used to evaluate the performance of material recovery facilities for municipal solid waste. For material recovery systems with more than one recovered valuable material streams, a weighted sum of grade and recovery rate are proposed in [100].

For our purpose, we will also use grade and recovery rate to evaluate the performance of a subsystem of our material recovery chain, as denoted by boundary 1 in Figure 6.1. In our Material Recovery Model, in addition to the dimension of material types, we have the added dimension of particle size due to separation by size, as discussed in Section 4.3. As we are only concerned with material types to evaluate performance, we aggregate the material flows over all size categories.

Grade measures the concentration of the target material(s) in the desired output stream while recovery rate measures the fraction of the target material(s) that is collected at the desired output stream. Our target materials depend on the output streams of a given separation network configuration: for example, ferrous in the ferrous scrap, aluminum in the Twitch scrap, and plastics in the ASR. To simplify the presentation in this section, we assume that each target material $m$ has a single target output stream denoted by $i_{(m)}$. We define grade $G_m$ and recovery rate $R_m$ of target material $m$ at output stream $i_{(m)}$ as follows:

$$G_m = \frac{f^m_{i_{(m)}}}{\sum_{m'} f^{m'}_{i_{(m)}}}$$

$$R_m = \frac{f^m_{i_{(m)}}}{\mu_m}$$

where $\mu_m$ denotes the total input flow of material $m$ to the recovery facility, and $f^m_{i_{(m)}}$ is the amount that is correctly sorted to output stream $i_{(m)}$.

It is useful to note that there can be a trade-off between grade and recovery rate, for a given input material feed to the system. For instance, by adding different recirculation steps to a given separation network configuration, we can increase the recovery rate at the expense of the grade. To affect this Pareto Curve, we can either increase the separation efficiency of the sorting units or increase the number of sorting units. However, this comes at a technological or economic cost to the facility, and is not something that is commonly done in industry as there needs to be an advantageous market for higher grade output scrap. Nevertheless, the concept of recirculation flow is being explored at the research level to increase grade or metal scrap [40].

The following example illustrates how the Pareto Curve is formed and what influences its shift. Let us assume a simple separation configuration of four ($s = 4$) separation units (U0 to U3), and a target output stream V0, and a landfill unit L1 (see Figure 6.2(left)). Each separation unit has separation efficiency $r$ for the target material, and a separation efficiency $q$ for the non-target material. While the material stream is a mixture of both target and non-target materials, the target stream progresses downstream from one unit to another towards V0 with probability or separation efficiency $r$, while the

non-target streams progresses upstream towards landfill unit L1 with probability or separation efficiency $q$. In the figure, as illustration for the target stream, each arc signifies the direction the target stream: $r$ fraction goes downstream, and $1-r$ fraction goes upstream. Note that depending on the recirculation flow, there can be several configuration designs. We explore 3 designs:

(i) Design 1: there is backward recirculation at each unit; that is, the target output stream from each separation unit goes to the next separation unit, while the non-target output stream is recirculated and fed back into the prior separation unit.

(ii) Design 2: there is upstream recirculation at each unit, where the non-target output streams from units U0, U1, and U2 are all sent back to U3 for recirculation.

(iii) Design 3: there is downstream recirculation at each unit where the target output streams from units U1, U2, and U3 are all sent forward to unit U0. We have different Pareto curves for each of these different designs

Furthermore, there can be several possible variations depending on where in the network the input stream is added to the system. We analytically solve for the grade and recovery rate, using a Markov Chain formulation, as detailed in Appendix C. Figure 6.2(right) shows the resulting Pareto curve for each system configuration, where $a_i$ denotes at which of unit U0 to U3 the input enters. We can observe the following: (i) if the input feed is put closer to the output stream, the recovery rate increases while the grade decreases; (ii) design 1 seems to dominate the other two. Figure 6.3 shows the positive effect on the Pareto Curve of increasing the number of separation units and of increasing their separation efficiencies.

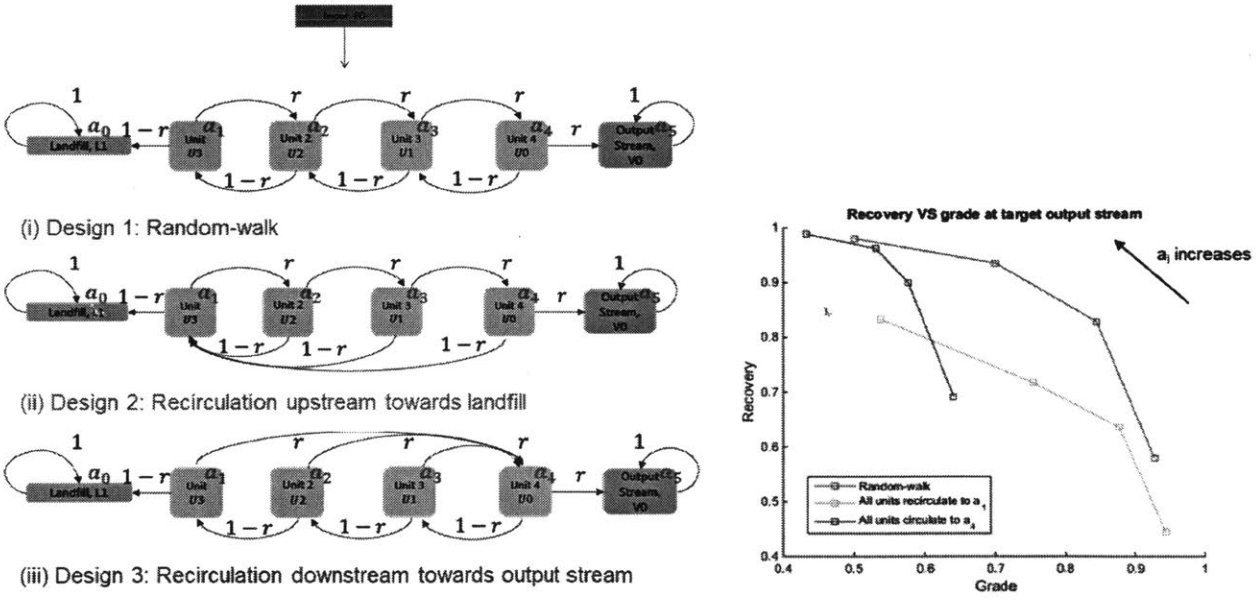


*Figure 6.2 left: Flow of target stream through different designs of separation networks; right: recovery-rate vs grade Pareto curves for different separation network designs (r=0.7, q=0.7).*

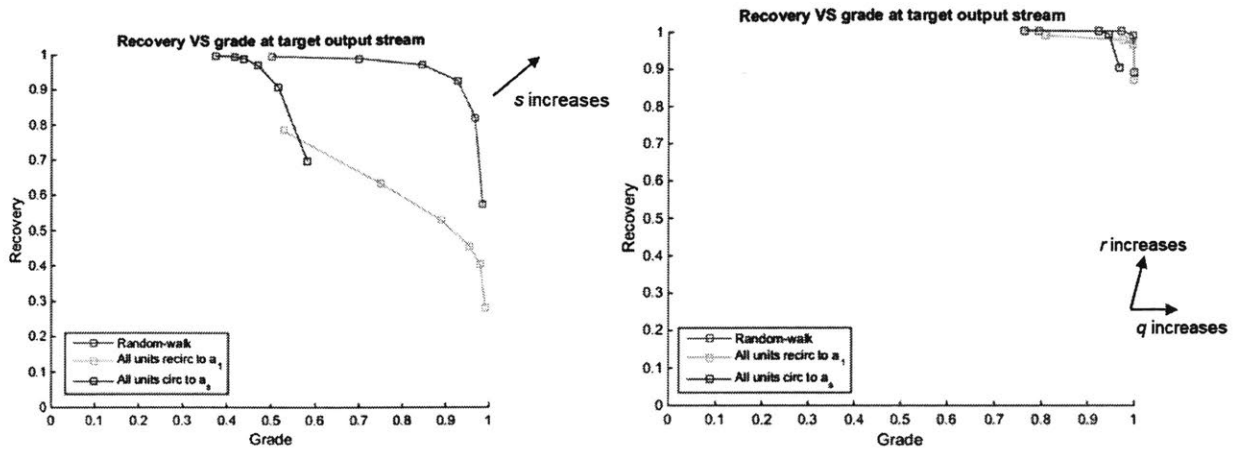


*Figure 6.3 Shift in Pareto curves with: (i) increase in s, the number of sorting units to 6 ($r = q = 0.7$), (ii) increase in separation efficiencies r and q to 0.9 ($s = 4$).*

### 6.1.2 Mixing entropy

In effect, grade and recovery rate only consider two materials or groups of materials, i.e. the target material(s) and non-target material(s). These metrics do not give consideration to the number of materials in the stream or the complexity of the product when there is heavy material mixing. In [4], [118], Gutowski and Dahmus propose a new metric to capture that: the normalized mixing entropy measure. This metric was derived based on observing an analogy between separation steps for materials in mixtures and decoding messages in information theory. Gutowski and Dahmus use this metric to determine the lower bound for the average number of separation steps needed (or for the average word length needed) in order to separate a mixture of a given number of materials of specified concentration. However, in our research we will use mixing entropy as a measure of how much of the material complexity in the material stream is removed or resolved by the separation system.

For a material stream consisting of a mixture of materials, its normalized mixing entropy measure is given by $H$ [4], [118]:

$$H = -\sum_{i=1}^{M} c_i \log_2 c_i$$

Where $c_i$ is the concentration fraction of material $i$, and there are $M$ component materials in the mixture. When the logarithm is taken to base 2, H is given in bits [4], [118]. A larger value of H signifies that there is a greater degree of mixing or complexity in the material stream. This measure tends to penalize mixtures which do not have high purity in one specific material, or which have a lot of materials, i.e. high $M$. As illustration, Figure 6.4 (i) and (ii) show these two effects. As a simple example, a binary mixture consisting of Material 1 and Material 2 has the highest total entropy when they both are equally concentrated, at $c_i = 0.5$, and the lowest total entropy when either Material 1 or 2 are highly concentrated. Figure 6.4 (ii) investigates 3 mixtures with different material compositions

for different number of materials $M$: (i) each material has equal concentration, (ii) a mixture with one main material at concentration $c = 0.7$ and the other materials equally distributed, (ii) a mixture with one material at concentration $c = 0.3$ and the other materials equally distributed. It shows that mixing entropy increases with the number of materials, and with the material composition having materials that are more diluted. We observe that the entropy is highest for the material mixture with materials of equal concentration, and lowest for the material mixture with one dominant material.

While this shows that the number of material types considered can impact the resulting mixing entropy, this metric can still be used for comparison as long as we keep the level and type of material differentiation constant.

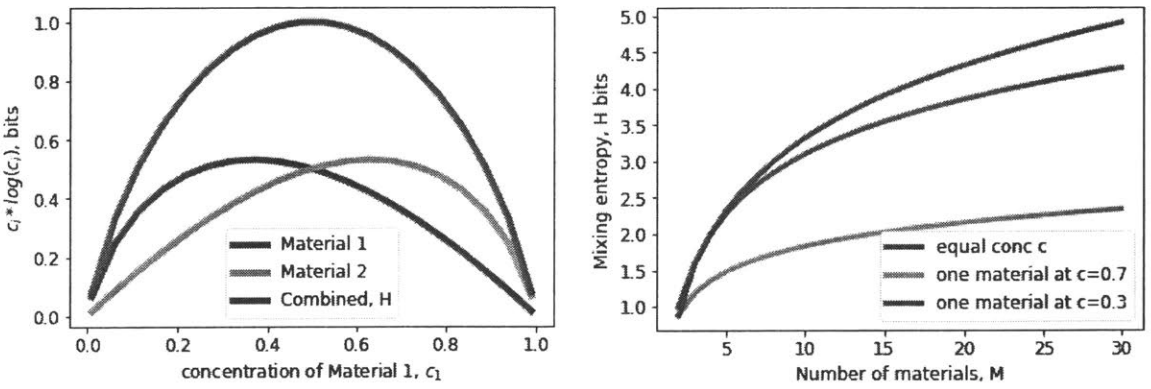


*Figure 6.4 Mixing entropy (i) for a binary material mixture, (ii) for mixtures of different number of materials & material compositions*

This metric comes with 3 shortcomings [118]: (i) it treats each material with equal value; (ii) differences in material size are not accounted for even though changes in size implies changes in entropy; (iii) thermodynamic entropy changes due to energy input to the system to allow for the minimum work for separation [119]. However, for our purpose, we will only use the metric for comparison between the material complexity of the material streams before and after the separation processes. As such, these shortcomings will not have much influence on the comparison.

In the context of evaluating the recovery chain, this mixing entropy measure is a good gauge of the material complexity of the end-of-life vehicle entering the chain. ELVs are growing more and more complex with some materials being partially replaced with less expensive or more lightweight materials or new materials being introduced through improved metal alloys (e.g. high-strength steel, magnesium or aluminum alloys) or new functionalities (e.g. new electronics sub-systems). In [4], [118], Dahmus and Gutowski show that material mixing in ELVs, as measured by mixing entropy, generally increased over the last half-century, with a 2000s era vehicle increasing in complexity by 0.7 bits as compared to a 1950s era vehicle, as shown in Figure 1.4. For our case, besides the base-case of a whole ELV, we will also look at the mixing entropy of partially-disassembled vehicles. Depending on what automotive parts are removed, the resulting ELV hulks can have either a higher (if the major materials decrease in quantity) or lower (if the minor materials decrease in quantity) mixing entropy as compared to a whole ELV.

While the original use of mixing entropy is to represent the difficulty of separating materials from their product, we can extend the use to examine the material composition of the recovered scrap outputs after separation at a material recovery facility. If separation has been effective, as compared to the input ELV's mixing entropy, we expect to have a lower mixing entropy in the valuable scraps' output streams, with the target material being in high concentration, relative to other minor materials that remain due to imperfect separation. Conversely, we expect a higher mixing entropy in the non-valuable output streams, due to the large number of non-valuable materials that should accumulate there.

## 6.2 Economic metrics

Economic metrics are useful when doing a cost or value analysis of recovery systems, with costs including raw material costs as well as investment and operation costs. In the literature in the field of material recovery, economic metrics have been applied in different studies looking at boundaries 1 & 2 of material recovery chains of different end-of-life products. In [101], [117], Ip, Testa et al. consider the inputs and outputs of an existing material recovery facility for municipal household waste to estimate its profits, given the operating costs, raw material costs and scrap revenues. Profit was used as an economic metric for evaluating and optimizing different network configurations of the sorting equipment. Similar economic evaluation was done in [100] to look at design of separation systems for plastics. It is useful to note that while the output scraps are sold as material commodities on global spot markets, there exists varying price-purity points [100], as well as additional revenues if a certain scrap grade is achieved, through certain governmental subsidies depending on the country [101], [117]. Other researchers have examined the economic benefits of processes upstream of boundary 1, i.e. disassembly. In the context of ELVs, Coates & Rahimifard have undertaken case-studies to examine the costs of dismantling plastic auto parts for direct recycling, with the manual labor costs outweighing the revenues from material sale [17]. In [120], Xu et al. examined the process costs of remanufacturing automotive parts.

Besides operational profit, a value-based metric is another type of economic metric suggested by [121]–[123]. A value-based metric augments mass-based recovery measures with the economic values of the material flows in and out of the system. In [121], Villalba et al. defines the "recyclability" index for a material as $V_p/V_m$, where $V_p$(\$/kg) and $V_m$(\$/kg) are respectively its post-recycle and minimum value in primary form, with the assumption that "the recyclability of materials will be reflected by their monetary value" [121]. Gregory, Atlee & Kirchain extend this metric to the boundaries of a material recovery system, i.e. boundary 2, and suggest 2 new value-based mass recovery indices [122], [123]:

$$\text{Value-Retention weighted mass recovery index} = \frac{\sum_j Vp_j m_j}{\sum_i \sum_k Vm_{ki} m_{ki}}$$

$$\text{Value-Added weighted mass recovery index} = \frac{\sum_j Vp_j m_j - \sum_i Vr_i m_i}{\sum_i \sum_k Vm_{ki} m_{ki} - \sum_i Vr_i m_i}$$

where $m_x$ represents mass of a given flow, subscripts $i$ and $j$ represent values for inflows and outflow, $k$ represents the kth embedded material in a given flow, and $V_{r_i}$ represents the value of flow $i$, i.e. price

of end-of-life product paid by recycler [122]. The value-retention measure aims to capture the effect of down-cycling reflected by the difference between the primary and secondary material values. The second measure aims to capture the added value of the recycling processes ($Vp - Vr$), normalized by the maximum possible added value ($Vm - Vr$). Using those 2 metrics, they compared different end-of-life scenarios involving part or all of dismantling, shredding and separation processes, using process-based cost models for end-of-life electronics recycling [122], [123].

Few research papers have looked beyond boundary 2 to incorporate the effect of material recovery on secondary metal production within an economic metric. In [124], Li et al. examined the cost-effective usage of secondary aluminum scraps of different grades produced by sorting to meet production specifications of the final aluminum alloys produced. However, their focus was only on the downstream material recovery processes, i.e. they consider a cost-optimization problem during secondary aluminum production from general aluminum scraps.

In this thesis work, we seek to evaluate the value of the scrap recovered from end-of-life vehicles as felt further downstream at the boundary 3 of the recovery system given in Figure 6.1. We thus propose the Effective Scrap Value as follows.

### 6.2.1 Effective Scrap Value

We desire to specify the economic value of the recovered scrap that is used as input to a secondary metal process to produce a valuable metal alloy. The effective scrap value will depend on the revenues for the mass of alloy produced and the cost of raw materials (for dilution and alloying) and the processing costs:

$$Real\ scrap\ value = revenue_{alloy} - cost_{raw\ materials} - cost_{processing}$$

However, this calculation is complicated for a couple of reasons: the revenue term depends on what alloy is produced from the scrap and is subject to market dynamics that determine the produced alloy pricing; and the processing cost varies by furnace operations. As we are concerned only with the effective value of the scrap, we will view this as the displaced costs of raw materials due to the use of scrap during secondary production instead of the use of primary metal during primary production, while accounting for costs for dilution and additional alloying needed during secondary production. To calculate it, we are going to compare the raw material costs during the secondary metal production (for the calculated addition as solved by the optimization formulation) to that which would have been incurred for the primary metal production of a final alloy of similar composition and mass. Thus, we define the effective scrap value as this difference normalized over the mass produced:

$$Effective\ scrap\ value = \frac{primary\ cost - Secondary\ cost}{mass\ produced}$$

$$= \frac{(\sum_j c_j z_j^* + \sum_j c_j x_j) - (\sum_j c_j z_j^* + c_{scrap} X)}{\sum_j z_j^* + x_j}$$

$$= \frac{\sum_j c_j x_j - c_{scrap} X}{\sum_j z_j^* + x_j}$$

Where $c_{scrap}$ is the cost/kg of the metal scrap, $X$ is the mass (kg) of scrap, $x_j$is the amount (kg) of material $j$ contained in the scrap, $c_j$ is the cost (\$/kg) of material $j$ in primary raw material form, $z_j^*$ is the calculated mass (kg) of material $j$ added as raw material to meet production requirements. This includes the primary metal added for dilution, as well as alloying elements, as shown in the figure below. The amount needed of these raw materials can be calculated by the blending model, as described in Chapter 5. Note that because we want to quantify the added value of using secondary materials to displace primary metals as raw materials, we use the cost of the displaced primary raw materials in our calculations. Additionally, $\sum_j x_j$ represents the useful and valuable materials found in the scrap, such that $\sum_j x_j \leq X$. For instance, if the metal scrap contains polymers, these materials would effectively get removed in the dross waste during the metallurgical pyrolysis process. Additionally, other non-valuable materials found in the scrap, could include the tramp metal elements (e.g. copper in ferrous scrap) if they are found in too high concentration. Hence, even though the scrap cost is inflated by such useless materials found in its composition, they contribute no effective value.

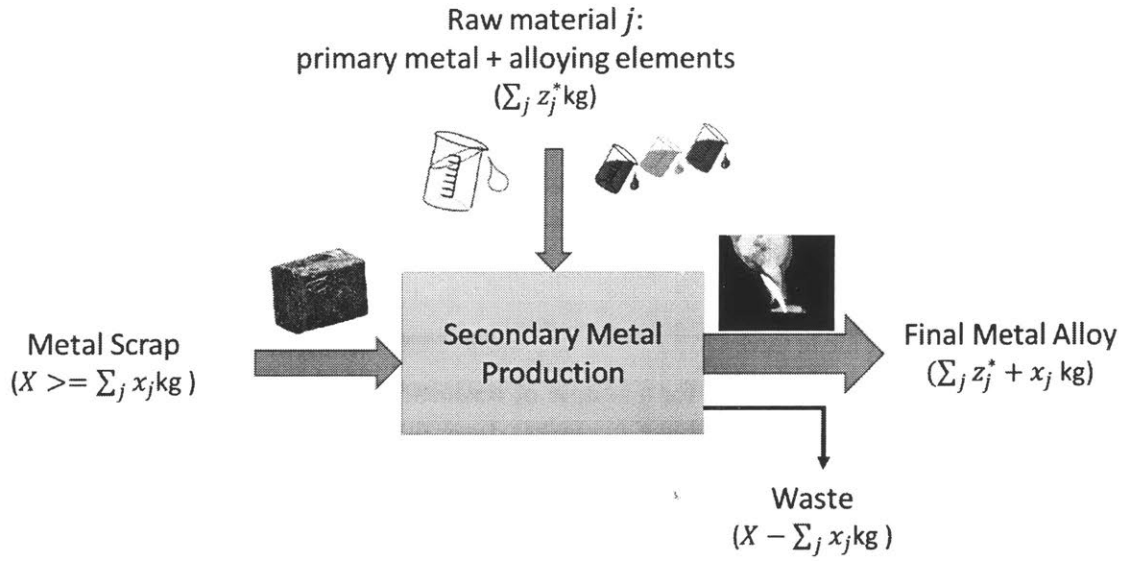


*Figure 6.5 Material flows during metal secondary production*

### 6.2.2 Economic Scrap Value Index

Similar to the value metrics proposed by [122], [123] for the case of material recovery up to boundary 2, we propose a new value metric to encompass the mass flow happening downstream at boundary 3 during secondary metal production. We define the economic scrap value index as follows, with the same nomenclature as in Figure 6.5:

$$EI = \frac{economic\ value\ of\ scrap}{economic\ value\ of\ produced\ alloy}$$

$$= \frac{\sum_j c_j x_j}{\sum_j c_j (x_j + z_j^*)}$$

Note that the actual market price of the scrap ($c_{scrap}X$) could also be used for the economic value of scrap. This would give a lower value of EI, as typically, $\sum_j c_j x_j > c_{scrap}X$. However, the scrap price only gives value to the main material, e.g. aluminum in Twitch scrap, while the economic values of other trace metals (useful if contributing to alloying needs) in the scrap are not accounted for. This metric serves to quantify the actual effectiveness of the metal scrap at secondary metal production. A high scrap value index means that the scrap is of high quality and content, and required little dilution against metal contaminants, or little amount of alloying elements to be added. Beyond using a ratio of mass flows, using cost as a weighting factor helps to capture the effects of different metal elements found in the metal scrap in minute amounts. These metal elements could either come from specific auto parts, e.g. chromium from chromium-plated wheels or bumpers, or from trace metal elements in major metal alloys, e.g. the magnesium content (3-5%) in aluminum alloys of 5000 series. As more and more alloys are adopted in vehicle designs to achieve lightweighting, we want to capture the effect of unintentional flows of alloying elements. If at secondary metal production they end up in a final metal alloy that unfortunately does not require them as an alloying elements, they are lost. In fact, Ohno et al calculated that 8% of the alloying elements used in steel production can come from ELV-derived steel scrap [125]. Despite being in minute amount, the fate of these alloying elements can be captured if their masses are weighted by the corresponding primary material cost, as these alloying elements are usually expensive, e.g. chromium, titanium etc. Thus, such a metric penalizes scrap metals that are down-cycled, i.e. the potential alloying elements in their composition end up unused in a final produced alloy, which does not require them.

## 6.3 Environmental metrics

For material recovery processes, the environmental potential of such processes are often measured in terms of the energy savings involved when using metal scrap for secondary production instead of primary raw materials for primary production. In [100], [126], Wolf & Gutowski show that the energy usage ($10^4$-$10^5$ J/kg) during the material recovery processes of shredding and separation are several orders of magnitude less than the thermal manufacturing processes ($10^6$-$10^7$ J/kg) for these materials, see Figure 6.6. Moreover, the embodied energy, i.e. total energy required for the life-cycle from mining to production, of materials, which are typically recycled, ranges from $10^7$-$10^9$ J/kg [5], which is much higher than the material recovery process energy usage. In [7], Sawyer-Beaulieu constructed the life-cycle inventory (LCI) of ELV shredding processes, using data collected from sites in Canadian facilities. The measured average electricity usage was comparable to the energy usage estimated in [100], [126], $10^5$ J/kg. In the LCI, Sawyer-Beaulieu accounted for processed-based water flow and air emissions associated with the shredding-separation processes, as well as for energy-based air emissions, see Table 6.1 below. Note that for energy-based air emissions, the system boundary was expanded to include the electricity production using Ontario data. However, Sawyer-Beaulieu did not account for energy costs or emissions for related transportation, heating systems, or landfilling.

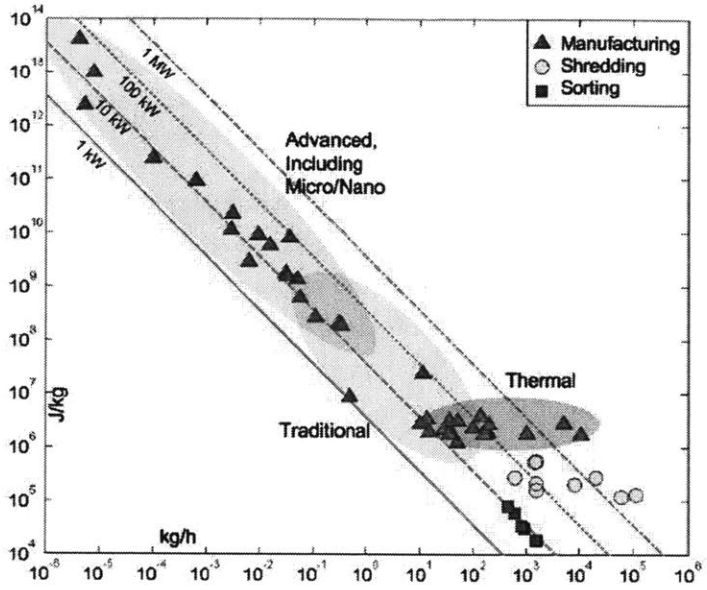


*Figure 6.6 Energy intensity and mass flow rate for a variety of manufacturing and recycling processes [100], [126]*

| **Shredder System Energy Input & Emission Outputs** | **Quantity per kg of shredder input feed** |
|---|---|
| Electrical energy usage | $1.0 \times 10^{5}$ J/kg |
| Process water usage | $5.7 \times 10^{-3}$ L/kg |
| $CO_2$ emission from electrical power generation | $8.6 \times 10^{-3}$ kg/kg |
| $SO_2$ emission from electrical power generation | $3.2 \times 10^{-2}$ g/kg |
| $NO_2$ emission from electrical power generation | $1.1 \times 10^{-2}$ g/kg |
| Particulate matter air emissions | $1.6 \times 10^{-2}$ g/kg |

*Table 6.1 Measured electricity usage and associated air emissions for an actual ELV shredder facility, adapted from [18]*

To look holistically at the environmental impact of a product, a life cycle assessment (LCA) is generally used to define the burden during the phases of production, use and end-of-life. For products such as waste electronics, the environmental impact of precious metals, as calculated by an LCA, stands out. For instance, in [127], Stevels et al. demonstrated that recovering 1 mg of gold has the same environmental effect as recovering 1-20g of common metals and plastics. However, while much LCA research has focused on the production and use phase, determination of the recycling burden during the end-of-use phase is still a challenge. In [128], Huisman et al. tackle this challenge by developing the QWERTY (Quotes for environmentally Weighted RecyclabiliTY and Eco-Efficiency) method by performing an LCA from the starting point of end-of-life phase only. Such a method accounts for the process flows surrounding collection, transportation, dismantling, shredding, separation, secondary material processing, disposal routes at landfill and incineration [128]. The environmental metric scoring is done using the Eco-Indicator'99 method, with the environmental data for these processes coming from [128]. In [129], Soo et al. focused only on the secondary aluminum processes, doing an LCA to evaluate the environmental impact of dilution and quality losses when processing different grades of aluminum scrap.

In theory, an environmental metric is an ideal metric to evaluate the recyclability of a product, as it accounts for different facets of environmental impact, including energy usage and associated emissions, process-based air and land emissions. However, it requires a large amount of environmental data, and it is very sensitive to the processes considered, i.e. where the system boundary is drawn. For the purpose of this thesis, we are not going to use any environmental metrics and instead will look to thermodynamic metrics as a proxy for evaluating environmental impact.

## 6.4 Thermodynamic metrics

While environmental metrics require in-depth accounting of the material and energy flows of all processes involved during material recovery as well as upstream of it, thermodynamic metrics can provide a more succinct accounting. In literature, exergy, a thermodynamic measure of the energy and resources in a system, has been recently used to evaluate the quality losses in resource systems. Exergy is defined as the available energy or the amount of energy that can be extracted as useful work [130], and is the maximum amount of work that may be theoretically performed [131].

There has been a recent push in literature to use exergy, as opposed to energy, as a measure of resource usage as it can capture energy amounts from energy resources together with chemical exergy of materials using the same physical units of joules [132]–[136]. Exergy captures quantity as well as quality: besides waste flows, irreversibilities and process inefficiencies are captured during conversion of resources into products. This thermodynamic approach has been developed in literature and software within Life-Cycle Assessment tools, and is known as the cumulative exergy demand (CExD) method: for instance, CExD indicators now exist within the database of LCA software, e.g. "ecoinvent", [133], [137] or "SimaPro" [136] . Cumulative exergy of materials is the sum of all exergies required to produce the minerals from their natural resources [114]. The exergy data in that database is taken from the works of Szargut, who coined the term cumulative exergy consumption instead [137]. The exergy data quantifies the total exergy requirement of a product, based on energy usage (chemical exergy of fossil fuels, thermal exergy, kinetic exergy, etc) and material resource usage (chemical exergy from mineral ores) [137], [138]. In the ecoinvent database, the chemical exergy of elementary metal from mineral ores included a CExD concentration factor and an allocation factor: the concentration factor penalized the exergy inversely proportional to its concentration if the elementary metal were in low concentration; the allocation factor divided the mineral's exergy between the elementary metals found in the ore according to their revenue or mass ratio [137].

For the purpose of this research, we are not concerned with the process energy flows during the material recovery processes. As discussed in the previous section, these energy flows, hence energy-based exergies, are of much smaller order of magnitude compared to energy requirements for other life-cycle processes such as extraction. However, if included, this could be a future consideration to improve the current proposed modeling framework, using namely the works of Sawyer-Beaulieu, who has estimated the energy consumption during dismantling, shredding and separation operations at a Canadian ELV dismantling and shredding facilities [7]. Further work will also be needed to account for energy flows for the downstream processes, i.e. smelting at steel or aluminum secondary production

plants, and waste recovery from the Automotive Shredder Residue (ASR) sent to waste-recovery facilities.

We will thus focus on the exergy content of our material flows. In the context of ELV treatment modeling, this metric was proposed by Amini et al. to evaluate Aluminum recovery in particular [114]. While grade and recovery rate metrics evaluate the quality of the material flow at the scrap outputs, they do not encompass the bigger picture, i.e. the impact on downstream process of secondary metal production. At this step, dilution and other third-order losses occur, due to material resources which enter the system, i.e. diluting materials (e.g. primary raw material for Aluminum during Aluminum metal production) and alloying materials. The need for these losses was explained in Chapter 5. Amini et al. used chemical exergy to quantify the quantity and quality losses, and cumulative exergy to quantify the dilution and other third-order losses [114]. In effect, Amini et al. augmented the mass flows involved by using exergy as a weight factor, in order to capture such losses.

More recently, Ortego et al. proposed thermodynamic rarity as a metric, as an extension of exergy [131], [139].

### 6.4.1 Thermodynamic rarity

The thermodynamic rarity is defined by Valero as "the amount of exergy resources needed to obtain a mineral commodity from bare rock" , and is the sum of the embodied exergy costs and the exergy replacement costs [131], [139]. The embodied exergy cost is similar to the term "cumulative exergy consumption" coined by Szargut [138]. As highlighted in Figure 6.7, from a life cycle assessment point of view, the embodied exergy costs represent the cradle-to-gate phase, which includes the processes of conventional mining and concentration and refining costs, similar to typical LCAs with exergy as described in the previous section. The novelty in the metric is the **exergy replacement costs**, which represent the grave-to-cradle phase. The exergy replacement costs bring an additional appreciation of the value of minerals, beyond their chemical exergy to include their concentration exergy. In fact, the authors argue that there is no difference in chemical exergy of the materials between the grave state and the cradle state, but there is significant difference in concentration exergies between these 2 states [131]. The concentration of a mineral element at the cradle, i.e. in mines or mineral deposits, is high, while at the grave state (referred to as the Thanatia crust by the author), its concentration is low as it is very much dispersed by comparison [140].

The exergy replacement cost ($b^*_{ci}$) of a mineral $i$ is thus derived from its difference in concentration exergies at the grave state in the Thanatia crust (mineral concentration $x = x_c$) and at the cradle state in mines (mineral concentration $x = x_m$). The concentration exergy at state $x$, $b_{ci_{(x)}}$, and exergy replacement cost, $b^*_{ci}$, are respectively given by [131], [139]:

$$b_{ci_{(x)}} = -RT_o\left[lnx + \frac{(1-x_i)}{x_i}\ln(1-x)\right]$$

$$b_{ci}^{*} = k_{(x=x_c)} b_{ci_{(x=x_c)}} - k_{(x=x_m)} b_{ci(x=x_m)}$$

Where $R$ is the universal gas constant (8314 kJ/kmol K), $T_0$ is the reference temperature set at 298.15 K, and $k$ is a dimensionless variable representing the unit exergy cost of the mineral at the cradle ($k_{(x=x_m)}$) or grave state ($k_{(x=x_c)}$). The variable $k$ represents the technological cost required for concentrating, as done in mineral extraction to ore grade minerals for example [131], [139]. Valero, after decades of work, has compiled the values of the parameters for the exergy replacement costs and embodied exergy costs for different metal minerals [131]. The resulting exergy replacement costs, embodies exergy costs and thermodynamic rarity are listed in Table 6.2 below.

Thermodynamic rarity was used as a metric in [139], [140] to highlight the importance of critical metals (Mo, Co, Nb, Ni) found in either auto-parts of such materials, or within other metal alloys. While these critical metals constitute less than 1% by weight of a car's metal content, they represent 7% of a car's thermodynamic rarity [139]. On the other hand, while Fe, Al and Cu constitute more than 90% by weight of the metal content, they represent only 60% of a car's thermodynamic rarity [140].

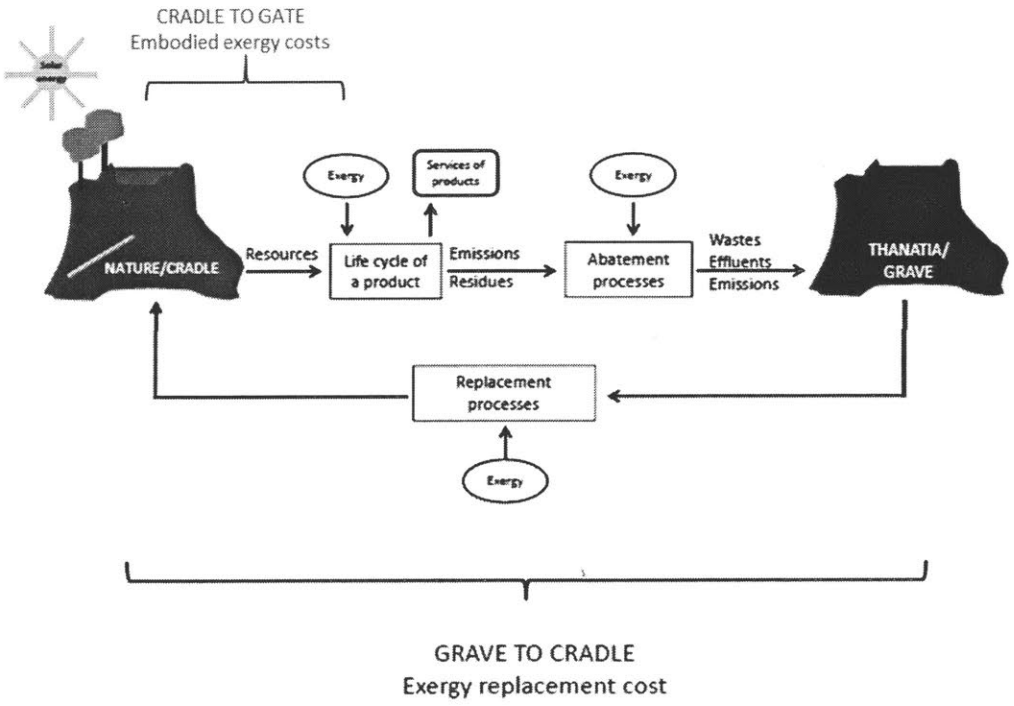


*Figure 6.7 Schematic of the two exergy components of thermodynamic rarity: embodied exergy costs (cradle-to-gate) and exergy replacement costs (grave-to-cradle), adapted from [131]*

| Metal | Embodied Exergy (GJ/ton) | Replacement Exergy Costs (GJ/ton) | Thermodynamic Rarity (GJ/ton) | Primary Ingot Price(€/ton) |
|---|---|---|---|---|
| **Ag** | 1,566.00 | 7,371 | 8,937 | 427,966 |
| **Al** | 34.4 | 627.24 | 661.64 | 1,644 |
| **As** | 28 | 399.84 | 427.84 | 716 |
| **Au** | 108,626 | 546,057 | 654,683 | 31,694,915 |
| **Ba** | 1 | 38.34 | 39.34 | 109 |

| | | | | |
|---|---|---|---|---|
| **Be** | 457.2 | 252.73 | 709.93 | 411,017 |
| **Bi** | 56.4 | 489.22 | 545.62 | 14,153 |
| **Cd** | 542.4 | 5,898 | 6,440.40 | 1,246 |
| **Ce** | 523 | 97 | 620 | 11,780 |
| **Co** | 138 | 10,872 | 11,010 | 50,254 |
| **Cr** | 36.4 | 4.5 | 40.9 | 1,907 |
| **Cu** | 56.7 | 291.7 | 348.4 | 4,788 |
| **Dy** | 384 | 348 | 732 | 11,780 |
| **Fe** | 14.1 | 17.75 | 31.85 | 69 |
| **Ga** | 610,000 | 144,828 | 754,828 | 268,644 |
| **Gd** | 3,607 | 478 | 4,085 | 11,780 |
| **Ge** | 498 | 23,749 | 24,247 | 1,059,322 |
| **Hg** | 409 | 28,298 | 28,707 | 45,508 |
| **In** | 3,320 | 360,598 | 363,918 | 440,508 |
| **La** | 297 | 39 | 336 | 11,780 |
| **Li** | 432 | 546 | 978 | 3,847 |
| **Mg** | 0 | 145.73 | 145.73 | 1,915 |
| **Mn** | 57 | 16 | 73 | 1,025 |
| **Mo** | 148 | 908 | 1,056 | 12,288 |
| **Nb** | 360 | 4,422 | 4,782 | 35,287 |
| **Nd** | 592 | 78 | 670 | 11,780 |
| **Ni** | 234 | 524 | 758 | 10,000 |
| **Pb** | 4 | 37 | 41 | 1,703 |
| **Pd** | 2,870,013.09 | | 2,870,013.09 | |
| **Pr** | 296 | 873 | 873 | 11,780 |
| **Pt** | 2,870,013.09 | | 2,870,013.09 | |
| **Rh** | 156 | 103,087 | 103,087 | 2,288,136 |
| **Ru** | 2,870,013.09 | | 2,870,013.09 | |
| **Sb** | 13.4 | 487.89 | 487.89 | 6,102 |
| **Sn** | 26.6 | 452.95 | 452.95 | 17,712 |
| **Ta** | 3,083 | 485,911 | 485,911 | 200,000 |
| **Te** | 589,405.30 | 2,825,104.30 | 2,825,104.30 | 65,254 |
| **Ti** | 196.45 | 203.12 | 203.12 | 3,195 |
| **V** | 517 | 1,572 | 1,572 | 19,153 |
| **W** | 594 | 8,023 | 8,023 | 32,034 |
| **Y** | 1,198 | 1,357 | 1,357 | 11,780 |
| **Zn** | 41.9 | 196.93 | 196.93 | 2,682 |
| **Zr** | 1,371.50 | 654.43 | 2,025.93 | 19,237 |

*Table 6.2 Thermodynamic rarity values for metals and their market prices, adapted from [139]*

Thermodynamic rarity is an ideal metric with which to value materials, as it captures and combines data about the energy needed for extraction and processing (embodied exergy), as well as about the

abundance of a material in Nature, such that a metal which is more abundant and concentrated in mines has less value. Therefore, we propose using thermodynamic rarity to weight the mass flows throughout the material recovery processes to create an additional metric. Similar to the Economic Scrap Value Index, we can weigh the mass flows surrounding scrap secondary processing, using thermodynamic rarity instead of material cost for $c_j$ for the material $j$:

$$\text{Thermodynamic Scrap Value Index} = \frac{\sum_j c_j x_j}{\sum_j c_j (x_j + z_j^*)}$$

We believe that thermodynamic rarity could be a better proxy than economic costs of materials to convey the inherent value of the materials recovered or lost. While its market price is affected by the geography, political situation, variable demand and supply, the specific thermodynamic rarity is an intensive property inherent to the material and is thus more stable metric than economic cost. To illustrate the correlation between economic value and thermodynamic rarity, we have plotted metals' thermodynamic rarity against the spot price for their metal ingots, with data from USGS and Valero's database for thermodynamic rarity [140]. One can observe a linear relationship for most metals (metals found in car parts and their alloys are in red), albeit with more variation for precious metals (upper right-hand corner). The only caveat for using thermodynamic rarity as a metric, is its sensitivity to the mineral ore being considered, as the ore determines the concentration exergy of a mineral. In the work of Valero [131], only *one* ore per mineral was considered when calculating the exergy costs. Some minerals, e.g. Aluminum, can come from different ores (bauxite, gibbsite, boehmite, and diaspore), but only gibbsite is considered in the exergy cost calculations in [131].

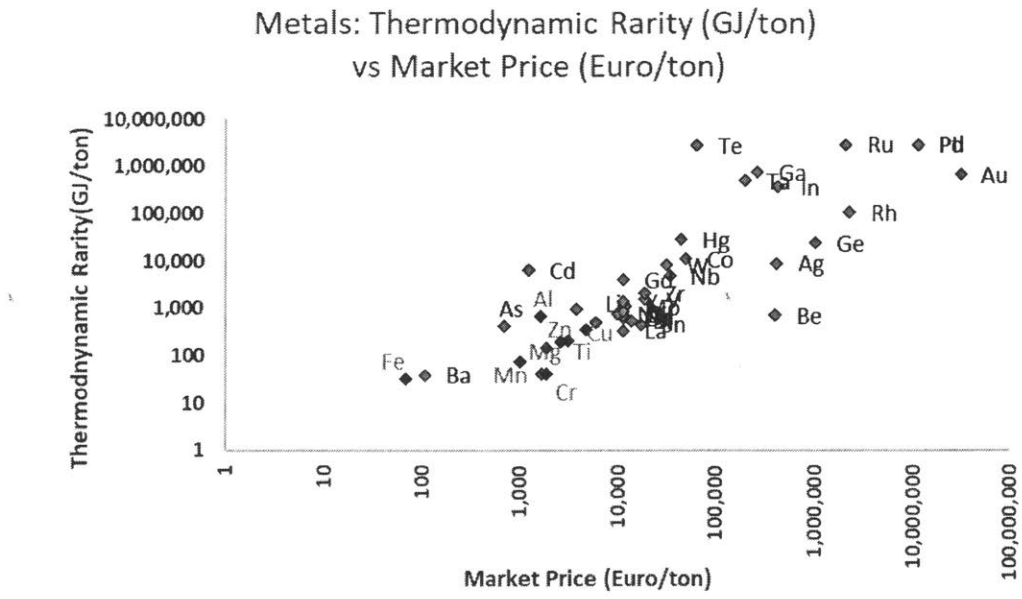


*Figure 6.8 Relationship between thermodynamic rarity and market price of metals, data from [139]*

## 6.5 Overall metrics

So far, we have covered metrics measuring performance at boundary 1 of our material recovery chain: recovery rate, grade and mixing entropy of the collected scrap streams. We then introduced three variations for a scrap value index (effective, economic and thermodynamic) to quantify the value of a scrap, with regard to dilution and alloying consequences downstream during secondary processes. To evaluate the effectiveness of the material recovery processes from an ELV, the overall performance metric needs to be able to capture valuable material recovery from *all* valuable scrap output streams.

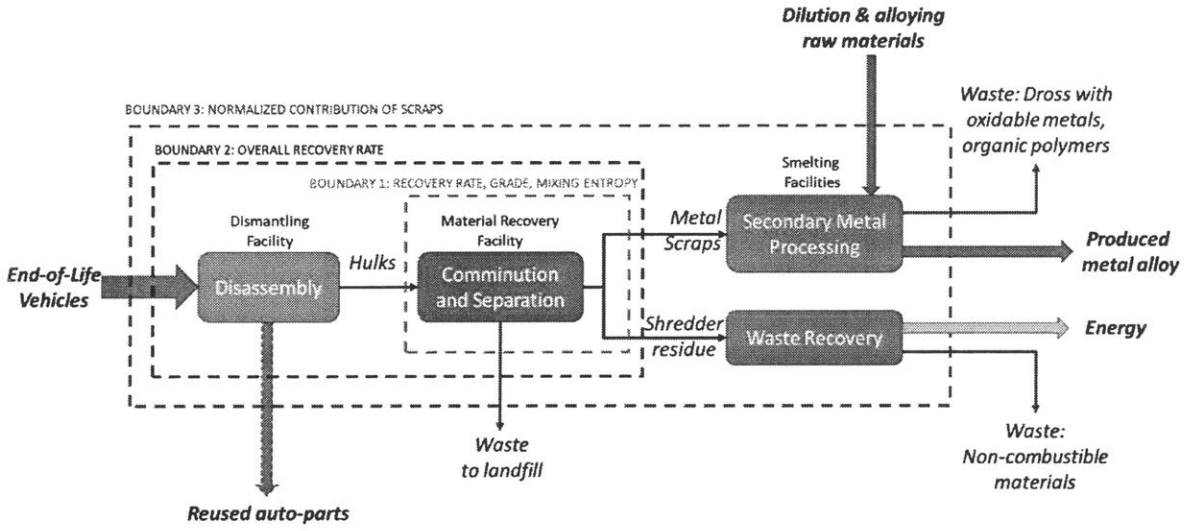


*Figure 6.9 System boundaries for material recovery processes from ELVs, with performance metrics to be used*

In literature, the overall recovery rate (ORR) of an ELV is typically used to determine a car's recyclability, with ORR typically defined as:

$$ORR = \frac{\sum_{j \in J} m_j}{\sum_{i \in I} M_i}$$

Where $m_j$ is the mass of target material $j$ that ends up in the appropriate target material output stream, $M_i$ is the mass of material $i$ that constitutes the input stream to the system, i.e. forms part of the hulk, the set $J$ consists of all the target materials recovered from the system, the set $I$ consists of all the materials within the hulk that enters the system. For our particular material recovery chain with the system boundary 3 as defined in Figure 6.9, we will consider 3 target output streams: Fe scrap with ferrous (Fe) as the target material, Al scrap with Aluminum (Al) as the target material, ASR fraction with plastics as the target material, i.e. $J = \{Ferrous, Aluminum, plastics\}$. Hence, ORR for our case would be:

$$ORR = \frac{(mass_{Fe})_{Fe\ Scrap} + (mass_{Al})_{Al\ Scrap} + (mass_{plastics})_{ASR}}{(\sum_{element\ j} mass_j)_{hulk}}$$

### 6.5.1 Normalized contribution of scraps

Similar to the development of the scrap value index, we want to expand the boundary from boundary 2 to boundary 3 (see Figure 6.9) to account for the downstream secondary processes. When we earlier proposed the scrap value index as a metric, we considered only one valuable scrap stream. Now we expand our system boundary to include all valuable scrap streams. We propose below the normalized contribution of scraps, NCS, to augment the general overall recovery rate metric. The inputs for calculating the NCS are:

- A weight $c_i$ to the mass of material $i$ to reflect the value associated with it, whether it is its economic cost or its thermodynamic rarity (value per kg);
- A set ($J'$) of useful and target materials of mass $m'_j$ that end up in the appropriate target material output streams, where a material is useful if it is not down-cycled and lost in the secondary metal produced. A useful material might not be the target material (e.g. Ferrous in the Ferrous scrap) but can still have value if it is also an alloying element within its alloy concentration limit;
- A set $I$ of all materials in the hulk, and $M_i$ the amount of such material $i$;
- The mass ($D_k^*$) of input raw materials $k$ needed for dilution and alloying at the secondary metal processes to produce a pre-determined final metal alloy, with the amount determined cost-optimally by the metal's corresponding blending model;
- A set $K$ of all input raw materials $k$ used for the secondary metal processing from aluminum or ferrous scrap.

Hence, we define NCS as follows:

$$NCS = \frac{\sum_{j\in J'} c_j m'_j}{\sum_{i\in I} c_i M_i + \sum_{k\in K} c_k D_k^*}$$

For our particular material recovery chain with the system boundary 3 as defined in Figure 6.9,

$$\hat{NCS} = \frac{\left(\sum_{j\in J'_{Fe}} c_j\, mass_j\right)_{Fe\ Scrap} + \left(\sum_{j\in J'_{Al}} c_j mass_j\right)_{Al\ Scrap} + \left(\sum_{j\in J'_{ASR}} c_j mass_j\right)_{ASR}}{\left(\sum_j c_j mass_j\right)_{hulk} + \left(\sum_{k\in K_{Fe}} c_k D_k^*\right)_{Dil\ Fe} + \left(\sum_{k\in K_{Al}} c_k D_k^*\right)_{Dil\ Al}}$$

In simpler terms, NCS is as follows with respect to the mass flows defined at points 1-6 in Figure 6.10:

$$NCS = \frac{(Target + useful\ elements^*)_{at\,2} + (Target + useful\ elements^*)_{at\,3} + (Target + useful\ elements^*)_{at\,4}}{(Target + alloying\ elements + non-target)_{hulk\ at\,1} + dilution^*_{at\,5} + dilution^*_{at\,6}}$$

In effect, such a formulation is able to capture quantity, quality as well as dilution losses: (i) quantity losses are captured by the ratio of target materials at nodes 2-4 and non-target elements at node 1 that end up at landfill; (ii) quality losses are captured by defining the subset of materials in the scrap at nodes 2-4 that are target or useful elements, as opposed to non-target elements; (iii) dilution losses are captured by the mass input at secondary processes, i.e. at nodes 5-6 .

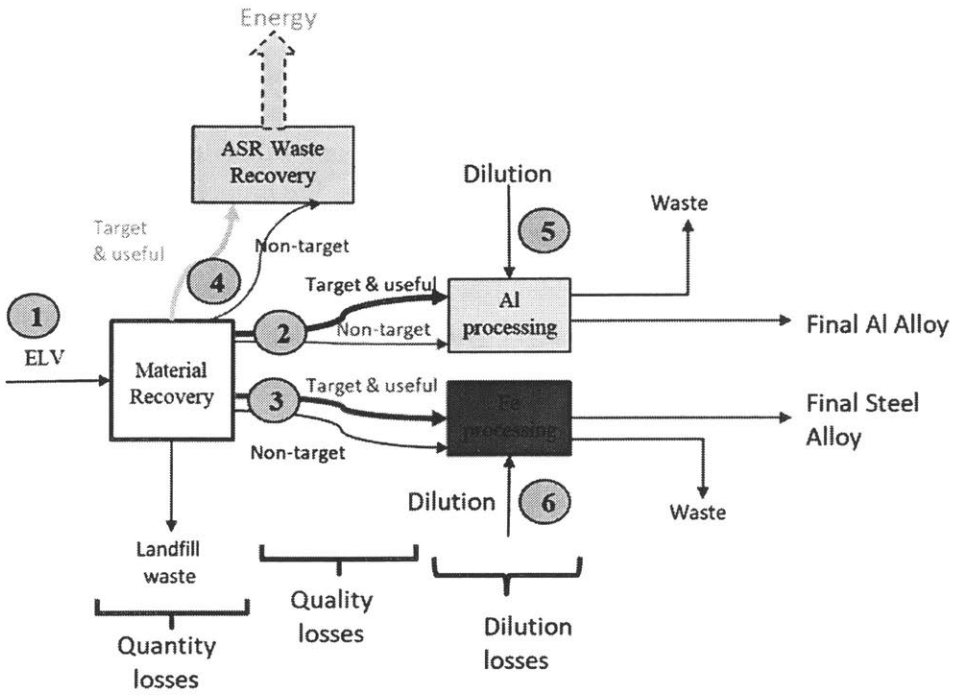


*Figure 6.10 Schematic with material flows of material recovery processes from ELVs, as captured in overall metric (NCS), with quantity, quality and dilution losses*

With NCS as an overall metric to evaluate and ELV's recyclability, we are able to:

(i) Quantify the effect of contamination in the scrap streams through calculated dilution losses;
(ii) Weigh the material flows by their economic or environmental (thermodynamic rarity) values;
(iii) Capture the effect of unintentional flows of valuable potential alloying elements from the hulk to the final metal alloys produced during secondary metal production.

As the material composition of future end-of-life vehicles will get more complex with the diversity of metal alloys as well as electronics used in modern vehicles [59], [125], [140], [141], it is crucial to use an appropriate metric to be able to capture their actual recyclability. With NCS as the objective to maximize, for a given recovery chain network, car designers can iterate over different vehicle input designs, with different sets of alloy compositions:

$$\underset{\substack{\textit{vehicle design}\\ \textit{alloy composition}}}{\arg\max} \quad X\,(\textit{vehicle input}, \textit{recovery chain structure})$$

For example, if at the downstream end of the recovery chain Aluminum alloy 3000 series are produced at secondary production, the sweet spot for an ideal alloy composition in the vehicle design could be a mixture of Aluminum alloy 5000 series and cast Aluminum. Through NCS, designing for effective recyclability can be achieved by even accounting for unintended flows of critical metals.

### 6.5.2 Example

As an illustration, we pose a hypothetical example with simplified material flows. In Table 6.3 below, we give the material flows for the material recovery chain through the nodes denoted as 1-6 (as defined in Figure 6.10), given in. Note that at nodes 5 and 6, there is input mass flow to the system with dilution and/or alloying materials, as calculated by the blending model for a particular wanted Al alloy (the values in the table are however fictitious).

| Material | Node 1 (Hulk) | Node 2 (Al scrap) | Node 3 (Fe scrap) | Node 4 (ASR fraction) | Node 5 (input at Al Production) | Node 6 (input at Fe Production) |
|---|---|---|---|---|---|---|
| **Fe** | 800 | 10 | 750 | 5 | | Dilution: 300 |
| **Al** | 100 | 80 | 10 | 5 | Dilution: 100 | |
| **Plastic** | 200 | 10 | 20 | 150 | | |
| **Cu** | 30 | 5 | 10 | | | |
| **Mg** | 20 | 5 | | | | |
| **Zn** | | | | | Alloying: 3 | |
| **Cr** | | | | | Alloying: 2 | |
| ***TOTAL (kg)*** | *1150* | *110* | *800* | *160* | *105* | *300* |

*Table 6.3 Example: simplified material flows throughout material recovery chain at nodes defined in Figure 6.10.*

We can calculate our metrics for the Al scrap (node 2) at boundary 1 as follows:

$$Grade_{Al\ scrap} = \frac{80}{110} = 0.72$$

$$Recovery\ Rate_{Al\ scrap} = \frac{80}{100} = 0.80$$

$$Mixing\ entropy_{Al\ scrap} = -\left(-\frac{10}{110} * \ln\left(\frac{10}{110}\right) - \frac{80}{110} * \ln\left(\frac{80}{110}\right) - \frac{10}{110} * \ln\left(\frac{10}{110}\right) - \frac{5}{110} * \ln\left(\frac{5}{110}\right) - \frac{5}{110} * \ln\left(\frac{5}{110}\right)\right)$$

$$= 1.4$$

As simplification, we assume all costs are of unit value ($c_i = \$1/kg$) for the raw materials and $c_i = \$0.5/kg$ for the scrap. For ferrous scrap, we assume that Al contaminant is removed by oxidation, and plastic is removed within the dross, but not Cu. Conversely for the Al scrap, we assume that Mg and plastic are useless, are removed by oxidation and through the dross, while Fe and Cu are contaminants that cannot be removed and create the need for dilution with Al. Thus, we can calculate our metrics for the Al scrap (node 2) at boundary 2 as follows:

$$Effective\ scrap\ value = \frac{(1 * 10 + 1 * 80 + 1 * 5) - 0.5 * 110}{(100 + 3 + 2) + (10 + 80 + 5)} = \frac{40}{200} = \$0.20/kg$$

$$Economic\ Scrap\ Value\ Index = \frac{(1*10+1*80+1*5)}{(1*100+1*3+1*2)+(1*10+1*80+1*5)} = \frac{95}{200} = 0.48$$

We define the material sets as:

$J = \{Fe\ in\ Fe\ scrap, Al\ in\ Al\ scrap, Plastics\ in\ ASR\}$;

$J'_{Fe} = \{Fe, Cu\ in\ Fe\ scrap\}$; $J'_{Al} = \{Al, Fe, Cu\ in\ Al\ scrap\}$; $J'_{ASR} = \{Plastics\ in\ ASR\}$.

Again for simplification, we assume all costs are of unit value ($1/kg). Thus, we can calculate our metrics for the entire system through boundary 3 as follows:

$$ORR = \frac{\sum_{j\in J} m_j}{\sum_{i\in I} M_i} = \frac{750+80+150}{1150} = \frac{980}{1150} = 85\%$$

$$NCS = \frac{\left(\sum_{j\in J'_{Fe}} c_j\ mass_j\right)_{Fe\ Scrap} + \left(\sum_{j\in J'_{Al}} c_j mass_j\right)_{Al\ Scrap} + \left(\sum_{j\in J'_{ASR}} c_j mass_j\right)_{ASR}}{\left(\sum_j c_j\ mass_j\right)_{hulk} + \left(\sum_{k\in K_{Fe}} c_k D^*_k\right)_{Dil\ Fe} + \left(\sum_{k\in K_{Fe}} c_k D^*_k\right)_{Dil\ Al}}$$

$$= \frac{(1*750+1*10)+(1*10+1*80+1*5)+(1*150)}{1*1150+1*105+1*300} = \frac{1005}{1555} = 65\%$$

As expected, accounting for dilution losses make the NCS less than ORR. Note that in this formulation, we have assumed the total mass of useful materials to include that of the contaminants in addition to the main target material (e.g. in Ferrous, 10 kg of copper in addition to the 750 kg of Ferrous), as the contaminant elements are within the concentration limits of the product once dilution is done. Another alternative would be to instead use the mass of the contaminants to meet the element's minimum concentration limits. That minimum concentration could be zero if the element is not an alloying element but a tramp element. In any case, the effect of the dilution costs in the denominator is much more significant than these added contributions of the useful materials in the numerator.

# Chapter 7 Baseline End-of-life Vehicle (ELV) Modeling

This chapter applies the whole material recovery model developed in chapter 2 to 6, on a complete representative end-of-life vehicle. Prior literature on modeling in ELV recycling has typically only used material composition of passenger cars as the starting data. This research project aims to incorporate additional product design and bill of material data, to incorporate the effect of disassembly on the rest of the material recovery processes, as well as the effect of non-liberated particles on metal scrap contamination. The non-liberated particles originate from joints between parts and hence require part definition with joints. At end-of-life, a vehicle can be subject to partial disassembly before arriving at a metal recycling facility (in the US) or a dedicated vehicle recycling facility (in Europe). In ELV disassembly, there is uncertainty about what automotive components are actually removed: as detailed in [7], [12], different components are removed from the ELV at different rates at junk-yards and u-pull-it facilities. This results in different part compositions for the ELV hulks (what is left of the car after the car is disassembled, i.e. after components are removed) that arrive as the input feed to an ELV material recovery facility for shredding and so on.

The end-of-life vehicle (ELV) data we have informs the type of disassembly model we will be using as well as the data processing needed to run it through the shredding and separation models. The data originates from the SM thesis of Zamudio-Ramirez [22] that includes data of a 1995 study with the Vehicle Recycling Development Center, where a vehicle tear-down was performed at a dismantling facility. The same data, in cleaner form, is found in the appendix of the PhD thesis of Kirchain [27], without the joint data. The data consists of an ELV's bill of materials, i.e. information about automotive components, including their weight and material types, and the components' hierarchy. In [22], the part data also contains the type and quantity of joints found in the each listed part.

The database has 550 named components where each component represents a physical entity that can be removed from the vehicle. Some components are stand-alone parts, while others are assemblies of parts. We can categorize each component as being one of the following:

1. an assembly in itself (e.g. drivetrain)
2. sub-assembly, or a part which is a component of an assembly (e.g. drivetrain.CradleSuspension)
3. a stand-alone part (e.g. battery)

To signify the part hierarchy, we use the nomenclature as follows: the assembly part (e.g. drivetrain) is the parent part, while the sub-assembly or child of the parent part is indicated following a ".". For instance, the part name "drivetrain.CradleSuspension" tells us that CradleSuspension is a sub-assembly of the bigger assembly, the drivetrain.

Several changes were made to the original ELV database to prepare it for the material recovery model:

(i) The battery was removed. This happens naturally during the depollution phase: at the junkyard, hazardous materials (e.g. battery, catalytic converter, fluids – see Table 1.1).

(ii) There were originally 74 parts with SKOS (some kind of stuff) as material type, totaling 67kg. From observation, a lot of these parts were electronics, and likely had some amounts of metals and plastics in them. It is important to capture the amounts of aluminum, copper, ferrous, magnesium, zinc, lead specifically, as they are quite prevalent in a car, and need to be accounted for during the downstream processes of secondary metal processing. Hence, we altered these SKOS parts using another ELV database, namely a bill of material for a recent U.S passenger car. For confidentiality, we cannot disclose this other ELV database. This other database is more complete with material types available at a more granular level. We identified the corresponding relevant parts in the baseline ELV database and then used their composition ratios of aluminum, copper, ferrous, magnesium, zinc, lead, plastics (SKOP) and other metals to calculate the corresponding amount of these materials in the original SKOS parts. In effect, we create a set of new parts to reflect this additional material information, identified with part IDs from 1000 onwards, to reflect the amount of aluminum, copper, ferrous, magnesium, zinc, lead, plastics (SKOP) and other metals (now labeled as SKOS in the new expanded database). As an example of this alteration, "InstrumentPanel.Cluster" now has 8 sub-assembly parts: "InstrumentPanel.Cluster.Al", "InstrumentPanel.Cluster.Cu", "InstrumentPanel.Cluster.Fe", "InstrumentPanel.Cluster.Mg", "InstrumentPanel.Cluster.Zn", "InstrumentPanel.Cluster.Pb", "InstrumentPanel.Cluster.SKOS", "InstrumentPanel.Cluster.SKOP". Originally, the ELV database consisted of a total of 44.7 kg of electronic parts originally labeled as SKOS. Using the new database for guidance, we have replaced the 44.7 kg of SKOS with the following material feeds: Al: 6.6kg, Cu: 5.8kg, Fe: 22.2kg, Mg: 0.05kg, Zn: 0.17kg, Pb: 0.002kg, SKOP: 1.1kg, SKOS: 8.9kg. The new expanded ELV database can be found in Table A-1 of Appendix A.

Section 7.1 expands on the material and joint data used for our baseline ELV case-study. For modeling disassembly, our formulation is on a part basis, i.e. we are only concerned with what parts are in an ELV, how the parts are connected to each other and which parts form assemblies. In addition, for disassembly optimization, we require a cost metric to evaluate the cost of removing each part, as described in Chapter 2. Section 7.3 synthetizes the data needed for disassembly modeling.

The results of the disassembly operations determine the material composition of the hulk, i.e. the input material feed to the downstream material recovery processes. In this chapter we will focus on the material recovery modeling of the whole ELV without disassembly, and in chapter 8, we will explore the case where the ELV hulk is subject to stochastic part removal. The modeling of the shredding and separation processes requires a basis transformation, from parts to material particles, and some assumptions to estimate the non-liberated particle flows. Section 7.1 explains the data transformation used on our baseline ELV. Additionally, in section 7.1.4 and section 7.1.5, we will describe the shredder and separation model parameters used. Section 7.2 gives the results of the material recovery model applied to the baseline ELV, i.e. the resulting material particle flows after the shredding and separation processes. The resulting material particle flows enable us to evaluate the output scraps, i.e. ferrous scrap, aluminum scrap and automotive shredder residue (ASR). In section 7.2.3, using the performance metrics developed in chapter 6, we will discuss the overall material recovery performance of an end-of-life vehicle.

## 7.1 Data for Material Recovery Model

### 7.1.1 Material data of automotive components

From the original database's bill of materials, each component is classified by a single material type from the categories: SKOP (some kind of plastics), SKOS (some kind of stuff), ABS (acrylonitrile butadiene styrene), Ferrous, Glass, Aluminum, Carpet, PUR (polyurethane), PE (polyethylene), PP (polypropylene), TPO (thermoplastic olefin), Lead, PC (polycarbonate), Elastomer, Xenoy, PET (Polyethylene terephthalate), Copper, Magnesium, Zinc, PC-ABS (polycarbonate- acrylonitrile butadiene styrene). Each material type has different material properties, and this causes them to have different behavior during the shredding and separation processes. Note the following:

- SKOP and SKOS were used by the database to denote some undetermined plastics, and unclassifiable materials respectively.
- The material properties of SKOP was set to be the average of the plastic materials in the list, i.e. {PET, PE, Xenoy, PC, PC-ABS, ABS, PP, TPO, PUR}.
- Recall that after the data alteration for original SKOS parts, SKOS now denotes metals other than copper, aluminum, ferrous, lead, zinc or magnesium. The material properties of SKOS was set to be the average of all these metals, except lead.
- In Table A-1 of Appendix A, some parts have the material type listed as "Mixed". This is the case for assembly components, as the assembly consists of sub-assembly parts of defined but different materials.

To calculate the material content of the whole ELV from the component database, some care is needed to account for the interrelationships between the components. We use an algorithm, listed in section 7.1.3, to find the material content for each assembly and sub-assembly component, without double-counting the mass of the sub-assembly components.

In the database, we found a few discrepancies between the weight of an assembly and the weights of its components:

- The assembly weight is greater than the sum of its childless sub-assemblies. We then set the effective mass of the assembly ($m_{rest}$) to be the difference, with the density calculated to be the average of those of the materials of the sub-assembly parts.
- The assembly weight is less than the sum of its their childless sub-assemblies. In this unusual case, we set the effective weight of the assembly to zero.

Figure 7.1 below illustrates the case for an assembly A which has 2 levels of sub-assemblies: $A.\alpha$ and $A.\beta$ , and $A.\alpha.\rho$ and $A.\alpha.\pi$. Note that in this case, the childless sub-assemblies (in orange) are $.\beta$ , $A.\alpha.\rho$ & $A.\alpha.\pi$. The effective mass of the assembly, i.e. mass of the rest of the assembly is calculated as follows:

$$m_{rest} = m_A - (m_{A.\beta} + m_{A.\alpha.\rho} + m_{A.\alpha.\pi})$$

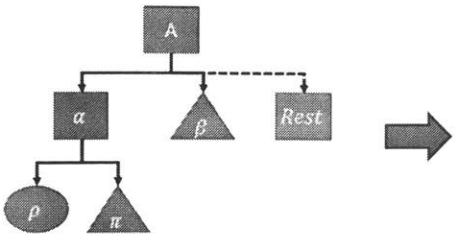


| Material | Mass |
|---|---|
| Mixed | $m_{rest}$ |
| Material_1 (triangle) | $m_\beta + m_\alpha$ |
| Material_2 (circle) | $m_\rho$ |

*Figure 7.1 Mass balance and part hierarchy for assembly parts (parents) and sub-assembly parts (children)*

For a more realistic ELV material composition, we update the material type for the assembly parts that were originally specified as "Mixed": in these cases, we set the material type of the remainder of the assembly ($m_{rest}$) to be the same as the dominating material type among their sub-assembly parts. In our ELV database, there was 162 such parts.

The table below shows the final material composition of the baseline ELV, as calculated from the parts database, making sure not to double-count the mass in sub-assembly or assembly parts. We can observe that there tends to be many lightweight automotive components made of a certain type of plastics, whereas there are bigger but fewer components made of metals. From Figure 7.2, we can observe that ferrous is the main material type (75 % of ELV weight), followed by plastics and elastomers (15%). While aluminum makes up only 7% of the material composition, we should keep in mind that the baseline ELV chosen is from the early 1990s, at which time vehicles were still steel-intensive.

| **Material** | | **Weight (kg)** | **Weight (%)** | **Part Frequency** |
|---|---|---|---|---|
| **Metal** | **Ferrous** | 1034.78 | 75.25 | 187 |
| | **Aluminum** | 96.63 | 7.03 | 72 |
| | **Copper** | 12.04 | 0.88 | 34 |
| | **Zinc** | 2.71 | 0.20 | 26 |
| | **Magnesium** | 1.73 | 0.13 | 28 |
| | **Lead** | 0.08 | 0.01 | 29 |
| | **SKOS** | 6.47 | 0.47 | 28 |
| **Plastics/ Elastomers** | **SKOP** | 59.24 | 4.31 | 180 |
| | **Elastomer** | 51.13 | 3.72 | 22 |
| | **Carpet** | 29.87 | 2.17 | 31 |
| | **Xenoy** | 18.24 | 1.33 | 2 |
| | **PUR** | 12.61 | 0.92 | 13 |
| | **ABS** | 9.75 | 0.71 | 27 |
| | **PP** | 9.10 | 0.66 | 36 |
| | **PET** | 4.69 | 0.34 | 3 |
| | **TPO** | 2.71 | 0.20 | 6 |
| | **PE** | 1.84 | 0.13 | 10 |
| | **PC** | 0.60 | 0.04 | 4 |
| | **PC-ABS** | 0.40 | 0.03 | 2 |
| **Others** | **Glass** | 20.53 | 1.49 | 9 |
| **TOTAL (kg)** | | 1375 | | |

*Table 7.1 Material composition and frequency in parts for baseline ELV*

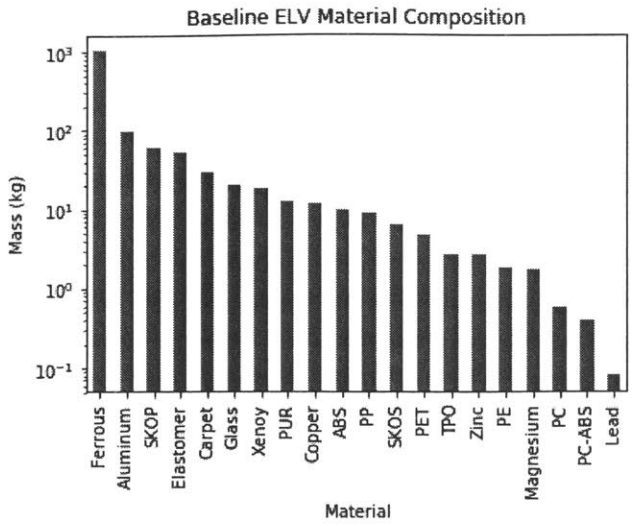


*Figure 7.2 Material composition for baseline ELV*

The above material composition only considers the material composition of the parts. However, an end-of-life vehicle also contains numerous joint fasteners, which form non-liberated material types downstream in subsequent material recovery processes. Hence, in order for our model to capture contamination due to such non-liberated particles, we need additional information about the joint fasteners that are present in the different parts.

### 7.1.2 Joint data of automotive components

The database from [22] contains joint data, specified as the quantity of each type of fasteners that each part has, if any. However, the database comes with a caveat that not all the existing joints in an ELV were actually recorded when the vehicle tear-down was done [22] . Hence, the calculated amount of contamination due to non-liberated joint particles further downstream is a lower bound of what might happen in reality. There are 697 joints of 43 types, whose names are as denoted in the database. We did not consider glue/adhesive as a joint type as it constitutes a form of non-liberated particles that is not as prevalent as mechanical fasteners and wire connections [109], [129]. Moreover, it was not clear what two parts the glue was holding together. In the database, there were 149 parts with at least 1 fastener. More details about the fasteners, their fastener classifications and their associated ELV parts can be found in tables A-1 and A-2 of Appendix A.

We note that our model only considers non-liberated particles that consist of the fastener material and of an attached fragment of part material. From the database from [22], there is no specification as to what is the corresponding part to which a certain fastener is attached. If such data were available, we could extend the model as future work, to characterize non-liberated particles with three material types, for the case where the fastener is attached to two parts of different material types.

Table 7.2 below lists the mechanical fastener classifications adopted for the joint data used for our modeling. This was done after analysis of the parts with fasteners, as well as weight measurements of such fasteners found at an automotive part shop. For each joint type, we have added the following information:

- Materials: Fasteners were either ferrous, copper or plastic. The ferrous fasteners were those which appeared to be bolts, screws or nuts. The fasteners (ECs- electrical connectors, QDCs- quick disconnects, etc) which are associated with electric parts, are assumed to contain an associated amount of copper wires. Copper and ferrous fasteners are of interest as ferrous and copper contribute to contamination in the aluminum and ferrous scraps respectively, obtained at the end of material recovery.
- Size, weight, volume: The screws and bolts were divided into 3 size classes (small, medium, large), with their associated weights measured from a sample of fasteners obtained from an automotive-part shop. A similar assessment was done for other fastener types (plastics rivets, ferrous rivets, ferrous clips and vacuum tees). The total mass of copper from copper wires was estimated by subtracting the existing weight of copper parts from the typical total copper weight in a passenger vehicle in literature [142]. The mass associated to each unit of copper wire was calculated by averaging over the total number of such units. Note that typical cars nowadays would have a much higher weight of copper wires due to more electronics and electric components: there can be as much as 18 kg of copper wires in a modern car[143]

| Classification | Unit Weight(kg) | Material | Density ($kg/m^3$) | Volume($m^3$) | Qty | Weight(kg) |
|---|---|---|---|---|---|---|
| **Bolt_small** | 0.010 | Ferrous | 7850 | 1.27E-06 | 15 | 0.15 |
| **VacTee_medium** | 0.010 | Ferrous | 7850 | 1.27E-06 | 2 | 0.02 |
| **Plastic_small** | 0.002 | SKOP | 1028 | 1.95E-06 | 51 | 0.10 |
| **Rivet_small** | 0.001 | Ferrous | 7850 | 1.27E-07 | 55 | 0.06 |
| **Qdisconnect_medium** | 0.204 | Ferrous | 7850 | 2.60E-05 | 5 | 1.02 |
| **Screw_large** | 0.111 | Ferrous | 7850 | 1.42E-05 | *63* | *7.02* |
| **lugnut_large** | 0.142 | Ferrous | 7850 | 1.81E-05 | 10 | 1.42 |
| **CopperWire** | 0.215 | Copper | 8940 | 2.40E-05 | 55 | 11.80 |
| **Clip_small** | 0.002 | Ferrous | 7850 | 2.55E-07 | 29 | 0.06 |
| **Bolt_large** | 0.056 | Ferrous | 7850 | 7.13E-06 | *5* | *0.28* |
| **Bolt_medium** | 0.023 | Ferrous | 7850 | 2.93E-06 | 59 | 1.36 |
| **Screw_small** | 0.006 | Ferrous | 7850 | 8.25E-07 | 117 | 0.76 |
| **Screw_medium** | 0.037 | Ferrous | 7850 | 4.71E-06 | *231* | *8.55* |
| **TOTAL** | | | | | 697 | 32..58 |
| | | | | | ***Copper*** | *11.80* |
| | | | | | ***Ferrous*** | *20.68* |
| | | | | | ***SKOP plastic*** | *0.10* |

*Table 7.2 Simplified list of fasteners in ELV, and their quantities and properties*

We thus end up with 32.6 kg of mechanical fasteners, which increases the total mass of the ELV to 1407 kg. We note that this amount of mechanical fasteners in the database is only a lower bound of the actual total weight of fasteners typically used in vehicles (less than 6% by weight [144]), since the database available did not report all the fasteners found in the ELV.

We require some further data wrangling to create non-liberated particles for fasteners attached to parts. We will create a non-liberated particle if and only if their respective materials are different, as we are only

concerned with non-liberated particles that can cause contamination. The next section will address the logic sequence (algorithm 2) for converting a part with joint(s) to non-liberated particles.

The baseline ELV is steel-intensive, and as such the automotive parts forming the body structure are set to be of ferrous material in the database. Additionally, as seen in the Table 7.3 below, welding joints, of ferrous materials, are prevalent in old car models. For our modeling, we are only concerned with joints causing non-liberation contamination, i.e. joints which are of different material from the automotive component to which they are attached. Hence, for the steel-intensive baseline ELV, we are not concerned with joints in the body structure.

Nevertheless, when we examine more recent vehicles, some further consideration is needed for joints that are not included in the database. For instance, joints that hold together the body structure, i.e. the body-in-white (BIW). As noted in [129], with new trends in lightweighting with non-conventional materials such as aluminum, there is an increase in mechanical fasteners as joints to join together dissimilar materials. For instance, we can use the new higher quantities of screw joints and rivets in new body structures (see Table 7.3 below) and add them to body parts listed in our database that would correspond to BIW, e.g. rear frame, front clips. This will be investigated in Chapter 9, in the case-study of the lightweight vehicle.

| Joint type | Audi A6 | | Trend | Audi A8 | | Trend |
|---|---|---|---|---|---|---|
| | 2001–2004 | 2005–2008 | | 1994–2002 | 2009-present | |
| *Share of point joints (%)* | | | | | | |
| Spot welding | 91.5 | 81.0 | ↓ | 28.1 | 7.5 | ↓ |
| Stud welding | 3.3 | 6.5 | ↑ | 0 | 0 | |
| Clinching | 0.9 | 1.3 | | 10.0 | 0 | ↓ |
| Screw joints | 0 | 0 | | 0 | 23.6 | ↑ |
| Rivets | 0 | 5.8 | ↑ | 61.9 | 68.9 | ↑ |
| *Share of linear joints (%)* | | | | | | |
| Laser welding | 8.3 | 3.3 | ↓ | 0 | 8 | ↑ |
| MIG welding | 6 | 4.3 | ↓ | 100 | 33.3 | ↓ |
| Laser brazing | 0 | 3.1 | ↑ | 0 | 0 | |
| Adhesive bonding | 85.7 | 89.3 | ↑ | 0 | 58.7 | ↑ |

*Table 7.3 Joining trends of different vehicle body structures [129]*

### 7.1.3 Data transformation from part to particle flows

The ELV database presents the data in the form of a bill of materials, with the material type and weight specified for each part and assembly in the product's hierarchical structure. However, we want to transform this data into material particle flows, as material type is the basis by which comminution and separation are performed further downstream. The first step is to flatten out the parts' hierarchy, so as to account for each material components once. The second step is to create the material flows for liberated particles as well as for non-liberated particles, i.e. particles containing fasteners with a part's fragment. To perform this data transformation, we coded a Java application to build classes representing the ELV parts and the material flows. In the section below, we describe the two algorithms that have been used to flatten the parts' hierarchy and create the particle material flows.

**Part hierarchies**

The first part of the data transformation involves building the parts' hierarchies, to make sure that the mass of subassemblies are not double-counted. In a complex product such as an ELV, there can be many assemblies with sub-assemblies that are themselves assemblies, as shown in Figure 7.1. To determine the part hierarchies, we first analyze the parts' names to find a part's assembly set, parent set, and whether it has a child. For instance, in the parts' structure in Figure 7.1, we establish their properties as follows:

| Part | Assembly Set | Parent Set | Has child |
|---|---|---|---|
| $A$ | $\{A.\alpha, A.\beta, A.\alpha.\rho, A.\alpha.\pi\}$ | | Yes |
| $A.\alpha$ | $\{A.\alpha.\rho, A.\alpha.\pi\}$ | $\{A\}$ | Yes |
| $A.\beta$ | - | $\{A\}$ | No |
| $A.\alpha.\rho$ | - | $\{A.\alpha, A\}$ | No |
| $A.\alpha.\pi$ | - | $\{A.\alpha, A\}$ | No |

*Table 7.4 Defining properties for parts' hierarchies*

The following algorithm is used to build the hulk list, a comprehensive list of parts and their respective masses, which will go into the shredder.

Algorithm 1

```
FOR each part p in ELV {
    IF part has NOT been removed during disassembly{

        IF p is stand-alone part{
            Add p to list
        }
         ELSEIF p is an assembly part{
            Add p to list, with its effective mass (restMass)
        }
         ELSEIF p is a sub-assembly part with child {
            IF all parts in p's parent-set present{
                Add p to list, with its effective mass (restMass)
            }
        }
         ELSEIF p is a sub-assembly part with NO child{
            IF all parts in p's parent-set present{
                Add p to list
            }
        }
    }
}
```

**Material flow in shredder**

The second part of the data transformation involves determining the mass of non-liberated particles originating from parts with joints. We assume that all parts are initially transformed to particles of the largest size possible (i.e. size of the shredder grates) before they undergo further break down, as captured by the shredder model. We transform a part with no joints into a particle stream of its particular material type. We do the same to a part which has joints for which the fasteners are the same material as the part. However, if the material types of the part and fasteners are different, then we transform the part into two or more streams: liberated particle stream of its material type, and non-liberated material streams, one for each fastener material type.

Let us consider a part $p$ of material $m$. It either has no joints and will generate a liberated material $m$, or has fastener(s) $j$ of material $\mu$ and will generate non-liberated material pair $m \Leftrightarrow \mu$. The following algorithm describes how we build the liberated particle stream $m$, and the non-liberated particle stream $m \Leftrightarrow \mu$. .

Algorithm 2

$mass_m = 0$

$mass_{(m-\mu)} = 0$

FOR each part $p$ of material $m$ in ELV hulk{

IF part $p$ does not have fastener{

$mass_m = mass_m + mass_{part\ p}$

} ELSE{

FOR each fastener $j$ of material $\mu$ in part $p${

IF materials m and $\mu$ are NOT the same{

Create non-liberated material ($m \Leftrightarrow \mu$):

$mass_{(m \Leftrightarrow \mu)} = mass_{fastener\ j} + mass_{attached\ fragment\ of\ part\ p}$

Update mass of that part $p$:

$mass_{part\ p} = mass_{part\ p} - mass_{attached\ fragment\ of\ part\ p}$

}

}

$mass_m = mass_m + mass_{part\ p}$

}

}

Note that we assume the following:

- To maintain mass balance from the bill of materials, we need to subtract the mass of unliberated particles formed from a part's joint and a broken part of the part, from its initial part mass.
- In a non-liberated particle, the volume of part material $m$ is assumed to be twice the volume of fastener of material $\mu$, such that:

$$mass_{fastener\ particles\ of\ part\ p} = vol_{fastener} * quantity_{fastener} * density_{\mu}$$

$$mass_{attached\ fragment\ of\ part\ p} = 2 * vol_{fastener} * quantity_{fastener} * density_{m}$$

### 7.1.4 Shredder model parameters

For the shredder model, we need to estimate the parameters that relate to the breakage of non-liberated joint particles and the comminution of all material particles. As described in the section on recovery models (Section 4.2), we will quantify the breakage by the survival probabilities and the comminution by the transition probabilities of the particles.

Both unbroken joint particles and material entanglement during shredding account for contamination downstream in the scrap output streams, but we will only model contamination due to unbroken joint particles (non-liberated particles). We do not account for material entanglement due to lack of data. Moreover, contamination due to material entanglement was found to occur at half the frequency of non-liberated joint particles during characterization experiments of ferrous and non-ferrous output streams [129]. An extension to this research could include material entanglement in shredding modeling: this might be done similar to the implementation of joint particle contaminations, using additional model parameters for the probability of entanglement for different material-pair combinations, with mass balance to account for the flow of the two material types involved, as done in [97].

Recall from section 4.2, that the mass balance for the material particle flows through the shredder is as follows: $\vec{p} = \bar{\bar{B}}\left(\left(\vec{1} - \vec{\pi}\right) \circ \vec{f}\right) + \vec{\pi} \circ \vec{f}$, where $\vec{f}$ is the input feed vector, $\vec{p}$ is the shredder output flow vector, $\vec{\pi}$ is the particle survival probability vector and $\bar{\bar{B}}$ is the transition probability matrix. Note that the input feed vector contains the material composition of the input flow, assuming that all particles are initially of the largest size. This comes from the assumption that although shredder feedstock is a giant ELV hulk eventually, the hulk fragments into large particles. We assume these large particles to be of the size of the shredder output grate, as only particles of that size or smaller will come out of the shredder.

We will now discuss how to obtain the two sets of shredder model parameters, i.e. the survival probabilities and the transition probabilities.

Survival probabilities

As per the shredding mass balance equation, the survival probability $\pi$ refers to the probability that the shredding process does not break a non-liberated joint, i.e. the probability that the joint survives the shredder. Based on the ELV's material and joint data, the non-liberated particles are of the following material type $i$:

- Particles originating from parts with ferrous fasteners: elastomer-ferrous, copper-ferrous, PUR-ferrous, PC-ferrous, aluminum-ferrous, PET-ferrous, Xenoy-ferrous, carpet-ferrous, ABS-ferrous, SKOS-ferrous, TPO-ferrous, PP-ferrous, PE-ferrous, SKOP-ferrous;
- Particles originating from parts with connected copper wires: aluminum-copper, ferrous-copper, SKOP-ferrous;
- Particles originating from parts with plastic (SKOP) fasteners: elastomer-SKOP, ferrous-SKOP, PP-SKOP, carpet-SKOP, ABS-SKOP.

For our model, we set the survival probabilities ($\pi_i$) of each of these non-liberated particles to a value of 0.5: as explanation, the literature has used values between 0.1 and 0.9 [90], and there does not seem to be

a definitive specification for these parameters. An extension to this research could look at modeling the non-liberated particles' survival probabilities proportional to the strength of the joint. For instance, one might use the literature from the field of structural mechanics to rate joint strength according to the shear strength or failure load of a joint T-peel specimen, estimated from simulation or experiments [145]–[147].

Class transition probabilities

In the shredder, the material particles, all initially of the largest size, undergo a series of breakage iterations. At each iteration, the particle can be broken into sub-particles of smaller sizes. We model these transitions as shown in the Markov-Chain diagram in Figure 7.3, from large to medium to small: i.e. a particle can be either large, medium or small at any one time. At each iteration, a large particle can either break into medium-sized particles with probability $p_1$ or stay as a large particle with probability $1 - p_1$. Similarly, a medium-sized particle can either break into small-sized particles with probability $p_2$, or stay as a medium-sized particle with probability $1 - p_2$. After n iterations, we can calculate the fraction of all particles that stay as large particles ($p_A$), break down into medium-sized particles ($p_B$), or break down into small-sized particles ($p_C$) as follows:

$$p_A = (1 - p_1)^n \qquad \textit{Equation 7.1}$$

$$p_B = p_1 * \sum_{x=0}^{n-1} (1 - p_1)^x (1 - p_2)^{n-1-x} \qquad \textit{Equation 7.2}$$

$$p_C = 1 - p_A - p_B \qquad \textit{Equation 7.3}$$

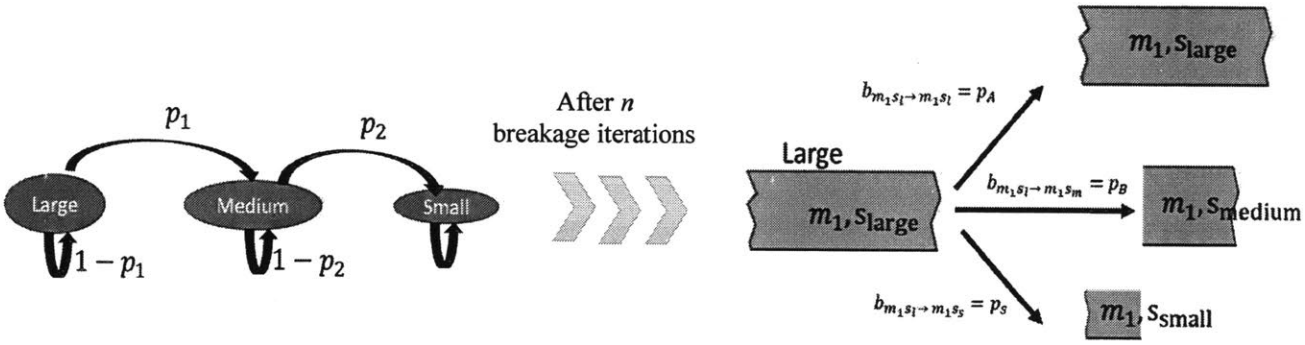


*Figure 7.3 Transition probabilities to different size classes for liberated particles, after one breakage iteration (left) and after multiple breakage iterations (right)*

In effect, the fractions $p_A, p_B, p_C$ for each particular material type are in fact the overall transition probabilities making up the elements of transition matrix $\bar{\bar{B}}$. For example, for large particles of material $m_1$, $b_{m_1 s_l \to m_1 s_l} = p_A$, $b_{m_1 s_l \to m_1 s_m} = p_B$, $b_{m_1 s_l \to m_1 s_s} = p_C$, as illustrated in Figure 7.3 (right). Figure 7.4(a) shows a plot of the overall transition probabilities ($p_A, p_B, p_C$) varying with the number of breakage iterations, for a given value for the individual probabilities $p_1$ and $p_2$. As shown, after only 5 breakage iterations, more than half of the initial population of large particles get shredded and end up in the medium and small size classes. The values of $p_1$and $p_2$ for a particular material particle of big and medium sizes can be estimated from the breakage frequency in experiments using hammer to simulate one shredder turn. The number of breakage iterations will be proportional to the shredder power and length of time material particles stay in the comminution process. Figure 7.4(b) shows a plot of the overall transition probabilities ($p_A, p_B$) with varying values of $n$ and $p_1 = p_2 = p$. We can see that high values of $p$ gives rise to most of

the particle population transitioning to smaller sizes, while low $p$ values require a lot of breakage iterations (high $n$) for any transitions.

The estimation of these transition probabilities can be another research topic, by fitting experimental data to the parameters of Equations 7.1 and 7.2 above. For the current project, we look at literature to obtain the shredding transition probabilities for our model. [89], [90] have performed experiments of ELV fed through shredders and have characterized the output to obtain such parameters. These parameters (see Table 7.5) are adapted for our model needs, i.e. 3 size categories and transition probabilities for liberated particles (see Table 7.6): large (>50mm), medium (10-50mm), small (<10mm). The right side of the table shows the result of solving the system of non-linear Equations 7.1-7.2 for the given material shredding transition probabilities. Thus, we observe that a large particle can undergo from 1 to 3 breakage iterations depending on the material types, to break down into smaller particles.

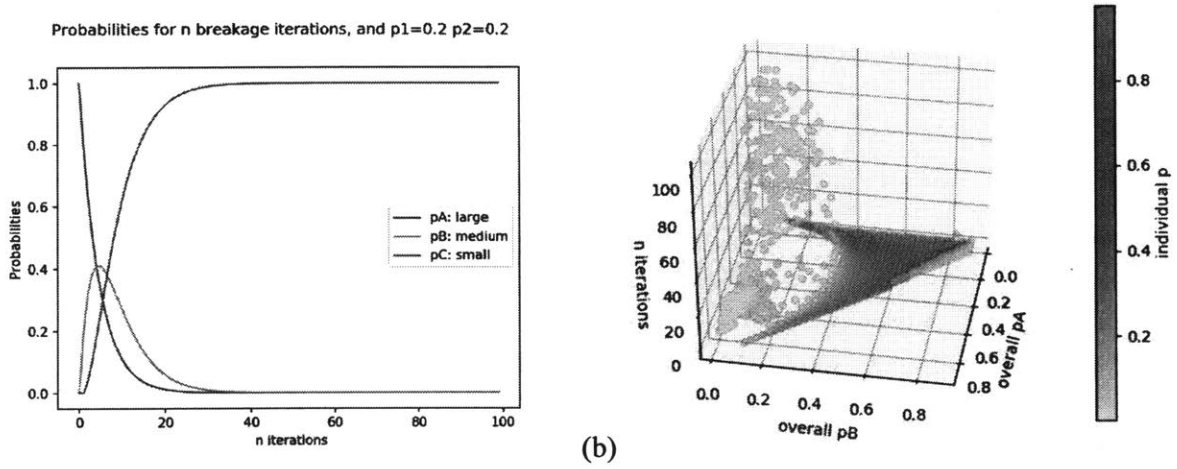


*Figure 7.4 Variation of shredding transition probabilities of initial particle stream to different class sizes, with increase in particle breakage iterations for (a) $\boldsymbol{p_1 = p_2 = 0.2}$, (b) for $\boldsymbol{p_1 = p_2 = p}$ distributed over [0.02, 0.9]*

| Schaik (2004) | | | | | |
|---|---|---|---|---|---|
| **Size category** | **>50mm** | **35-50mm** | **20-35mm** | **10-20mm** | **<10mm** |
| | 1 | 2 | 3 | 4 | 5 |
| **All materials** | 0.2 | 0.3 | 0.3 | 0.1 | 0.1 |
| **Castro (2005)** | | | | | |
| **Size category** | **>50mm** | **35-50mm** | **20-35mm** | **10-20mm** | **<10mm** |
| **Aluminum_cast (Al_c)** | 0.1 | 0.3 | 0.3 | 0.15 | 0.1 |
| **Al_wrought (Al_w)** | 0.15 | 0.2 | 0.4 | 0.1 | 0.1 |
| **Copper (Cu)** | 0.15 | 0.4 | 0.3 | 0.2 | 0.05 |
| **Ferrous (Fe)** | 0.1 | 0.2 | 0.4 | 0.3 | 0.1 |
| **Rest** | 0.1 | 0.2 | 0.3 | 0.3 | 0.1 |
| **Alc_Fe** | 0.15 | 0.15 | 0.2 | 0.3 | 0.2 |
| **Alw_Cu** | 0.1 | 0.2 | 0.3 | 0.3 | 0.1 |
| **Alw_rest** | 0.05 | 0.1 | 0.15 | 0.3 | 0.4 |
| **Cu_Fe** | 0.1 | 0.2 | 0.2 | 0.3 | 0.2 |
| **Cu_Rest** | 0.1 | 0.2 | 0.2 | 0.4 | 0.1 |

*Table 7.5 Shredding parameters (overall size transition probabilities of $\overline{\overline{\boldsymbol{B}}}$) from models in literature*

| | $P_A$ | $P_B$ | $P_C$ | Estimated p | Estimated n |
|---|---|---|---|---|---|
| All materials | 0.2 | 0.7 | 0.1 | 0.75 | 1.15 |
| | | | | | |
| | $P_A$ | $P_B$ | $P_C$ | Estimated p | Estimated n |
| Aluminum_cast (Al_c) | 0.1 | 0.75 | 0.1 | 0.87 | 1.1 |
| Al_wrought (Al_w) | 0.15 | 0.7 | 0.1 | 0.8 | 1.2 |
| Copper (Cu) | 0.15 | 0.9 | 0.05 | 0.1 | 3 |
| Ferrous (Fe) | 0.1 | 0.9 | 0.1 | 0.1 | 3 |
| Rest | 0.1 | 0.8 | 0.1 | 0.89 | 1.1 |

*Table 7.6 Possible shredding parameters (overall size transition probabilities $P_A, P_B, P_C$ in $\bar{\bar{B}}$) to be used in current model for liberated material particles*

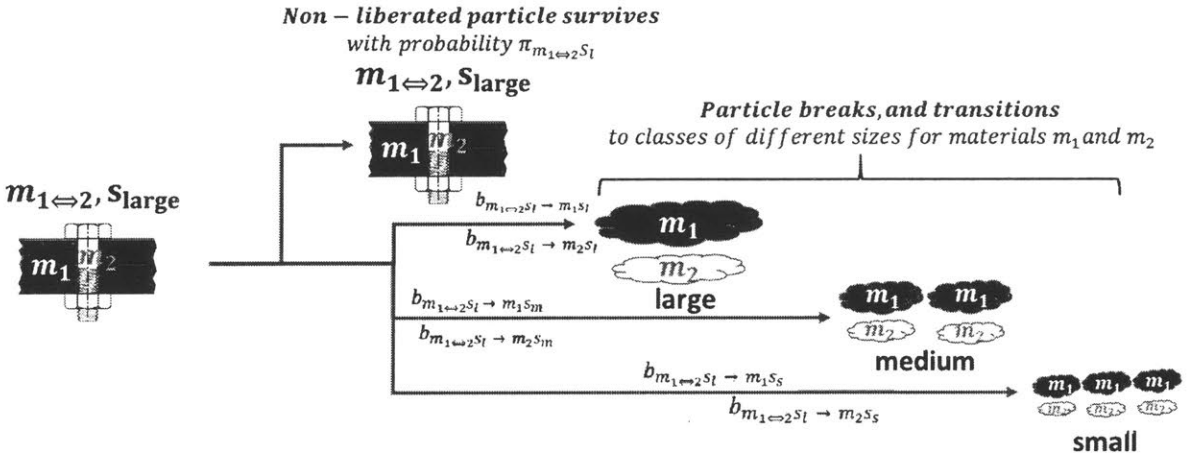


*Figure 7.5 Schematic for class transition to different size and material classes for non-liberated particles*

$$b_{m_{1\Leftrightarrow 2}s_l \rightarrow m_1 s_l} = p_{A_{m_1}} * \frac{m_1}{m_1+m_2} \qquad \textit{Equation 7.4}$$

$$b_{m_{1\Leftrightarrow 2}s_l \rightarrow m_2 s_l} = p_{A_{m_2}} * \frac{m_2}{m_1+m_2} \qquad \textit{Equation 7.5}$$

$$b_{m_{1\Leftrightarrow 2}s_l \rightarrow m_1 s_m} = p_{B_{m_1}} * \frac{m_1}{m_1+m_2} \qquad \textit{Equation 7.6}$$

$$b_{m_{1\Leftrightarrow 2}s_l \rightarrow m_2 s_m} = p_{B_{m_2}} * \frac{m_2}{m_1+m_2} \qquad \textit{Equation 7.7}$$

$$b_{m_{1\Leftrightarrow 2}s_l \rightarrow m_1 s_s} = p_{C_{m_1}} * \frac{m_1}{m_1+m_2} \qquad \textit{Equation 7.8}$$

$$b_{m_{1\Leftrightarrow 2}s_l \rightarrow m_2 s_s} = p_{C_{m_2}} * \frac{m_2}{m_1+m_2} \qquad \textit{Equation 7.9}$$

For non-liberated particles of say material type $m_{1\Leftrightarrow 2}$, i.e. containing materials $m_1$ and $m_2$ joined together, and size large, which break with probability $(1-\pi)$, we model the shredding transitions as described in the schematic of Figure 7.5. Equations 7.4-7.9 describe how the transition probabilities of the non-liberated particles are calculated from using the mass-weighted transition probabilities of their constituent material types ($m_1$ and $m_2$) . We make the following assumptions:

- A non-liberated particle undergoes size transition only if it undergoes breakage, i.e. the joint does not survive the shredding process;
- Upon breakage, the particle, for both the material type of the joint and the original part, can transition to large, medium or small size class;
- The transition probability to each material and size class is proportional to the mass ratio of these 2 material types, and is proportional to the transition probabilities $(p_{A_{m_1}}, p_{A_{m_2}}, p_{B_{m_1}}, p_{B_{m_2}}, p_{C_{m_1}}, p_{C_{m_2}})$ of the liberated material types $m_1$ and $m_2$.

For simplicity, we chose the final transition probabilities to be independent of the material types, and from Table 7.6: $p_A = 0.2, p_B = 0.7, p_C = 0.1$. We can now build the transition matrix using these values for liberated particles, and Equations 7.4-7.9 for the non-liberated particles.

For our ELV case-study, we have three particle size categories and 42 material type classes. Thus our transition matrix is of size 146 by 146.

The particle size classes and material classes are as follows:

- Size class: $\{small, medium, large\}$;
- Material class:
  - 20 liberated particle types: $\{ferrous, aluminum, copper, zinc, magnesium, lead, SKOS; glass; elastomer, carpet, PET, PE, Xenoy, PC, PC-ABS, ABS, PP, TPO, PUR, SKOP\}$;
  - 22 non-liberated particle types: $\{elastomer-ferrous, copper-ferrous, PUR-ferrous, PC-ferrous, aluminum-ferrous, PET-ferrous, Xenoy-ferrous, carpet-ferrous, ABS-ferrous, SKOS-ferrous, TPO-ferrous, PP-ferrous, PE-ferrous, SKOP-ferrous; aluminum-copper, ferrous-copper, SKOP-copper; elastomer-SKOP, ferrous-SKOP, PP-SKOP, carpet-SKOP, ABS-SKOP\}$.

We have now explained how we characterize the shredding model parameters, i.e. survival probability vector $\vec{\pi}$, and the transition probability matrix $\bar{\bar{B}}$.

### 7.1.5 Separation model parameters

The output from the shredder becomes the input to the separation system. Based on the network configuration of separation units, the particles undergo a series of separation steps and eventually end up in one of the output collection units. Recall from section 4.3 , that the mass balance for the material particle flows through the network of separation units is as follows through each unit $j$:
$f_j^{m,s} = \sum_i q_{i,j}^{m,s} f_i^{m,s} + p_j^{m,s}$, where $p_j^{m,s}$ represents the flow of input to the system, $f_j^{m,s}$ is the flow through each unit $j$, $q_{i,j}^{m,s}$ is the separation efficiency of unit $j$ to unit $i$, for material type $m$ and size $s$. To establish the separation models we need to define the network configuration, i.e. what unit $j$ is connected to unit $i$, as well as the separation efficiency of each of these units, on a material type basis and size basis.

**Network configuration**

To model the separation process, we need to define the network configuration of separation units. Most existing network configurations as described in the literature, contain at least an air separation unit, a magnet, and an eddy current. Depending on the grade of output scrap streams collected and the recovery facility's country and setup, there can be more than one unit. Additionally, there can be other separation units: density media separators (DMS) which separate between different types of metals, based on different media used ( e.g. silica, water, etc), and trommels that separate by particle size.

The typical network configurations used by shredding and separation facilities in the US have been discussed in Section 1.5. For our model, we choose the separation facility network design that is simple and yet captures the most common separation equipment and the typical output scrap: ferrous scrap, Zorba (aluminum) scrap, Twitch (aluminum) scrap, and automotive shredder residue (ASR). We use the separation network of a Massachusetts-based metal recycling facility that we visited, shown in the Figure 7.6 below. Note that the manual unit (U1) represents manual workers who are sometimes employed to remove copper wires from the collected Ferrous scrap, as a form of quality control. These wires are often found in non-liberated form when attached to a ferrous element, such as a magnet.

Additionally, we will extend the separation network to include density separators, called heavy-medium separators (HMS), which take in the aluminum scrap (Zorba) and concentrate it to form a higher-grade aluminum scrap (Twitch), see Figure 7.7 below. We chose a sequence of two HMS units of different specific gravities. As described in Section 1.5, an HMS operates by using a medium of a certain density so as to float out a target material that has a much different density. Typically, the first HMS has a specific gravity (2.1-2.5) to separate magnesium and dense plastics from the other metals; the second HMS has a higher specific gravity (3.1-3.5) to float aluminum and sink the heavier metals [43].

In practice, there are few shredding and separation facilities in the U.S which include HMS, unlike in Europe. This is because the prices of Zorba and Twitch do not differ by much on the scrap market, and thus this does not warrant the addition of HMS separation units, given their operational costs. In some countries, the HMS units are found at secondary metal production plants, where scraps are mechanically sorted further on-site before secondary processing.

Table 7.7 describes the separation units used in the selected network configuration (Figure 7.7) for our material recovery facility, the units they are connected to, and the material types they target. Table 7.8 lists the possible output collection units, of which the main valuable scraps sold on the scrap markets are the ferrous and aluminum scraps. Output units V4, V5, V6, V7, and V8 are waste that is typically sent to landfill. However, this waste output contains automotive shredder residue (ASR) as described in Section 1.6.2. While ASR is not further processed to recover materials, ASR is used to cover landfills in the US, and sometimes processed at waste energy recovery facilities in Europe. We will consider the light ASR (V4 and V5) as an output stream that is burnt, and as such, targets plastic particles.

| UNIT ID | UNIT TYPE | DESCRIPTION | Target Material | Target Unit | Other Unit |
|---|---|---|---|---|---|
| **U0** | Mechanical | Magnet | Ferrous | U1 | U2 |
| **U2** | Mechanical | Air Separation | Light material (Plastics) | U3 | V4 |
| **U3** | Mechanical | Trommel (19mm) | <19 mm sized particles | U5 | U4 |
| **U4** | Mechanical | Eddy Current | Aluminum | U7 | V6 |
| **U5** | Mechanical | Eddy Current | Aluminum | U6 | V5 |
| **U7** | Mechanical | DensitySeparation | Of density > 2300 kg/m$^3$ | U8 | V7 |
| **U8** | Mechanical | DensitySeparation | Of density <3500 kg/m$^3$ | V8 | V3 |

*Table 7.7 Separation units in selected network configuration for the material recovery facility shown in Figure 7.7*

| Output Unit ID | Description | Collected Material |
|---|---|---|
| **V1** | Ferrous Scrap | Ferrous |
| **V3** | Twitch Scrap | Aluminum |
| **V4** | Landfill | Light ASR (Plastic) |
| **V5** | Landfill | Heavy ASR (Plastic) |
| **V6** | Landfill | N/A |
| **V7** | Landfill | N/A |
| **V8** | Landfill | N/A |

*Table 7.8 Output collection units in selected network configuration for the material recovery facility shown in Figure 7.7*

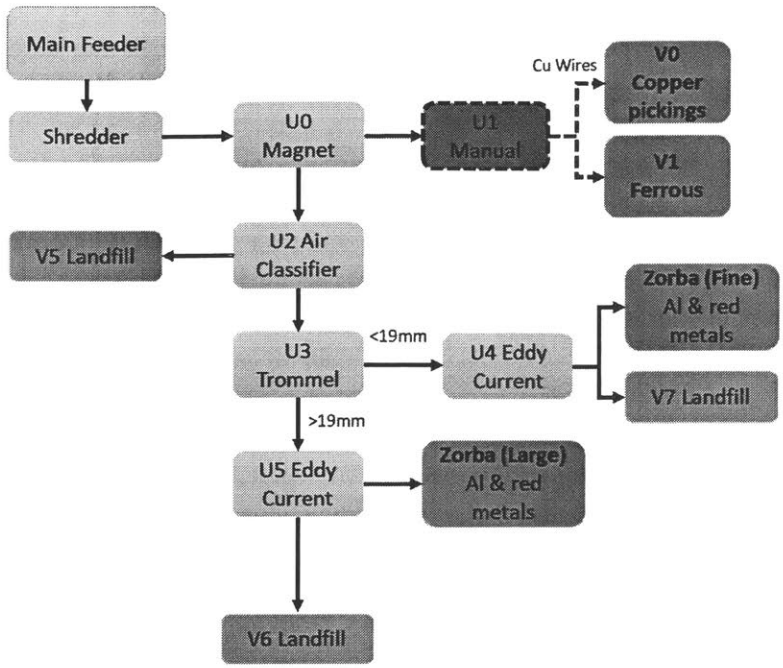


*Figure 7.6 Network configuration for material recovery facility in the MA, USA (Site visit)*

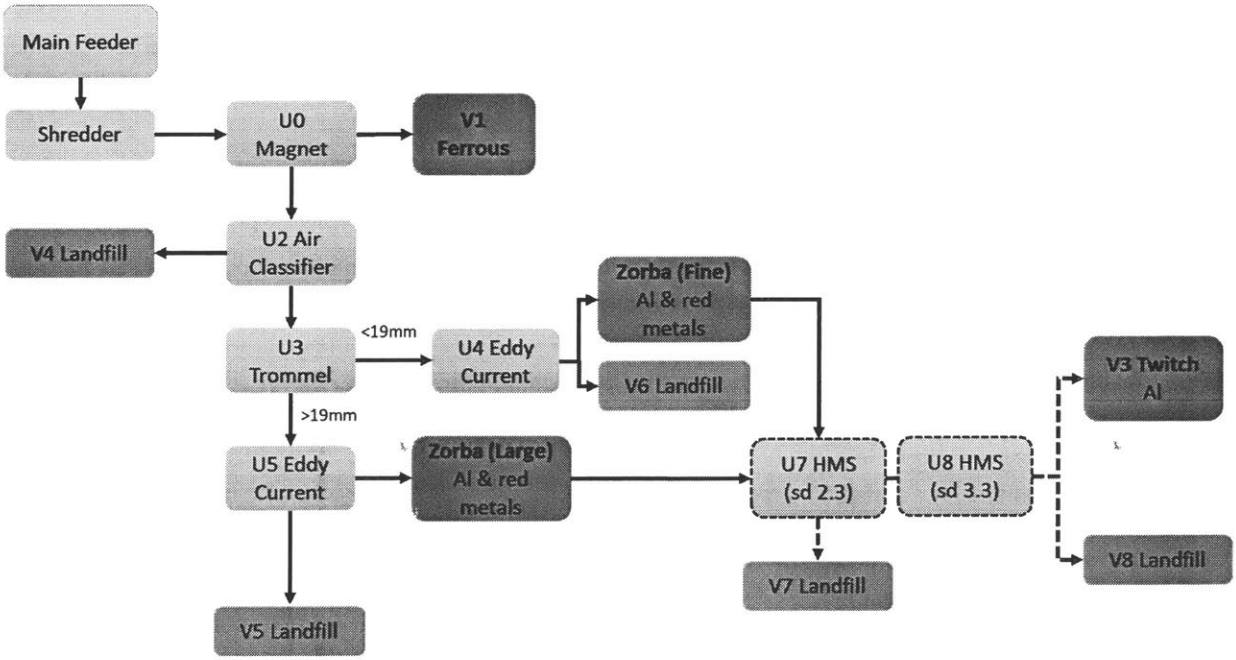


*Figure 7.7 Separation network configuration extended to include heavy-medium separation units to produce Twitch*

**Unit separation parameters**

Once we set a network configuration for the separation process, we need to determine the separation efficiencies for each unit as model parameters. These parameters can be estimated by fitting the measurements for several runs with characterization of all output material streams, with a known input feed

composition, as done in [102]. However, due to a lack of experimental data, we rely on the literature for such data.

Literature data

In Table 7.9, we show separation efficiency parameters for different separation units by material type and size, adapted from the literature [89]: Schaik et al. defined the separation efficiencies of 3 sorting units (magnet, eddy-current and air separation) for 5 different material types (cast aluminum, wrought aluminum, copper, ferrous and rest). While the data is reasonable, it is hard to extrapolate for material types that have not been included in their model. For this reason, we turn to partition curves, which we can use to infer the separation efficiencies based on the physical properties of a material type.

| | | Unit separation efficiency to target stream | | |
|---|---|---|---|---|
| **Material Type** | **Particle Size** | **Magnet** | **Eddy Current** | **Air Separation** |
| **Aluminum_cast (Al_c)** | **Large** | 0.058 | 0.94 | 0.982 |
| | **Medium** | 0.058 | 0.94 | 0.962 |
| | **Small** | 0.058 | 0.28 | 0.942 |
| **Al_wrought (Al_w)** | **Large** | 0.058 | 0.94 | 0.982 |
| | **Medium** | 0.058 | 0.94 | 0.962 |
| | **Small** | 0.058 | 0.28 | 0.942 |
| **Copper (Cu)** | **Large** | 0.088 | 0.768 | 0.94 |
| | **Medium** | 0.088 | 0.868 | 0.927 |
| | **Small** | 0.088 | 0.408 | 0.86 |
| **Ferrous (Fe)** | **Large** | 0.95 | 0.19 | 0.95 |
| | **Medium** | 0.95 | 0.19 | 0.93 |
| | **Small** | 0.95 | 0.19 | 0.91 |
| **Rest** | **Large** | 0.1 | 0.64 | 0.66 |
| | **Medium** | 0.1 | 0.64 | 0.62 |
| | **Small** | 0.1 | 0.354 | 0.58 |

*Table 7.9 Separation efficiency parameters for different separation units by material type and size, adapted from literature [89]*

Using partition curves

A partition curve is a logistic function that maps the value of a separation property to the corresponding partition coefficient, which is the probability of a particle being correctly sorted. As explained in the Section 3.2 on separation system models, these partitions require two parameters proper to the separation unit, to determine the shape of the curve: *fcutPoint, fEp*. The third parameter, $f_{material}$, is the relevant material property of the input particles, and is the function argument for generating the partition curve. Recall, the Napier equation gives the logistic function as:

$$\text{Partition coefficient} = \frac{1}{1+exp(1.099*(f_{cutPoint}-f_{material})/f_{Ep}} \qquad \textit{Equation 7.10}$$

In Figure 7.8, we show the generated curves for the different separation units. For a non-liberated particle consisting of material $m_1$ (from the part) and material $m_2$ (from the joint fastener), we calculate $f_{material}$ as a convex combination of the respective values of the two materials' physical property. We set a heavier

weight on the property of the part's material, because we assume that the part is bigger than the fastener (which can be hidden) that it contains, and has more influence on the separation. In particular, for a non-liberated particle consisting of a part fragment of material $m_1$ and of a fastener of material $m_2$, we define the effective material property of a non-liberated particle, $f_{material}$, as follows :

$$f_{material}^{non-lib} = \frac{(w*mass_{m_1}*f_{m_1}+mass_{m_2}*f_{m_2})}{w*mass_{m_1}+mass\_m_2} \qquad \textit{Equation 7.11}$$

Where we use weight $w > 1$ to increase the influence of the part material. Based on Twitch sample data from [43], there was around 0.3% by weight of steel fasteners that was collected into Twitch scrap. For these non-liberated particles made up of aluminum with steel fasteners to avoid the magnet and yet get sucked away by the eddy-current, this is evidence that the part material has a greater influence. We found that setting $w = 4$ would produce a weight percentage of ferrous in Twitch close to 0.3% in our numerical tests.

Table 7.10 lists the parameters ($f_{cutPoint}$, $f_{Ep}$) that we use to define the partition curve for each of the separation units in our chosen separation network configuration. These parameters were adjusted from those Coates and Rahimifard used in their model [97], in particular for the magnet, air separation and trommel, so as to give sensible results.

| **Separation unit and property** | **Unit** | $f_{cutPoint}$ | $f_{Ep}$ |
|---|---|---|---|
| **Magnetic separator** | Relative magnetic permeability | 0.52 | 0.18 |
| **Heavy media separator: magnetite solution (specific density 2.3)** | density (kg/m$^3$) | 2325 | 200 |
| **Heavy media separator: ferro-silicate solution (specific density 3.5)** | density (kg/m$^3$) | 3525 | 500 |
| **Eddy current: conductivity and density** | Conductivity/density e-3 (m$^4$/(kgΩ ) | 3 | 1 |
| **Air separation: mass** | Particle mass (kg) | -4.9e-6 | 3.2e-4 |
| **Trommel 1 of screen aperture 19 mm** | Particle size (mm) | 15 | 5 |

*Table 7.10 Parameters for partition curves of separation units, adapted from [97]*

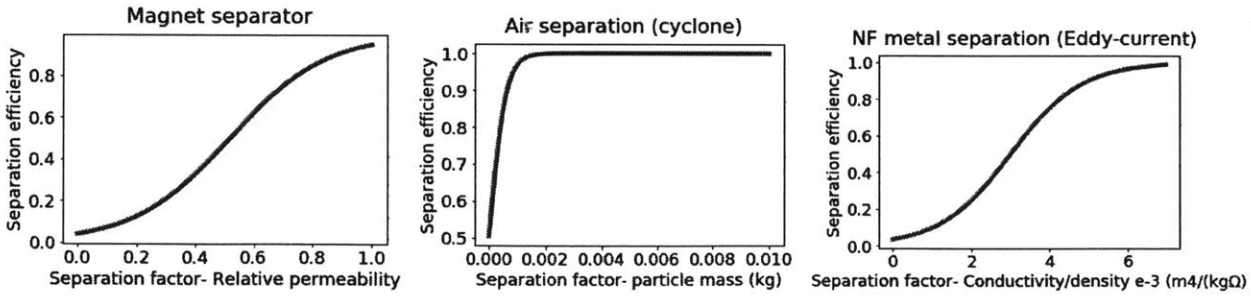


(a) (b) (c)

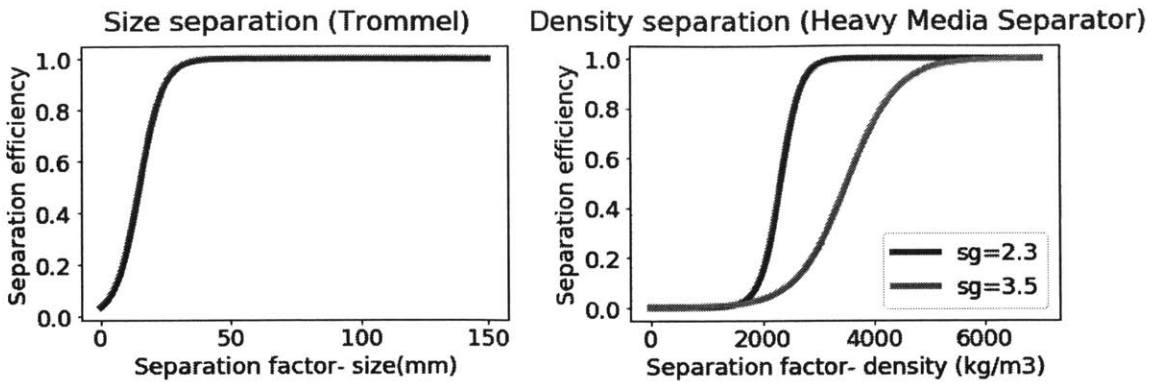


(d) (e)

*Figure 7.8 Partition curves generated for different separation units used during the material separation stage*

In Appendix A, Table A-3 lists the values of the separation material properties of the liberated material types found in our material flows. Using these values, the values generated by Equation 7.11 for non-liberated materials and the partition curve parameters, we apply Equation 7.10 to generate the partition coefficient and hence the separation probabilities of each separation unit. These values can be found in Table A-4 of Appendix A.

We have now established the separation model parameters, i.e. the separation probability matrix $Q^{m,s}$.

## 7.2 Material Recovery Model results

### 7.2.1 Shredder input and output material composition

Input to the shredding model

With the whole ELV intact, no parts removed, the following is the input flow ($f_i$) to the Shredder Model, i.e. the masses of particles by particle classes. The particle classes are by material type (liberated and non-liberated) and size. Note that this particle flow is prior to any class transition or any joint-particle breakage occurring during shredding, and hence all particles are assumed to be in this temporary state of large size. Table 7.11 below shows the list of large particles and their mass available at the start of the shredding process. We obtain this after applying algorithm 1 and 2 to the ELV parts database. We can observe that ferrous-copper particles (ferrous part fragments with attached copper wires) form the largest mass of non-liberated particles, while there are about 2 kg of aluminum-ferrous particles (aluminum part fragments with attached ferrous mechanical fasteners).

| MATERIAL | SIZE | Mass(kg) | Part Fragment Mass(kg) | Fastener/Wire Mass(kg) |
|---|---|---|---|---|
| ***Ferrous-Copper*** | *Large* | *19.515* | *12.434* | *7.080* |
| ***SKOP-Copper*** | *Large* | *5.806* | *1.085* | *4.720* |
| ***SKOP-Ferrous*** | *Large* | *4.906* | *1.018* | *3.888* |
| ***Aluminum-Ferrous*** | *Large* | *2.037* | *0.832* | *1.205* |

| | | | | |
|---|---|---|---|---|
| ***Elastomer-Ferrous*** | *Large* | *1.611* | *0.170* | *1.441* |
| ***PP-Ferrous*** | *Large* | *1.319* | *0.270* | *1.049* |
| ***PUR-Ferrous*** | *Large* | *0.709* | *0.006* | *0.703* |
| ***PET-Ferrous*** | *Large* | *0.646* | *0.165* | *0.481* |
| ***Xenoy-Ferrous*** | *Large* | *0.578* | *0.135* | *0.444* |
| ***Copper-Ferrous*** | *Large* | *0.487* | *0.338* | *0.148* |
| ***TPO-Ferrous*** | *Large* | *0.420* | *0.086* | *0.334* |
| ***ABS-Ferrous*** | *Large* | *0.255* | *0.056* | *0.198* |
| ***PE-Ferrous*** | *Large* | *0.251* | *0.060* | *0.190* |
| ***PC-Ferrous*** | *Large* | *0.192* | *0.044* | *0.148* |
| ***Ferrous-SKOP*** | *Large* | *0.163* | *0.153* | *0.010* |
| ***PP-SKOP*** | *Large* | *0.095* | *0.063* | *0.032* |
| ***SKOS-Ferrous*** | *Large* | *0.075* | *0.029* | *0.046* |
| ***Elastomer-SKOP*** | *Large* | *0.053* | *0.025* | *0.028* |
| ***Carpet-SKOP*** | *Large* | *0.022* | *0.016* | *0.006* |
| ***Carpet-Ferrous*** | *Large* | *0.009* | *0.002* | *0.006* |
| ***ABS-SKOP*** | *Large* | *0.006* | *0.004* | *0.002* |
| **PP** | Large | 8.767 | 0.000 | 0.000 |
| **Aluminum** | Large | 95.795 | 0.000 | 0.000 |
| **Ferrous** | Large | 1032.123 | 0.000 | 0.000 |
| **Glass** | Large | 20.525 | 0.000 | 0.000 |
| **Carpet** | Large | 29.852 | 0.000 | 0.000 |
| **ABS** | Large | 9.689 | 0.000 | 0.000 |
| **TPO** | Large | 2.624 | 0.000 | 0.000 |
| **Lead** | Large | 0.082 | 0.000 | 0.000 |
| **SKOS** | Large | 6.443 | 0.000 | 0.000 |
| **Magnesium** | Large | 1.735 | 0.000 | 0.000 |
| **Copper** | Large | 11.700 | 0.000 | 0.000 |
| **SKOP** | Large | 57.159 | 0.000 | 0.000 |
| **Elastomer** | Large | 50.935 | 0.000 | 0.000 |
| **PUR** | Large | 12.604 | 0.000 | 0.000 |
| **Xenoy** | Large | 18.105 | 0.000 | 0.000 |
| **Zinc** | Large | 2.707 | 0.000 | 0.000 |
| **PC-ABS** | Large | 0.400 | 0.000 | 0.000 |
| **PC** | Large | 0.556 | 0.000 | 0.000 |
| **PE** | Large | 1.780 | 0.000 | 0.000 |
| **PET** | Large | 4.525 | 0.000 | 0.000 |
| | | | | |
| | TOTAL | 1407.3 | | |

*Table 7.11 Masses of particles (liberated and non-liberated – in italic) by material type at the start of the shredding process*

Recall the shredding model represented by the equation : $\vec{p} = \bar{\bar{B}}\left(\left(\vec{1} - \vec{\pi}\right) \circ \vec{f}\right) + \vec{\pi} \circ \vec{f}$. The shredding process modifies the input feed of material particles represented in Table 7.11, $\vec{f}$, by: (i) breaking down non-liberated particles to liberated particles represented by survival vector $\left(\vec{1} - \vec{\pi}\right)$; (ii) comminution of particles to smaller size categories, represented by transition matrix $\bar{\bar{B}}$. The full output flow of material particles, $\vec{p}$, can be found in Table A-5 of Appendix A. Table 7.12 and Table 7.13 below summarize the effect of the shredding process, which uses the parameters defined in Section 7.1.4: (i) half of the non-liberated particles survive; (ii) 70% of the input particles transition to the medium size class; (ii) 10% of the input particles transition to the small size class.

| Particle Type | Size | Mass (kg) |
|---|---|---|
| **Liberated** | Large | 1368.1 |
| **Non-liberated** | Large | 39.2 |
| **TOTAL** | Large | 1407.3 |

*Table 7.12 Total mass of liberated and non-liberated particles at the start of the shredding process*

| Particle type | Weight (kg) | Large (kg) | Medium (kg) | Small (kg) |
|---|---|---|---|---|
| **Liberated** | 1387.7 | 277.5 | 971.4 | 138.8 |
| **Non-liberated** | 19.6 | 19.6 | 0.0 | 0.0 |
| **TOTAL** | 1407.3 | 297.1 | 971.4 | 138.8 |

*Table 7.13 Masses of particles (liberated and non-liberated) by material type at the start of the shredding process*

### 7.2.2 Separation output: scrap quality and material composition

After the shredding process, the particle flows undergo a sequence of separation processes through the network of separation units (see Figure 7.7). The material mass flows are calculated using the mass balance equation for the separation processes, recall equation: $f_j^{m,s} = \sum_i q_{i,j}^{m,s} f_i^{m,s} + p_j^{m,s}$. The calculated mass flow vectors (per material class $m$ and size class $s$) for each separation unit or output unit $j$, $f_j^{m,s}$, are listed in Table A-6 of Appendix A. Using these material flows , we are able to calculate the grade and recovery rate of the valuable scraps collected at the end of the separation processes.

The whole goal of the separation processes is to route the different material types in the feed to the correct target output streams, to be collected as valuable scraps, which ideally would have a high concentration of the target material type. The grade and recovery rate of the recovered scraps are never 100% because of the following: (i) the routing of material particles during separation processes is imperfect, i.e. the separation efficiencies are below 1; (ii) non-liberated particles with two joined fragments of dissimilar material types, end up in only one of the material's target scrap output, the other material thus contributing to contamination.

To illustrate the overall material flow, we draw up the Sankey diagram in Figure 7.9 to see in which collected output streams the materials eventually end up. We follow the fate of six main material categories: (i) ferrous (in red), (ii) aluminum (in black); (iii) copper (in green); (iv) other metals (in pink), which include zinc, magnesium and lead; (v) glass (in purple); (vi) plastics (in yellow) which here also include elastomers/rubber and carpet. As described in Section 7.1.5, we have two valuable output streams: ferrous scrap (unit V1), and Twitch (unit V3). However, we also have two other output streams of interest, labeled

as ASR (light) and ASR. Here, we define the material flow at output unit V4 as ASR (light) as it is the light fraction coming from the air cyclone separation unit. Conversely, we define the other heavier ASR as the remaining.material flows that are the waste streams of the metal separation processes downstream: (i) waste streams from the eddy-current separation units (V5+V6) and waste streams from the density HMS units further downstream (V7+V8).

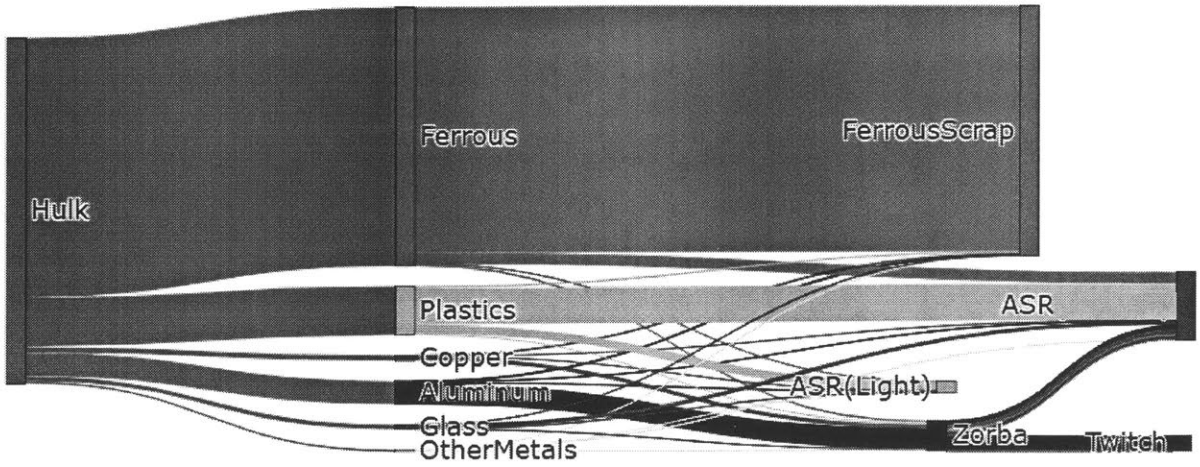


*Figure 7.9 Sankey diagram for material flows before and after separation for a whole ELV*

In the Sankey diagram, the width of the line is proportional to the actual mass of that material. We can thus visualize the following:

- the general material composition of the ELV hulk before the separation processes: Ferrous, plastics, aluminum and copper have the highest mass in the hulk.
- Most of the targeted materials end up in their respective target output streams: ferrous in ferrous scrap; aluminum in the Zorba then Twitch scraps, plastics in the waste streams of ASR (light) and ASR.
- The target output streams (on the right side of the Sankey diagram), all have contaminants, although in different proportions.
- Copper and other metals are considered non-valuable, as they do not have a specific target scrap output stream. As a result, they end up dispersed among the output streams.
- The heavier ASR contains a lot of metal contaminants, including valuable metals (ferrous and aluminum) that have been imperfectly sorted by the upstream metal separation units.
- Zorba scrap is an intermediate aluminum scrap, before further separation steps using heavy-medium separators concentrate the aluminum into Twitch scrap; hence there is increase in grade from Zorba to Twitch.

To further investigate the possible causes of quality and dilution losses in the collected scraps, we examine more closely the material composition of each scrap. The Ferrous scrap has a high quality grade of 98.2%, but does contain contamination with aluminum (0.4% or 4 kg) and copper (0.4% or 4 kg), see Figure 7.10. Although this contamination is in minute quantities, it is of high enough concentration to require dilution of the ferrous scrap during secondary steel production. From Figure 7.10 (right), one can see that this contamination is largely due to non-liberated particles (1.2% by weight of the ferrous scrap). Further

inspection from the material flows (Table A-6 of Appendix A) show that this is largely caused by the accumulation of ferrous-copper particles (8.8 kg), while there are also plastic-ferrous particles and aluminum-ferrous particles in smaller amounts. This is an issue that is often reported during characterization of ferrous scraps [5]: for instance, one common issue is copper wire from electric motors that remains attached to the ferrous fragments that get sorted by the magnet.

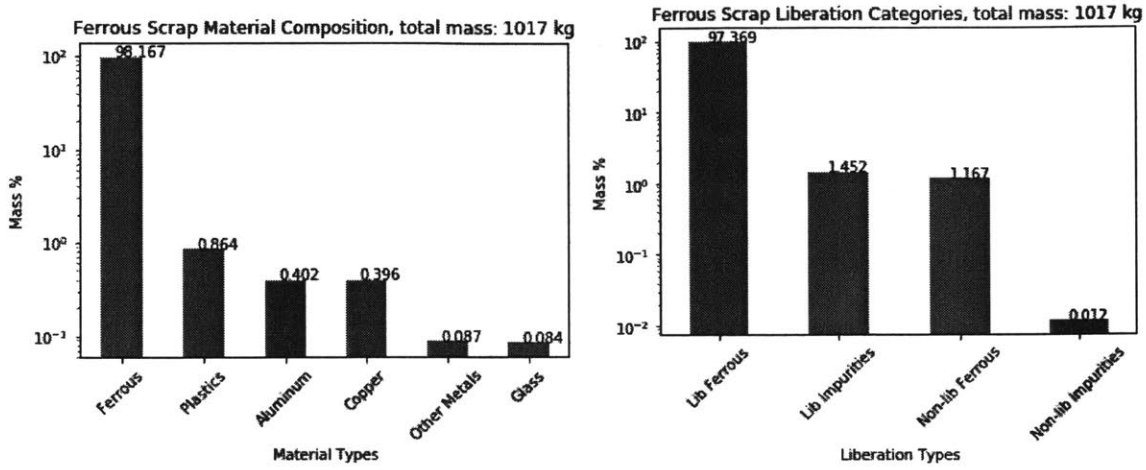


*Figure 7.10 Ferrous scrap (at output unit V1): main material composition (left); liberation categories (right)*

In Figure 7.11 and Figure 7.12, we compare the material composition of the Zorba scrap and the Twitch scrap respectively. From these figures, one can see the benefit of the additional separation steps used to produce Twitch. When going through the eddy-currents (U4 and U5), the other non-ferrous metals (Copper, OtherMetals) do not get sufficiently separated from the aluminum particles: this is because these non-ferrous metals have conductivity/density material properties that are not starkly different from that of aluminum. From the material composition of Twitch (Figure 7.12), one can see that the HMS separation units have removed a large proportion of the plastics from the Zorba feed, as well as the metals, in particular copper, that is much denser than aluminum. However, the amount of glass has not decreased by much (0.46 kg in Zorba compared to 0.33 kg in Twitch): this is because glass has a similar density (2600 kg/m$^3$) to aluminum (2699 kg/m$^3$) . More importantly, there is still some ferrous contaminants in the Twitch scrap. Inspection of the material flows in Table A-6 of Appendix A shows that: while liberated ferrous particles are largely removed by the HMS, non-liberated particles of aluminum-ferrous are still prevalent (yet decreased from 0.84kg in Zorba to 0.19kg in Twitch).

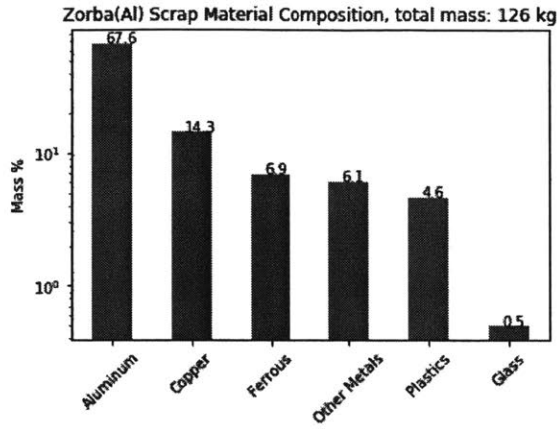


*Figure 7.11 Zorba Al scrap (received at unit U7): main material composition*

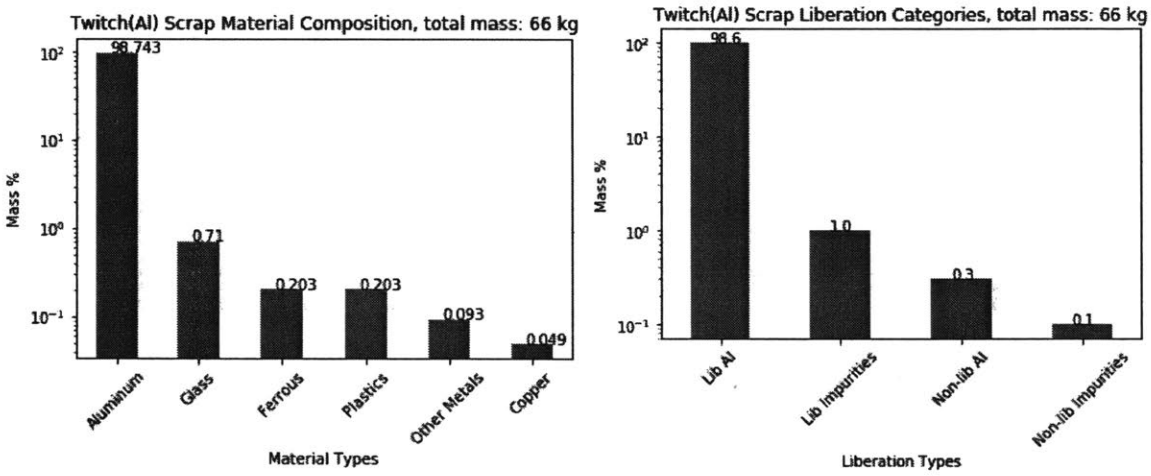


*Figure 7.12 Twitch Al scrap (at output unit V3): main material composition (left); liberation categories (right)*

Next, we examine the material composition of the ASR streams (light & heavy). As expected, the light ASR contains largely lightweight plastic particles. However, it also contains a significant amount (7 kg) of aluminum, which is thus not recovered properly. In the heavier ASR stream, we can observe a more heterogeneous mixture of material types: the heavier plastics, as well as a significant amount of ferrous, which is sorted into the waste stream by the eddy-current, because of the low conductivity/density ratio of ferrous.

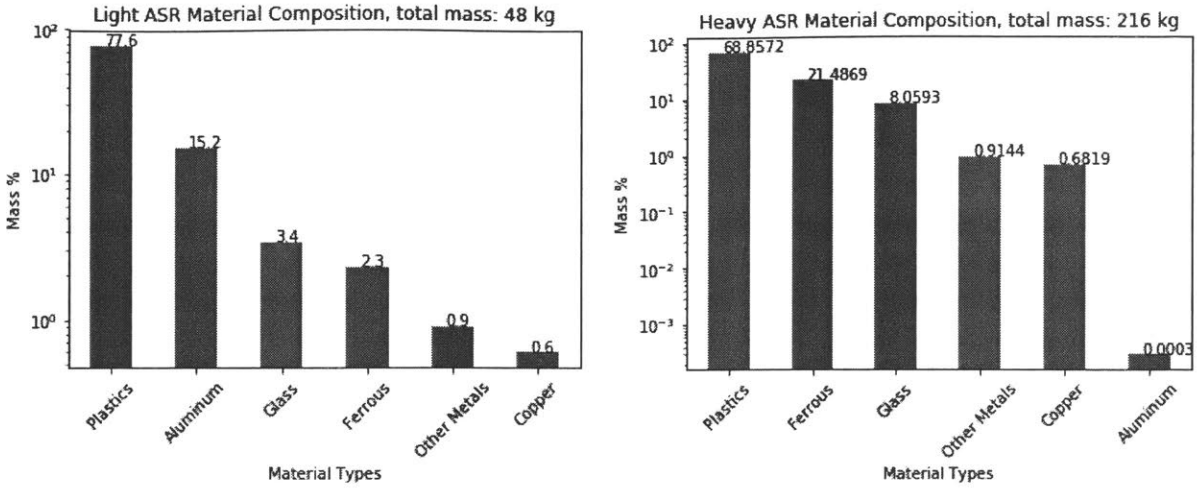


*Figure 7.13 Main material composition for automotive shredder residue: light ASR at output unit V1 (left); heavy ASR at output units V5 & V6 (right)*

### 7.2.3 Performance metrics

Recovery & grade

The general performance of the material recovery processes can be measured using typical performance metrics on the valuable scraps. Table 7.14 shows the recovery rate and grade of the ferrous and aluminum scraps. With a higher recovery rate and grade, we can deduce that ferrous is more easily recovered than aluminum from our baseline ELV. It is also interesting to note that the additional separation steps that convert Zorba to Twitch Al scrap are effective in increasing the grade from 68% to 99%. However, this comes at a cost of the recovery rate, since there can only be a trade-off between grade and recovery rate, as discussed in Section 6.1. When evaluating the ASR streams, we assume that plastic/elastomers are the target materials, as they can be used as fuel at waste energy recovery facilities. We can observe that most of the plastic mass ends up in the heavy ASR stream. Overall, the ASR streams have poor grade, as all the unwanted wastes (non-metals and non-target metals) or badly-separated valuable metal (ferrous and aluminum) materials end up there.

| Scrap | Weight (kg) | Recovery Rate | Grade |
|---|---|---|---|
| **Ferrous** | 1017 | 94.6 % | 98.2 % |
| **Aluminum: Zorba** | 126 | 88.3 % | 67.6 % |
| **Aluminum: Twitch** | 66 | 67.1 % | 98.7 % |
| **ASR (Light)** | 48 | 18.4 % | 77.6 % |
| **ASR (Heavy)** | 216 | 74.2 % | 68.9 % |

*Table 7.14 Recovery & grade metrics of output scraps for baseline ELV case-study*

Entropy

We now apply entropy as a performance measure to evaluate the material separation processes. Recall that a higher entropy is a measure of material mixing. Hence, a good separation process would produce output

streams for the valuable target materials with low entropy, but with higher entropy in the waste streams. In Table 7.15, we report the entropy measure for the input stream, namely the ELV, and for the output streams for the valuable target materials. We see that an ELV is a complex product with high material mixing, while its scrap products (ferrous scrap and Twitch Al scrap) have low entropy due to the high concentration of the target material. It is also useful to note that Zorba, the intermediate Al stream, actually has a higher entropy than the ELV. This is because Zorba is a rather heterogeneous mixture of non-ferrous metals and non-metals, although aluminum has a relatively high concentration. As expected, the ASR streams, being the waste streams, have the highest entropy due to the relatively high concentration of non-conductive metals, and the wide variety of plastic materials.

| Material Stream | Material Mixing, H (bits) |
|---|---|
| **Whole ELV** | 1.62 |
| **Ferrous scrap** | 0.19 |
| **Al scrap: Zorba** | 1.73 |
| **Al scrap: Twitch** | 0.12 |
| **ASR (Light)** | 3.30 |
| **ASR (Heavy)** | 3.09 |

*Table 7.15 Mixing entropy for the material streams before and after the shredding/separation processes, for baseline ELV case-study*

Overall performance metrics

To evaluate the overall material recovery performance from an ELV, we use the overall recovery rate (ORR) metric to combine the recovery rates for the three target materials of interest: ferrous scrap, aluminum from the Twitch scrap, plastic from the ASR streams. Table 7.16 shows the calculation of the ORR, with an 88.8% ORR achieved with the baseline ELV. Note that this is below the European standard of 95% recovery to be achieved by 2020 [10]. However, an improved ORR is possible by improving the separation efficiencies, using more efficient technologies or using recirculation in the separation network configuration). Increasing the number of separation units might only increase the grade of the scrap output but not the recovery rate of the valuable materials. The ORR can also be improved through selective disassembly of parts that can be fully recovered through resale/resuse or direct recycling.

| Flow | Mass (kg) |
|---|---|
| **Hulk** | 1407.3 |
| **Collected Ferrous (at Ferrous scrap)** | 998.8 |
| **Collected Aluminum (at Twitch scrap)** | 64.9 |
| **Collected Plastic (at light and heavy ASR)** | 185.7 |
| **ORR (%)** | (998.8+64.9+185.7)/1407 = 88.8 % |

*Table 7.16 Calculation of the overall recovery rate of the baseline ELV, from material flows of interest*

To evaluate the repercussions of the contaminants in the scrap streams, we make use of the normalized contribution of the scraps (NCS) described in Section 6.5. We are interested in quantifying the dilution losses due to metal contaminants in the ferrous and aluminum scraps that cannot be removed by oxidation. We use the blending model described in Section 5.1, with the input feed specified based on the material composition in the ELV Twitch scrap above, as well as the ratio of cast aluminum and wrought aluminum, which is calculated from the ELV's part database. Thus, we calculate the cost-optimal amounts of alloying elements and primary Aluminum for dilution, in order to meet the element concentration constraints of different possible Al alloys. Table 7.17 lists the calculated alloying and dilution needed when using our baseline ELV's Twitch scrap as input feed during the secondary aluminum production. We can observe that for the production of some of the cast Al alloys (A319 and A380), there is no dilution costs (no Al added) but only alloying costs (Si and Cu added). This is because all the elements (from Si to Ti) are within the maximum concentration limits allowed in A380 and 319, but their minimum concentrations of Si and Cu are not achieved. On the other hand, for the other Al sink alloys, we need both alloying as well as dilution to achieve their respective elements' concentration requirements.

Similarly, Table 7.18 lists the calculated dilution needed when using the ferrous scrap as input feed for secondary steel production, with different final steel product scenarios. For the dilution calculation, the effective concentration of copper is 0.402%, assuming all other metals are oxidized and plastics burnt. Thus, the production of steel bars, requiring a maximum of 0.400% copper, needs the least dilution (5 kg) of pig iron. On the other hand, the production of steel sheets, requiring a maximum of 0.060% copper, needs a dilution of 6859 kg of pig iron.

Table 7.17 and Table 7.18 both illustrate the huge difference in the dilution amount needed for the different final metal alloy scenarios. We note that this exercise is largely illustrative. In practice, due to the high dilution otherwise needed, secondary metals are usually downgraded to the lowest quality of produced alloys. For instance, secondary aluminum is usually used to produce cast Aluminum, e.g. A380, which requires very little dilution.

| Final Al Alloys | Si added (kg) | Fe added (kg) | Cu added (kg) | Mn added (kg) | Mg added (kg) | Cr added (kg) | Ni added (kg) | Zn added (kg) | Ti added (kg) | Al added (kg) |
|---|---|---|---|---|---|---|---|---|---|---|
| **P0506A** | NaN | NaN | NaN | NaN | NaN | NaN | NaN | NaN | NaN | NaN |
| **P1020A** | 0.0 | 0.0 | 312.7 | 313.5 | 313.7 | 0.0 | 313.9 | 313.3 | 0.0 | 104290 0.7 |
| **1070A** | 0.0 | 0.8 | 0.0 | 0.0 | 0.0 | 0.0 | 0.0 | 0.0 | 0.0 | 2398.0 |
| **3103** | 0.0 | 3.5 | 0.0 | 6.5 | 0.0 | 0.0 | 0.0 | 0.0 | 0.0 | 664.9 |
| **5182** | 0.0 | 0.0 | 0.0 | 7.1 | 72.2 | 0.0 | 0.0 | 3.6 | 0.0 | 1308.2 |
| **5754** | 0.0 | 1.1 | 0.0 | 0.0 | 18.6 | 0.0 | 0.0 | 0.0 | 0.0 | 656.4 |
| **6061** | 0.0 | 0.0 | 0.0 | 0.0 | 1.1 | 0.0 | 0.0 | 0.0 | 0.0 | 153.5 |
| **6082** | 2.9 | 1.9 | 0.0 | 2.8 | 3.7 | 0.0 | 0.0 | 0.0 | 0.0 | 663.2 |
| **A356** | 242.2 | 0.0 | 5.7 | 3.1 | 14.5 | 0.0 | 1.5 | 3.2 | 0.0 | 2890.7 |
| **301** | 77.0 | 11.3 | 23.9 | 4.0 | 2.1 | 0.0 | 8.1 | 0.0 | 0.0 | 629.3 |
| **319** | 2.2 | 0.0 | 1.3 | 0.0 | 0.0 | 0.0 | 0.0 | 0.0 | 0.0 | 0.0 |
| **A380** | 3.7 | 0.0 | 1.3 | 0.0 | 0.0 | 0.0 | 0.0 | 0.0 | 0.0 | 0.0 |

*Table 7.17 Alloying and dilution additions needed for secondary processing of Twitch Al scrap for different final Al alloy scenarios, baseline ELV study*

| | Steel Sheet | Rolled Steel | Steel Section | Steel Bar |
|---|---|---|---|---|
| **Pig iron added for dilution (kg)** | 6859.0 | 3364.9 | 352.6 | 5.1 |

*Table 7.18 Dilution addition needed for secondary processing of ferrous scrap for different scenarios of final steel products, baseline ELV study*

We use the above calculated alloying and dilution costs to calculate the NCS for the different possible aluminum alloys and steel products produced during secondary metal production. Table 7.19 shows the resulting matrix of possible NCS. For this exercise, we do not use any cost-based or thermodynamic-based weight to the masses. We can observe that if we use our Twitch scrap to produce low grade Aluminum alloy such as 319 or A380, and our ferrous scrap to produce steel bars, we do not require much dilution. In such case, the NCS is 88%, or 1% lower than the ORR calculated above.

| | P1020A | 1070A | 3103 | 5182 | 5754 | 6061 | 6082 | A356 | 301 | 319 | A380 |
|---|---|---|---|---|---|---|---|---|---|---|---|
| **Steel Sheet** | 0.12 | 11.71 | 13.97 | 12.94 | 13.97 | 14.84 | 13.97 | 10.93 | 13.85 | 15.11 | 15.10 |
| **Rolled Steel** | 0.12 | 17.42 | 22.94 | 20.27 | 22.93 | 25.36 | 22.94 | 15.75 | 22.60 | 26.16 | 26.15 |
| **Steel Section** | 0.12 | 30.04 | 51.31 | 39.65 | 51.29 | 65.26 | 51.32 | 25.39 | 49.67 | 70.85 | 70.79 |
| **Steel Bar** | 0.12 | 32.78 | 59.86 | 44.56 | 59.82 | 79.73 | 59.86 | 27.32 | 57.63 | 88.24 | 88.14 |

*Table 7.19 Matrix of NCS metric, calculated over the different possible scenarios of produced steel products (rows) and produced aluminum alloys (columns), for our baseline ELV case-study*

The NCS metric is useful to evaluate the different scenarios of metal alloys produced during secondary metal production. While the convention in industry is to downgrade to the lowest quality alloy, it is also possible and actually advantageous to explore other possible sink alloys, the reason being that the market for Al cast alloys is actually saturating, i.e. supply is exceeding demand [43]. For example, for our particular profile of baseline ELV, using 6061 alloy as the final sink alloy does not cause too much dilution losses, with a NCS of 80%. This is because we assume the wrought aluminum fraction (63% by weight) of all aluminum in the ELV is taken to be 6061 Al alloy. As such, the output scrap tends to have a similar element composition to that of the produced 6061 Al alloy, and hence we incur less alloying costs in the secondary metal processing. However, if we used more granular data, with more information about what specific wrought and cast alloys are associated to what parts, it is not clear that the best wrought sink alloy to use would still be 6061 Al alloy.

Recall from Section 6.5.1 that during the calculation of the NCS metric, the recovered materials can be weighted according to either their respective economic cost or respective thermodynamic rarity. As discussed in Section 6.4, thermodynamic rarity encompasses the exergy costs for material production as well as for resource depletion, and tends to correlate with the material market price for many metals. Figure 7.14 summarizes the economic cost and thermodynamic rarity of the main metals found in a vehicle, and as elements of aluminum alloys. To examine the effects of those weights, we now focus on two scenarios of sink metal alloys produced: (i) Al A380 & steel bar, (ii) Al 6061 & rolled steel. Table 7.20 lists the resulting calculated NCS metrics with: (i) no weights; (ii) metal market prices, i.e. economic costs as weights; (iii) metal thermodynamic rarity as weights. We observe that the NCS metrics weighted by economic cost and thermodynamic rarity do not differ significantly, as these two costs are generally correlated for the metals under consideration. In the first scenario with the production of low quality alloys, the weighted NCS metrics are lower than the non-weighted NCS metric by around 18 %. Note that in this scenario, the dilution costs are minimal such that the NCS metric is highly influenced by the respective

recovery rates of ferrous and aluminum. For our baseline ELV study, we previously found that the recovery rate of ferrous is much higher than that of aluminum in our model's recovery chain infrastructure. Because aluminum has higher economic and thermodynamic costs than ferrous, the weighted NCS metrics penalize the bad recovery rate of aluminum more strongly, thus leading to lower values than the non-weighted NCS metric. However, in the second scenario where high quality metal alloys are produced, the weighted NCS metrics are not different from the non-weighted NCS metric. This is because the dilution costs are significant, but the dilution costs for steel production is higher than that for aluminum production; this balances out the higher economic or thermodynamic cost of aluminum as compared to that of ferrous.

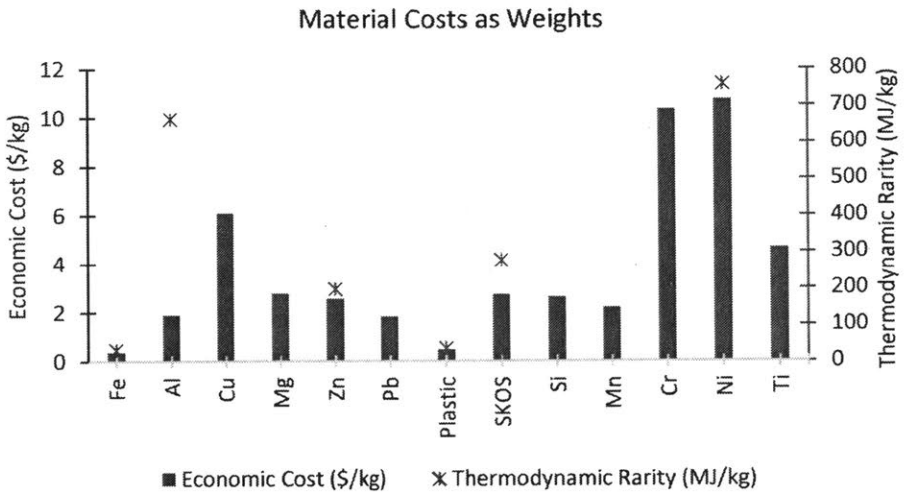


*Figure 7.14 Economic cost and thermodynamic rarity of recovered materials, used as weights in NCS calculation, data from [139]*

| | Al A380 & Steel Bar | Al 6061 & Rolled Steel |
|---|---|---|
| **NCS ($c_j$=1)** | 88 % | 25 % |
| **NCS ($c_j$=economic cost)** | 69 % | 24 % |
| **NCS ($c_j$=thermodynamic cost)** | 70 % | 25 % |

*Table 7.20 NCS metrics with different weights, for baseline ELV study*

## 7.3 Data for Disassembly Optimization

With the ELV database described in Section 7.1, we can now apply the integer-programming optimization developed in Section 2.2 to determine the automotive parts that are cost-optimally removed for resale from an end-of-life vehicle. In the following section, we describe the ELV data wrangling that is needed to form the IP model parameters. We then the present the optimization results in Section 7.3.2.

### 7.3.1 Data transformation

2-level part hierarchy

The dismantling data comes from the work of [22], where two mid-sized family cars manufactured in 1993 were dismantled at the Vehicle Recycling Development Center. The original data contained 616 total parts (including subparts and assemblies), and 451 part precedence constraints. We simplify the data to contain only two-levels of assembly to be able to apply it to the disassembly model developed in Section 2.2.1. For example, in the original data, a door assembly contained the following subassemblies at level 2: panel, shoddy, structure. These subassemblies were themselves assemblies containing smaller subassemblies at level 3: e.g. the structure contained the base and mirror.

Besides the parts' precedence data, the dismantling data also contains the removal time (in seconds) and part resale value (in $) for each part. For parts which are difficult to remove (as determined by the prior studies), we assign an arbitrarily large value of $10^9$ seconds. The final data used, consisting of only components of an ELV with 2-level part hierarchies, is listed in Appendix B. Table B-1 contains the 335 components, including: (i) assemblies; (ii) subassembly components; (iii) standalone parts. Table B-2 contains the 319 precedence constraints, where a precedence constraint is defined for a pair of parts (source and target), with the source part being the one removed before the target part can be removed.

From precedence constraints to disassembly jobs

For a complex product like an end-of-life vehicle, we have a complex network of parts (nodes) and connections (arcs). The connections are determined by the available precedence constraints data. A part can have more than one precedence constraint. In the data table (Table B-2 in Appendix B), this corresponds to a target part having more than one source part. For instance: the "headliner" has as precedence the "APillarTrimLeft", "APillarTrimRight", "sunversorRight", "SunvisorLeft", "Handles", "CPillarLeft", "CPillarRight", "BPillarUpperRight", and "BPillarUpperLeft". The original dataset had no mention as to whether the constraints were OR or AND relationships. For our example, we will assume that the precedence constraints are AND constraints. Thus, for the "headliner" to be removed, all of the nine precedence parts listed need to be removed.

Disassembly path search

We formulate our disassembly problem in such a way that disassembly jobs (i.e. sets of parts which are to be removed together) are defined to facilitate the listing of feasible disassembly jobs based on expert knowledge of the disassembly process, or as determined by experiment.

However, for our case, we have to use the part precedence constraint list (Appendix A) to determine the feasible disassembly jobs. To define complete assembly jobs (in this section, complete means the job can stand alone, i.e. the removal of these parts do not require the precedence of any other parts), we do the following:

(i) Define source and end nodes
From the available list of precedence constraints, i.e. arcs with between a source part and target part, we can build the list of source nodes, namely the nodes that have no predecessors. Similarly, the end nodes are the target parts that are not predecessors for any other parts.

(ii) Graph-search algorithms
Depth-first search (DFS) and breadth-first search (BFS) are two algorithms that use recurrence for searching through graphs. We use DFS to list the complete feasible paths between all possible combinations of source and end nodes determined above.

We note that using these complete feasible paths as disassembly jobs provides a lower bound on the possible parts to be removed: the first set of constraints ( $x_j = \sum_{k=1}^{K} a_{jk} y_k$ ) used in the disassembly optimization formulation does not allow a part to be taken from more than one disassembly job; if a part is found on more than one complete feasible paths (this is the case if the path branches off into more than one path), only one of these paths is chosen. One solution would be to relax the first set of constraints to an inequality and enable the paths to overlap, in which case the extra costs of the overlapping parts need to be adjusted for. Alternatively, further algorithms can be explored to determine subsets of jobs along these complete paths, as well as the precedence constraints between these incomplete jobs.

### 7.3.2 Optimized disassembly results

For this section, we use the notation of Section 2.2, where the optimization formulation was presented. We now have a list of disassembly jobs $k$, and the list of parts $j$ and their associated removal times and values ($v_j$). We do an additional calculation to transform the removal time of the parts into a cost using a labor rate of ($9/h). From the part removal costs, we calculate $c_k$, the total costs of a disassembly job, by summing the costs of all parts found in that particular job. For the current optimization, we are only concerned with finding the cost-optimal solution from the perspective of the dismantler, who does not bear any of the shredder value. Hence, we put the shredder values to 0, i.e. $u_j = 0 \, \forall j$. Note that with the way the disassembly jobs are generated here, we do not require the third set of constraints ( $y_k \le \sum_{l=1}^{K} s_{kl} y_l, \forall k = 1, 2...K$ ); as each job is from a starting node to an end node, there are no precedence

constraints across the jobs. Additionally, the list of parts within each disassembly job $k$ is used to define the job-listing matrix $\{a_{jk}\}$ where $a_{jk} = 0,1$ to denote whether or not part $j$ is to be removed using job $k$.

We now have all the components to use the 2-level hierarchical structure of the ELV on the optimization formulation in Section 2.2.1. The optimization problem was solved using Gurobi package in a Java interface. The solution, i.e. all the parts that are cost-optimally removed, is listed in Table B-3 of Appendix B. In all, we find that 84 parts are to be removed: 39 parts have an associated resale value (see Table 7.21 below), while 45 parts have no resale value. Most of the valuable parts do not require the simultaneous disassembly of one or more parts to be reached: e.g., the doors, decklid, "InstrumentPanel.Radio", etc. However, some parts require that one or more parts be removed before they can themselves be removed, as defined by the list of feasible disassembly jobs built through the precedence constraints. For illustration, some of these parts are sketched with their disassembly jobs in Figure 7.15. In these sketches, the direction of the arrow goes from the preceding part to the succeeding part. On the left, we can see a disassembly job consisting of the following parts: {"FasciaRearlower", "EnergyAbsorberRearLeft", "EnergyAbsorberRearRight"}. According to the precedence constraints (refer to Table B-1 of Appendix B), the "EnergyAbsorberRearLeft" and "EnergyAbsorberRearRight" are both preceded by the "FasciaRearlower". While in this case, it happens that the preceding part is also valuable, it often happens that a preceding part is of no value but needs to be removed to reach a valuable part. This can be seen in the example on the right of Figure 7.15: the disassembly job consists of {"WiperAssemblies", "CowlVent", "WindshieldWiperMotor"}. While the "CowlVent" and "WiperAssemblies" have zero resale value, they are removed to be able to access the "WindshieldWipermotor", which has a resale value of $40. Note that the sub-assembly parts ("WiperAssemblies.Steel", "WiperAssemblies.Blade") of the "WiperAssemblies" are themselves not removed from the "WiperAssemblies" as they are not valuable.

In this example, the optimization algorithm removes most of the parts with value in an ELV. This is because these parts with a resale value are typically easy to remove. However, we also observe that some non-valuable parts are also removed in order to reach valuable parts, which they precede.

| Part ID | Part Name | Resale Value ($) | Removal Time (s) | Removal Cost($) |
|---|---|---|---|---|
| **501** | DriveTrain.Engine | 730 | 1519 | 3.80 |
| **505** | DriveTrain.Transmission | 478 | 240 | 0.60 |
| **508** | DriveTrain.CradleSuspension | 459 | 1 | 0.0025 |
| **28** | DoorFrontLeft | 450 | 33 | 0.08 |
| **1** | DoorFrontRight | 450 | 33 | 0.08 |
| **56** | DoorRearRight | 425 | 21 | 0.05 |
| **74** | DoorRearLeft | 425 | 21 | 0.05 |
| **476** | FrontClip.FasciaFrontLower | 225 | 115 | 0.29 |
| **481** | FrontClip.Hood | 200 | 100 | 0.25 |
| **277** | SteeringColumnAssembly | 200 | 140 | 0.35 |
| **307** | FasciaRearlower | 200 | 117 | 0.29 |
| **310** | DeckLid | 163 | 110 | 0.27 |
| **535** | InstrumentPanel.Cluster | 125 | 15 | 0.04 |
| **530** | InstrumentPanel.Radio | 125 | 232 | 0.58 |
| **321** | AirCleanerAssembly | 113 | 21 | 0.05 |

| | | | | |
|---|---|---|---|---|
| **449** | FrontClip.RadiatorHeatExchanger | 85 | 164 | 0.41 |
| **515** | WheelFrontLeft.Rim | 85 | 126 | 0.32 |
| **389** | CoolingFanShroudAssembly | 70 | 17 | 0.04 |
| **302** | TailLightCoverLeft | 65 | 91 | 0.23 |
| **299** | TailLightCoverRight | 65 | 91 | 0.23 |
| **117** | SeatFrontLeft | 50 | 91 | 0.23 |
| **92** | SeatFrontRight | 50 | 91 | 0.23 |
| **281** | SteeringColumnAssembly.Base | 50 | 0 | 0.00 |
| **479** | FrontClip.EnergyAbsorberFrontLeft | 45 | 44 | 0.11 |
| **432** | WheelRearLeft.Rim | 45 | 126 | 0.32 |
| **384** | BrakeBooster | 45 | 100 | 0.25 |
| **428** | WheelRearRight.Rim | 45 | 126 | 0.32 |
| **241** | SeatBeltRearLeft | 40 | 47 | 0.12 |
| **192** | SeatBeltFrontLeft | 40 | 12 | 0.03 |
| **183** | SeatBeltFrontRight | 40 | 12 | 0.03 |
| **259** | SeatbeltRearLeftLower | 40 | 8 | 0.02 |
| **442** | WindshieldWiperMotor | 40 | 30 | 0.08 |
| **308** | EnergyAbsorberRearLeft | 40 | 25 | 0.06 |
| **309** | EnergyAbsorberRearRight | 40 | 35 | 0.09 |
| **351** | HeatBoxAssembly.Motor | 28 | 60 | 0.15 |
| **143** | SeatRearBottom | 25 | 43 | 0.11 |
| **320** | Battery | 20 | 48 | 0.12 |
| **332** | HeatBoxAssembly | 20 | 780 | 1.95 |
| **463** | FrontClip.MarkerLightFrontLeft | 17 | 80 | 0.20 |
| **464** | FrontClip.MarkerLightFrontRight | 17 | 40 | 0.10 |
| | **TOTAL** | 5875 | 5005 | 12.5 |
| | **TOTAL for non-valuable parts** | 0 | 4112 | 10.29 |
| | **NET TOTAL** | **5875** | **9117** | **22.79** |

*Table 7.21 Disassembly optimization solution: valuable parts removed, and their associated value and removal cost*

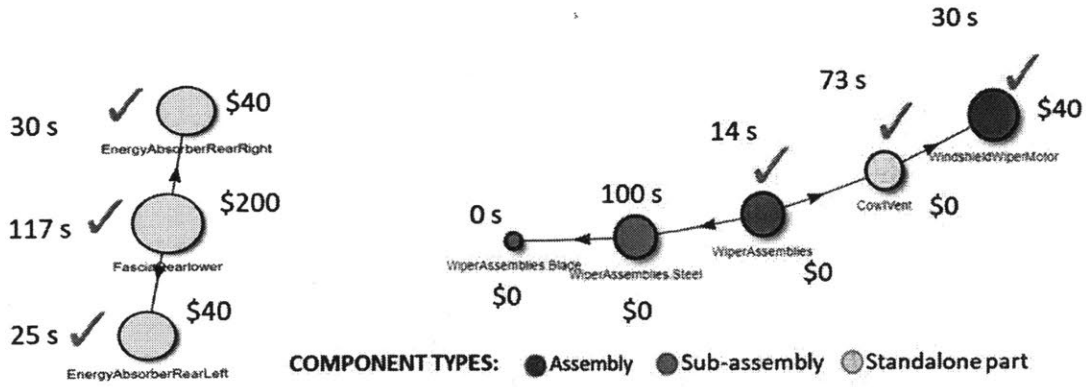


*Figure 7.15 Illustration for disassembly optimization solution: parts removed as part of a disassembly job of length > 1*

# Chapter 8 Case-study A: Partially-disassembled ELV Hulk Composition Variation

For the baseline ELV case-study, we have examined the material recovery processes assuming that a complete ELV enters the shredding/separation facility. However, this is not the case in practice, especially in the US, as old vehicles are usually sent to junk-yards or U-Pull-It yards, where automotive parts are removed for resale. This is highly common in the U.S due to the existing market for resale auto-parts, i.e. the many retail/wholesale businesses that remove and keep an inventory high-value parts for resale or remanufacture. Thus, the ELV hulks that enter the shredding/separation facility are of different material compositions from that of a complete ELV. It is important to account for the disassembled parts as resale parts can constitute on average 6-9% by weight of a car [7], [25], i.e. around 100 kg of materials that do not end up in the shredder. If parts that are removed for direct recycling are included, that could represent 19% by weight of an average European car [2]. Moreover, these parts are usually of valuable materials, and can represent a decrease in the valuable scraps actually collected, than if a complete end-of-life vehicle were shredded. Additionally, the level of contamination in the scraps can vary, depending on whether a part that is removed has a lot of ferrous fasteners or copper wires that contribute to non-liberated particles ending up in the scrap streams.

To explore the above points, we will:

(i) Run a Monte-Carlo simulation to simulate the variation in partially disassembled hulks for a fleet of 1000 ELVs;
(ii) Use each of the generated profiles of the 1000 partially-disassembled ELV hulks as input to the material recovery model.
(iii) Average the ELV hulk profiles and scrap output compositions to get a representation of the recovery performance for an average partially-disassembled hulk.
(iv) With the generated 1000 sets of scrap output compositions, we look at the distribution in their compositions, as well as in the overall performance metrics.

In the next section, we will discuss the automotive parts' reuse rates that we will use, and how we will generate the different probability distributions of the different reused auto parts. Our Monte Carlo simulations will sample from these distributions to generate the 1000 possible ELV hulks.

## 8.1 Automotive components' reuse rates

There are two databases available in the literature that could be used to define our list of reuse rates for the different car parts. The database from Sawyer-Beaulieu's work provides detailed information about the reuse of 144 car parts for both high-salvage and low-salvage (usually older) vehicles [7]. However, this data is in terms of mass flow, i.e. a part's mass fraction out of all the ELVs processed. As such,

## 8.1 Automotive components' reuse rates

There are two databases available in the literature that could be used to define our list of reuse rates for the different car parts. The database from Sawyer-Beaulieu's work provides detailed information about the reuse of 144 car parts for both high-salvage and low-salvage (usually older) vehicles [7]. However, this data is in terms of mass flow, i.e. a part's mass fraction out of all the ELVs processed. As such, there are too many assumptions to be made about the actual mass of the part as named in the database, as the data collected covers different vehicle make and model. In contrast, the database in [24] contains the direct reuse rates of 41 car components. We have adapted this data to our ELV database to match the parts' names, and the final reuse list (for 46 named parts, accounting for 4 wheels, 2 front doors and 2 front seats) is as in the table below.

The table below reports the parts and their reuse rates, along with the associated mass and material type. We also show the mapping between the part names between the two databases. We note that some parts are part of an assembly that is itself also reused, e.g. front door and front door glass, rearFrame and rearFrame.B. In such cases, we write the algorithm (similar to algorithm 1 in Section 7.1.3) will recognize that the sub-assembly has been removed if we opt to remove the assembly. In the table, if a material is noted mixed, this is because it comprises of sub-assembly components of different material types. Nevertheless, the major material in this mixed category is usually ferrous or aluminum.

| Duranceau Part Type | Reuse rate, fraction | Part in ELV database | Part ID | Weight (kg) | Material |
|---|---|---|---|---|---|
| **Front Door** | 0.37 | DoorFrontRight | 1 | 33.34 | Mixed: Ferrous |
| **Front Door Glass** | 0.15 | DoorFrontRight.Structure.Base.Glass | 19 | 2.34 | Glass |
| **Door Mirror** | 0.17 | DoorFrontRight.Structure.Mirror | 20 | 0.92 | Mixed |
| **Front Door** | 0.37 | DoorFrontLeft | 28 | 33.34 | Mixed: Ferrous |
| **Front Door Glass** | 0.15 | DoorFrontLeft.Structure.Base.Glass | 46 | 2.34 | Glass |
| **Door Mirror** | 0.17 | DoorFrontLeft.Structure.Mirror | 47 | 0.92 | Mixed |
| **Rear Door** | 0.17 | DoorRearRight | 56 | 25.5 | Mixed: Ferrous |
| **Rear Door Glass** | 0.03 | DoorRearRight.Structure.Glass | 73 | 1.79 | Glass |
| **Rear Door** | 0.17 | DoorRearLeft | 74 | 25.5 | Mixed: Ferrous |
| **Rear Door Glass** | 0.03 | DoorRearLeft.Structure.Glass | 91 | 1.79 | Glass |
| **Front Seat** | 0.12 | SeatFrontRight | 92 | 21.72 | Mixed: Ferrous |
| **Front Seat** | 0.12 | SeatFrontLeft | 117 | 21.72 | Mixed: Ferrous |
| **Rear Seat** | 0.03 | SeatRearBack | 150 | 7.2 | Mixed: Ferrous |
| **Roof Assembly** | 0.01 | Headliner | 180 | 2 | SKOS |
| **Column** | 0.14 | SteeringColumnAssembly | 277 | 10.06 | Mixed |
| **Air Bag** | 0.05 | SteeringColumnAssembly.AirBag | 278 | 1.7 | Mixed |
| **Tail lamp** | 0.12 | TailLightCoverRight | 299 | 0.54 | SKOP |
| **Tail lamp** | 0.12 | TailLightCoverLeft | 302 | 0.54 | SKOP |
| **Rear Bumper** | 0.24 | FasciaRearUpper | 306 | 1.73 | PUR |
| **Rear Bumper** | 0.24 | FasciaRearLower | 307 | 8.56 | Xenoy |
| **Deck Lid** | 0.15 | Decklid | 310 | 13.26 | Mixed: Ferrous |
| **Heater Housing** | 0.004 | HeatBoxAssemblyBase | 331 | 2.24 | PET |

| | | | | | |
|---|---|---|---|---|---|
| **Heater Core** | 0.03 | HeatBoxAssembly | 332 | 8.64 | Mixed:Aluminum |
| **Full Interior** | 0.004 | carpet | 371 | 15.88 | Mixed |
| **Wheels** | 0.87 | WheelRearRight | 426 | 16.28 | Mixed: Aluminum |
| **Wheels** | 0.87 | WheelRearLeft | 430 | 16.28 | Mixed: Aluminum |
| **Wiper Motor** | 0.01 | WindshieldWiperMotor | 442 | 1.98 | Mixed |
| **Windshield** | 0.13 | WindShieldFront | 446 | 11.76 | Glass |
| **Front End** | 0.14 | FrontClip | 448 | 175.54 | Mixed: Ferrous, Aluminum |
| **Headlamp** | 0.20 | FrontClip.LightFrontAssembly.HeadLightL | 466 | 0.86 | SKOP |
| **Headlamp** | 0.20 | FrontClip.LightFrontAssembly.HeadLightR | 470 | 0.86 | SKOP |
| **Front Bumper** | 0.11 | FrontClip.FasciaFrontLower | 476 | 9.68 | Xenoy |
| **Front Bumper** | 0.11 | FrontClip.FasciaFrontUpper | 477 | 1.2 | PUR |
| **Hood** | 0.08 | FrontClip.Hood | 481 | 22.56 | Mixed: Ferrous |
| **AC Compressor** | 0.19 | DriveTrain.ACCompressor | 486 | 6.36 | Mixed |
| **Engine** | 0.41 | DriveTrain.Engine | 501 | 200 | Mixed: Ferrous |
| **Transmission** | 0.50 | DriveTrain.Transmission | 505 | 94.55 | Mixed: Ferrous, Aluminum |
| **Wheels** | 0.87 | WheelFrontRight | 509 | 16.28 | Mixed: Aluminum |
| **Wheels** | 0.87 | WheelFrontLeft | 513 | 16.28 | Mixed: Aluminum |
| **Instrument Panel** | 0.004 | InstrumentPanel | 517 | 35.96 | Mixed |
| **Consoles** | 0.01 | InstrumentPanel.TrayAssembly | 533 | 0.5 | TPO |
| **Dash Assembly** | 0.02 | InstrumentPanel.Cluster | 535 | 1.54 | SKOS |
| **Temperature Control** | 0.06 | InstrumentPanel.HeaterControl | 536 | 0.26 | SKOS |
| **Air Bag** | 0.05 | InstrumentPanel.AirBagPassenger | 548 | 4.86 | Mixed |
| **Rear Clip** | 0.02 | RearFrame | 600 | 279 | Ferrous |
| **Quarter Assembly** | 0.08 | RearFrame.B | 602 | 101 | Ferrous |

*Table 8.1 Parts in the ELV database that are potentially removed during partial disassembly*

## 8.2 Monte-Carlo run methods

We generate a fleet of 1000 ELVs, disassembled to different degrees according to the parts' reuse rates using Monte-Carlo simulations. A part's reuse rate is its probability of removal.

Let part $i$ have probability $p_i$ of removal

Let $X_i$ denote that part $i$ stays in hulk if $X_i = 1$

Assume $X_1, X_2, \ldots, X_i$follow independent Bernoulli distributions:

$$X_i \sim Bernoulli(1 - p_i)$$

For each part $i$, 1000 Bernoulli trials are generated to specify whether or not the part is removed from the hulk. Thus, we end up with a matrix representation of the parts' list for the 1000 ELVs. For an ELV of $N$ defined parts, the matrix is of size $(1000\ X\ N)$:

$$\begin{pmatrix} & part\ 1 & part\ 2 & \cdots & part\ i \\ car\ 1 & 1 & 1 & \cdots & 0 \\ car\ 2 & 1 & 0 & \cdots & 1 \\ \vdots & \vdots & \vdots & \ddots & \vdots \\ car\ 1000 & 1 & 1 & \cdots & 1 \end{pmatrix}$$

For generating these 1000 hulks, we assume that the automotive parts are removed independently of one another. This might not be the case in practice: for instance, if the car is still in good physical condition, all the body structures might be removed, i.e. the removal of the 4 doors, hood, deck-lid, bumpers will happen altogether.

Each of the 46 parts that can be removed has a probability of removal or reuse of $p_i$, as given in Table 8.1. These probabilities vary from 0.87 for the most popular resale automotive component (wheels), to 0.004 for the least popular one (instrument panel). Note that if a part $i$ is not in the list in Table 8.1, $X_i = 1$ for all 1000 cars. Thus, the hulk profiles of 1000 cars which are partially-disassembled are generated from the matrix above, where each row represents a partially-disassembled car, with different possible combinations of removed parts.

## 8.3 Monte-Carlo run results

### 8.3.1 Average partially-disassembled ELV hulk

For our fleet of 1000 Monte-Carlo generated partially-disassembled ELV hulks, we observe that on average, 9 auto-parts are actually removed per car. The maximum and minimum number of car parts actually removed from an ELV in the fleet are 16 and 3 respectively.

We calculate the profile of the average disassembled ELV by averaging the material composition of the 1000 Monte-Carlo generated ELV hulks. Figure 8.1 shows the resulting material composition for the average disassembled ELV hulk, as well as for the parts removed for reuse, in comparison to the material composition of the complete ELV. We observe the following:

- The average partially disassembled hulk has a weight of 1120 kg. With a baseline whole ELV weight of 1407 kg, this means that an average of 287 kg of auto-parts were removed during disassembly for resale.
- The resale parts removed were predominantly of ferrous material (182 kg), but this represents only 17 % of total ferrous materials in the whole ELV. On the other hand, on average 52 kg of aluminum are in the resale parts, i.e. 54 % of the aluminum in the whole ELV is removed. This can be attributed to the high resale rates of aluminum wheels (total of 28 kg of aluminum), and of the transmission which contains 47 kg of aluminum.

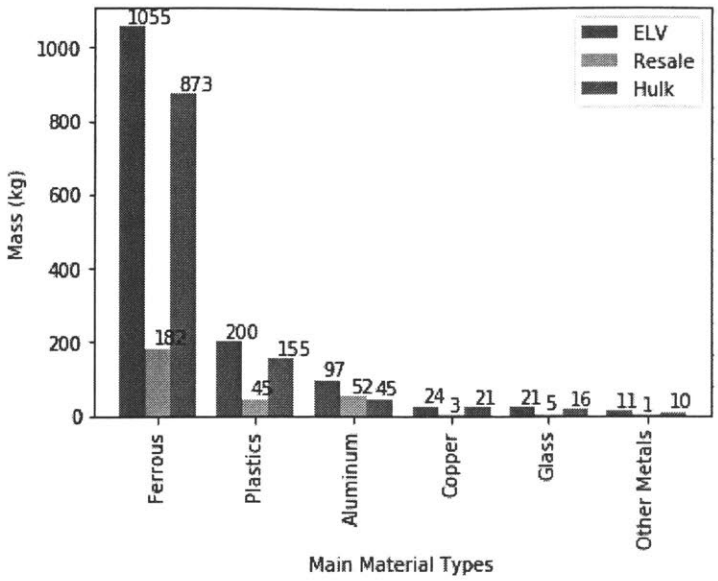


*Figure 8.1Main material composition of the average partially-disassembled ELV, resale parts, and remaining hulk*

We now look at the compositions of the scrap streams produced by the average partially-disassembled ELV. The Sankey diagram in Figure 8.2 allows us to visualize the main material flows: a relatively high proportion of the initial ferrous still remains and makes it to the ferrous scrap, and conversely a relatively small proportion of the initial aluminum remains to end up in the Twitch scrap. The resulting grade and recovery rate metrics of the scrap streams are shown in Table 8.2. As expected, we see that the recovery rate does not change much, as compared to the baseline ELV case-study: since the recovery processes are modeled by a linear system, what goes out is proportional to what comes in. On the other hand, we observe a slight increase in ferrous grade and a slight decrease in Twitch grade. This can be explained as follows: the majority of ferrous parts removed for resale (e.g. doors, engine) contains sub-components of other materials with a lot of fasteners. Thus removing these also removes the contaminants from non-liberated particles. Conversely, the main aluminum parts removed for resale (wheels, transmission) do not have a significant amount of other materials. Thus, removing these parts leaves a higher concentration of contaminants that end up in the Twitch stream. Figure 8.3 below provides a breakdown of the main material composition of each output stream: ferrous scrap, Twitch aluminum scrap, light ASR and heavy ASR). We can observe that the concentration of copper contaminant in ferrous increases slightly to 0.405 %, as compared to 0.396 % in the baseline ELV case-study. This can be the case if most of the removed parts do not contain a lot of copper wire contaminants.

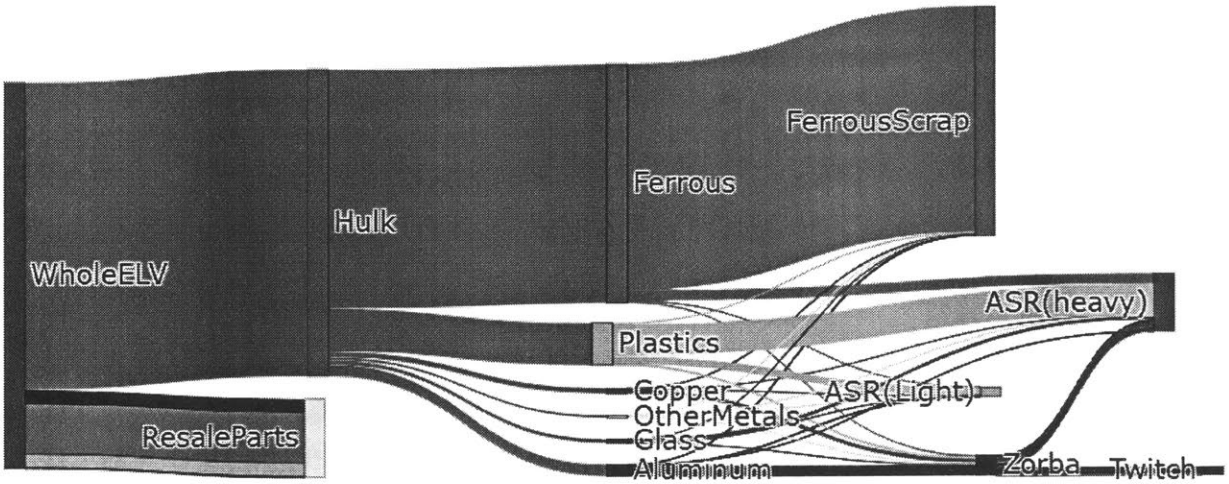


*Figure 8.2 Sankey diagram for material flows at disassembly and after separation, average partially-disassembled ELV case-study*

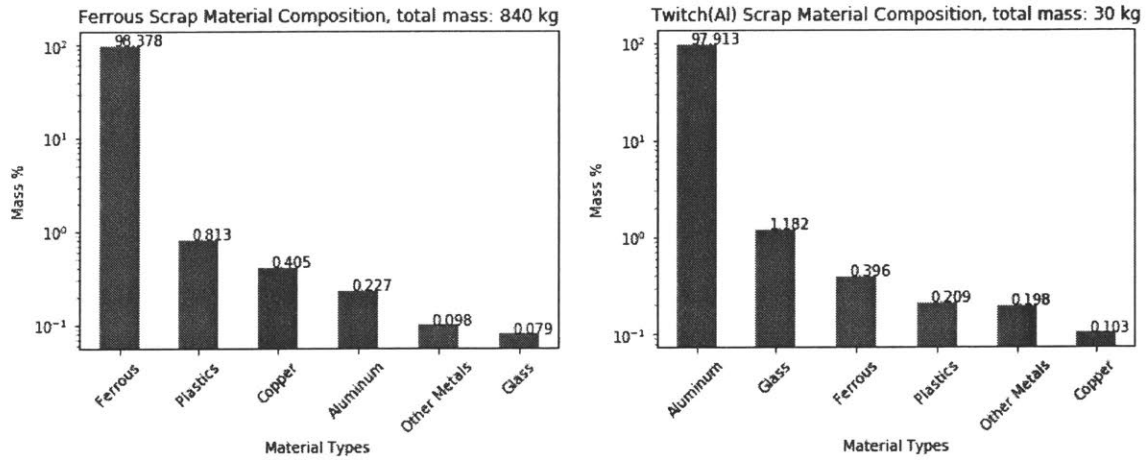


(i) (ii)

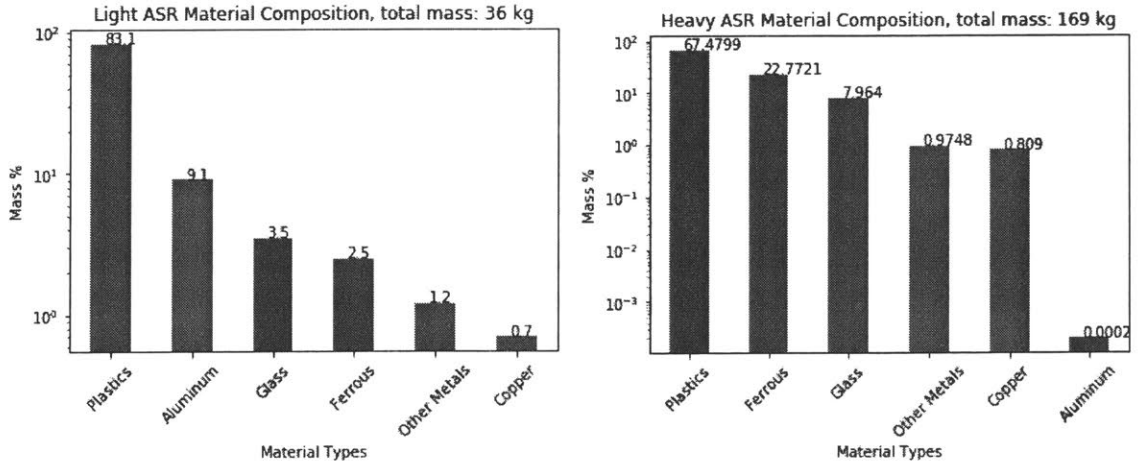

(iii) (iv)

*Figure 8.3 Main material composition for each output stream for average partially-disassembled ELV case-study: (i) Ferrous scrap; (ii) Twitch Al scrap; (iii) light ASR; (iv) heavy ASR*

| | Baseline ELV | | | Average partially-disassembled ELV | | |
|---|---|---|---|---|---|---|
| **Scrap** | **Weight (kg)** | **Recovery Rate** | **Grade** | **Weight (kg)** | **Recovery Rate** | **Grade** |
| **Ferrous** | 1017 | 94.6 % | 98.2% | 840 | 94.7 % | 98.4 % |
| **Aluminum: Zorba** | 126 | 88.3 % | 67.6 % | 75 | 88.3 % | 52.5 % |
| **Aluminum: Twitch** | 66 | 67.1 % | 98.7 % | 30 | 66.9 % | 97.9 % |
| **ASR (Light)** | 48 | 18.4 % | 77.6 % | 36 | 19.5 % | 83.1 % |
| **ASR (Heavy)** | 216 | 74.2 % | 68.9 % | 169 | 73.2 % | 67.5 % |

*Table 8.2 Recovery & grade metrics of output scraps for average partially-disassembled ELV, compared to baseline ELV case-study*

Overall performance metrics

We now calculate the overall recovery rate (ORR) using the above scrap compositions (see Table 8.3), in order to evaluate if there is any difference in the overall material recovery performance from the ELV hulk, as compared to the baseline ELV case-study. We observe that the ORR slightly increases to 89.3%. By contrast, if we consider the material recovery performance from the whole ELV by treating the parts removed for resale as recovered, the ORR increases even more to 91.5%.

| **Flow** | **Baseline ELV Mass (kg)** | **Average partially-disassembled ELV Mass (kg)** |
|---|---|---|
| **Hulk** | 1407.3 | 1120 |
| **Collected Ferrous (at Ferrous scrap)** | 998.8 | 826.8 |
| **Collected Aluminum (at Twitch scrap)** | 64.9 | 29.8 |
| **Collected Plastic (at light and heavy ASR)** | 185.7 | 30.3+113.8=144.1 |
| **ORR from hulk (%)** | (998.8+64.9+185.7)/1407 = 88.8 % | (826.8+29.8+144.1)/1120=89.3% |
| **ORR from ELV, including reused parts (%)** | | (826.8+29.8+144.1+287)/(1120+287) =91.5% |

*Table 8.3 Calculation of the overall recovery rate of average partially-disassembled ELV, from material flows of interest*

Similar to the baseline ELV case-study, we calculate the dilution costs in the secondary metal production from the ferrous and Twitch scrap streams. We will not go into the details of the dilution cost calculation, which was covered in Section 7.2.3, and more generally in Chapter 5. However, we observe that the dilution costs for secondary Aluminum production do not change much, as the composition of the Twitch is still of good quality similar to that in the baseline case-study. On the other hand, because of the higher concentration of copper contaminant in the ferrous scrap, dilution costs are

slightly worse for the low quality steel products (see Table 7.18). We use these dilution costs to calculate the NCS (normalized contribution of scrap) metric for all final metal alloy scenarios (see Table 8.5).

| | Steel Sheet | Rolled Steel | Steel Section | Steel Bar |
|---|---|---|---|---|
| **Max Cu conc in Steel product** | 0.06 % | 0.10 % | 0.30 % | 0.40% |
| **Pig iron added for dilution (kg)** | 5804.4 | 2855.7 | 313.7 | 20.4 |

*Table 8.4 Dilution addition needed for secondary processing of ferrous scrap for different scenarios of final steel products, for average partially-disassembled ELV*

| | P1020A | 1070A | 3103 | 5182 | 5754 | 6061 | 6082 | A356 | 301 | 319 | A380 |
|---|---|---|---|---|---|---|---|---|---|---|---|
| **Steel Sheet (deep-drawn)** | 0.671 | 13.47 | 14.20 | 14.11 | 14.20 | 14.40 | 14.20 | 11.75 | 13.82 | 14.44 | 14.45 |
| **Rolled Steel** | 0.685 | 22.32 | 24.43 | 24.15 | 24.43 | 25.02 | 24.43 | 17.98 | 23.30 | 25.15 | 25.15 |
| **Steel Section** | 0.697 | 51.56 | 64.36 | 62.47 | 64.37 | 68.64 | 64.36 | 33.08 | 57.10 | 69.63 | 69.65 |
| **Steel Bar** | 0.698 | 60.74 | 79.33 | 76.47 | 79.33 | 85.93 | 79.32 | 36.63 | 68.58 | 87.48 | 87.51 |

*Table 8.5 Matrix of NCS metric, calculated over the different possible scenarios of produced steel products (rows) and produced aluminum alloys (columns), for average partially-disassembled ELV*

### 8.3.2 Variation in ELV hulk & output scrap compositions

In this section, we will look at the variation in ELV hulk and output scrap compositions using the fleet of 1000 partially-disassembled ELV hulks generated by the Monte-Carlo simulations.

ELV hulk

We first analyze the variation in the ELV hulk mass going into the shredder, as depicted in Figure 8.4. From this left-skewed distribution, we can observe the following:

- A partially-disassembled hulk can have a weight as low as 681 kg. Hulks with a high degree of disassembly are a rare occurrence as that would imply having several big and heavy parts, of low probability of removal, to be removed altogether in the same hulk.
- There are a few heavy parts that have a low probability of removal, .e.g.: the rear clip with a mass of 279 kg and reuse rate of 2%, quarter assembly with a mass of 101 kg and reuse rate of 8%, instrument panel with a mass of 36 kg and reuse rate of 0.4%.
- There are more hulks on the right-side of the distribution as there are many parts that have a low probability of removal: 26 of the 46 removable parts (from Table 8.1) have a probability of less than 20%. Recall that the whole ELV has 550 named parts (including stand-alone parts, assemblies and sub-assembly components). Additionally, most of the removable parts have a low weight: 33 of the 46 removable parts (from Table 8.1) have a weight of less than 20 kg, for e.g. wheels, bumper, mirrors, etc.).

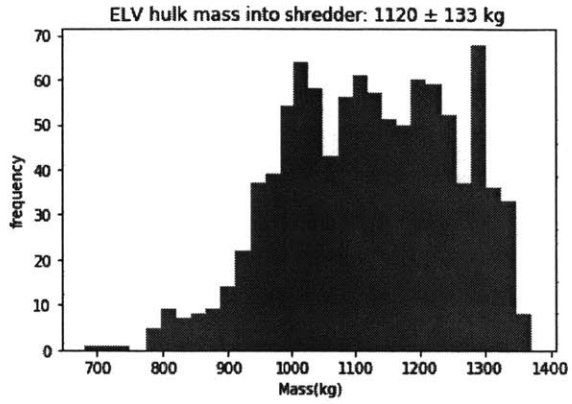


*Figure 8.4 Variation in the mass of partially-disassembled ELV hulks, from the Monte-Carlo simulations*

Ferrous scrap

We now visualize the variation in mass of the most important constituents of the ferrous scrap: ferrous and copper contaminant (see Figure 8.5). Similar to the distribution of ELV hulk weight, we can observe a left skew in the distribution of ferrous mass. This is because the low mass of Fe remaining in the hulk is possible but highly unlikely when all the massive ferrous parts are all removed, i.e. front clip, rear frame, body parts, engine and transmission. However, we can also observe a bimodal distribution. This results from the removal of reuse parts containing ferrous material, and having a reuse rate of close to 50%: (i) the engine with a reuse rate of 41% and ferrous content of 150kg; (ii) the transmission, with a reuse rate of 50% and ferrous content of 47 kg. Together, the removal of both the engine and transmission causes a total loss of Fe mass of ~200 kg, corresponding to the distance between the 2 modes. From Figure 8.5 (right), we can deduce that the distribution of the copper content follows that of ferrous. This is because the ferrous parts have associated copper wires which end up as non-liberated ferrous-copper particles.

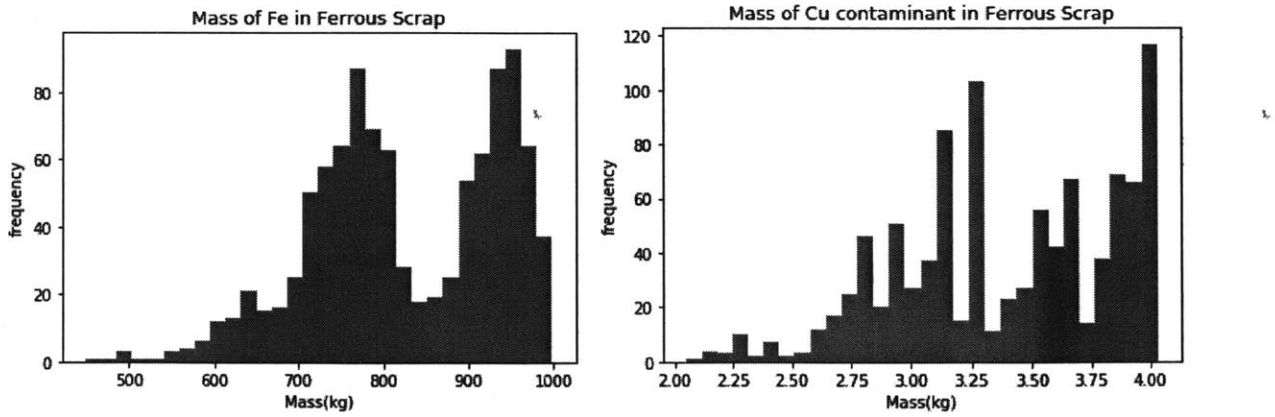


*Figure 8.5 Variation of ferrous (left) and copper contaminant (right) collected in the ferrous scrap, from the Monte-Carlo simulations of partially-disassembled ELV hulks,*

Al scrap

We now visualize the variation in mass of the most important constituents of the Twitch Al scrap: the target material aluminum (see Figure 8.6), and the contaminants ferrous and copper (see Figure 8.7). We can observe a distinctly bimodal distribution for the variation of aluminum. This can be attributed to one specific removable part containing aluminum: the transmission, which has a removal rate of 50%, and has an aluminum content of 47 kg, which corresponds to the distance between the 2 modes.

The distributions for the mass of contaminants, ferrous and copper, look different because there are few parts (among the removable parts list in Table 8.1) that have the copper wires or ferrous fasteners which contribute to the presence of these contaminants within non-liberated particles found in Twitch. Such parts when removed, result in less contamination in the Twitch scrap stream; in the figures, these removals create a distinct mode on the left. The main contributor of copper is SKOP-Copper particles (~0.04kg of them in Twitch), which represent SKOP part fragment with attached copper wires. SKOP-Copper particles originate from the instrument panel, and front clip. When the front clip is removed (at a reuse rate of 14%), this causes the drop in copper content represented by the second peak from the right. We note that this peak shows a frequency of 142: out of 1000 runs, which corresponds to the probability of 14% for removing the front-clip. Additionally, when the instrument panel is removed (reuse rate of 0.004%), this causes the third peak from the right, which shows a very low probability of occurrence.

We see a similar trend in the distribution of ferrous contaminant mass. The ferrous contaminant present in the Twitch originates from non-liberated Aluminum-Ferrous particles (~0.19 kg in Twitch) and SKOP-Ferrous particles (~0.01 kg in Twitch). Some of these particles come from the removable parts found in the list of Table 8.1: the HeatBoxAssembly and FrontClip contribute to aluminum-ferrous particles and the doors contribute to SKOP-Ferrous particles. The removal of the Fron Clip (reuse rate of 14%) causes the third peak from the right, while the removal of HeatBoxAssembly (reuse rate of 0.03%) causes the tiny peak on the left.

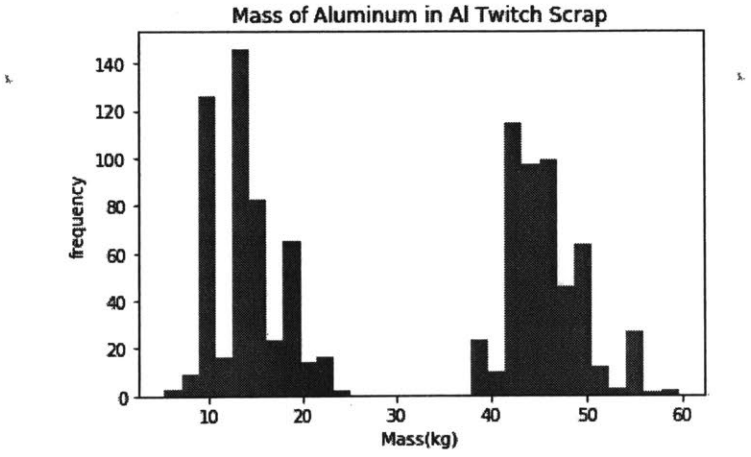


*Figure 8.6 Variation of aluminum collected in the Twitch scrap, from the Monte-Carlo simulations of partially-disassembled ELV hulks*

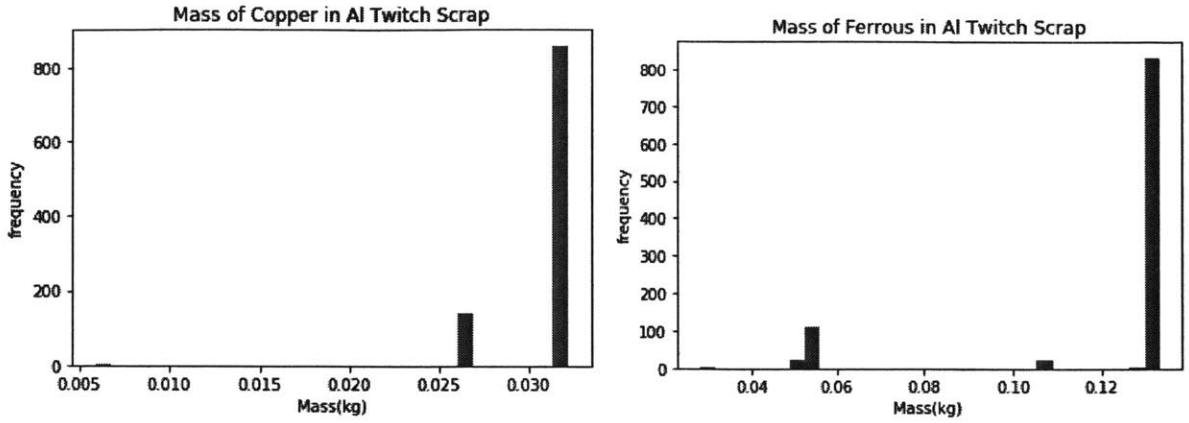


*Figure 8.7 Variation of copper and ferrous contaminants in the Twitch scrap, from the Monte-Carlo simulations of partially-disassembled ELV hulks*

### 8.3.3 Variation in performance metrics

Lastly, we look at the variation of the overall performance metrics: overall recovery rate (ORR) and Normalized Contribution of Scraps (NCS). For each Monte-Carlo generated hulk run through the material recovery model, we use the hulk and scrap material compositions to calculate the ORR, similar to calculations done in Table 8.3 . The resulting distribution for the ORR is shown in Figure 8.8 below. On average, the partially-disassembled hulks have an ORR of 89.3%, similar to the average partially-disassembled ELV hulk, with a standard deviation of 0.7 %. This is of the same order as the ORR of the baseline complete ELV.

To produce the distribution in NCS metrics, we first calculate the dilution and alloying costs from the secondary production models for aluminum and ferrous for each Monte-Carlo run. To illustrate the variation in NCS metrics, which depends on what final Al alloy and steel product are chosen, we choose three representative cases: max NCS represent the case when steel bar and A380 are produced during secondary metal production; mid NCS is the case for producing rolled steel and 6061 ; min NCS is the case for producing steel sheet and P01020A production. From Figure 8.9, we can observe that max NCS distribution is left-skewed while the min NCS distribution is right-skewed. For most ELV hulks generated, the contamination levels are low enough to require little dilution (high NCS) for the production of low-quality alloys. Conversely, the contaminations levels are too high for the production of high-quality alloys, and require substantial dilution (low NCS).

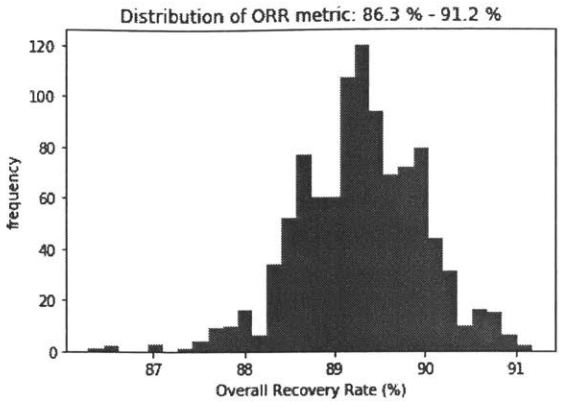


*Figure 8.8 Variation of in the overall recovery rate metric, from the Monte-Carlo simulations of partially-disassembled ELV hulks*

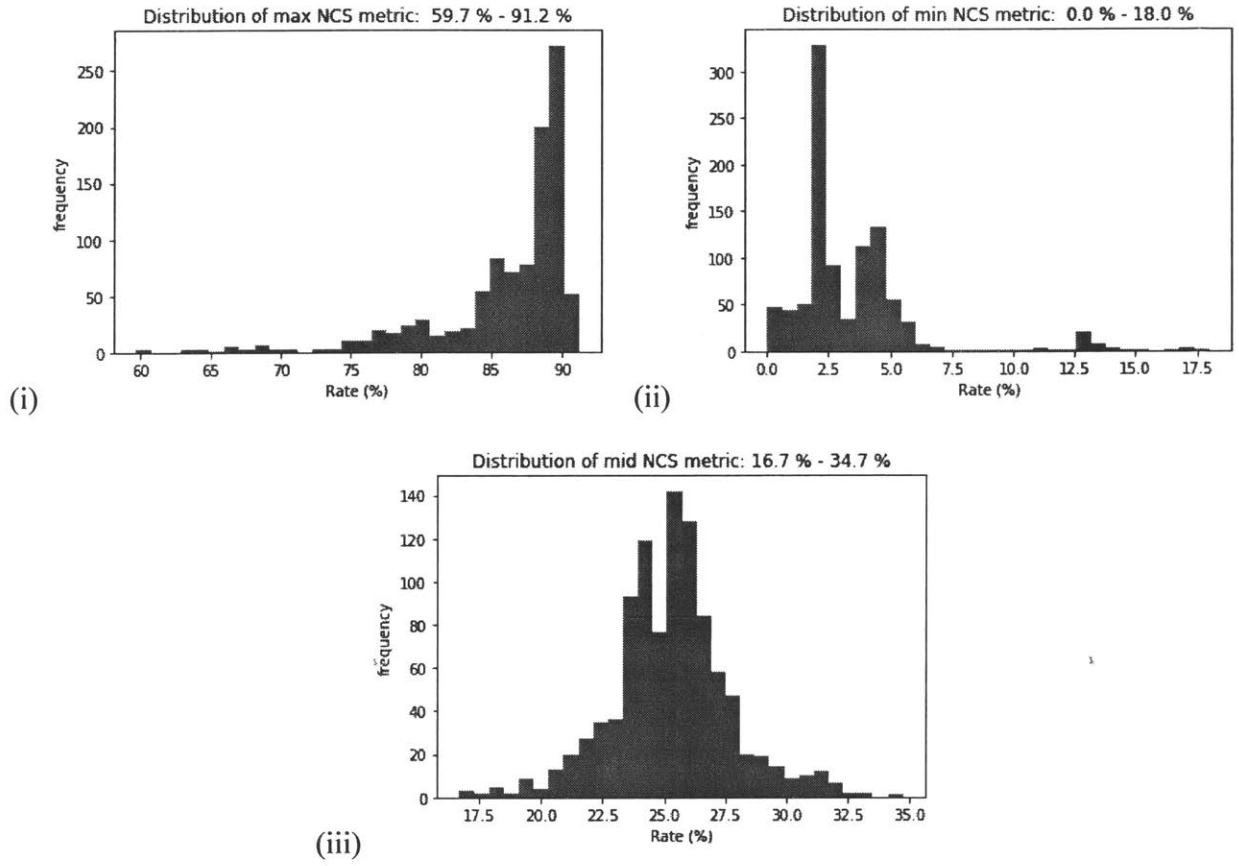


*Figure 8.9 Variation of in the NCS metric, from the Monte-Carlo simulations of partially-disassembled ELV hulks, for three final alloy production scenarios: max- steel bar and A380 Al alloy; mid- rolled steel and 6061 Al alloy; min- steel sheet and P01020A Al alloy production.*

# Chapter 9 Case-study B: Lightweight vehicles

## 9.1 Background on lightweighting

There has been a growing trend in lightweighting of vehicles in the automotive industry both in the US and the EU. In the EU, this is driven by EU directive – Regulation (EC) No 443/2009, of the European parliament, which pushes manufacturers to limit $CO_2$ emissions from light-duty vehicles [148]. In the US, in addition to emission control, lightweighting trends are driven by fuel economy improvement regulated by the government-mandated CAFE (Corporate Average Fuel Economy) standard [149]. The fuel economy for a US vehicle manufacturer's fleet of passenger cars is set to increase to 35 mpg (miles per US gallon) by 2020 [149]. A vehicle's powertrain architecture plays a huge role in determining its fuel economy and/or emissions, with powertrain options including: hybrid-electric vehicles (HEV), plug-in hybrid-electric vehicles (PHEV), electric vehicles (EV) and internal combustion vehicles (ICV). In our study, we will focus only on ICVs. An internal combustion vehicle's fuel economy depends on engine and transmission efficiencies, the fuel type and the vehicle's power requirement. The vehicle's power requirement itself can be reduced by reducing its weight: 10% reduction in vehicle weight results in 5-8% greater fuel efficiency, and 100kg of reduced vehicle weight results in up to 12.5 g/km reduction in $CO_2$ emissions [149].

With addition of new technological features such as safety equipment and entertainment systems only adding more weight, downsizing is not a long-term option for lightweighting, but *material substitution* and *design optimization* are [149]. As seen in Section 7.1, the baseline 1990's vehicle has a high ferrous content. To change this, new lightweighting technologies with new material designs are applied to the following major vehicle component groups by the automotive industry [150], [151] :

(i) Body-in-white (BIW) and closures (~34% of vehicle weight):
   a. Ultra high-strength steels
   b. Aluminum stampings, extrusions, and castings
   c. Carbon fiber and polymer matrix composites (PMC) structure

(ii) Powertrain (~26% of vehicle weight):
   a. Magnesium and Aluminum high-pressure vacuum die casting
   b. Carbon-fiber filament winding

(iii) Chassis and suspension (~25% of vehicle weight):
   a. Aluminum castings, forgings and extrusions
   b. Carbon fiber wheels

As seen in Figure 9.1 below, the structure (BIW and closures) makes up about a third of a vehicle's weight, followed by the powertrain and chassis and suspension. As noted above, the main material options being adopted by the automotive industry to enable lightweight structure are: Aluminum, advanced/high strength steels (AHSS) and carbon fiber, also referred to as carbon fiber reinforced plastic (CFRP). In [152], Lutsey provides a comprehensive list of lightweighting technologies and the corresponding components already used in existing vehicles. Numerous studies have examined

different lightweight vehicle hypothetical scenarios (based on different material technology mixes) to calculate their life-cycle energy and GHG (greenhouse gas) emission savings [150], [153]–[155]. The life-cycle calculations include the material feedstock extraction and transportation phase, fuel production and transportation phase, vehicle operation or in-use phase [150], [153]–[155]. There is significant reduction in vehicle weight when substituting conventional or advanced high-strength steel with wrought-aluminum, magnesium or CFRP in different vehicle components, as seen in Figure 9.2 [153]. However, these materials actually contribute to a higher whole vehicle-cycle GHG emissions, with CFRP contributing the most [153]. However, depending on the electricity source at production, these GHG emissions can vary [155]. AHSS produce similar GHG emissions as conventional steel, since the only difference is addition of alloying elements or thermally treating the metal, and these account for less than 5% of overall production impacts [155]. On the other hand, cast aluminum contributes to lower GHG emissions due to the high amount of recycled content used in their studies [153]. The conclusions from these analyses also depend on the lifetime assumptions for the in-use phase, as a lifetime of 50,000 mile compared to 200,000 miles or more affects the energy savings and emissions [154].

| Approximate vehicle mass breakdown[a] | System | Major components in system |
|---|---|---|
| 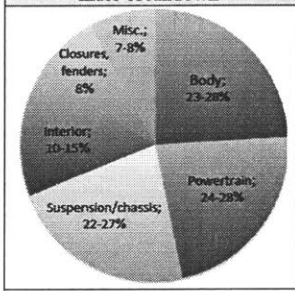 | Body-in-white | Passenger compartment frame, cross and side beams, roof structure, front-end structure, underbody floor structure, panels |
| | Powertrain | Engine, transmission, exhaust system, fuel tank |
| | Chassis | Chassis, suspension, tires, wheels, steering, brakes |
| | Interior | Seats, instrument panel, insulation, trim, airbags |
| | Closures | Front and rear doors, hood, lift gate |
| | Miscellaneous | Electrical, lighting, thermal, windows, glazing |

*Figure 9.1 Vehicle mass breakdown by system and component lists [152]*

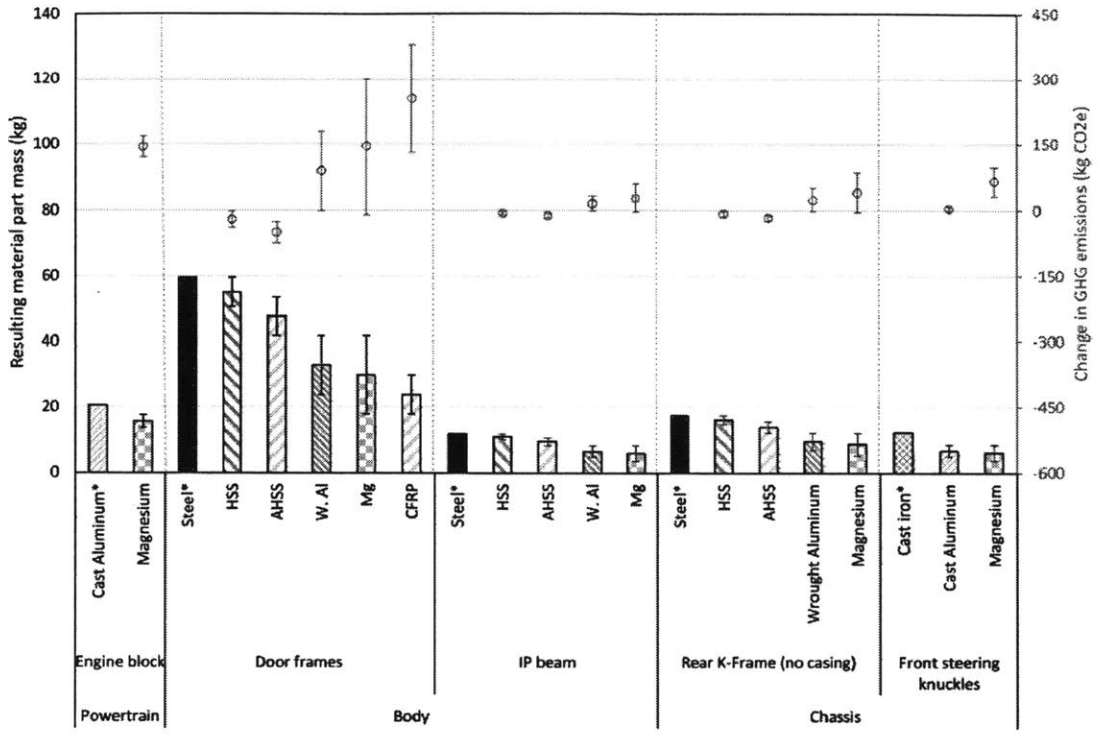


*Figure 9.2 Different material substitution scenarios in the different vehicle components, with the resulting mass savings and increase in GHG emissions, compared to the baseline conventional steel parts (with *) [153]*

While the benefits of lightweighting are well explored, the different material choices have their own different market penetration rates, as well as different pros and cons. Figure 9.3 shows the increasing use of aluminum, plastic composites and high-strength steels (as opposed to conventional steels) in vehicle design over time. However, we will focus only on the materials used in the main automotive components, i.e. the body structure, powertrain and chassis systems. Carbon fiber, or CFRP, is used in the body structure in limited applications in low-production-volume vehicles [152], such as the sports cars. Despite CFRP's higher weight-saving potential, it presents high-costs [156] and, the recycling infrastructure for CFRP is non-existent commercially [157]. As for aluminum, there was an increase in its use in European cars from 62 kg in 1990 to 157kg in 2010: while the major aluminum components are found in the powertrain, the greatest increase is happening in the car body sheets [158]. Even though aluminum provides a greater weight saving than high-strength steels, it is projected to grow from 1% in 2012 to only 19% by weight of body structures, while high-strength steels will grow from 15% to 40%, see Figure 9.4 [159].

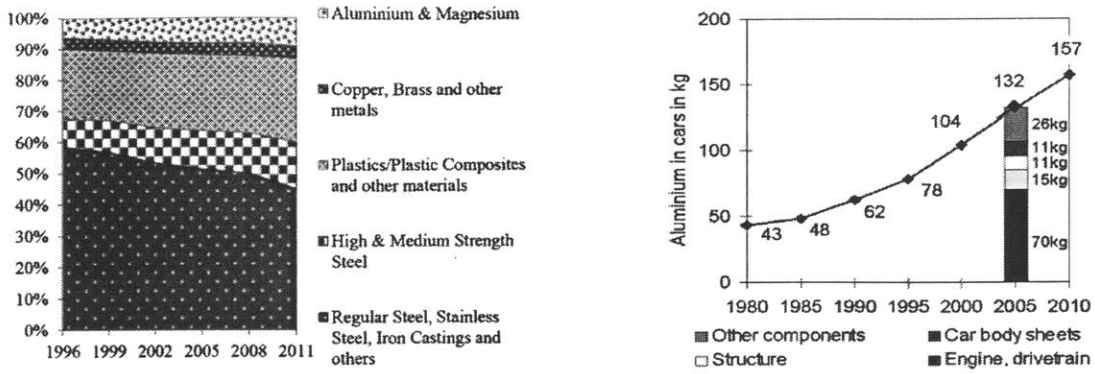


*Figure 9.3 Left: Increase use of lightweight materials in past vehicle design [160]. Right: Aluminum increase over time in European cars [158]*

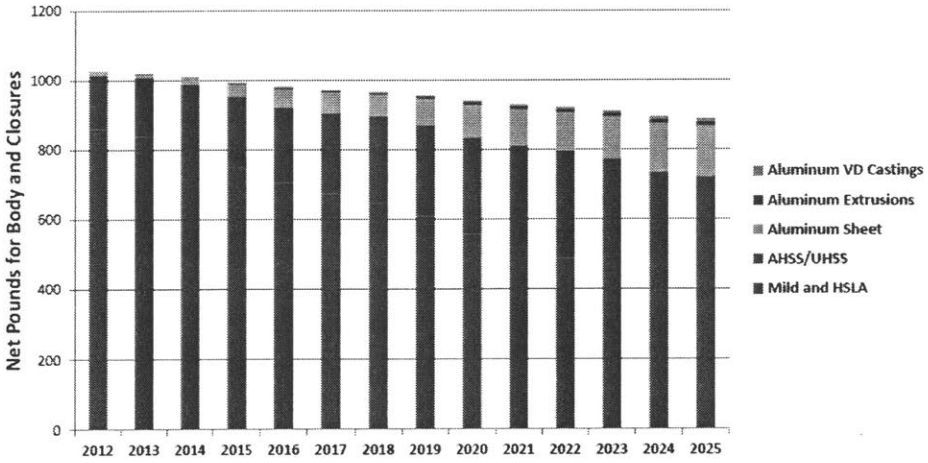


*Figure 9.4 Projected increase use of Aluminum and high-strength steels in vehicle body structures in North America[159]*

| Vehicle system | Subcomponent | New material or technique[a] | Weight reduction (lb)[b] | Example automaker (models)[c] | Source(s) |
|---|---|---|---|---|---|
| Power-train | Block | Aluminum block | 100 | Ford (Mustang); most vehicles | Tyell, 2010; Ford, 2010 |
| | Engine, housing, etc | Alum-Mg-composite | 112 | BMW (R6) | Kulekci, 2008 |
| | Engine | Smaller optimized molds (Al) | 55 | Toyota (Camry) | Simpson, 2007 |
| | Valvetrain | Titanium intake valves | 0.74 | GM (Z06) | Gerard, 2008 |
| | Connecting rod (8) | Titanium | 3.5 | GM (Z06); Honda (NSX) | Gerard, 2008 |
| | Driveshaft | Composite | 7 | Nissan; Mazda; Mitsubishi | ACC, 2006 |
| | Cradle system | Aluminum | 22 | GM (Impala) | Taub et al, 2007 |
| | Engine cradle | Magnesium | 11-12 | GM (Z06) | Gerard, 2008; US AMP, 200x |
| | Intake manifold | Magnesium | 10 | GM (V8); Chrysler | Kulekci, 2008; US AMP |
| | Camshaft case | Magnesium | 2 | Porsche (911) | Kulekci, 2008; US AMP |
| | Auxiliaries | Magnesium | 11 | Audi (A8) | Kulekci, 2008 |
| | Oil pan | Modular composite | 2 | Mercedes (C class) | Stewart, 2009 |
| | Trans. housing | Aluminum | 8 | BMW (730d); GM (Z06) | Gerard, 2008 |
| | Trans. housing | Magnesium | 9-10 | Volvo; Porsche (911); Mercedes; VW (Passat); Audi (A4, A8) | Kulekci, 2008; US AMP |
| Body and closures | Unibody design | Vs. truck body-on-frame | 150-300 | Honda (Ridgeline); Ford; Kia; most SUV models | Honda, 2010; Motor Trend, 2009 |
| | Frame | Aluminum-intensive body | 200-350 | Audi (TT, A2, A8); Jaguar (XJ); Lotus; Honda (NSX, Insight) | Brooke and Evans, 2009; Autointel, 1999; EAA, 2007; Audi, 2010 |
| | Frame | Aluminum spaceframe | 122 | GM (Z06) | Taub et al, 2007 |
| | Panel | Thinner, aluminum alloy | 14 | Audi (A8) | Audi, 2010 |
| | Panel | Composite | 42 | BMW | Diam et al, 2002 |
| | Doors (4) | Aluminum-intensive | 5-50 | Nissan (370z); BMW (7); Jaguar (XJ) | Keith, 2010; BMW, 2008; Birch, 2010 |
| | Doors (4) | New production process | 86 | Porsche (Cayenne) | Stahl, 2010 |
| | Door inner (4) | Magnesium | 24-47 | | Kulekci, 2008; US AMP |
| | Hood | Aluminum | 15 | Honda (MDX); Nissan (370z) | Monaghan, 2007; Keith, 2010 |
| | Roof | Aluminum | 15 | BWW (7 series) | BMW, 2008 |
| | Lift gate | Magnesium | 5-10 | | Kulekci, 2008; US AMP |
| Suspen. and chassis | Chassis | Aluminum | 145 | Porsche (Cayenne) | Carney, 2010 |
| | Chassis | Hydroformed steel structure, tubular design | 100 | Ford (F150) | FordF150.net, 2010 |
| | Steering wheel | Magnesium | 1.1 | Ford (Thunderbird, Taurus); Chrysler (Plymouth); Toyota (LS430); BMW (Mini); GM (Z06) | Kulekci, 2008; Gerard, 2008 |
| | Steering column | Magnesium | 1-2 | GM (Z06) | Kulekci, 2008; Gerard, 2008; US AMP |
| | Wheels (4) | Magnesium | 26 | Toyota (Supra); Porsche (911); Alfa Romeo | Kulekci, 2008; US AMP |
| | Wheels (4) | Lighterweight alloy, design | 13 | Mercedes (C-class) | Tan, 2008 |
| | Brake system | Heat dissipation, stainless steel pins, aluminum caps | 30 | Audi (A8) | Audi, 2010 |
| | Tires | Design (low RR) | 4 | Mercedes (C-class) | Tan, 2008 |
| | Suspension | Control arms (3) | 6 | Dodge (Ram) | SSAB, 2009 |
| Interior | Seat frame (4) | Magnesium | 28 | Toyota (LS430); Mercedes (Roadster) | Kulekci, 2008; US AMP |
| | Instrument panel | Magnesium | 7-13 | Chrysler (Jeep); GM; Ford (Explorer, F150); Audi (A8); Toyota (Century); GM | Kulekci, 2008; US AMP; Taub et al, 2007 |
| | Dashboard | Fiber-reinforced thermoplastic | 18 | VW (Golf) | Stewart, 2009 |
| | Console and shifter | Injection molded glass reinforced polypropylene | 5 | Ford (Flex) | Stewart, 2009 |
| Misc. | Windows | Design, material thickness | 3 | Mercedes (C-class) | Tan, 2008 |
| | Running board | Glass-reinforced polypropylene | 9 | Ford (Escape) | Stewart, 2009 |

*[a] These technologies can include a change in design, a reduction in parts, a reduction in material amount, and use of various metallic alloys; note that weight (lb) and mass (kg) variables are used in this report. 1 kg = 2.205 lb.*

*[b] Weight reduction estimates are approximate, based on media sources and technical reports*

*[c] A number of these models are not available in the U.S.; some model names have changed in recent product changes*

*Table 9.1 Component weight-reduction potential from technologies on production vehicles [152]*

As seen through the above-mentioned literature, automotive manufacturers have looked at a wide array of material substitution for lightweighting vehicles. However, for this case-study, we will focus on the aluminum-intensive vehicle (AIV), due to its high weight-saving potential and the emerging design changes needed for joining technologies. While there is a comprehensive data on the hypothetical lightweight vehicle profile used in the GREET (Greenhouse gases, Regulated Emissions, and Energy use in Transportation) model [161], [162, p.], the lightweight vehicle profile includes CFRP for the body structure components, and aluminum used partially in the other components. For AIVs in

particular, we have relied on aluminum component-specific data in [163], where the weight-saving in switching from steel to aluminum structure components is detailed, based on Ford's Mercury Sable aluminum-body concept car. We also note that we need alloy-specific information if we are to delve into a more granular level. As discussed in Chapter 5, different aluminum alloys have different chemical compositions due to different ratios of alloying elements added to give different physical properties. As such, different vehicle components in an AIV use different aluminum alloys based on the components' functionalities, production and safety requirements. While cast aluminum is used mainly in the powertrain components such as engine components and transmission, wrought aluminum is used mostly in the body structure parts. Such parts require extrusion, stamping or forming in production, and high strength, toughness and machinability are needed in the material properties [164]. While wrought and cast aluminum categories are often used for component-specific data (e.g. in the GREET model Burnham 2012), the work of Modaresi details component alloy compositions broken down into seven alloy categories of different aluminum series, see Table 9.2 [52].

| Alloys categories Components | 1xxx | 3xxx | 5xxx | 6xxx | 2xxx/7xxx/ 6xxx | 4xxx + cast alloys with low impurity | High Si cast alloys |
|---|---|---|---|---|---|---|---|
| **C1: Full body in white (BIW) and partial BIW** | 0 % | 0 % | 40 % | 45 % | 0 % | 15 % | 0 % |
| **C2: Closures** | 0 % | 0 % | 35 % | 65 % | 0 % | 0 % | 0 % |
| **C3: Bumpers and crash boxes** | 0 % | 0 % | 5 % | 80 % | 15 % | 0 % | 0 % |
| **C4: Heat shields** | 75 % | 25 % | 0 % | 0 % | 0 % | 0 % | 0 % |
| **C5: Heat exchangers** | 45 % | 25 % | 5 % | 5 % | 0 % | 20 % | 0 % |
| **C6: Engine block and cylinder heads** | 0 % | 0 % | 0 % | 0 % | 0 % | 45 % (A319 and 380) | 55 % (A319 and 380) |
| **C7: Suspension frames** | 0 % | 0 % | 40 % | 20 % | 0 % | 40 % | 0 % |
| **C8: Suspension and steering arms** | 0 % | 0 % | 5 % | 80 % | 0 % | 15 % | 0 % |
| **C9: Wheels** | 0 % | 0 % | 0 % | 10 % | 0 % | 90 % (A356) | 0 % |
| **C10: Transmission and driveline** | 0 % | 0 % | 0 % | 10 % | 0 % | 10 % | 80% |
| **C11: Brake components** | 0 % | 0 % | 10 % | 30 % | 0 % | 60 % | 0 % |
| **C12: All other engine components** | 0 % | 0 % | 5 % | 10 % | 5 % | 0 % | 80 %(301 in pistons due to Ni) |
| **C13: All other steering components** | 0 % | 0 % | 10 % | 25 % | 0 % | 25 % | 40 % |
| **C14: All other interior and exterior components** | 30 % | 5 % | 10 % | 40 % | 0 % | 15 % | 0 % |

*Table 9.2 Components of aluminum used in passenger cars and corresponding alloy composition [52]*

Together with material substitution, a concurrent aspect is the need for changes in joining and assembly technologies (Mascarin et al. 2015). In a lightweight vehicle with a multi-material design, different components with dissimilar materials that are assembled together, need to be joined with new or different joining technologies [165]. Traditional joining methods used on conventional steel body structures include spot welding and metal-inert gas (MIG) welding because they are easily automated and flexible during production [165]. However, there are several issues with achieving high-quality welds with aluminum sheets: (i) the aluminum oxide layer increases contact resistance; (ii) as aluminum has a lower melting temperature, it melts and forms a porous weld nugget at the electrode/Al

interface and not with Al/steel interface [165]. While GM has been able to use resistant spot welding on their vehicles (Cadillac, Chevrolet, GMC), other automotive manufacturers (Ford in the F-150, Audi in the A8, Land Rover in their SUV) have turned to mechanical joining techniques [166]. Overall, with an increased use of aluminum in the vehicle body structure, traditional welding techniques are used less, while mechanical joining techniques (e.g. screws and rivets, together with adhesive bonding) are increasing in use, as seen in red in Table 9.3 [129].

| Joint type | Audi A6 | | | | Audi A8 | | | |
|---|---|---|---|---|---|---|---|---|
| | 2001-2004 | | 2005-2008 | | 1994-2002 | | 2009-present | |
| ***Share of point joints (%, quantity)*** | | | | | | | | |
| **Spot welding** | 91.5% | 6147 | 81.0% | 5102 | 28.1% | 500 | 7.5% | 202 |
| **Stud welding** | 3.3% | 220 | 6.5% | 408 | 0.0% | 0 | 0.0% | 0 |
| **Clinching** | 0.9% | 63 | 1.3% | 83 | 10.0% | 178 | 0.0% | 0 |
| **Screw joints** | 0.0% | 0 | 0.0% | 364 | 0.0% | 0 | 23.6% | 632 |
| **Rivets** | 0.0% | 0 | 5.8% | | 61.9% | 1100 | 68.9% | 1847 |
| ***Share of linear joints (%, m)*** | | | | | | | | |
| **Laser welding** | 8.3% | 3.5m | 3.3% | 4.5m | 0.0% | 0m | 8.0% | 6m |
| **MIG welding** | 6.0% | 2.5m | 4.3% | 5.9m | 100.0% | 70m | 33.3% | 25m |
| **Laser brazing** | 0.0% | 0m | 3.1% | 4.2m | 0.0% | 0m | 0.0% | 0m |
| **Adhesive bonding** | 85.7% | 36m | 89.3% | 122m | 0.0% | 0m | 58.7% | 44m |

*Table 9.3 Joining trends of different vehicle models' body structure, adapted from [129], [164], [167]*

## 9.2 Lightweight Vehicle profile data

### 9.2.1 Aluminum automotive components

As seen in the literature review above, while there exist different material-substitution scenarios with different materials used in different components, the two main trends are *high-strength steel-intensive vehicles and aluminum-intensive vehicles*. For our simple case-study of a lightweight vehicle, we will create an aluminum-intensive vehicle (AIV) profile, by substituting aluminum for ferrous in specific components either completely or partially. Note that we need to calculate the associated aluminum mass after material substitution. While it entails a decrease in mass from its prior ferrous counterpart, there are different design considerations (e.g. safety) that might require a different volume of the components. Where possible, our calculations take material substitution data from the literature in [161], [163] . Thus, we consider the components and material substitution as follows:

(i) Powertrain:

This includes the engine, transmission, exhaust system and fuel tank. The latter two components were not specifically labeled in our baseline ELV database and were thus not considered. However, the transmission in our database already has a 50% Al-50% ferrous material composition and was not changed. Incidentally, in the GREET 2 model lightweight vehicle, the transmission does not see any increase in aluminum from the conventional ICV [161]. We thus assume that the aluminum content cannot be increased

due to design constraints. We increase the aluminum content in the engine from 0% in our baseline vehicle to 42% in our AIV as noted in the GREET model lightweight vehicle. In our calculation for the amount of substitute aluminum, we assume that the original volume of the engine stays constant, and we used densities of 2725 km/m$^3$ and 7900 kg/m$^3$ for the ferrous and aluminum materials respectively.

(ii) Chassis and suspension:
This includes the chassis, suspension, wheels, steering and brakes. In our ELV database, the wheels are already of aluminum, and the brakes and steering parts partially contain aluminum. As the GREET 2 model does not increase aluminum content in these parts, we do not change them either. However, we replace the ferrous with aluminum in the "CradleSuspension" part, using the following conversion equation:

$$part\ mass_{Al\ in\ LW\ ELV} = \frac{GREET\ part\ mass_{Al\ in\ LW\ ELV}}{GREET\ part\ mass_{Fe\ in\ ELV}} * part\ mass_{Fe\ in\ ELV}$$

As the GREET 2 model represents the "CradleSuspension" part with the "Driveshaft/axle" (change in mass from 163 to 65 kg) and the "suspensions" (change in mass from 90 to 44 kg) [161], we calculate the new mass of the aluminum "CradleSuspension" in our model as: $\frac{(65+44)}{(90+163)} * 108 = 47kg$. Henceforth. We will refer as this conversion rate as the GREET 2 ratio. Table 9.4 lists the ratios for all the ferrous parts substituted with aluminum.

In our ELV database, the chassis is integrated with the body-in-white frame in parts labeled as "RearFrame" and "FrontClip.Frame". As the GREET model substituted 100% of the chassis for a lightweight material (glass-fiber composite), we will do so but with aluminum.

(iii) Body structure:
This includes the body-in-white frame, and closures i.e. roof, fenders, hood, decklid, doors, crash-elements/bumpers (see Figure 9.5). The roof and fender were not specifically labeled in our baseline ELV database and were thus not considered. The energy absorbers in our database were identified as the crash-elements and the mass for the substitute aluminum was calculated from GREET ratio (5/22) of bumper mass before and after lightweighting [161]. For the hood, decklid, doors, and body-in-white (labeled as "RearFrame" and "FrontClip.Frame" in our database), the mass-substitution calculation used the corresponding component mass ratio in [163], labeled as "ANL_1995 ratio" in Table 9.4 below.

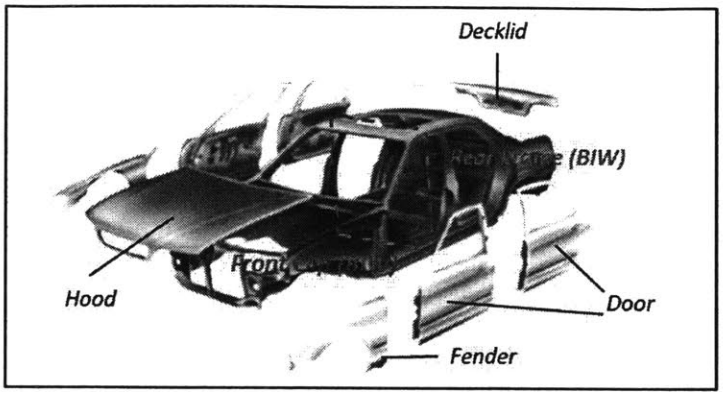


*Figure 9.5 Body structure components considered in the material substitution of our ELV (adapted from [154])*

Table 9.4 below lists all the parts for which the steel has been partially or completely substituted with aluminum, as well as the assumptions used for mass amount calculations. We should highlight that this lightweight vehicle profile is hypothetical and provides an upper-bound for the possible amount of substitution with aluminum: design constraints, which might limit the percentage of aluminum used in the body-in-white, were not taken into consideration, being beyond the scope of this research.

| Part ID | Name | Weight (kg) | Material | Calculation Assumptions | New Part ID | New Weight (kg) | New Material |
|---|---|---|---|---|---|---|---|
| **502** | DriveTrain.Engine.Steel | 150 | Ferrous | GREET 2 ratio: assume 42% Al Cast,using density ratio, keeping total volume constant | 2000 | 68.3 | Ferrous |
| **503** | DriveTrain.Engine.SKOM | 30 | Ferrous | GREET 2 ratio: assume 42% Al Cast,using density ratio, keeping total volume constant | 2001 | 49.5 | Aluminum _cast |
| **508** | DriveTrain. CradleSuspension | 107.96 | Ferrous | GREET 2 ratio: (65+44)/(90+163) | 2002 | 46.5 | Aluminum _cast |
| **478** | FrontClip. EnergyAbsorberFrontRight | 2.5 | Ferrous | GREET 2 ratio: (5/22) | 2003 | 0.6 | Aluminum _wrought |
| **479** | FrontClip. EnergyAbsorberFrontLeft | 2.5 | Ferrous | GREET 2 ratio: (5/22) | 2004 | 0.6 | Aluminum _wrought |
| **308** | EnergyAbsorberRearLeft | 2.46 | Ferrous | GREET 2 ratio: (5/22) | 2005 | 0.6 | Aluminum _wrought |
| **309** | EnergyAbsorberRearRight | 2.46 | Ferrous | GREET 2 ratio: (5/22) | 2006 | 0.6 | Aluminum _wrought |
| **311** | DeckLid.Lid | 10.88 | Ferrous | ANL_1995 ratio: (5.4/17) | 2007 | 3.5 | Aluminum _wrought |
| **483** | FrontClip.Hood.Lid | 17.49 | Ferrous | ANL_1995 ratio: (9.1/22.2) | 2008 | 7.2 | Aluminum _wrought |
| ***484*** | *FrontClip.Frame* | *125* | *Ferrous* | *ANL_1995 ratio: (145/270.3)* | *2009* | *67.1* | Aluminum _wrought |
| **615** | FrontClip.Frame.A | 72 | Ferrous | ANL_1995 ratio: (145/270.3) | 2010 | 38.6 | Aluminum _wrought |
| **616** | FrontClip.Frame.B | 53 | Ferrous | ANL_1995 ratio: (145/270.3) | 2011 | 28.4 | Aluminum _wrought |
| ***600*** | *RearFrame* | *279* | *Ferrous* | *ANL_1995 ratio: (145/270.3)* | *2012* | *149.7* | Aluminum _wrought |
| **601** | RearFrame.A | 178 | Ferrous | ANL_1995 ratio: (145/270.3) | 2013 | 95.5 | Aluminum _wrought |
| **602** | RearFrame.B | 101 | Ferrous | ANL_1995 ratio: 145/270.3) | 2014 | 54.2 | Aluminum _wrought |
| **17** | DoorFrontRight.Structure. Base.Steel | 24.21 | Ferrous | ANL_1995 ratio: (9.8/17) | 2015 | 14.0 | Aluminum _wrought |

| | | | | | | | |
|---|---|---|---|---|---|---|---|
| 44 | DoorFrontLeft.Structure.Base.Steel | 24.21 | Ferrous | ANL_1995 ratio: (9.8/17) | 2016 | 14.0 | Aluminum_wrought |
| 71 | DoorRearRight.Structure.Steel | 18.58 | Ferrous | ANL_1995 ratio: (8.2/12.9) | 2017 | 11.8 | Aluminum_wrought |
| 89 | DoorRearLeft.Structure.Steel | 18.58 | Ferrous | ANL_1995 ratio: (8.2/12.9) | 2018 | 11.8 | Aluminum_wrought |

*Table 9.4 Material substitution used in baseline ELV data for case-study of AIV as lightweight car*

### 9.2.2 Joints in Aluminum-Intensive Vehicles

From Table 9.3, we saw that body structures of the aluminum-intensive vehicles such as the Audi A8, have a high proportion of mechanical fasteners, specifically 632 screws and 1847 rivets. As we do not have data about the ratio of steel to aluminum in the Audi A8, we assume that these quantities of mechanical fasteners are evenly distributed among our all-aluminum body-structure parts in our lightweight ELV database, in proportion to their weight, as detailed in Table 9.5 below. These quantities would thus represent the upper-bound of the number of aluminum-ferrous joints, assuming that the screw and rivet joints are of steel.

As detailed in [166], flow-drill screws (FDS), self-piercing rivets (SPR) and clinching joints are used together with aluminum in the vehicle body structures. We will assume the scrap contamination due to clinching joints is negligible because (i) they are not as widely used compared to FDS and SPR (see Table 9.3); (ii) clinching joints are formed by plastic deformation of the joined metal sheets, causing interlocking, and do not use external elements [165]. Thus, while clinching joints might result in some contamination if dissimilar sheets are joined together and can give rise to non-liberated joint particles, in our study, we are only looking at contamination due to additional elements of mechanical fasteners.

| PartID | Name | Weight (kg) | Screw joints (qty) | Rivets (qty) |
|---|---|---|---|---|
| 2010 | FrontClip.Frame.A | 38.6 | 113 | 329 |
| 2011 | FrontClip.Frame.B | 28.4 | 83 | 242 |
| 2013 | RearFramè.A | 95.5 | 278 | 814 |
| 2014 | RearFrame.B | 54.2 | 158 | 462 |
| | **TOTAL** | **216.7** | **632** | **1847** |

*Table 9.5 Joint types and quantities added to body structure of AIV in case-study of lightweight vehicle*

SPR rivets are formed by pushing the rivet element through the joined sheets against a die, and deformation of the rivets and sheets produces mechanical interlocking [168]. This can be seen in the cross-section example in Figure 9.6. The rivets used in SPR joints in industry are typically of high-strength steel, as aluminum alloys would not have enough strength to prevent severe deformation during compression into the metal sheets to be joined, although research on achieving functional aluminum rivets is ongoing [169]. Hence, as observed by Soo et al. [109], [129], SPR rivets contribute to contamination and impede recycling.

Flow-drill screws work as follows: (i) the rotating screws heats up the materials being joined, facilitating penetration; (ii) the materials are concurrently extruded into a funnel shape; (iii) threads form within this funnel, creating a deep interlock depth as seen in Figure 9.7 [165]. FDS are said to perform better than the typical spot-welded joints [170]. FDS, along with structural adhesives, are used in the BIW and closure joints when there are limitations for self-piercing rivets due to single-side access or insufficient gun clearance. Other types of joints less commonly used in such cases are RivTac and Huck rivets [171]. While aluminum flow-drill screws exist, they are used to drill in plastics, but are not sufficient in mechanical strength to drill into harder steel or aluminum sheets [170].

Therefore, we assign FDS and SPR joints to have elements made of ferrous. Additionally, we calculate their typical volume based on dimensions listed in [147], [169] for the rivet and screw elements respectively, as depicted in Figure 9.6 and Figure 9.7. The volumes calculated are listed in Table 9.6 Properties of additional joints in AIV in case-study of lightweight vehicle below. The ferrous fasteners add a total of 2kg.

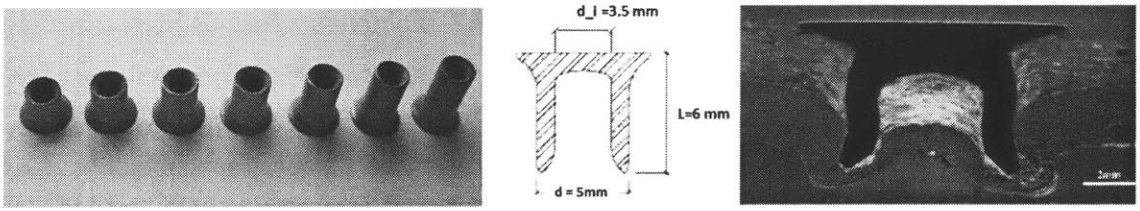


*Figure 9.6 Left: stand-alone SPRs; middle: dimensions of SPR joint used in our study; right: Cross-section of an SPR joint in a 2mm glass fiber composite and 2mm Aluminum alloy sheet [168], [169]*

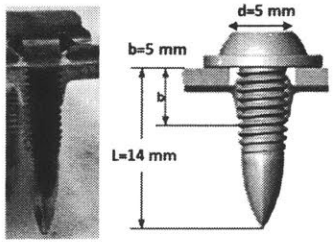


*Figure 9.7 Left: Flow-drill screw steel-Al joint [165]; right: dimensions of flow-drill screw joint used in our study, adapted from [147]*

| JointName | Material | Density | Volume(m3) |
|---|---|---|---|
| **FlowDrillScrew** | Ferrous | 7850 | 1.3E-07 |
| **SelfPiercingRivet** | Ferrous | 7850 | 9.3E-08 |

*Table 9.6 Properties of additional joints in AIV in case-study of lightweight vehicle*

## 9.3 Lightweighting case-study results

### 9.3.1 Shredder input material composition

Due to the changes in the material part data and the joint data, the shredder input material composition of the lightweight aluminum-intensive vehicle (AIV) is different from that of our baseline steel-intensive vehicle. The complete material flow into the shredder in listed in Table A-7 of Appendix A. Table 9.7 describes the main changes to the material composition that results from the lightweighting assumptions described in Section 9.2:

- The lightweight AIV is 367 kg lighter than our baseline vehicle.
- The weight of aluminum in the AIV is more than four times that in our baseline vehicle, while the weight of ferrous materials decreases to about a fourth.
- There is a greater fraction of wrought aluminum than cast aluminum. This is because most of the new aluminum components are body structures, which are typically of wrought aluminum for structural integrity.
- There is an increase in non-liberated particles, namely in aluminum-ferrous and aluminum-copper particles. The increase in the former is due to aluminum fragments with ferrous fasteners attached, with the fragments coming from the aluminum body structure and energy absorbers. The aluminum-copper particles come from the doors, deck lid and hood which have copper wires running through them.

| | Baseline (Steel-Intensive) vehicle | Lightweight (Aluminum-Intensive) vehicle |
|---|---|---|
| **Total Weight (kg)** | 1407 | 1040 |
| **Aluminum (kg)** | 96 | 471 |
| **Cast Al: Wrought Al ratio** | 0.48:1 | 0.37:1 |
| **Ferrous (kg)** | 1032 | 285 |
| **Aluminum-Ferrous (kg)** | 2.0 | 7.3 |
| **Aluminum-Copper (kg)** | 0.0 | 1.4 |

*Table 9.7 Main changes in weight and material composition for lightweight aluminum intensive vehicle*

### 9.3.2 Separation output: scrap quality and material composition

We run our aluminum-intensive ELV through the shredder and separation models, keeping the same model parameters as used in the baseline ELV case-study. Through the Sankey diagram in Figure 9.8 below, we can visualize the material flows through the separation units to the collected scraps. We use the same notation as the Sankey diagram in Section 7.2.2, with the color codes denoting the material types, and the right-hand side representing the output streams. As we model the material flows in each process as a linear system, the output changes proportionally with the input. Hence, with the aluminum-intensive ELV as opposed to the baseline ELV, the higher input of aluminum but lower input of ferrous results in an increase in collected aluminum at the Twitch scrap, and lower amount of ferrous collected at the ferrous scrap.

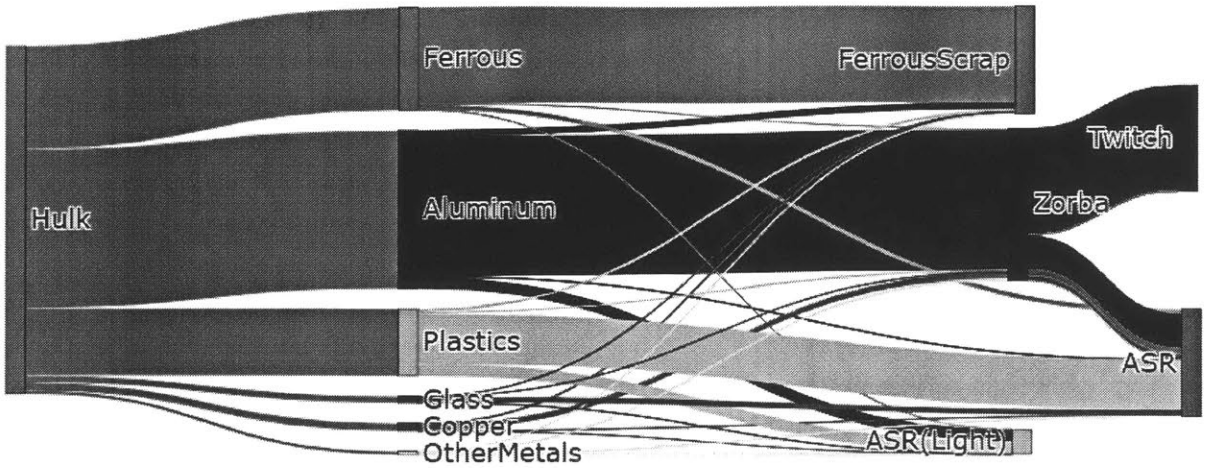


*Figure 9.8 Sankey diagram for material flows before and after separation, lightweight ELV case-study*

We now look more closely at the composition of each collected scrap to see the impact of lightweighting on contamination levels. From the material composition of ferrous scrap in Figure 9.9, we can see an increased amount of aluminum (to 20 kg or 6.2 % weight), which also contributes to an increase in liberated impurities. There is a slight decrease in the amount of copper (3.5 kg as compared to 4.1kg in the baseline ELV); however, the concentration of the copper contaminant actually increases (to 1.1% as compared to 0.4% in the baseline ELV) as the total mass of the ferrous scrap decreases. We note that when examining the dilution costs of secondary steel production from ferrous, we are only concerned with contamination from copper, because copper is a tramp element that cannot be removed by oxidation, like aluminum. From Figure 9.9 (right), we can also see an increase in non-liberated ferrous impurities, but this results from the decrease in total mass of the ferrous scrap, as the amount of impurities with attached ferrous fasteners stay about the same (11kg).

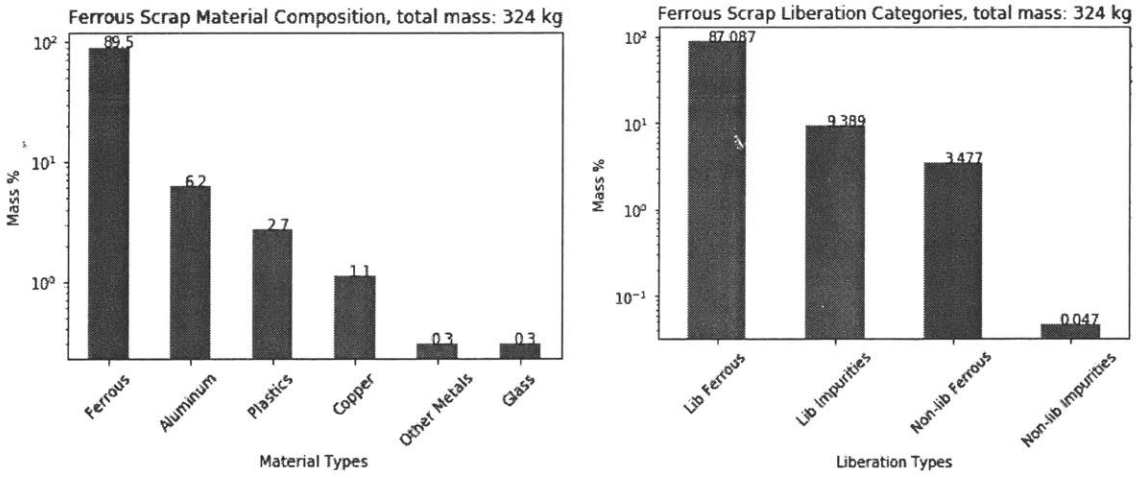


*Figure 9.9 Ferrous scrap (at output unit V1): main material composition (left); liberation categories (right), lightweight ELV case-study*

Figure 9.10 and Figure 9.11 show that the grade of both Zorba (92% from 68%) and Twitch (96.7% to 99.6%) scrap increases. This can be attributed to the increase of aluminum in the ELV hulk entering

the system. From Figure 9.11, one can calculate the mass of ferrous in Twitch scrap to be 0.4kg, as compared to only 0.1kg in the baseline ELV scenario. This increase in ferrous comes from the increase in non-liberated aluminum-ferrous joints ending up in Twitch (0.7kg as compared to 0.2kg in baseline ELV scenario). This is a consequence of the additional joints: the aluminum body-frame is held together by ferrous flow-drill screws and self-piercing rivets, as described in Section 9.2.2. However, there is no consequential change in the amount of contamination due to non-liberated aluminum-ferrous particles. This is because the increase of aluminum-ferrous joints in the input stream is not enough to cause an increase in concentration of ferrous. As for copper contaminant, there is a slight increase in mass (0.07kg as compared to 0.03kg in the baseline ELV scenario). This comes from the change in material from ferrous to aluminum for certain body structure parts having copper wires, and the resulting increase in non-liberated aluminum-copper particles in the feed, at the expense of ferrous-copper particles. However, similarly, there is no increase in concentration of copper contaminant due to the large mass of aluminum going through.

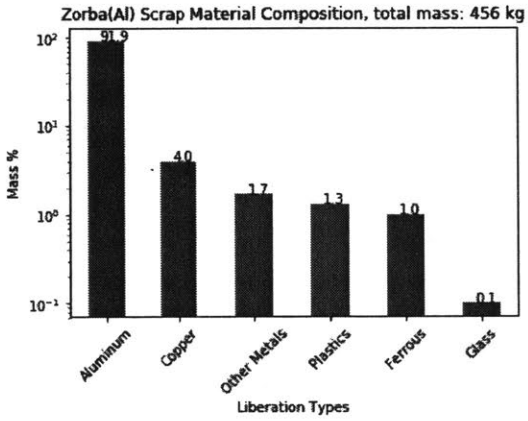


*Figure 9.10 Zorba Al scrap (received at unit U7): main material composition, lightweight ELV case-study*

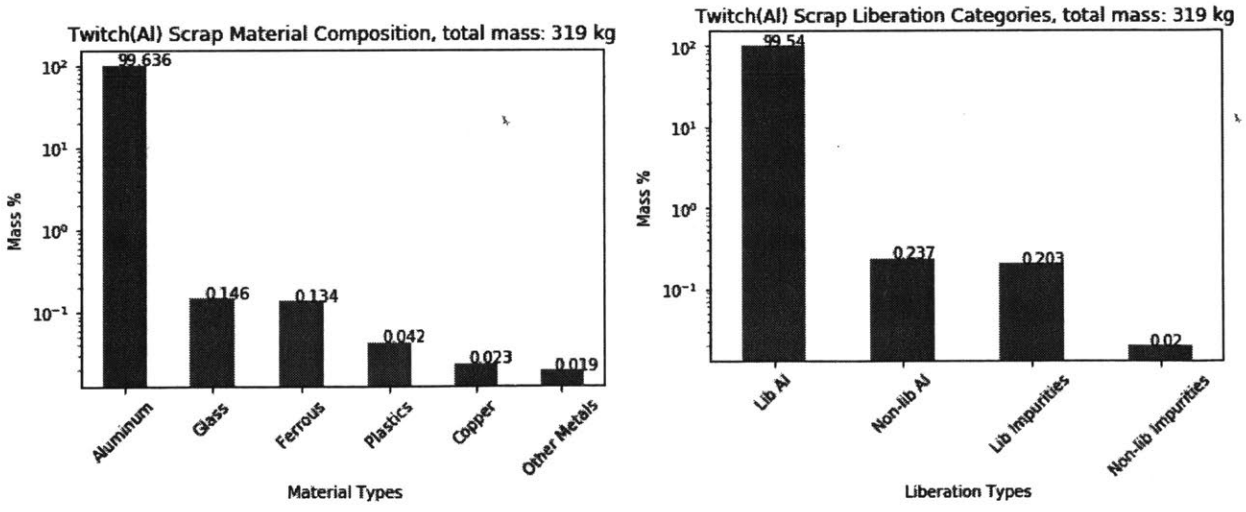


*Figure 9.11 Twitch Al scrap (at output unit V3): main material composition (left); liberation categories (right), lightweight ELV case-study*

The heavy and light ASR compositions remain a heterogeneous mixture of materials. We can see from Figure 9.12, an increase in the amount and concentration of aluminum in the light ASR. Again, this stems from the increased amount of aluminum with an AIV, combined with the fact that the air cyclone separation unit that produced the light ASR has a relatively high separation efficiency for small-sized aluminum particles due to their light density and weight. In the heavy ASR, we see a decrease in the amount and concentration of ferrous. This arises due to the decreased input of ferrous in the body structure of the AIV, and thus in the amount of ferrous that does not get sorted by the magnet or are in non-liberated form (as mechanical fasteners attached to other materials).

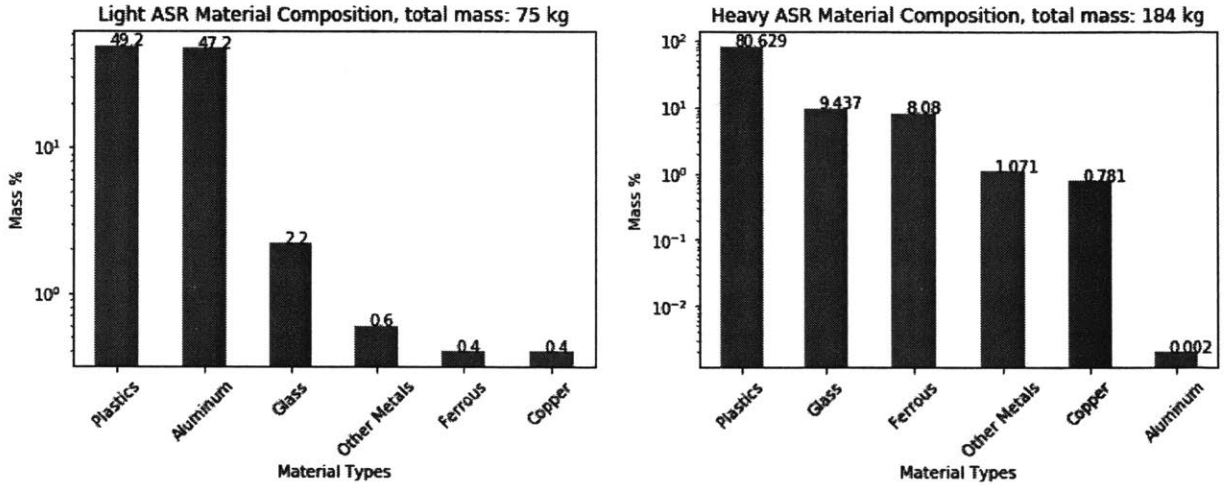


*Figure 9.12 Main material composition for automotive shredder residue: light ASR at output unit V1 (left); heavy ASR at output units V5 & V6 (right), lightweight ELV case-study*

### 9.3.3 Performance metrics

To quantify the general performance of the material recovery processes on an AIV, we first look at the grade and recovery rate of the output scraps. From the comparison in Table 8.2, we can see a decrease in grade in the ferrous scrap, and an increase in the grade of Twitch Al scrap, while the recovery rates do not change much because we model the separation processes as linear systems for mass flow. The changes in grade result from the fact that the mass of contaminants does not change much while the mass of the target materials respectively decreases and increases in the ferrous and aluminum scraps.

| | Baseline ELV | | | Lightweight AIV | | |
|---|---|---|---|---|---|---|
| **Scrap** | **Weight (kg)** | **Recovery Rate** | **Grade** | **Weight (kg)** | **Recovery Rate** | **Grade** |
| **Ferrous** | 1017 | 94.6 % | 98 % | 324 | 93.7 % | 89.5 % |
| **Aluminum: Zorba** | 126 | 88.3 % | 67.6 % | 456 | 90.0 % | 91.9 % |
| **Aluminum: Twitch** | 66 | 67.1 % | 98.7 % | 319 | 67.4 % | 99.6 % |
| **ASR (Light)** | 48 | 18.4 % | 77.6 % | 75 | 18.5 % | 49.2 % |
| **ASR (Heavy)** | 216 | 74.2 % | 68.9 % | 184 | 80.6 % | 74.2 % |

*Table 9.8 Recovery & grade metrics of output scraps for lightweight ELV case-study, compared to baseline ELV case-study*

Entropy

While entropy does not give a comprehensive picture of the separation processes, it helps us understand the degree of material homogeneity in a mixture. In Table 9.9 below, we compare the entropy in the baseline ELV and lightweight AIV case-studies. As expected, the lightweight AIV has a higher entropy as the ferrous is no longer the main material. The increase in entropy in the ferrous scrap reflects the higher concentration of the contaminants, while the decrease in entropy in the aluminum scrap reflects the lower concentration of the contaminants.

| Material Stream | Baseline ELV Material Mixing, H (bits) | Lightweight AIV Material Mixing, H (bits) |
|---|---|---|
| **Whole ELV** | 1.62 | 2.34 |
| **Ferrous scrap** | 0.19 | 0.73 |
| **Al scrap: Zorba** | 1.73 | 0.61 |
| **Al scrap: Twitch** | 0.12 | 0.04 |
| **ASR (Light)** | 3.30 | 2.64 |
| **ASR (Heavy)** | 3.09 | 3.16 |

*Table 9.9 Mixing entropy for the material streams before and after the shredding/separation processes, for lightweight ELV case-study*

Overall performance metrics

A lightweight aluminum-intensive ELV has a lower ORR (calculated in Table 8.3 below) than our baseline steel-intensive ELV: 76% as compared to 89%. This is because the amount of ferrous decreases while the amount of aluminum increases, but the recovery of aluminum is less than that for ferrous.

| Flow | Mass (kg) |
|---|---|
| **Hulk** | 1039.6 |
| **Collected Ferrous (at Ferrous scrap)** | 290.3 |
| **Collected Aluminum (at Twitch scrap)** | 318.3 |
| **Collected Plastic (at light and heavy ASR)** | 185.7 |
| **ORR (%)** | (290+318+186) / 1039 = 76.4 |

*Table 9.10 Calculation of the overall recovery rate of the lightweight ELV, from material flows of interest*

We will now turn to our NCS metric to evaluate the effect of contamination in the scrap streams. Similar to the baseline ELV case-study (see Section 7.2.3), we first calculate the dilution costs incurred during the secondary production of aluminum and steel. The calculated dilution results during secondary aluminum production are quite similar to Table 17, as the Twitch composition coming from the lightweight vehicle is quite similar to that from the baseline ELV. However, the copper

concentration in the ferrous scrap produced from the lightweight AIV is 1.0 % as compared to 0.4 % in the baseline ELV scenario. Hence, the dilution costs are thus higher for all possible scenarios of produced steel (see Table 8.5 below).

| | Steel Sheet | Rolled Steel | Steel Section | Steel Bar |
|---|---|---|---|---|
| **Max Cu conc in Steel product** | 0.06 % | 0.10 % | 0.30 % | 0.40% |
| **Pig iron added for dilution (kg)** | 6974.8 | 3744.2 | 959.3 | 637.9 |

*Table 9.11 Dilution addition needed for secondary processing of ferrous scrap for different scenarios of final steel products, lightweight ELV case-study*

We use the calculated alloying and dilution costs to calculate the NCS metrics for the different scenarios of possible aluminum alloys and steel products produced during secondary metal production, see Table 7.18 below. The NCS metrics are lower over for all scenarios, as compared to the baseline ELV case-study, as the total dilution costs are much higher. This is due to the increased dilution required due to the increase in the concentration of copper contaminant in ferrous scrap is more significant, and the quality of the Twitch scrap does not improve by much. In fact, focusing on the lowest quality alloy production (A380 aluminum alloy and steel bar production), the NCS in a lightweight vehicle decreases from 88% to 46%

| | P1020A | 1070A | 3103 | 5182 | 5754 | 6061 | 6082 | A356 | 301 | 319 | A380 |
|---|---|---|---|---|---|---|---|---|---|---|---|
| **Steel Sheet (deep-drawn)** | 0.031 | 5.58 | 8.22 | 7.07 | 8.22 | 9.65 | 8.22 | 3.87 | 6.90 | 9.88 | 9.87 |
| **Rolled Steel** | 0.031 | 7.21 | 12.34 | 9.93 | 12.34 | 15.89 | 12.35 | 4.59 | 9.60 | 16.52 | 16.50 |
| **Steel Section** | 0.031 | 9.65 | 21.77 | 15.24 | 21.76 | 35.89 | 21.78 | 5.48 | 14.48 | 39.28 | 39.13 |
| **Steel Bar** | 0.031 | 10.04 | 23.87 | 16.24 | 23.86 | 41.99 | 23.89 | 5.60 | 15.38 | 46.70 | 46.49 |

*Table 9.12 Matrix of NCS metric, calculated over the different possible scenarios of produced steel products (rows) and produced aluminum alloys (columns), for our lightweight ELV case-study*

# Chapter 10 Conclusions and Future Work

This thesis has developed a holistic modeling framework for materially-complex products, in particular, end-of-life vehicles. We will now summarize the contributions of this thesis, in terms of the width of scope provided by the developed grave-to-cradle material recovery model, and in terms of its applications in investigating the material recovery performance of typical ELVs, i.e. steel-intensive vehicles, as well as future ELVs, i.e. aluminum-intensive light-weight vehicles.

## 10.1 Contributions and findings

Holistic model developed

We have developed a holistic material recovery model to cover the four important stages of the material recovery chain of an ELV: disassembly, shredding, separation and secondary metal production. Prior research papers in the literature have only analyzed one or two of these stages in detail. Our holistic model remedies that situation by following the material flows, starting from the vehicle's bill of materials, i.e. a defined material breakdown and parts' hierarchical structure.

In Section 1.4, we see that during disassembly in industry, different parts are removed for reuse,at different rates, depending on the parts' demand and vehicle models, i.e. their parts' hierarchical structure. In Chapter 2, we analyze the disassembly process and propose an integer-programming formulation to solve for the best automotive components to remove, i.e. targeting components with the highest resale value but least disassembly costs. As constraints to the optimization, we consider the precedence relationships existing between the automotive components.

In Chapter 4, we propose our material recovery model that uses a system of linear equations to represent mass balance of the material streams at the shredding and separation steps. The model caters for: (i) survival of non-liberated particles (consisting of parts' fragments with attached fasteners or wires) and size transition of the liberated particles during the shredding process; (ii) inefficiencies of the different separation technologies in the network of separation units used during the separation processes. With a complete material flow characterization, we determine the material composition of the ELV scraps obtained at the end of the separation processes, namely ferrous scrap, Twitch aluminum scrap and automotive shredder residue (ASR). As discussed in Chapter 5, the detailed material flow composition of the metal scraps enables us to calculate the dilution costs due to the non-target metal contaminants when the metal scraps are used as input feedstock during secondary metal production of aluminum and steel. If the metal production has several element concentration limits as constraints (this is the case for how we model secondary aluminum production), we calculate the dilution and alloying costs using a cost-optimized blending model, formulated as a linear programming problem. We also see that the production of sink metal alloys of different quality and composition requirements gives different dilution and alloying costs. In general, down-cycling the metal scraps to low-quality

alloys requires barely any dilution. Comparatively, significant dilution is required for the production of medium-quality alloys of the level of closed-loop recycling, i.e. alloys that are typically found in the ELV (e.g. 6000 series aluminum alloy, and rolled steel).

New overall performance metrics proposed

Typically, the overall recovery rate (ORR) has been used in the existing literature to evaluate the performance of material recovery from products. In addition, it is also used as a metric to drive environmental consciousness about how ELVs are treated at end-of-life in EU countries., with the EU Directive 2000/53/EC putting a target of an ORR of 95% of ELV's total weight [10]. While the ORR aggregates the masses of recovered target materials from the output scraps, it does not capture the effect of contaminants in ELV metal scraps on the downstream processes of secondary metal production. We therefore propose an improved overall performance metric, the normalized contribution of scrap (NCS). The NCS metric weighs down the ORR by including the masses of dilution and alloying raw materials added during secondary metal production. Thus, the NCS metric gives a more accurate representation of the actual value of the scraps: of two metal scrap feeds of the same grade, the one with the higher contaminant concentration has a lower inherent value.

Additionally, we can extend the NCS metric by adding cost-based weights or thermodynamic rarity-based weights to the masses of collected scraps. As seen in Chapter 5, this allows us to put more value on the recovered materials that are more cost-worthy or have a bigger environmental impact.

Applications and numerical analysis findings

In Chapter 7, we apply the holistic material recovery model to an ELV (1990s passenger vehicle) bill of materials database from literature. This first required some data wrangling to convert the hierarchical structure data to a characterized material flow for the ELV hulk, and to determine the amount of non-liberated particles originating from fasteners or wires attached to parts' fragments. This formed the input for our baseline ELV analysis. We observe that while our baseline ELV has an ORR of 89%, it has an NCS of 88% in the best-case scenario, i.e. choosing the lowest grade sink alloy during secondary metal production. However, if higher grade sink alloys were chosen, e.g. shifting from A380 to 6061 aluminum alloy, the NCS decreases by 30% due to the increase in dilution costs needed.

In chapter 8, we investigate the variation in the composition of the partially-disassembled ELV hulks due to removal of automotive components for resale. This case study is a more realistic scenario as resale statistics have shown that some components can have probability of resale as high as 87 % (wheels) or as low as 0.4% (instrument panel). Using these components' reuse probability rates to generate Monte Carlo runs, we model 1000 ELV hulks, each disassembled to different degrees. We observe the following: on average, 287 kg of automotive components are removed. For the average partially-disassembled hulk, this results in an ORR of 89%. If the average mass of reused parts removed during disassembly is included as source of material recovery, the ORR increases to 91%, still short of

the EU Directive 2000/53/EC target of 95% ELV total weight. This implies that European facilities need more efficient material separation system than the simple one used as our model parameters.

Furthermore, our analysis allows us to see the variation in performance metrics over our generated fleet of 1000 partially-disassembled ELVs. The calculated metrics are as follows: the ORR varied from 86 % to 91 %; the NCS for the best-case scenario (380 Al alloy and steel bar production) varied from 60% to 91 %. This variation shows that even for the same vehicle model, variation in hulk composition affects the recovery performance, as well as the contamination level in metal scraps, and hence the dilution costs incurred during secondary metal production.

In chapter 9, we conduct a second case study, to investigate the material recovery performance of an aluminum-intensive lightweight vehicle. The profile of our lightweight vehicle implies the following change in composition from our baseline ELV: a decrease in ferrous content from 1032 to 285 kg, and an increase in aluminum content from 96 to 471 kg, an increase in non-liberated aluminum-ferrous particles from 2 to 7 kg, an increase in non-liberated aluminum-copper particles from 0 to 1 kg. For this lightweight vehicle profile, we found out that the ORR decreases to 76%, due to the higher separation inefficiencies of aluminum as compared to those of ferrous materials. Furthermore, the NCS also decreases, as the quality of the ferrous scrap decreases, due to increased concentration of the copper contaminant. There is an increase in non-liberated aluminum-ferrous particles due to the increase in ferrous fasteners in the aluminum body-structure. However, as there is a comparable increase in the overall aluminum material flow, the concentration of the contaminants in the aluminum does not increase.

While the performance results depend on the model parameters representing the material recovery infrastructure, these case studies highlight that different profiles of ELV hulk lead to different material recovery performances. Moreover, small changes to a vehicle design, such as different metal alloys used, more copper wires due to a larger electronics system, different types of mechanical fasteners, can all contribute to scrap contamination and dilution losses during the secondary metal production processes. Hence, we have shown the need for a holistic material recovery model able to capture unintended dilution loss consequences due to changes in vehicle designs.

## 10.2 Future work

The holistic modeling framework presented in this thesis has the capacity to relate changes in product design and hulk composition to the overall material recovery performance. Better model parameters and more granular data about the ELV composition can improve the accuracy of our findings from our numerical analyses. Through our case studies of lightweight vehicles and partially-disassembled ELVs, we have examined only a few possibilities of the applications of this holistic model. Future work can investigate other applications of this model, namely how the evaluated material recovery performance can affect decisions upstream during the disassembly stage or product design stage.

ELV data improvement

We devise the model to be able to follow the fate of particles stemming from specific automotive parts, from within the shredder flow to the scrap flows for secondary metal production. A more granular ELV data can provide a more accurate material recovery performance evaluation. In particular, we can account for a wider range of trace metals, which although found in minute amounts in a vehicle, can accumulate in metal scraps. As discussed in Chapter 5, even in small concentrations, such trace metals can be contaminants and cause dilution losses in the production of certain final sink alloys. Alternatively, some trace metals could possibly find their way into metal scrap streams, where they are neither an alloying element nor a contaminating tramp element. Then, at the secondary metal production stage, such metals could be dissipated through the slag waste [125]. Not recovering these trace metals represents an opportunity cost, especially if these trace metals have a high value (economic or thermodynamic rarity).

These trace metals are usually present as alloying elements in the different aluminum alloys, steel alloys and other metal alloys, or as elements within electronic parts in the vehicle. Hence, more granular input data is needed in the following respects:

- More detailed Al alloy denomination (different types of wrought and cast alloys) for specific automotive parts. In this thesis work, we only use the overall ratio of the total amount of wrought aluminum (assumed to be A6061) to cast aluminum (assumed to be A380) present in a vehicle. These aluminum alloys contain different ratios of trace elements such as silicon, magnesium, manganese, titanium, etc.
- Similarly for steel alloy denomination in the automotive parts. Steel alloys contain trace elements such as chromium, nickel and molybdenum. Moreover while stainless steel is estimated to compose 1.2% of a vehicle by weight [142], our ELV database only contained ferrous as the material type encompassing steel and stainless steel. Hence, a more accurate modeling will account for stainless steel.
- Electronics components in vehicles. Embedded electronic systems with electronic control units (ECUs) are increasingly used in sensors and sub-systems such as engine, air-conditioning, entertainment and safety systems [9]. While still small in mass, these electronic systems account for more than 30% of a vehicle's total cost [9]. These electronic components include "critical" materials, in particular, precious metals and rare earths elements (REEs) [172]. These metals can contaminate main material flows (i.e. recovery of aluminum and steel) and require separate material recovery chains with chemical separation processes (e.g. acid/caustic leaching) as done for waste electrical and electronic equipment (WEEE) recycling [173], [174].

Another area of improvement for our model is using better joint data. The ELV database used did not contain a complete list of all joints, and their material types and weight were estimated to the best of our ability. Hence, the actual contamination due to non-liberated joint particles in the ferrous and aluminum scraps might actually be higher than estimated by our model. Moreover, the ELV database did not specify to what other component a part's fastener is attached to. If such data were available, our model could be extended to account for contamination from non-liberated particles having part fragments of different materials. Similarly, we can expand on the types of joints accounted for: besides

mechanical fasteners and wires, chemical surface joints such as adhesives and welding can also be sources of contamination [90], [109] if two parts of different materials are thus joined together.

Model parameter improvement

The main model parameters that could benefit from some improvement in accuracy are the shredding and separation model parameters. We saw in Section 7.1.4 that the shredding model equation required an estimation of the survival probabilities of non-liberated particles, as well as of the transition probabilities of non-liberated particles to smaller size classes. In this thesis, we have adapted general values used in the literature, but better estimates for non-liberated particles of specific joint types and material combinations can be obtained from simulation or physical experiments. Using experiment data, a model can be built to map the material properties (e.g. Young's modulus, yield strength and Poisson's ratio) and joint types onto the survival and transition probabilities.

The separation model parameters are the partition curves' shape parameters for all separation units used to define the separation network configuration. In this thesis, we have adapted values used in the literature. Better estimates can be obtained from actual characterization measurements done in situ. For example, as done in [117], several sampling sets can be taken concurrently at all the input feeds and output streams: the measured material masses for each material type can then be used in an optimization best-fit model for that particular separation network configuration to determine the best-fit separation efficiencies for all separation units. Subsequently, the estimated separation efficiencies for the different material types can be used to find the best-fit shape parameters, using their respective separation material properties.

Other applications

With the grave-to-cradle span of the model, future work can investigate how the evaluated performance for a particular material recovery infrastructure and ELV model can affect decisions upstream during disassembly. In particular, we could observe the effects of pre-emptive removal of specific parts that contribute to scrap contamination or quality reduction. For instance, we suspect that the removal of copper wires would reduce contamination due to non-liberated particles in ferrous and aluminum scraps, thus reducing dilution losses. Similarly, the removal of large plastic components might improve scrap grade. A part can be removed for (i) reuse or (ii) directly recycling. Typically, a part is directly recycled if it might have an economic benefit for the shredding facilities when the part trades at a higher price point than leaving it in the hulk or selling it for reuse. While this form of disassembly represents a local optimization with respect to the parts' immediate removal values (as described in Section 2.2), disassembly can also be a form of global optimization if the a part's value incorporates its influence on the overall material recovery performance. A part's removal value would then include its contribution to improving scrap grade or reducing scrap contamination. To do this, there needs several iterations of the recovery chain evaluation, with the performance metrics updating the parts' removal values until there is solution convergence of the disassembly optimization.

Another interesting aspect to investigate would be how the disassembly process could change for the case of future ELVs, such as lightweight vehicles. As these vehicles would contain automotive parts

of different material types than the typical ferrous or plastics, their inherent material resale values would be different from their corresponding parts in a typical steel-intensive vehicle. An additional consideration would be the system dynamics of the supply chain of resale parts as it changes over time: as lightweight vehicles see an increase in market share, the supply of resale parts from the lightweight vehicles having reached end of life would need to balance the demand for resale parts from existing lightweight vehicles that need repair. This difference implies that the parts' reuse rates would be different from the historical reuse rates used in the Monte-Carlo simulations of case-study A. Future work could involve simulation of the system dynamics of this reuse supply chain, in order to calculate the average reuse rates of the parts in a lightweight vehicle.

Future work can investigate how the evaluated performance of a particular ELV design can inform decisions upstream during the iterative product design stage. For example, designers can vary the material composition or alloy choices, within the constraints of structural and safety requirements, and explore the resulting material recovery performances. They could thus pick the set of material and alloys that maximize the material recovery performance. Some vehicle manufacturers promote the sustainability aspect of a vehicle by touting the recycled material content, amongst other specifications: for instance, Ford reports the recycled content of their F-150 truck to contain recycled aluminum from industrial in-house factory scraps. They also report the use of recycled tires, plastic bottles, cotton and nylon carpeting in the different automotive components of the F-150 [175]. Picking the right material and alloy set can additionally contribute to this kind of closed-loop recycling: the set corresponding to the highest material recovery performance can help reduce the contamination problem during secondary metal processing and thus avoid down-cycling by producing high quality metal alloys (e.g. wrought aluminum alloys as opposed to cast aluminum alloy). These high quality alloys can then be recycled in parts requiring structural integrity (e.g. stamped body panels).

# Appendix A ELV database and recovery model parameters

| PartID | Name | Weight (kg) | Material | Fasteners |
|---|---|---|---|---|
| 1 | DoorFrontRight | 33.34 | Mixed | 2-13; 3-EC |
| 2 | DoorFrontRight.Panel | 2.96 | Mixed | 4-Ph |
| 3 | DoorFrontRight.Panel.Handle | 0.4 | SKOP | 4-Ph; 4-Rivets |
| 4 | DoorFrontRight.Panel.Light | 0.02 | SKOP | 6-Rivets |
| 5 | DoorFrontRight.Panel.SpeakerCover | 0.01 | SKOP | 6-Rivets |
| 6 | DoorFrontRight.Panel.BottomCover | 0.04 | SKOP | |
| 7 | DoorFrontRight.Panel.TopCover | 0.34 | Mixed:ABS | |
| 8 | DoorFrontRight.Panel.TopCover.TopPlastic | 0.06 | SKOP | |
| 9 | DoorFrontRight.Panel.TopCover.CarpetCover | 0.02 | SKOP | |
| 10 | DoorFrontRight.Panel.TopCover.Foam | 0.02 | SKOP | |
| 11 | DoorFrontRight.Panel.TopCover.Base | 0.26 | ABS | |
| 12 | DoorFrontRight.Panel.Base | 1.96 | ABS | |
| 13 | DoorFrontRight.MirrorPanel | 0.02 | ABS | 1-Ph |
| 14 | DoorFrontRight.Shoddy | 0.12 | Carpet | 3-Pushin |
| 15 | DoorFrontRight.Structure | 31.7 | Mixed | |
| 16 | DoorFrontRight.Structure.Base | 30.34 | Mixed:Ferrous | |
| 17 | DoorFrontRight.Structure.Base.Steel | 24.21 | Ferrous | |
| 18 | DoorFrontRight.Structure.Base.SKOS | 3.79 | Mixed:Ferrous | |
| 19 | DoorFrontRight.Structure.Base.Glass | 2.34 | Glass | |
| 20 | DoorFrontRight.Structure.Mirror | 0.92 | Mixed:SKOP | 3-8mm |
| 21 | DoorFrontRight.Structure.Mirror.House | 0.63 | Mixed:SKOP | |
| 22 | DoorFrontRight.Structure.Mirror.House.SKOP | 0.07 | SKOP | 5-Ph; 3-2way screws |
| 23 | DoorFrontRight.Structure.Mirror.House.SKOP2 | 0.35 | SKOP | |
| 24 | DoorFrontRight.Structure.Mirror.House.Steel | 0.03 | Ferrous | |
| 25 | DoorFrontRight.Structure.Mirror.House.Alum | 0.18 | Aluminum_wrought | |
| 26 | DoorFrontRight.Structure.Mirror.Lens | 0.14 | Glass | Glass and plastic |
| 27 | DoorFrontRight.Structure.Mirror.Electrical | 0.16 | Mixed:Ferrous | 3-Ph |
| 28 | DoorFrontLeft | 33.34 | Mixed | 2-13; 1-10 |
| 29 | DoorFrontLeft.Panel | 2.96 | Mixed | 4-Ph |
| 30 | DoorFrontLeft.Panel.Handle | 0.4 | SKOP | 4-Ph; 4-Rivets |
| 31 | DoorFrontLeft.Panel.Light | 0.02 | SKOP | |
| 32 | DoorFrontLeft.Panel.SpeakerCover | 0.01 | SKOP | 6-Rivets |
| 33 | DoorFrontLeft.Panel.BottornCover | 0.04 | SKOP | 6-Rivets |
| 34 | DoorFrontLeft.Panel.TopCover | 0.34 | Mixed:ABS | |
| 35 | DoorFrontLeft.Panel.TopCover.TopPlastic | 0.06 | SKOP | |
| 36 | DoorFrontLeft.Panel.TopCover.CarpetCover | 0.02 | SKOP | |

| | | | | |
|---|---|---|---|---|
| 37 | DoorFrontLeft.Panel.TopCover.Foam | 0.02 | SKOP | |
| 38 | DoorFrontLeft.Panel.TopCover.Base | 0.26 | ABS | |
| 39 | DoorFrontLeft.Panel.Base | 1.96 | ABS | |
| 40 | DoorFrontLeft.MirrorPanel | 0.02 | ABS | |
| 41 | DoorFrontLeft.Shoddy | 0.12 | Carpet | 1-Ph |
| 42 | DoorFrontLeft.Structure | 31.7 | Mixed | 3-Pushin |
| 43 | DoorFrontLeft.Structure.Base | 30.34 | Mixed:Ferrous | |
| 44 | DoorFrontLeft.Structure.Base.Steel | 24.21 | Ferrous | |
| 45 | DoorFrontLeft.Structure.Base.SKOS | 3.79 | Mixed:Ferrous | |
| 46 | DoorFrontLeft.Structure.Base.Glass | 2.34 | Glass | |
| 47 | DoorFrontLeft.Structure.Mirror | 0.92 | Mixed:SKOP | |
| 48 | DoorFrontLeft.Structure.Mirror.House | 0.63 | Mixed:SKOP | |
| 49 | DoorFrontLeft.Structure.Mirror.House.SKOP | 0.07 | SKOP | 5-Ph; 3-2way screws |
| 50 | DoorFrontLeft.Structure.Mirror.House.SKOP2 | 0.35 | SKOP | |
| 51 | DoorFrontLeft.Structure.Mirror.House.Steel | 0.03 | Ferrous | |
| 52 | DoorFrontLeft.Structure.Mirror.House.Alum | 0.18 | Aluminum_wrought | |
| 53 | DoorFrontLeft.Structure.Mirror.Lens | 0.14 | Glass | |
| 54 | DoorFrontLeft.Structure.Mirror.Electrical | 0.16 | Mixed:Ferrous | |
| 56 | DoorRearRight | 25.5 | Mixed | 2-13; 1-EC |
| 57 | DoorRearRight.Panel | 2.2 | Mixed | 1-Ph; 2-5.5 |
| 58 | DoorRearRight.Panel.Ashtray | 0.22 | Mixed:Ferrous | 1-Ph; 2-Rivets |
| 59 | DoorRearRight.Panel.Ashtray.Steel | 0.11 | Ferrous | |
| 60 | DoorRearRight.Panel.Ashtray.SKOS | 0.11 | SKOP | |
| 61 | DoorRearRight.Panel.Light | 0.01 | SKOP | 6-Pi |
| 62 | DoorRearRight.Panel.Handle | 0.3 | SKOP | |
| 63 | DoorRearRight.Panel.BottomCover | 0.06 | Carpet | |
| 64 | DoorRearRight.Panel.TopCover | 0.36 | Mixed:ABS | 9-Rivets |
| 65 | DoorRearRight.Panel.TopCover.TopPlastic | 0.06 | SKOP | |
| 66 | DoorRearRight.Panel.TopCover.CarperCover | 0.02 | Carpet | |
| 67 | DoorRearRight.Panel.TopCover.Foam | 0.02 | SKOP | |
| 68 | DoorRearRight.Panel.TopCover.Base | 0.26 | ABS | |
| 69 | DoorRearRight.Panel.Base | 1.14 | ABS | |
| 70 | DoorRearRight.Structure | 23.28 | Mixed | |
| 71 | DoorRearRight.Structure.Steel | 18.58 | Ferrous | |
| 72 | DoorRearRight.Structure.SKOS | 2.91 | Mixed:Ferrous | |
| 73 | DoorRearRight.Structure.Glass | 1.79 | Glass | |
| 74 | DoorRearLeft | 25.5 | Mixed | 2-13; 1-EC |
| 75 | DoorRearLeft.Panel | 2.2 | Mixed | 1-Ph; 2-5.5 |
| 76 | DoorRearLeft.Panel.Ashtray | 0.22 | Mixed:Ferrous | 1-Ph; 2-Rivets |
| 77 | DoorRearLeft.Panel.Ashtray.Steel | 0.11 | Ferrous | |
| 78 | DoorRearLeft.Panel.Ashtray.SKOS | 0.11 | SKOP | |
| 79 | DoorRearLeft.Panel.Light | 0.01 | SKOP | 6-Pi |
| 80 | DoorRearLeft.Panel.Handle | 0.3 | SKOP | |

| | | | | |
|---|---|---|---|---|
| **81** | DoorRearLeft.Panel.BottomCover | 0.06 | Carpet | |
| **82** | DoorRearLeft.Panel.TopCover | 0.36 | Mixed:ABS | 9-Rivets |
| **83** | DoorRearLeft.Panel.TopCover.TopPlastic | 0.06 | SKOP | |
| **84** | DoorRearLeft.Panel.TopCover.CarperCover | 0.02 | Carpet | |
| **85** | DoorRearLeft.Panel.TopCover.Foam | 0.02 | SKOP | |
| **86** | DoorRearLeft.Panel.TopCover.Base | 0.26 | ABS | |
| **87** | DoorRearLeft.Panel.Base | 1.14 | ABS | |
| **88** | DoorRearLeft.Structure | 23.28 | Mixed | |
| **89** | DoorRearLeft.Structure.Steel | 18.58 | Ferrous | |
| **90** | DoorRearLeft.Structure.SKOS | 2.91 | Mixed:Ferrous | |
| **91** | DoorRearLeft.Structure.Glass | 1.79 | Glass | |
| **92** | SeatFrontRight | 21.72 | Mixed | 3-13; 1-18 |
| **93** | SeatFrontRight.HeadRest | 0.88 | Mixed | |
| **94** | SeatFrontRight.HeadRest.Cover | 0.14 | Carpet | |
| **95** | SeatFrontRight.HeadRest.Base | 0.76 | Mixed:Ferrous | |
| **96** | SeatFrontRight.HeadRest.Base.Foam | 0.62 | PUR | |
| **97** | SeatFrontRight.HeadRest.Base.Steel | 0.12 | Ferrous | |
| **98** | SeatFrontRight.LateralCover | 0.22 | SKOP | |
| **99** | SeatFrontRight.BackFoam | 0.68 | PUR | |
| **100** | SeatFrontRight.BackCover | 0.8 | Carpet | |
| **101** | SeatFrontRight.ArmRestCovers | 0.04 | SKOP | |
| **102** | SeatFrontRight.ArmRest | 0.7 | Mixed | |
| **103** | SeatFrontRight.ArmRestBigCover | 0.08 | SKOP | |
| **104** | SeatFrontRight.ArmRest.Cover | 0.16 | Carpet | |
| **105** | SeatFrontRight.ArmRest.Base | 0.56 | Mixed:Ferrous | |
| **106** | SeatFrontRight.ArmRest.Base.Foam | 0.16 | PUR | |
| **107** | SeatFrontRight.ArmRest.Base.Steel | 0.4 | Ferrous | |
| **108** | SeatFrontRight.BottomCover | 0.58 | Carpet | |
| **109** | SeatFrontRight.BottomFoam | 0.88 | PUR | |
| **110** | SeatFrontRight.BottomBase | 16.36 | Mixed | |
| **111** | SeatFrontRight.BottomBase.Steel | 16.2 | Ferrous | |
| **112** | SeatFrontRight.BottomBase.SKOS | 0.16 | Mixed:SKOP | |
| **113** | SeatFrontRight.SeatBeltFrontMid | 0.22 | Mixed | |
| **114** | SeatFrontRight.SeatBeltFrontMid.Latch | 0.09 | Ferrous | |
| **115** | SeatFrontRight.SeatBeltFrontMid.Bracket | 0.05 | Ferrous | |
| **116** | SeatFrontRight.SeatBeltFrontMid.Strap | 0.08 | PE | |
| **117** | SeatFrontLeft | 21.72 | Mixed | |
| **118** | SeatFrontLeft.HeadRest | 0.88 | Mixed | |
| **119** | SeatFrontLeft.HeadRest.Cover | 0.14 | Carpet | |
| **120** | SeatFrontLeft.HeadRest.Base | 0.76 | Mixed:Ferrous | |
| **121** | SeatFrontLeft.HeadRest.Base.Foam | 0.62 | PUR | |
| **122** | SeatFrontLeft.HeadRest.Base.Steel | 0.12 | Ferrous | |
| **123** | SeatFrontLeft.LateralCover | 0.22 | SKOP | |

| | | | | |
|---|---|---|---|---|
| 124 | SeatFrontLeft.BackFoam | 0.68 | PUR | |
| 125 | SeatFrontLeft.BackCover | 0.8 | Carpet | |
| 126 | SeatFrontLeft.ArmRestCovers | 0.04 | SKOP | |
| 127 | SeatFrontLeft.ArmRest | 0.7 | Mixed | 3-Ph |
| 128 | SeatFrontLeft.ArmRestBigCover | 0.08 | SKOP | |
| 129 | SeatFrontLeft.ArmRest.Cover | 0.16 | Carpet | |
| 130 | SeatFrontLeft.ArmRest.Base | 0.56 | Mixed:Ferrous | |
| 131 | SeatFrontLeft.ArmRest.Base.Foam | 0.16 | PUR | 1-LongScrew |
| 132 | SeatFrontLeft.ArmRest.Base.Steel | 0.4 | Ferrous | |
| 133 | SeatFrontLeft.BottomCover | 0.58 | Carpet | |
| 134 | SeatFrontLeft.BottomFoam | 0.88 | PUR | |
| 135 | SeatFrontLeft.BottomBase | 16.36 | Mixed | |
| 136 | SeatFrontLeft.BottomBase.Steel | 16.2 | Ferrous | |
| 137 | SeatFrontLeft.BottomBase.SKOS | 0.16 | Mixed:SKOP | |
| 138 | SeatFrontLeft.SeatBeltFrontMid | 0.22 | Mixed | |
| 139 | SeatFrontLeft.SeatBeltFrontMid.Latch | 0.09 | Ferrous | |
| 140 | SeatFrontLeft.SeatBeltFrontMid.Bracket | 0.05 | Ferrous | |
| 141 | SeatFrontLeft.SeatBeltFrontMid.Strap | 0.08 | PE | |
| 142 | RearViewMirror | 0.3 | Mixed | |
| 143 | SeatRearBottom | 6.64 | Mixed | 2-Clips |
| 144 | SeatRearBottom.Cover | 1 | Carpet | |
| 145 | SeatRearBottom.Base | 5.58 | Mixed | |
| 146 | SeatRearBottom.Base.Foam | 2.52 | PUR | |
| 147 | SeatRearBottom.Base.Steel | 3.06 | Mixed:SKOP | |
| 148 | SeatRearBottom.Base.Steel.Steel | 2.91 | Ferrous | |
| 149 | SeatRearBottom.Base.Steel.SKOP | 0.15 | SKOP | |
| 150 | SeatRearBack | 7.2 | Mixed | 10-Feb |
| 151 | SeatRearBack.Base | 6.02 | Mixed | |
| 152 | SeatRearBack.Base.Steel | 3.28 | Mixed:SKOP | |
| 153 | SeatRearBack.Base.Steel.Steel | 0.03 | Ferrous | |
| 154 | SeatRearBack.Base.Steel.SKOP | 3.25 | SKOP | |
| 155 | SeatRearBack.Base.Foam | 2.7 | Mixed:PUR | |
| 156 | SeatRearBack.Base.Foam.Foam | 2.48 | PUR | |
| 157 | SeatRearBack.Base.Foam.SKOS | 0.22 | SKOP | |
| 158 | SeatRearBack.Cover | 1.14 | Carpet | |
| 159 | APillarTrimLeft | 0.2 | Mixed | 3-Clips |
| 160 | APillarTrimLeft.Clips | 0.01 | Ferrous | |
| 161 | APillarTrimLeft.ABS | 0.19 | ABS | |
| 162 | APillarTrimRight | 0.2 | Mixed | 3-Clips |
| 163 | APillarTrimRight.Clips | 0.01 | Ferrous | |
| 164 | APillarTrimRight.Clips.ABS | 0.19 | ABS | |
| 165 | SunvisorRight | 0.52 | SKOP | 3-Ph |
| 166 | SunvisorLeft | 0.8 | SKOP | 3-Ph |

| | | | | |
|---|---|---|---|---|
| **167** | Handles | 0.32 | SKOP | 2-Ph |
| **168** | DomeLight | 0.2 | Mixed | 2-Ph |
| **173** | SeatbeltFrontLeftCover | 0.01 | SKOP | 1-Ph |
| **174** | CPillarLeft | 0.4 | PP | |
| **175** | CPillarRight | 0.4 | PP | |
| **176** | SeatbeltFrontRightCover | 0.01 | SKOP | |
| **177** | BPillarUpperRight | 0.1 | PP | |
| **179** | BPillarUpperLeft | 0.1 | PP | |
| **180** | Headliner | 2 | SKOP | |
| **181** | BPillarLowerRight | 0.71 | TPO | 5-Ph; 1-500T |
| **182** | BPillarLowerLeft | 0.71 | TPO | 5-Ph; 1-500T |
| **183** | SeatBeltFrontRight | 1.4 | Mixed | 1-Ph; 1-500T |
| **184** | SeatBeltFrontRight.Steelcase | 0.86 | Mixed | |
| **185** | SeatBeltFrontRight.Steelcase.Steel | 0.82 | Ferrous | |
| **186** | SeatBeltFrontRight.Steelcase.SKOP | 0.04 | SKOP | |
| **187** | SeatBeltFrontRight.Strap | 0.16 | PE | |
| **188** | SeatBeltFrontRight.Other | 0.1 | Mixed | |
| **189** | SeatBeltFrontRight.Other.Steel | 0.09 | Ferrous | |
| **190** | SeatBeltFrontRight.Other.SKOP | 0.01 | SKOP | |
| **191** | SeatBeltFrontRight.Lead | 0.02 | Lead | |
| **192** | SeatBeltFrontLeft | 1.4 | Mixed | 1-Ph; 1-500T |
| **193** | SeatBeltFrontLeft.Steelcase | 0.86 | Mixed | |
| **194** | SeatBeltFrontLeft.Steelcase.Steel | 0.82 | Ferrous | |
| **195** | SeatBeltFrontLeft.Steelcase.SKOP | 0.04 | SKOP | |
| **196** | SeatBeltFrontLeft.Strap | 0.16 | PE | |
| **197** | SeatBeltFrontLeft.Other | 0.1 | Mixed | |
| **198** | SeatBeltFrontLeft.Other.Steel | 0.09 | Ferrous | |
| **199** | SeatBeltFrontLeft.Other.SKOP | 0.01 | SKOP | |
| **200** | SeatBeltFrontLeft.Lead | 0.02 | Lead | |
| **201** | BPillarShoddyRight | 0.1 | Mixed | 2-Snaps |
| **202** | BPillarShoddyRight.Shoddy | 0.04 | Carpet | |
| **203** | BPillarShoddyRight.SKOP | 0.06 | SKOP | |
| **204** | BPillarShoddyLeft | 0.1 | Mixed | 2-Snaps |
| **205** | BPillarShoddyLeft.Shoddy | 0.04 | Carpet | |
| **206** | BPillarShoddyLeft.SKOP | 0.06 | SKOP | |
| **207** | QuartertrimRight | 0.18 | Mixed | 1-Pi; 1-500T |
| **208** | QuartertrimRight.Shoddy | 0.08 | Carpet | |
| **209** | QuartertrimRight.PP | 0.1 | PP | |
| **210** | QuartertrimLeft | 0.18 | Mixed | 1-Pi; 1-500T |
| **211** | QuartertrimLeft.Shoddy | 0.08 | Carpet | |
| **212** | QuartertrimLeft.PP | 0.1 | PP | |
| **213** | KickPanelRight | 0.06 | PP | 1-Ph |
| **214** | KickPanelLeft | 0.06 | PP | 1-Ph |

| | | | | |
|---|---|---|---|---|
| **215** | ThirdBrakeLight | 0.34 | Mixed | 2-Ph |
| **216** | ThirdBrakeLight.Lens | 0.01 | SKOP | |
| **217** | ThirdBrakeLight.Reflector | 0.04 | PC | |
| **218** | ThirdBrakeLight.Case | 0.26 | Mixed | |
| **219** | ThirdBrakeLight.Case.Steel | 0.06 | Ferrous | |
| **220** | ThirdBrakeLight.Case.Plastic | 0.2 | SKOP | |
| **221** | SpeakerCovers | 0.22 | Ferrous | |
| **222** | ParcelTray | 1.58 | Mixed | |
| **223** | SpeakerRearLeft | 0.7 | Mixed | 3-5mm; 1-EC |
| **224** | SpeakerRearLeft.Steel | 0.67 | Ferrous | |
| **225** | SpeakerRearLeft.SKOP | 0.03 | SKOP | |
| **226** | SpeakerRearRight | 0.7 | Mixed | 3-5mm; 1-EC |
| **227** | SpeakerRearRight.Steel | 0.67 | Ferrous | |
| **228** | SpeakerRearRight.SKOP | 0.03 | SKOP | |
| **229** | ParcelTrayShoddy | 0.68 | Carpet | |
| **230** | BackSeatShoddy | 2.18 | Carpet | |
| **231** | SeatBeltRearRight | 0.96 | Mixed | 1-500T; 1-40 |
| **232** | SeatBeltRearRight.Steelcase | 0.62 | Mixed | |
| **233** | SeatBeltRearRight.Steelcase.Steel | 0.59 | Ferrous | |
| **234** | SeatBeltRearRight.Steelcase.SKOP | 0.03 | SKOP | |
| **235** | SeatBeltRearRight.Strap | 0.14 | PE | |
| **236** | SeatBeltRearRight.PlasticCase | 0.02 | SKOP | |
| **237** | SeatBeltRearRight.Other | 0.1 | Mixed | |
| **238** | SeatBeltRearRight.Other.Steel | 0.09 | Ferrous | |
| **239** | SeatBeltRearRight.Other.SKOP | 0.01 | SKOP | |
| **240** | SeatBeltRearRight.Lead | 0.02 | Lead | |
| **241** | SeatBeltRearLeft | 0.96 | Mixed | |
| **242** | SeatBeltRearLeft.Steelcase | 0.62 | Mixed | |
| **243** | SeatBeltRearLeft.Steelcase.Steel | 0.59 | Ferrous | |
| **244** | SeatBeltRearLeft.Steelcase.SKOP | 0.03 | SKOP | |
| **245** | SeatBeltRearLeft.Strap | 0.14 | PE | |
| **246** | SeatBeltRearLeft.PlasticCase | 0.02 | SKOP | |
| **247** | SeatBeltRearLeft.Other | 0.1 | Mixed | |
| **248** | SeatBeltRearLeft.Other.Steel | 0.09 | Ferrous | |
| **249** | SeatBeltRearLeft.Other.SKOP | 0.01 | SKOP | |
| **250** | SeatBeltRearLeft.Lead | 0.02 | Lead | |
| **251** | SeatbeltRearRightLower | 0.36 | Mixed | 1-18mm |
| **252** | SeatbeltRearRightLower.Other | 0.1 | Mixed | |
| **253** | SeatbeltRearRightLower.Other.Steel | 0.09 | Ferrous | |
| **254** | SeatbeltRearRightLower.Other.SKOP | 0.01 | SKOP | |
| **255** | SeatbeltRearRightLower.Strap | 0.08 | PE | |
| **256** | SeatbeltRearRightLower.Buckle | 0.08 | Mixed | |
| **257** | SeatbeltRearRightLower.Latch | 0.1 | Ferrous | |

| | | | | |
|---|---|---|---|---|
| 258 | SeatbeltRearRightLower.PlasticCase | 0.02 | SKOP | |
| 259 | SeatbeltRearLeftLower | 0.26 | Mixed | 1-18mm |
| 260 | SeatbeltRearLeftLower.Strap | 0.04 | PE | |
| 261 | SeatbeltRearLeftLower.PlasticCase | 0.02 | SKOP | |
| 262 | SeatbeltRearLeftLower.Steel | 0.1 | Ferrous | |
| 263 | SeatbeltRearLeftLower.Buckles | 0.14 | Mixed | |
| 264 | LowerIP | 1.12 | Mixed | 4-27T |
| 265 | LowerIP.Steel | 1.09 | Ferrous | |
| 266 | LowerIP.SKOP | 0.03 | SKOP | |
| 267 | LowerIPReinforcement | 0.18 | Ferrous | 2-8mm |
| 268 | LowerIPReinforcement2 | 1.22 | Ferrous | 4-13mm |
| 271 | SteeringColumnSupport | 2.26 | Mixed | 5-10mm |
| 272 | SteeringColumnSupport.Electrical | 0.28 | Mixed | |
| 273 | SteeringColumnSupport.Case | 1.8 | Aluminum_wrought | |
| 274 | SteeringColumnSupport.Bracket | 0.14 | Ferrous | |
| 275 | SteeringColumnTurnSignal | 0.22 | Mixed | |
| 276 | SteeringColumnLowerPanel | 0.08 | SKOP | |
| 277 | SteeringColumnAssembly | 10.06 | Mixed | 4-13mm; 2-20T; 5-EC; 1-8mm; 4-Ph; 2-Clips |
| 278 | SteeringColumnAssembly.AirBag | 1.7 | Mixed | |
| 279 | SteeringColumnAssembly.AirBag.Steel | 1.19 | Ferrous | |
| 280 | SteeringColumnAssembly.AirBag.SKOS | 0.51 | SKOP | |
| 281 | SteeringColumnAssembly.Base | 8.36 | Mixed | |
| 282 | SteeringColumnAssembly.Base.Steel | 7.52 | Ferrous | |
| 283 | SteeringColumnAssembly.Base.SKOP | 0.84 | SKOP | |
| 284 | TrunkCloseOut | 0.84 | Mixed | |
| 285 | TrunkCloseOut.Shoddy | 0.26 | Carpet | |
| 286 | TrunkCloseOut.SKOS | 0.58 | SKOP | |
| 287 | TrunkScuffPlateRear | 0.12 | PP | |
| 288 | TrunkSpareTireCover | 1.8 | Mixed | |
| 289 | TrunkSpareTireCover.Carpet | 0.19 | Carpet | |
| 290 | TrunkSpareTireCover.Carboard | 1.61 | SKOP | |
| 291 | SpareTire | 11.3 | Mixed | |
| 292 | SpareTire.Rim | 6.55 | Ferrous | |
| 293 | SpareTire.Rubber | 4.73 | Elastomer | |
| 294 | Jack | 2.44 | Ferrous | |
| 295 | TrunkLiner | 3.56 | Mixed | |
| 296 | TrunkLiner.Shoddy | 0.24 | Carpet | |
| 297 | TrunkLiner.Carpet | 3.32 | Carpet | |
| 298 | WeatherStripping | 6.78 | Elastomer | |
| 299 | TailLightCoverRight | 0.54 | SKOP | 3-wing nuts |
| 300 | TailLightCoverRight.Red | 0.16 | SKOP | |
| 301 | TailLightCoverRight.Black | 0.38 | ABS | |

| | | | | |
|---|---|---|---|---|
| **302** | TailLightCoverLeft | 0.54 | SKOP | 3-wing nuts |
| **303** | TailLightCoverLeft.Red | 0.16 | SKOP | |
| **304** | TailLightCoverLeft.Black | 0.38 | ABS | |
| **305** | TailLightCoverCenter | 1.28 | SKOP | 12-10mm |
| **306** | FasciaRearUpper | 1.73 | PUR | 10-11mm |
| **307** | FasciaRearlower | 8.56 | Xenoy | 6-10mm |
| **308** | EnergyAbsorberRearLeft | 2.46 | Ferrous | |
| **309** | EnergyAbsorberRearRight | 2.46 | Ferrous | |
| **310** | DeckLid | 13.26 | Mixed | 4-8mm; 1-EC |
| **311** | DeckLid.Lid | 10.88 | Ferrous | |
| **312** | DeckLid.SKOS | 0.13 | SKOP | |
| **313** | WiringHarnessCloseOut | 0.3 | SKOP | |
| **314** | WiperAssemblies | 0.92 | Mixed | |
| **315** | WiperAssemblies.Steel | 0.86 | Ferrous | |
| **316** | WiperAssemblies.Blade | 0.06 | Mixed | |
| **317** | WiperAssemblies.Blade.Elastomer | 0.04 | Elastomer | |
| **318** | WiperAssemblies.Blade.SKOM | 0.02 | Aluminum_wrought | |
| **319** | CowlVent | 0.54 | ABS | 10-Ph |
| **321** | AirCleanerAssembly | 1.7 | Mixed | |
| **322** | AirCleanerAssembly.Hose | 0.4 | Mixed | |
| **323** | AirCleanerAssembly.Hose.Clamp | 0.06 | Aluminum_wrought | |
| **324** | AirCleanerAssembly.Hose.SKOR | 0.34 | Elastomer | |
| **325** | AirCleanerAssembly.Top | 0.4 | PP | 4-9mm |
| **326** | AirCleanerAssembly.Bottom | 0.88 | PP | |
| **327** | AirCleanerAssembly.Filter | 0.18 | SKOP | |
| **328** | WasherCoolantBottleAssembly | 0.9 | Mixed | 1-8mm |
| **329** | WasherCoolantBottleAssembly.Bottles | 0.82 | PP | |
| **330** | WasherCoolantBottleAssembly.Rubber | 0.08 | Elastomer | |
| **331** | HeatBoxAssemblyBase | 2.24 | PET | |
| **332** | HeatBoxAssembly | 8.64 | Mixed | 1-7mm; 1-8mm; 5-11mm; 1-QDC; 1-Vac |
| **333** | HeatBoxAssembly.EC | 0.24 | Mixed | 3-5/16th |
| **334** | HeatBoxAssembly.LateralCover | 0.05 | PP | 4-5/16th |
| **335** | HeatBoxAssembly.Elastomer | 0.05 | Elastomer | |
| **336** | HeatBoxAssembly.Filter1 | 0.81 | Aluminum_wrought | |
| **337** | HeatBoxAssembly.SpringHeater | 0.04 | SKOS | 2-5/16th |
| **338** | HeatBoxAssembly.Panel1 | 0.23 | Mixed | 2-Clips |
| **339** | HeatBoxAssembly.Panel1.Sponge | 0.02 | SKOP | |
| **340** | HeatBoxAssembly.Panel1.PP | 0.21 | PP | |
| **341** | HeatBoxAssembly.Duct1 | 0.77 | Mixed | 2-5/16th |
| **342** | HeatBoxAssembly.Duct1.Pump | 0.1 | Mixed:Aluminum | 2-5/16th; 1-Clips |
| **343** | HeatBoxAssembly.Duct1.Pump.Alum | 0.08 | Aluminum_wrought | |
| **344** | HeatBoxAssembly.Duct1.Pump.SKOP | 0.02 | SKOP | |

| | | | | |
|---|---|---|---|---|
| **345** | HeatBoxAssembly.Duct1.Structure | 0.67 | Mixed:PP | |
| **346** | HeatBoxAssembly.Duct1.Structure.Steel | 0.04 | Ferrous | |
| **347** | HeatBoxAssembly.Duct1.Structure.PP | 0.56 | PP | |
| **348** | HeatBoxAssembly.Duct1.Structure.SKOS | 0.07 | SKOP | |
| **349** | HeatBoxAssembly.Elastomer2 | 0.13 | Elastomer | |
| **350** | HeatBoxAssembly.Fan | 0.12 | PP | 1-Clips |
| **351** | HeatBoxAssembly.Motor | 1.6 | Mixed | 5-5/16th |
| **352** | HeatBoxAssembly.Motor.Steel | 1.2 | Ferrous | |
| **353** | HeatBoxAssembly.Motor.Copper | 0.24 | Copper | |
| **354** | HeatBoxAssembly.Motor.SKOS | 0.16 | Mixed:Ferrous | |
| **355** | HeatBoxAssembly.Duct2 | 0.5 | Mixed | 2-5/16th; 2-3/16th |
| **356** | HeatBoxAssembly.Duct2.SKOS | 0.03 | SKOP | |
| **357** | HeatBoxAssembly.Duct2.PP | 0.47 | PP | |
| **358** | HeatBoxAssembly.Box | 3.85 | Mixed | |
| **359** | HeatBoxAssembly.Box.SKOP | 0.09 | SKOP | |
| **360** | HeatBoxAssembly.Box.Filter2 | 1.81 | Aluminum_wrought | 8-5/16th; 3-Clips |
| **361** | HeatBoxAssembly.Box.PP | 1.95 | PP | |
| **362** | GasPedalAssembly | 0.52 | Mixed | 2-13mm; 1-Clips |
| **363** | GasPedalAssembly.Steel | 0.48 | Ferrous | |
| **364** | GasPedalAssembly.SKOP | 0.04 | SKOP | |
| **365** | BreakPedalAssembly | 2.23 | Mixed | 4-13mm; 1-10mm; 1-Clips |
| **366** | BreakPedalAssembly.Bracket | 0.26 | Ferrous | 1-8mm |
| **367** | BreakPedalAssembly.Rubber | 0.07 | Elastomer | |
| **368** | BreakPedalAssembly.Base | 1.9 | Ferrous | |
| **369** | SteeringColumnSupport2 | 0.62 | SKOP | 3-11mm |
| **370** | TrunkReleaseCase | 0.04 | ABS | 1-Ph; 1-Pushin |
| **371** | carpet | 15.88 | Mixed | |
| **372** | carpet.Shoddy | 6.38 | Carpet | |
| **373** | carpet.Carpet | 9.5 | Carpet | |
| **374** | RearHeaterDuct | 0.78 | PP | 2-7mm |
| **375** | ECU | 1.08 | Mixed | 2-11mm |
| **376** | ECU.Steel | 0.11 | Ferrous | |
| **377** | ECU.AIuminum | 0.22 | Aluminum_cast | |
| **378** | ECU.SKOS | 0.76 | Mixed | |
| **379** | EmergencyBrake | 1.62 | Ferrous | 3-10mm |
| **380** | FrontInsulator | 6.34 | Mixed | |
| **381** | FrontInsulator.Shoddy | 0.98 | Carpet | |
| **382** | FrontInsulator.SKOS | 5.36 | SKOS | |
| **383** | BatteryCase | 0.76 | SKOP | 3-10mm |
| **384** | BrakeBooster | 4.14 | Mixed | 2-12mm; 2-14mm |
| **385** | BrakeBooster.Steel | 2.28 | Ferrous | |
| **386** | BrakeBooster.Aluminum | 1.24 | Aluminum_wrought | |

| | | | | |
|---|---|---|---|---|
| **387** | BrakeBooster.SKOP | 0.62 | SKOP | |
| **388** | FirewallInsulation | 0.44 | SKOP | 3-Pi |
| **389** | CoolingFanShroudAssembly | 3.68 | Mixed | 2-11mm |
| **390** | CoolingFanShroudAssembly.Steel | 1.47 | Ferrous | |
| **391** | CoolingFanShroudAssembly.SKOS | 2.21 | SKOP | |
| **392** | CoolingFanModule | 0.72 | Mixed | 2-11mm |
| **393** | CoolingFanModule.Steel | 0.5 | Ferrous | |
| **394** | CoolingFanModule.SKOS | 0.22 | SKOP | |
| **395** | AirBagSensor | 0.34 | Mixed | 4-8mm |
| **398** | CruiseServo | 1.08 | Mixed | 2-13mm |
| **399** | CruiseServo.Steel | 0.22 | Ferrous | |
| **400** | CruiseServo.SKOS | 0.86 | Mixed | |
| **401** | EngineHarness | 3.16 | Mixed | 1-8mm |
| **402** | EngineHarness.Steel | 0.63 | Ferrous | |
| **403** | EngineHarness.Copper | 0.03 | Copper | |
| **404** | EngineHarness.SKOS | 2.05 | Mixed | |
| **405** | ACManifold | 3.9 | Mixed | 3-8mm |
| **406** | ACManifold.Steel | 3.32 | Ferrous | |
| **407** | ACManifold.SKOS | 0.59 | SKOP | |
| **408** | AirBagSensor2 | 0.26 | Mixed | 2-8mm |
| **412** | AirDam | 0.34 | Elastomer | 3-Ph |
| **413** | WheelHouseLinerFrontRight | 1.22 | Mixed | 4-Pushin |
| **414** | WheelHouseLinerFrontRight.SKOS | 1.13 | SKOP | |
| **415** | WheelHouseLinerFrontRight.PP | 0.09 | PP | |
| **416** | WheelHouseLinerFrontLeft | 1.22 | Mixed | 4-Pushin |
| **417** | WheelHouseLinerFrontLeft.SKOS | 1.13 | SKOP | |
| **418** | WheelHouseLinerFrontLeft.PP | 0.09 | PP | |
| **419** | CharcoalCanister | 0.82 | SKOP | 1-8mm |
| **420** | VacuumTank | 0.74 | SKOP | 1-8mm |
| **421** | HornAssembly | 0.6 | Mixed | 1-13mm |
| **424** | RockerMoldingRight | 1.44 | Elastomer | 7-Pushin; 1-Rivets |
| **425** | RockerMoldingLeft | 1.4 | Elastomer | 7-Pushin |
| **426** | WheelRearRight | 16.28 | Mixed | 5-lognuts |
| **427** | WheelRearRight.Cover | 0.18 | PC | |
| **428** | WheelRearRight.Rim | 7.18 | Aluminum_cast | |
| **429** | WheelRearRight.Rubber | 8.84 | Elastomer | |
| **430** | WheelRearLeft | 16.28 | Mixed | 5-lognuts |
| **431** | WheelRearLeft.Cover | 0.18 | PC | |
| **432** | WheelRearLeft.Rim | 7.18 | Aluminum_cast | |
| **433** | WheelRearLeft.Rubber | 8.84 | Elastomer | |
| **434** | WireHarnessCover | 0.48 | PP | 16-Pushin |
| **435** | TrunkRelease | 0.42 | Mixed | 2-Pushin; 2-Clips |
| **436** | TrunkRelease.Steel | 0.38 | Ferrous | |

| | | | | |
|---|---|---|---|---|
| 437 | TrunkRelease.SKOP | 0.04 | SKOP | |
| 438 | WireHarness | 3.94 | Mixed | |
| 439 | WireHarness.Steel | 0.79 | Ferrous | |
| 440 | WireHarness.Copper | 0.59 | Copper | |
| 441 | WireHarness.SKOP | 2.56 | SKOP | |
| 442 | WindshieldWiperMotor | 1.98 | Mixed | 3-8mm; 1-Clips |
| 443 | WindshieldWiperMotor.Steel | 1.49 | Ferrous | |
| 444 | WindshieldWiperMotor.Magnesium | 0.2 | Magnesium | |
| 445 | WindshieldWiperMotor.Copper | 0.3 | Copper | |
| 446 | WindShieldFront | 11.76 | Glass | |
| 448 | FrontClip | 175.54 | Mixed | |
| 449 | FrontClip.RadiatorHeatExchanger | 4.76 | Mixed | 4-10mm; 3-8mm |
| 450 | FrontClip.RadiatorHeatExchanger.Hoses | 0.28 | Ferrous | |
| 451 | FrontClip.RadiatorHeatExchanger.Fittings | 0.06 | Ferrous | |
| 452 | FrontClip.RadiatorHeatExchanger.Elastomer | 0.09 | Elastomer | |
| 453 | FrontClip.RadiatorHeatExchanger.LeftEnd | 0.38 | PP | |
| 454 | FrontClip.RadiatorHeatExchanger.Nuts | 0.05 | Ferrous | |
| 455 | FrontClip.RadiatorHeatExchanger.RightEnd | 0.56 | Mixed:Ferrous | |
| 456 | FrontClip.RadiatorHeatExchanger.RightEnd.Cap | 0.49 | Ferrous | |
| 457 | FrontClip.RadiatorHeatExchanger.RightEnd.PA | 0.08 | Ferrous | |
| 458 | FrontClip.RadiatorHeatExchanger.CoolantTube | 0.52 | Copper | |
| 459 | FrontClip.RadiatorHeatExchanger.Fins | 2.56 | Aluminum_wrought | |
| 460 | FrontClip.ACCondensor | 2.12 | Mixed | 3-8mm; 2-QDC; 2-Clips |
| 461 | FrontClip.ACCondensor.Alum | 1.8 | Aluminum_wrought | |
| 462 | FrontClip.ACCondensor.Steel | 0.32 | Ferrous | |
| 463 | FrontClip.MarkerLightFrontLeft | 0.34 | SKOP | 1-Ph; 2-11mm; 2-EC |
| 464 | FrontClip.MarkerLightFrontRight | 0.34 | SKOP | 1-Ph; 2-11mm; 2-EC |
| 465 | FrontClip.LightFrontAssembly | 4.26 | Mixed | 13-8mm |
| 466 | FrontClip.LightFrontAssembly.HeadLightL | 0.86 | SKOP | 3-Pi |
| 467 | FrontClip.LightFrontAssembly.HeadLightL.St | 0.02 | Ferrous | |
| 468 | FrontClip.LightFrontAssembly.HeadLightL.PI1 | 0.36 | SKOP | |
| 469 | FrontClip.LightFrontAssembly.HeadLightL.PI2 | 0.47 | SKOP | |
| 470 | FrontClip.LightFrontAssembly.HeadLightR | 0.86 | SKOP | 3-Pi |
| 471 | FrontClip.LightFrontAssembly.HeadLightR.St | 0.02 | Ferrous | |
| 472 | FrontClip.LightFrontAssembly.HeadLightR.PI1 | 0.36 | SKOP | |
| 473 | FrontClip.LightFrontAssembly.HeadLightR.PI2 | 0.47 | SKOP | |
| 474 | FrontClip.LightFrontAssembly.Center | 1.06 | SKOP | 4-8mm |
| 475 | FrontClip.LightFrontAssembly.Frame | 2.45 | PET | |
| 476 | FrontClip.FasciaFrontLower | 9.68 | Xenoy | 6-10mm |
| 477 | FrontClip.FasciaFrontUpper | 1.2 | PUR | 4-11mm; 2-Pi |
| 478 | FrontClip.EnergyAbsorberFrontRight | 2.5 | Ferrous | |
| 479 | FrontClip.EnergyAbsorberFrontLeft | 2.5 | Ferrous | |

| | | | | |
|---|---|---|---|---|
| 480 | FrontClip.RadiatorShroud | 0.28 | TPO | 4-8mm |
| 481 | FrontClip.Hood | 22.56 | Mixed | 4-8mm; 1-EC; 2-Clips |
| 482 | FrontClip.Hood.Insulation | 0.64 | SKOP | 7-Pi |
| 483 | FrontClip.Hood.Lid | 17.49 | Ferrous | |
| 484 | FrontClip.Frame | 125 | Ferrous | |
| 485 | DriveTrain | 457.85 | Mixed | 2-10mm; 8-13mm; 5-8mm; 10-EC; 1-Clamp; 1-11mm; 1-Clips; 1-VacLine; 1-7mm; 2-QDC; 2-15mm; 4-18mm; 2-7/16th |
| 486 | DriveTrain.ACCompressor | 6.36 | Mixed | 4-10mm; 1-EC |
| 487 | DriveTrain.ACCompressor.Steel | 3.62 | Ferrous | |
| 488 | DriveTrain.ACCompressor.Zinc | 2.54 | Zinc | |
| 489 | DriveTrain.Alternator | 6.58 | Mixed | 1-15mm; 1-10mm |
| 490 | DriveTrain.Alternator.Copper | 2.8 | Copper | |
| 491 | DriveTrain.Alternator.Magnesium | 1 | Magnesium | |
| 492 | DriveTrain.Alternator.Steel | 2.78 | Ferrous | |
| 493 | DriveTrain.PowerSteering | 6.34 | Mixed | 3-13mm; 1-10mm; 1-18mm |
| 494 | DriveTrain.PowerSteering.Steel | 3.01 | Ferrous | |
| 495 | DriveTrain.PowerSteering.Aluminum | 3.01 | Aluminum_wrought | |
| 496 | DriveTrain.PowerSteering.SKOP | 0.32 | SKOP | |
| 497 | DriveTrain.Starter | 3.5 | Mixed | 3-13mm;1-15mm;1-EC |
| 498 | DriveTrain.Starter.Steel | 2.1 | Ferrous | |
| 499 | DriveTrain.Starter.Magnesium | 0.53 | Magnesium | |
| 500 | DriveTrain.Starter.Copper | 0.88 | Copper | |
| 501 | DriveTrain.Engine | 200 | Mixed | 8-15mm; 2-18mm; 7-EC; 2-13mm |
| 502 | DriveTrain.Engine.Steel | 150 | Ferrous | |
| 503 | DriveTrain.Engine.SKOM | 30 | Ferrous | |
| 504 | DriveTrain.Engine.SKOS | 20 | Mixed:Ferrous | |
| 505 | DriveTrain.Transmission | 94.55 | Mixed | |
| 506 | DriveTrain.Transmission.Steel | 47.28 | Ferrous | |
| 507 | DriveTrain.Transmission.Aluminum | 47.28 | Aluminum_wrought | |
| 508 | DriveTrain.CradleSuspension | 107.96 | Ferrous | |
| 509 | WheelFrontRight | 16.28 | Mixed | |
| 510 | WheelFrontRight.Cover | 0.2 | PC-ABS | |
| 511 | WheelFrontRight.Rim | 7.18 | Aluminum_cast | |
| 512 | WheelFrontRight.Tire | 8.84 | Elastomer | |
| 513 | WheelFrontLeft | 16.28 | Mixed | |
| 514 | WheelFrontLeft.Cover | 0.2 | PC-ABS | |
| 515 | WheelFrontLeft.Rim | 7.18 | Aluminum_cast | |
| 516 | WheelFrontLeft.Tire | 8.84 | Elastomer | |
| 517 | InstrumentPanel | 35.96 | Mixed | 11-8mm; 16-EC; 1-10mm; 1-awc; 1-cable |

| | | | | |
|---|---|---|---|---|
| 518 | InstrumentPanel.DuctWork | 0.52 | PE | 8-20T; 1-7mm |
| 519 | InstrumentPanel.EvapDuct | 1.14 | SKOP | |
| 520 | InstrumentPanel.DuctWork2 | 0.44 | PE | |
| 521 | InstrumentPanel.Hoses | 0.26 | SKOP | |
| 522 | InstrumentPanel.WireHarness | 5.62 | Mixed | 5-2T; 9-Pi |
| 523 | InstrumentPanel.WireHarness.Steel | 1.12 | Ferrous | |
| 524 | InstrumentPanel.WireHarness.Copper | 0.84 | Copper | |
| 525 | InstrumentPanel.WireHarness.SKOP | 3.65 | SKOP | |
| 526 | InstrumentPanel.DashBrain | 0.2 | Mixed | |
| 527 | InstrumentPanel.Dimmer | 0.26 | Mixed | |
| 528 | InstrumentPanel.Dimmer.Steel | 0.12 | Ferrous | |
| 529 | InstrumentPanel.Dimmer.SKOP | 0.14 | SKOP | |
| 530 | InstrumentPanel.Radio | 1.48 | Mixed | |
| 533 | InstrumentPanel.TrayAssembly | 0.5 | TPO | 2-Clips |
| 534 | InstrumentPanel.ClusterBezel | 1.32 | SKOP | |
| 535 | InstrumentPanel.Cluster | 1.54 | Mixed | 4-20T |
| 536 | InstrumentPanel.HeaterControl | 0.26 | Mixed | 4-20T |
| 537 | InstrumentPanel.GloveBox | 2.52 | Mixed | 3-20T |
| 538 | InstrumentPanel.GloveBox.Front | 0.56 | Mixed:TPO | 9-Ph |
| 539 | InstrumentPanel.GloveBox.Front.PPO | 0.51 | TPO | 2-Ph |
| 540 | InstrumentPanel.GloveBox.Front.SKOP | 0.05 | SKOP | |
| 541 | InstrumentPanel.GloveBox.Steel | 1.37 | Ferrous | |
| 542 | InstrumentPanel.GloveBox.SKOP | 0.59 | SKOP | |
| 543 | InstrumentPanel.Ashtray | 1.04 | Mixed | 2-20T; 2-10mm |
| 544 | InstrumentPanel.Ashtray.Steel | 0.99 | Ferrous | |
| 545 | InstrumentPanel.Ashtray.SKOP | 0.05 | SKOP | |
| 546 | InstrumentPanel.CenterBezel | 0.18 | ABS | |
| 547 | InstrumentPanel.Clock | 0.1 | Mixed | 2-15T |
| 548 | InstrumentPanel.AirBagPassenger | 4.86 | Mixed | 4-20T; 3-8mm |
| 549 | InstrumentPanel.AirBagPassenger.Steel | 3.89 | Ferrous | |
| 550 | InstrumentPanel.AirBagPassenger.SKOS | 0.97 | SKOP | |
| 551 | InstrumentPanel.AirBagCover | 0.2 | PC | 4-Pi |
| 552 | InstrumentPanel.Frame | 5.94 | Ferrous | |
| 553 | InstrumentPanel.Skin | 6.5 | SKOP | |
| 600 | RearFrame | 279 | Ferrous | |
| 601 | RearFrame.A | 178 | Ferrous | |
| 602 | RearFrame.B | 101 | Ferrous | |
| 605 | DeckLid.Hinge | 2.25 | Ferrous | |
| 610 | FrontClip.Hood.Hinges | 4.43 | Ferrous | |
| 615 | FrontClip.Frame.A | 72 | Ferrous | |
| 616 | FrontClip.Frame.B | 53 | Ferrous | |
| 1000 | InstrumentPanel.Radio.Al | 0.046042 | Aluminum | |
| 1001 | InstrumentPanel.Radio.Cu | 0.076143 | Copper | |

| | | | | |
|---|---|---|---|---|
| **1002** | InstrumentPanel.Radio.Fe | 0.63438 | Ferrous | |
| **1003** | InstrumentPanel.Radio.Mg | 0.00062 | Magnesium | |
| **1004** | InstrumentPanel.Radio.Zn | 0.030218 | Zinc | |
| **1005** | InstrumentPanel.Radio.Pb | 0.000133 | Lead | |
| **1006** | InstrumentPanel.Radio.OtherMetals | 0.019338 | SKOS | |
| **1007** | InstrumentPanel.Radio.NonMetals | 0.673125 | SKOP | |
| **1008** | HornAssembly.Al | 0.025421 | Aluminum | |
| **1009** | HornAssembly.Cu | 0.005998 | Copper | |
| **1010** | HornAssembly.Fe | 0.404727 | Ferrous | |
| **1011** | HornAssembly.Mg | 0 | Magnesium | |
| **1012** | HornAssembly.Zn | 0.005764 | Zinc | |
| **1013** | HornAssembly.Pb | 1.65E-06 | Lead | |
| **1014** | HornAssembly.skos | 0.002819 | SKOS | |
| **1015** | HornAssembly.skop | 0.155269 | SKOP | |
| **1016** | InstrumentPanel.Cluster.Al | 0.027286 | Aluminum | |
| **1017** | InstrumentPanel.Cluster.Copper | 0.06282 | Copper | |
| **1018** | InstrumentPanel.Cluster.Fe | 0.271587 | Ferrous | |
| **1019** | InstrumentPanel.Cluster.Mg | 0.000622 | Magnesium | |
| **1020** | InstrumentPanel.Cluster.Zn | 0.002437 | Zinc | |
| **1021** | InstrumentPanel.Cluster.Pb | 1.74E-05 | Lead | |
| **1022** | InstrumentPanel.Cluster.SKOS | 0.026875 | SKOS | |
| **1023** | InstrumentPanel.Cluster.SKOP | 1.148357 | SKOP | |
| **1024** | ECU.SKOS.Al | 0.013466 | Aluminum | |
| **1025** | ECU.SKOS.Cu | 0.031002 | Copper | |
| **1026** | ECU.SKOS.Fe | 0.13403 | Ferrous | |
| **1027** | ECU.SKOS.Mg | 0.000307 | Magnesium | |
| **1028** | ECU.SKOS.Zn | 0.001203 | Zinc | |
| **1029** | ECU.SKOS.Pb | 8.61E-06 | Lead | |
| **1030** | ECU.SKOS.skos | 0.013263 | SKOS | |
| **1031** | ECU.SKOS.skop | 0.566722 | SKOP | |
| **1032** | HeatBoxAssembly.EC.Al | 0.004252 | Aluminum | |
| **1033** | HeatBoxAssembly.EC.Cu | 0.00979 | Copper | |
| **1034** | HeatBoxAssembly.EC.Fe | 0.042325 | Ferrous | |
| **1035** | HeatBoxAssembly.EC.Mg | 9.69E-05 | Magnesium | |
| **1036** | HeatBoxAssembly.EC.Zn | 0.00038 | Zinc | |
| **1037** | HeatBoxAssembly.EC.Pb | 2.72E-06 | Lead | |
| **1038** | HeatBoxAssembly.EC.SKOS | 0.004188 | SKOS | |
| **1039** | HeatBoxAssembly.EC.SKOP | 0.178965 | SKOP | |
| **1040** | InstrumentPanel.DashBrain.Al | 8.35E-07 | Aluminum | |
| **1041** | InstrumentPanel.DashBrain.Cu | 0.000725 | Copper | |
| **1042** | InstrumentPanel.DashBrain.Fe | 0.00012 | Ferrous | |
| **1043** | InstrumentPanel.DashBrain.Mg | 0 | Magnesium | |
| **1044** | InstrumentPanel.DashBrain.Zn | 1.34E-05 | Zinc | |

| | | | | |
|---|---|---|---|---|
| **1045** | InstrumentPanel.DashBrain.Pb | 3.38E-08 | Lead | |
| **1046** | InstrumentPanel.DashBrain.skos | 2.98E-05 | SKOS | |
| **1047** | InstrumentPanel.DashBrain.skop | 0.199111 | SKOP | |
| **1048** | DomeLight.Al | 0 | Aluminum | |
| **1049** | DomeLight.Cu | 0.009043 | Copper | |
| **1050** | DomeLight.Fe | 0.004804 | Ferrous | |
| **1051** | DomeLight.Mg | 0 | Magnesium | |
| **1052** | DomeLight.Zn | 0.00106 | Zinc | |
| **1053** | DomeLight.Pb | 1.98E-07 | Lead | |
| **1054** | DomeLight.skos | 0.004373 | SKOS | |
| **1055** | DomeLight.skop | 0.18072 | SKOP | |
| **1056** | InstrumentPanel.HeaterControl.Al | 0 | Aluminum | |
| **1057** | InstrumentPanel.HeaterControl.Cu | 0.011756 | Copper | |
| **1058** | InstrumentPanel.HeaterControl.Fe | 0.006245 | Ferrous | |
| **1059** | InstrumentPanel.HeaterControl.Mg | 0 | Magnesium | |
| **1060** | InstrumentPanel.HeaterControl.Zn | 0.001378 | Zinc | |
| **1061** | InstrumentPanel.HeaterControl.Pb | 2.57E-07 | Lead | |
| **1062** | InstrumentPanel.HeaterControl.skos | 0.005685 | SKOS | |
| **1063** | InstrumentPanel.HeaterControl.skop | 0.234935 | SKOP | |
| **1064** | InstrumentPanel.Clock.Al | 0 | Aluminum | |
| **1065** | InstrumentPanel.Clock.Cu | 0.004522 | Copper | |
| **1066** | InstrumentPanel.Clock.Fe | 0.002402 | Ferrous | |
| **1067** | InstrumentPanel.Clock.Mg | 0 | Magnesium | |
| **1068** | InstrumentPanel.Clock.Zn | 0.00053 | Zinc | |
| **1069** | InstrumentPanel.Clock.Pb | 9.89E-08 | Lead | |
| **1070** | InstrumentPanel.Clock.SKOS | 0.002187 | SKOS | |
| **1071** | InstrumentPanel.Clock.SKOP | 0.09036 | SKOP | |
| **1072** | DriveTrain.Engine.SKOS.Al | 4.588788 | Aluminum | |
| **1073** | DriveTrain.Engine.SKOS.Cu | 1.239569 | Copper | |
| **1074** | DriveTrain.Engine.SKOS.Fe | 11.06077 | Ferrous | |
| **1075** | DriveTrain.Engine.SKOS.Mg | 0.002741 | Magnesium | |
| **1076** | DriveTrain.Engine.SKOS.Zn | 0.110727 | Zinc | |
| **1077** | DriveTrain.Engine.SKOS.Pb | 0.000726 | Lead | |
| **1078** | DriveTrain.Engine.SKOS.skos | 0.696293 | SKOS | |
| **1079** | DriveTrain.Engine.SKOS.skop | 2.300389 | SKOP | |
| **1080** | AirBagSensor.Al | 0.078009 | Aluminum | |
| **1081** | AirBagSensor.Cu | 0.021073 | Copper | |
| **1082** | AirBagSensor.Fe | 0.188033 | Ferrous | |
| **1083** | AirBagSensor.Mg | 4.66E-05 | Magnesium | |
| **1084** | AirBagSensor.Zn | 0.001882 | Zinc | |
| **1085** | AirBagSensor.Pb | 1.23E-05 | Lead | |
| **1086** | AirBagSensor.skos | 0.011837 | SKOS | |
| **1087** | AirBagSensor.skop | 0.039107 | SKOP | |

| | | | | |
|---|---|---|---|---|
| **1088** | AirBagSensor2.Al | 0.059654 | Aluminum | |
| **1089** | AirBagSensor2.Cu | 0.016114 | Copper | |
| **1090** | AirBagSensor2.Fe | 0.14379 | Ferrous | |
| **1091** | AirBagSensor2.Mg | 3.56E-05 | Magnesium | |
| **1092** | AirBagSensor2.Zn | 0.001439 | Zinc | |
| **1093** | AirBagSensor2.Pb | 9.44E-06 | Lead | |
| **1094** | AirBagSensor2.skos | 0.009052 | SKOS | |
| **1095** | AirBagSensor2.skop | 0.029905 | SKOP | |
| **1096** | DoorFrontRight.Structure.Mirror.Electrical.Al | 0.01816 | Aluminum | |
| **1097** | DoorFrontRight.Structure.Mirror.Electrical.Cu | 0.032019 | Copper | |
| **1098** | DoorFrontRight.Structure.Mirror.Electrical.Fe | 0.097926 | Ferrous | |
| **1099** | DoorFrontRight.Structure.Mirror.Electrical.Mg | 0 | Magnesium | |
| **1100** | DoorFrontRight.Structure.Mirror.Electrical.Zn | 5.38E-06 | Zinc | |
| **1101** | DoorFrontRight.Structure.Mirror.Electrical.Pb | 1.08E-05 | Lead | |
| **1102** | DoorFrontRight.Structure.Mirror.Electrical.skos | 0.002251 | SKOS | |
| **1103** | DoorFrontRight.Structure.Mirror.Electrical.skop | 0.009629 | SKOP | |
| **1104** | DoorFrontLeft.Structure.Mirror.Electrical.Al | 0.01816 | Aluminum | |
| **1105** | DoorFrontLeft.Structure.Mirror.Electrical.Cu | 0.032019 | Copper | |
| **1106** | DoorFrontLeft.Structure.Mirror.Electrical.Fe | 0.097926 | Ferrous | |
| **1107** | DoorFrontLeft.Structure.Mirror.Electrical.Mg | 0 | Magnesium | |
| **1108** | DoorFrontLeft.Structure.Mirror.Electrical.Zn | 5.38E-06 | Zinc | |
| **1109** | DoorFrontLeft.Structure.Mirror.Electrical.Pb | 1.08E-05 | Lead | |
| **1110** | DoorFrontLeft.Structure.Mirror.Electrical.skos | 0.002251 | SKOS | |
| **1111** | DoorFrontLeft.Structure.Mirror.Electrical.skop | 0.009629 | SKOP | |
| **1112** | DoorRearRight.Structure.SKOS.Al | 0.330276 | Aluminum | |
| **1113** | DoorRearRight.Structure.SKOS.Cu | 0.58234 | Copper | |
| **1114** | DoorRearRight.Structure.SKOS.Fe | 1.781026 | Ferrous | |
| **1115** | DoorRearRight.Structure.SKOS.Mg | 0 | Magnesium | |
| **1116** | DoorRearRight.Structure.SKOS.Zn | 9.78E-05 | Zinc | |
| **1117** | DoorRearRight.Structure.SKOS.Pb | 0.000197 | Lead | |
| **1118** | DoorRearRight.Structure.SKOS.skos | 0.040937 | SKOS | |
| **1119** | DoorRearRight.Structure.SKOS.skop | 0.175127 | SKOP | |
| **1120** | DoorRearLeft.Structure.SKOS.Al | 0.330276 | Aluminum | |
| **1121** | DoorRearLeft.Structure.SKOS.Cu | 0.58234 | Copper | |
| **1122** | DoorRearLeft.Structure.SKOS.Fe | 1.781026 | Ferrous | |
| **1123** | DoorRearLeft.Structure.SKOS.Mg | 0 | Magnesium | |
| **1124** | DoorRearLeft.Structure.SKOS.Zn | 9.78E-05 | Zinc | |
| **1125** | DoorRearLeft.Structure.SKOS.Pb | 0.000197 | Lead | |
| **1126** | DoorRearLeft.Structure.SKOS.skos | 0.040937 | SKOS | |
| **1127** | DoorRearLeft.Structure.SKOS.skop | 0.175127 | SKOP | |
| **1128** | CruiseServo.SKOS.Al | 0.097607 | Aluminum | |
| **1129** | CruiseServo.SKOS.Cu | 0.172101 | Copper | |
| **1130** | CruiseServo.SKOS.Fe | 0.526351 | Ferrous | |

| | | | | |
|---|---|---|---|---|
| **1131** | CruiseServo.SKOS.Mg | 0 | Magnesium | |
| **1132** | CruiseServo.SKOS.Zn | 2.89E-05 | Zinc | |
| **1133** | CruiseServo.SKOS.Pb | 5.82E-05 | Lead | |
| **1134** | CruiseServo.SKOS.skos | 0.012098 | SKOS | |
| **1135** | CruiseServo.SKOS.skop | 0.051756 | SKOP | |
| **1136** | SeatFrontRight.BottomBase.SKOS.Al | 8.33E-06 | Aluminum | |
| **1137** | SeatFrontRight.BottomBase.SKOS.Cu | 0.014819 | Copper | |
| **1138** | SeatFrontRight.BottomBase.SKOS.Fe | 0.005578 | Ferrous | |
| **1139** | SeatFrontRight.BottomBase.SKOS.Mg | 0 | Magnesium | |
| **1140** | SeatFrontRight.BottomBase.SKOS.Zn | 6.66E-05 | Zinc | |
| **1141** | SeatFrontRight.BottomBase.SKOS.Pb | 1.46E-06 | Lead | |
| **1142** | SeatFrontRight.BottomBase.SKOS.skos | 0.007583 | SKOS | |
| **1143** | SeatFrontRight.BottomBase.SKOS.skop | 0.131943 | SKOP | |
| **1144** | SeatFrontLeft.BottomBase.SKOS.Al | 8.33E-06 | Aluminum | |
| **1145** | SeatFrontLeft.BottomBase.SKOS.Cu | 0.014819 | Copper | |
| **1146** | SeatFrontLeft.BottomBase.SKOS.Fe | 0.005578 | Ferrous | |
| **1147** | SeatFrontLeft.BottomBase.SKOS.Mg | 0 | Magnesium | |
| **1148** | SeatFrontLeft.BottomBase.SKOS.Zn | 6.66E-05 | Zinc | |
| **1149** | SeatFrontLeft.BottomBase.SKOS.Pb | 1.46E-06 | Lead | |
| **1150** | SeatFrontLeft.BottomBase.SKOS.skos | 0.007583 | SKOS | |
| **1151** | SeatFrontLeft.BottomBase.SKOS.skop | 0.131943 | SKOP | |
| **1152** | SteeringColumnSupport.Electrical.Al | 1.46E-05 | Aluminum | |
| **1153** | SteeringColumnSupport.Electrical.Cu | 0.025934 | Copper | |
| **1154** | SteeringColumnSupport.Electrical.Fe | 0.009762 | Ferrous | |
| **1155** | SteeringColumnSupport.Electrical.Mg | 0 | Magnesium | |
| **1156** | SteeringColumnSupport.Electrical.Zn | 0.000117 | Zinc | |
| **1157** | SteeringColumnSupport.Electrical.Pb | 2.56E-06 | Lead | |
| **1158** | SteeringColumnSupport.Electrical.skos | 0.01327 | SKOS | |
| **1159** | SteeringColumnSupport.Electrical.skop | 0.230901 | SKOP | |
| **1160** | SteeringColumnTurnSignal.Al | 1.14E-05 | Aluminum | |
| **1161** | SteeringColumnTurnSignal.Cu | 0.020377 | Copper | |
| **1162** | SteeringColumnTurnSignal.Fe | 0.00767 | Ferrous | |
| **1163** | SteeringColumnTurnSignal.Mg | 0 | Magnesium | |
| **1164** | SteeringColumnTurnSignal.Zn | 9.16E-05 | Zinc | |
| **1165** | SteeringColumnTurnSignal.Pb | 2.01E-06 | Lead | |
| **1166** | SteeringColumnTurnSignal.skos | 0.010427 | SKOS | |
| **1167** | SteeringColumnTurnSignal.skop | 0.181422 | SKOP | |
| **1168** | EngineHarness.SKOS.Al | 0.05116 | Aluminum | |
| **1169** | EngineHarness.SKOS.Cu | 1.323587 | Copper | |
| **1170** | EngineHarness.SKOS.Fe | 0.231862 | Ferrous | |
| **1171** | EngineHarness.SKOS.Mg | 0.000367 | Magnesium | |
| **1172** | EngineHarness.SKOS.Zn | 0.009387 | Zinc | |
| **1173** | EngineHarness.SKOS.Pb | 0.000113 | Lead | |

| | | | | |
|---|---|---|---|---|
| **1174** | EngineHarness.SKOS.skos | 0.030151 | SKOS | |
| **1175** | EngineHarness.SKOS.skop | 1.513372 | SKOP | |
| **1176** | HeatBoxAssembly.Motor.SKOS.Al | 0.01816 | Aluminum | |
| **1177** | HeatBoxAssembly.Motor.SKOS.Cu | 0.032019 | Copper | |
| **1178** | HeatBoxAssembly.Motor.SKOS.Fe | 0.097926 | Ferrous | |
| **1179** | HeatBoxAssembly.Motor.SKOS.Mg | 0 | Magnesium | |
| **1180** | HeatBoxAssembly.Motor.SKOS.Zn | 5.38E-06 | Zinc | |
| **1181** | HeatBoxAssembly.Motor.SKOS.Pb | 1.08E-05 | Lead | |
| **1182** | HeatBoxAssembly.Motor.SKOS.SKOS | 0.002251 | SKOS | |
| **1183** | HeatBoxAssembly.Motor.SKOS.SKOP | 0.009629 | SKOP | |
| **1184** | DoorFrontRight.Structure.Base.SKOS.Al | 0.430153 | Aluminum | |
| **1185** | DoorFrontRight.Structure.Base.SKOS.Cu | 0.758443 | Copper | |
| **1186** | DoorFrontRight.Structure.Base.SKOS.Fe | 2.319618 | Ferrous | |
| **1187** | DoorFrontRight.Structure.Base.SKOS.Mg | 0 | Magnesium | |
| **1188** | DoorFrontRight.Structure.Base.SKOS.Zn | 0.000127 | Zinc | |
| **1189** | DoorFrontRight.Structure.Base.SKOS.Pb | 0.000256 | Lead | |
| **1190** | DoorFrontRight.Structure.Base.SKOS.skos | 0.053316 | SKOS | |
| **1191** | DoorFrontRight.Structure.Base.SKOS.skop | 0.228086 | SKOP | |
| **1192** | DoorFrontLeft.Structure.Base.SKOS.Al | 0.430153 | Aluminum | |
| **1193** | DoorFrontLeft.Structure.Base.SKOS.Cu | 0.758443 | Copper | |
| **1194** | DoorFrontLeft.Structure.Base.SKOS.Fe | 2.319618 | Ferrous | |
| **1195** | DoorFrontLeft.Structure.Base.SKOS.Mg | 0 | Magnesium | |
| **1196** | DoorFrontLeft.Structure.Base.SKOS.Zn | 0.000127 | Zinc | |
| **1197** | DoorFrontLeft.Structure.Base.SKOS.Pb | 0.000256 | Lead | |
| **1198** | DoorFrontLeft.Structure.Base.SKOS.skos | 0.053316 | SKOS | |
| **1199** | DoorFrontLeft.Structure.Base.SKOS.skop | 0.228086 | SKOP | |
| **1200** | RearViewMirror.PP | 0.15 | Glass | |
| **1201** | RearViewMirror.Glass | 0.075 | PP | |
| **1202** | ParcelTray.Steel | 0.79 | Ferrous | |
| **1203** | ParcelTray.skop | 0.395 | SKOP | |
| **1204** | SeatbeltRearRightLower.Buckle.Steel | 0.04 | Ferrous | |
| **1205** | SeatbeltRearRightLower.Buckle.PP | 0.02 | PP | |
| **1206** | SeatbeltRearLeftLower.Buckles.Steel | 0.07 | Ferrous | |
| **1207** | SeatbeltRearLeftLower.Buckles.PP | 0.035 | PP | |

*Table A- 1 ELV database, data about parts' material and weight and fasteners (types and quantities), adapted from [22], [27]*

| Joint Name | Quantity | Classification | Unit Weight(kg) | Material | Total Weight (kg) | Density (kg/m3) | Volume(m3) |
|---|---|---|---|---|---|---|---|
| wing nuts | 6 | Bolt_small | 0.010 | Ferrous | 0.060 | 7850 | 1.2739E-06 |
| VacLine | 1 | VacTee_medium | 0.010 | Ferrous | 0.010 | 7850 | 1.2739E-06 |
| Vac | 1 | VacTee_medium | 0.010 | Ferrous | 0.010 | 7850 | 1.2739E-06 |
| Snaps | 4 | Plastic_small | 0.002 | SKOP | 0.008 | 1028 | 1.9455E-06 |
| Rivets | 55 | Rivet_small | 0.001 | Ferrous | 0.055 | 7850 | 1.2739E-07 |
| QDC | 5 | Qdisconnect_medium | 0.204 | Ferrous | 1.021 | 7850 | 2.6003E-05 |
| Pushin | 47 | Plastic_small | 0.002 | SKOP | 0.094 | 1028 | 1.9455E-06 |
| LongScrew | 1 | Screw_large | 0.111 | Ferrous | 0.111 | 7850 | 1.4187E-05 |
| lognuts | 10 | lugnut_large | 0.142 | Ferrous | 1.420 | 7850 | 1.8089E-05 |
| EC | 53 | CopperWire | 0.215 | Copper | 11.371 | 8940 | 2.3998E-05 |
| Clips | 29 | Clip_small | 0.002 | Ferrous | 0.058 | 7850 | 2.5478E-07 |
| Clamp | 1 | Screw_large | 0.111 | Ferrous | 0.111 | 7850 | 1.4187E-05 |
| cable | 1 | CopperWire | 0.215 | Copper | 0.215 | 8940 | 2.3998E-05 |
| awc | 1 | CopperWire | 0.215 | Copper | 0.215 | 8940 | 2.3998E-05 |
| 7/16th | 2 | Bolt_large | 0.056 | Ferrous | 0.112 | 7850 | 7.1338E-06 |
| 500T | 4 | Bolt_large | 0.056 | Ferrous | 0.224 | 7850 | 7.1338E-06 |
| 5/16th | 28 | Bolt_medium | 0.023 | Ferrous | 0.644 | 7850 | 2.9299E-06 |
| 3/16th | 2 | Bolt_small | 0.010 | Ferrous | 0.020 | 7850 | 1.2739E-06 |
| 2way screws | 6 | Screw_small | 0.006 | Ferrous | 0.039 | 7850 | 8.2484E-07 |
| 2T | 5 | Bolt_small | 0.010 | Ferrous | 0.050 | 7850 | 1.2739E-06 |
| 27T | 4 | Bolt_medium | 0.023 | Ferrous | 0.092 | 7850 | 2.9299E-06 |
| 20T | 27 | Bolt_medium | 0.023 | Ferrous | 0.621 | 7850 | 2.9299E-06 |
| 15T | 2 | Bolt_small | 0.010 | Ferrous | 0.020 | 7850 | 1.2739E-06 |
| Pi | 42 | Screw_medium | 0.037 | Ferrous | 1.554 | 7850 | 4.7134E-06 |
| Ph | 96 | Screw_small | 0.006 | Ferrous | 0.622 | 7850 | 8.2484E-07 |
| 9mm | 4 | Screw_medium | 0.037 | Ferrous | 0.148 | 7850 | 4.7134E-06 |
| 8mm | 82 | Screw_medium | 0.037 | Ferrous | 3.034 | 7850 | 4.7134E-06 |
| 7mm | 5 | Screw_small | 0.006 | Ferrous | 0.032 | 7850 | 8.2484E-07 |
| 5mm | 6 | Screw_small | 0.006 | Ferrous | 0.039 | 7850 | 8.2484E-07 |
| 18mm | 9 | Screw_large | 0.111 | Ferrous | 1.002 | 7850 | 1.4187E-05 |
| 15mm | 12 | Screw_large | 0.111 | Ferrous | 1.336 | 7850 | 1.4187E-05 |
| 14mm | 2 | Screw_large | 0.111 | Ferrous | 0.223 | 7850 | 1.4187E-05 |
| 13mm | 37 | Screw_large | 0.111 | Ferrous | 4.121 | 7850 | 1.4187E-05 |
| 12mm | 2 | Screw_medium | 0.037 | Ferrous | 0.074 | 7850 | 4.7134E-06 |
| 11mm | 33 | Screw_medium | 0.037 | Ferrous | 1.221 | 7850 | 4.7134E-06 |
| 10mm | 57 | Screw_medium | 0.037 | Ferrous | 2.109 | 7850 | 4.7134E-06 |
| 40 | 2 | Screw_large | 0.111 | Ferrous | 0.223 | 7850 | 1.4187E-05 |
| 18 | 1 | Screw_medium | 0.037 | Ferrous | 0.037 | 7850 | 4.7134E-06 |
| 13 | 11 | Screw_medium | 0.037 | Ferrous | 0.407 | 7850 | 4.7134E-06 |
| 10 | 3 | Screw_medium | 0.037 | Ferrous | 0.111 | 7850 | 4.7134E-06 |
| 5.5 | 4 | Screw_small | 0.006 | Ferrous | 0.026 | 7850 | 8.2484E-07 |

*Table A-2 Joint data, adapted from[22] and from collected data from an auto-part shop*

| Material | Magnet-Relative per (Km/150) | EddyCurrent-Con/den e+3 | DensitySeparation-kg/m^3 | AirSeparation-kg/m^3 |
|---|---|---|---|---|
| Aluminum | 0.006667 | 13.723 | 2698.9 | 2698.9 |
| Magnesium | 0.006667 | 12.494 | 1740 | 1740 |
| Copper | 0.006667 | 6.565 | 8960 | 8960 |
| Zinc | 0.006667 | 2.304 | 7000 | 7000 |
| Ferrous | 1 | 1.428 | 7870 | 7870 |
| Lead | 0.006667 | 0.424 | 11340 | 11340 |
| Glass | 0.006667 | 0 | 2600 | 2600 |
| PC | 0.006667 | 0 | 1200 | 1200 |
| ABS | 0.006667 | 0 | 1045 | 1045 |
| PC-ABS | 0.006667 | 0 | 1122.5 | 1122.5 |
| PP | 0.006667 | 0 | 937 | 937 |
| Carpet | 0.006667 | 0 | 1314 | 1314 |
| Xenoy | 0.006667 | 0 | 1230 | 1230 |
| TPO | 0.006667 | 0 | 1250 | 1250 |
| PE | 0.006667 | 0 | 1161.75 | 1161.75 |
| PUR | 0.006667 | 0 | 453.5 | 453.5 |
| Elastomer | 0.006667 | 0 | 1870 | 1870 |
| PET | 0.006667 | 0 | 1300 | 1300 |
| SKOP | 0.006667 | 0 | 1171.25 | 1171.25 |
| SKOS | 0.172222 | 6.156333333 | 6601.483 | 6601.483 |

*Table A-3 Material Properties used to calculate separation efficiencies using the partition curves of separation units, adapted from [107]*

| | | Magnet | | Air Separation | | Trommel | | Eddy-Current | | HMS (sg:3.5) | | HMS (sg:2.3) | |
|---|---|---|---|---|---|---|---|---|---|---|---|---|---|
| MATERIAL | Size | Efficiency | Material Property Value | Efficiency | Material Property Value | Efficiency | Material Property Value | Efficiency | Material Property Value | Efficiency | Material Property Value | Efficiency | Material Property Value |
| ABS | Large | 4.2E-02 | 6.7E-03 | 9.7E-01 | 1.0E-03 | 1.0E+00 | 1.0E+02 | 3.6E-02 | 0.0E+00 | 1.0E+00 | 1.0E+03 | 8.8E-04 | 1.0E+03 |
| ABS | Medium | 4.2E-02 | 6.7E-03 | 7.5E-01 | 3.1E-04 | 9.6E-01 | 3.0E+01 | 3.6E-02 | 0.0E+00 | 1.0E+00 | 1.0E+03 | 8.8E-04 | 1.0E+03 |
| ABS | Small | 4.2E-02 | 6.7E-03 | 5.5E-01 | 5.2E-05 | 1.0E-01 | 5.0E+00 | 3.6E-02 | 0.0E+00 | 1.0E+00 | 1.0E+03 | 8.8E-04 | 1.0E+03 |
| ABS-Ferrous | Large | 1.5E-01 | 2.3E-01 | 1.0E+00 | 7.9E-03 | 1.0E+00 | 1.0E+02 | 5.0E-02 | 3.3E-01 | 1.7E-01 | 4.2E+03 | 1.0E+00 | 4.2E+03 |
| ABS-Ferrous | Medium | 1.5E-01 | 2.3E-01 | 1.0E+00 | 2.4E-03 | 9.6E-01 | 3.0E+01 | 5.0E-02 | 3.3E-01 | 1.7E-01 | 4.2E+03 | 1.0E+00 | 4.2E+03 |
| ABS-Ferrous | Small | 1.5E-01 | 2.3E-01 | 8.0E-01 | 3.9E-04 | 1.0E-01 | 5.0E+00 | 5.0E-02 | 3.3E-01 | 1.7E-01 | 4.2E+03 | 1.0E+00 | 4.2E+03 |
| ABS-SKOP | Large | 4.2E-02 | 6.7E-03 | 9.8E-01 | 1.2E-03 | 1.0E+00 | 1.0E+02 | 3.6E-02 | 0.0E+00 | 1.0E+00 | 1.1E+03 | 9.5E-04 | 1.1E+03 |
| ABS-SKOP | Medium | 4.2E-02 | 6.7E-03 | 7.7E-01 | 3.5E-04 | 9.6E-01 | 3.0E+01 | 3.6E-02 | 0.0E+00 | 1.0E+00 | 1.1E+03 | 9.5E-04 | 1.1E+03 |

| | | | | | | | | | | | | | |
|---|---|---|---|---|---|---|---|---|---|---|---|---|---|
| ABS-SKOP | Small | 4.2E-02 | 6.7E-03 | 5.5E-01 | 5.9E-05 | 1.0E-01 | 5.0E+00 | 3.6E-02 | 0.0E+00 | 1.0E+00 | 1.1E+03 | 9.5E-04 | 1.1E+03 |
| Aluminum | Large | 4.2E-02 | 6.7E-03 | 1.0E+00 | 2.7E-03 | 1.0E+00 | 1.0E+02 | 1.0E+00 | 1.4E+01 | 8.6E-01 | 2.7E+03 | 8.9E-01 | 2.7E+03 |
| Aluminum | Medium | 4.2E-02 | 6.7E-03 | 9.4E-01 | 8.1E-04 | 9.6E-01 | 3.0E+01 | 1.0E+00 | 1.4E+01 | 8.6E-01 | 2.7E+03 | 8.9E-01 | 2.7E+03 |
| Aluminum | Small | 4.2E-02 | 6.7E-03 | 6.2E-01 | 1.4E-04 | 1.0E-01 | 5.0E+00 | 1.0E+00 | 1.4E+01 | 8.6E-01 | 2.7E+03 | 8.9E-01 | 2.7E+03 |
| Aluminum-Ferrous | Large | 5.2E-01 | 5.3E-01 | 1.0E+00 | 7.9E-03 | 1.0E+00 | 1.0E+02 | 9.9E-01 | 7.2E+00 | 2.3E-01 | 4.1E+03 | 1.0E+00 | 4.1E+03 |
| Aluminum-Ferrous | Medium | 5.2E-01 | 5.3E-01 | 1.0E+00 | 2.4E-03 | 9.6E-01 | 3.0E+01 | 9.9E-01 | 7.2E+00 | 2.3E-01 | 4.1E+03 | 1.0E+00 | 4.1E+03 |
| Aluminum-Ferrous | Small | 5.2E-01 | 5.3E-01 | 8.0E-01 | 3.9E-04 | 1.0E-01 | 5.0E+00 | 9.9E-01 | 7.2E+00 | 2.3E-01 | 4.1E+03 | 1.0E+00 | 4.1E+03 |
| Carpet | Large | 4.2E-02 | 6.7E-03 | 9.9E-01 | 1.3E-03 | 1.0E+00 | 1.0E+02 | 3.6E-02 | 0.0E+00 | 9.9E-01 | 1.3E+03 | 3.9E-03 | 1.3E+03 |
| Carpet | Medium | 4.2E-02 | 6.7E-03 | 8.0E-01 | 3.9E-04 | 9.6E-01 | 3.0E+01 | 3.6E-02 | 0.0E+00 | 9.9E-01 | 1.3E+03 | 3.9E-03 | 1.3E+03 |
| Carpet | Small | 4.2E-02 | 6.7E-03 | 5.6E-01 | 6.6E-05 | 1.0E-01 | 5.0E+00 | 3.6E-02 | 0.0E+00 | 9.9E-01 | 1.3E+03 | 3.9E-03 | 1.3E+03 |
| Carpet-Ferrous | Large | 2.0E-01 | 2.9E-01 | 1.0E+00 | 7.9E-03 | 1.0E+00 | 1.0E+02 | 5.5E-02 | 4.1E-01 | 2.3E-01 | 4.1E+03 | 1.0E+00 | 4.1E+03 |
| Carpet-Ferrous | Medium | 2.0E-01 | 2.9E-01 | 1.0E+00 | 2.4E-03 | 9.6E-01 | 3.0E+01 | 5.5E-02 | 4.1E-01 | 2.3E-01 | 4.1E+03 | 1.0E+00 | 4.1E+03 |
| Carpet-Ferrous | Small | 2.0E-01 | 2.9E-01 | 8.0E-01 | 3.9E-04 | 1.0E-01 | 5.0E+00 | 5.5E-02 | 4.1E-01 | 2.3E-01 | 4.1E+03 | 1.0E+00 | 4.1E+03 |
| Carpet-SKOP | Large | 4.2E-02 | 6.7E-03 | 9.8E-01 | 1.2E-03 | 1.0E+00 | 1.0E+02 | 3.6E-02 | 0.0E+00 | 9.9E-01 | 1.3E+03 | 3.6E-03 | 1.3E+03 |
| Carpet-SKOP | Medium | 4.2E-02 | 6.7E-03 | 7.7E-01 | 3.5E-04 | 9.6E-01 | 3.0E+01 | 3.6E-02 | 0.0E+00 | 9.9E-01 | 1.3E+03 | 3.6E-03 | 1.3E+03 |
| Carpet-SKOP | Small | 4.2E-02 | 6.7E-03 | 5.5E-01 | 5.9E-05 | 1.0E-01 | 5.0E+00 | 3.6E-02 | 0.0E+00 | 9.9E-01 | 1.3E+03 | 3.6E-03 | 1.3E+03 |
| Copper | Large | 4.2E-02 | 6.7E-03 | 1.0E+00 | 9.0E-03 | 1.0E+00 | 1.0E+02 | 9.8E-01 | 6.6E+00 | 6.5E-06 | 9.0E+03 | 1.0E+00 | 9.0E+03 |
| Copper | Medium | 4.2E-02 | 6.7E-03 | 1.0E+00 | 2.7E-03 | 9.6E-01 | 3.0E+01 | 9.8E-01 | 6.6E+00 | 6.5E-06 | 9.0E+03 | 1.0E+00 | 9.0E+03 |
| Copper | Small | 4.2E-02 | 6.7E-03 | 8.3E-01 | 4.5E-04 | 1.0E-01 | 5.0E+00 | 9.8E-01 | 6.6E+00 | 6.5E-06 | 9.0E+03 | 1.0E+00 | 9.0E+03 |
| *Copper-Ferrous* | *Large* | *3.4E-01* | *4.1E-01* | 1.0E+00 | 7.9E-03 | 1.0E+00 | 1.0E+02 | 8.3E-01 | 4.5E+00 | 8.2E-06 | 8.9E+03 | 1.0E+00 | 8.9E+03 |
| *Copper-Ferrous* | *Medium* | *3.4E-01* | *4.1E-01* | 1.0E+00 | 2.4E-03 | 9.6E-01 | 3.0E+01 | 8.3E-01 | 4.5E+00 | 8.2E-06 | 8.9E+03 | 1.0E+00 | 8.9E+03 |
| *Copper-Ferrous* | *Small* | *3.4E-01* | *4.1E-01* | 8.0E-01 | 3.9E-04 | 1.0E-01 | 5.0E+00 | 8.3E-01 | 4.5E+00 | 8.2E-06 | 8.9E+03 | 1.0E+00 | 8.9E+03 |
| Elastomer | Large | 4.2E-02 | 6.7E-03 | 1.0E+00 | 1.9E-03 | 1.0E+00 | 1.0E+02 | 3.6E-02 | 0.0E+00 | 9.7E-01 | 1.9E+03 | 7.6E-02 | 1.9E+03 |
| Elastomer | Medium | 4.2E-02 | 6.7E-03 | 8.7E-01 | 5.6E-04 | 9.6E-01 | 3.0E+01 | 3.6E-02 | 0.0E+00 | 9.7E-01 | 1.9E+03 | 7.6E-02 | 1.9E+03 |
| Elastomer | Small | 4.2E-02 | 6.7E-03 | 5.8E-01 | 9.4E-05 | 1.0E-01 | 5.0E+00 | 3.6E-02 | 0.0E+00 | 9.7E-01 | 1.9E+03 | 7.6E-02 | 1.9E+03 |
| Elastomer-Ferrous | Large | 9.3E-01 | 9.5E-01 | 1.0E+00 | 7.9E-03 | 1.0E+00 | 1.0E+02 | 1.4E-01 | 1.4E+00 | 4.8E-03 | 5.9E+03 | 1.0E+00 | 5.9E+03 |
| Elastomer-Ferrous | Medium | 9.3E-01 | 9.5E-01 | 1.0E+00 | 2.4E-03 | 9.6E-01 | 3.0E+01 | 1.4E-01 | 1.4E+00 | 4.8E-03 | 5.9E+03 | 1.0E+00 | 5.9E+03 |
| Elastomer-Ferrous | Small | 9.3E-01 | 9.5E-01 | 8.0E-01 | 3.9E-04 | 1.0E-01 | 5.0E+00 | 1.4E-01 | 1.4E+00 | 4.8E-03 | 5.9E+03 | 1.0E+00 | 5.9E+03 |
| Elastomer-SKOP | Large | 4.2E-02 | 6.7E-03 | 9.8E-01 | 1.2E-03 | 1.0E+00 | 1.0E+02 | 3.6E-02 | 0.0E+00 | 9.8E-01 | 1.7E+03 | 3.4E-02 | 1.7E+03 |
| Elastomer-SKOP | Medium | 4.2E-02 | 6.7E-03 | 7.7E-01 | 3.5E-04 | 9.6E-01 | 3.0E+01 | 3.6E-02 | 0.0E+00 | 9.8E-01 | 1.7E+03 | 3.4E-02 | 1.7E+03 |
| Elastomer-SKOP | Small | 4.2E-02 | 6.7E-03 | 5.5E-01 | 5.9E-05 | 1.0E-01 | 5.0E+00 | 3.6E-02 | 0.0E+00 | 9.8E-01 | 1.7E+03 | 3.4E-02 | 1.7E+03 |
| Ferrous | Large | 9.5E-01 | 1.0E+00 | 1.0E+00 | 7.9E-03 | 1.0E+00 | 1.0E+02 | 1.5E-01 | 1.4E+00 | 7.1E-05 | 7.9E+03 | 1.0E+00 | 7.9E+03 |
| Ferrous | Medium | 9.5E-01 | 1.0E+00 | 1.0E+00 | 2.4E-03 | 9.6E-01 | 3.0E+01 | 1.5E-01 | 1.4E+00 | 7.1E-05 | 7.9E+03 | 1.0E+00 | 7.9E+03 |
| Ferrous | Small | 9.5E-01 | 1.0E+00 | 8.0E-01 | 3.9E-04 | 1.0E-01 | 5.0E+00 | 1.5E-01 | 1.4E+00 | 7.1E-05 | 7.9E+03 | 1.0E+00 | 7.9E+03 |
| *Ferrous-Copper* | *Large* | *2.2E-01* | *3.1E-01* | 1.0E+00 | 9.0E-03 | 1.0E+00 | 1.0E+02 | 9.0E-01 | 5.0E+00 | 5.3E-05 | 8.0E+03 | 1.0E+00 | 8.0E+03 |
| *Ferrous-Copper* | *Medium* | *2.2E-01* | *3.1E-01* | 1.0E+00 | 2.7E-03 | 9.6E-01 | 3.0E+01 | 9.0E-01 | 5.0E+00 | 5.3E-05 | 8.0E+03 | 1.0E+00 | 8.0E+03 |
| *Ferrous-Copper* | *Small* | *2.2E-01* | *3.1E-01* | 8.3E-01 | 4.5E-04 | 1.0E-01 | 5.0E+00 | 9.0E-01 | 5.0E+00 | 5.3E-05 | 8.0E+03 | 1.0E+00 | 8.0E+03 |
| Ferrous-SKOP | Large | 9.4E-01 | 9.8E-01 | 9.8E-01 | 1.2E-03 | 1.0E+00 | 1.0E+02 | 1.5E-01 | 1.4E+00 | 9.0E-05 | 7.8E+03 | 1.0E+00 | 7.8E+03 |
| Ferrous-SKOP | Medium | 9.4E-01 | 9.8E-01 | 7.7E-01 | 3.5E-04 | 9.6E-01 | 3.0E+01 | 1.5E-01 | 1.4E+00 | 9.0E-05 | 7.8E+03 | 1.0E+00 | 7.8E+03 |
| Ferrous-SKOP | Small | 9.4E-01 | 9.8E-01 | 5.5E-01 | 5.9E-05 | 1.0E-01 | 5.0E+00 | 1.5E-01 | 1.4E+00 | 9.0E-05 | 7.8E+03 | 1.0E+00 | 7.8E+03 |

| | | | | | | | | | | | | | |
|---|---|---|---|---|---|---|---|---|---|---|---|---|---|
| **Glass** | **Large** | 4.2E-02 | 6.7E-03 | 1.0E+00 | 2.6E-03 | 1.0E+00 | 1.0E+02 | 3.6E-02 | 0.0E+00 | 8.8E-01 | 2.6E+03 | 8.2E-01 | 2.6E+03 |
| **Glass** | **Medium** | 4.2E-02 | 6.7E-03 | 9.4E-01 | 7.8E-04 | 9.6E-01 | 3.0E+01 | 3.6E-02 | 0.0E+00 | 8.8E-01 | 2.6E+03 | 8.2E-01 | 2.6E+03 |
| **Glass** | **Small** | 4.2E-02 | 6.7E-03 | 6.1E-01 | 1.3E-04 | 1.0E-01 | 5.0E+00 | 3.6E-02 | 0.0E+00 | 8.8E-01 | 2.6E+03 | 8.2E-01 | 2.6E+03 |
| **Lead** | **Large** | 4.2E-02 | 6.7E-03 | 1.0E+00 | 1.1E-02 | 1.0E+00 | 1.0E+02 | 5.6E-02 | 4.2E-01 | 3.5E-08 | 1.1E+04 | 1.0E+00 | 1.1E+04 |
| **Lead** | **Medium** | 4.2E-02 | 6.7E-03 | 1.0E+00 | 3.4E-03 | 9.6E-01 | 3.0E+01 | 5.6E-02 | 4.2E-01 | 3.5E-08 | 1.1E+04 | 1.0E+00 | 1.1E+04 |
| **Lead** | **Small** | 4.2E-02 | 6.7E-03 | 8.8E-01 | 5.7E-04 | 1.0E-01 | 5.0E+00 | 5.6E-02 | 4.2E-01 | 3.5E-08 | 1.1E+04 | 1.0E+00 | 1.1E+04 |
| **Magnesium** | **Large** | 4.2E-02 | 6.7E-03 | 1.0E+00 | 1.7E-03 | 1.0E+00 | 1.0E+02 | 1.0E+00 | 1.2E+01 | 9.8E-01 | 1.7E+03 | 3.9E-02 | 1.7E+03 |
| **Magnesium** | **Medium** | 4.2E-02 | 6.7E-03 | 8.6E-01 | 5.2E-04 | 9.6E-01 | 3.0E+01 | 1.0E+00 | 1.2E+01 | 9.8E-01 | 1.7E+03 | 3.9E-02 | 1.7E+03 |
| **Magnesium** | **Small** | 4.2E-02 | 6.7E-03 | 5.8E-01 | 8.7E-05 | 1.0E-01 | 5.0E+00 | 1.0E+00 | 1.2E+01 | 9.8E-01 | 1.7E+03 | 3.9E-02 | 1.7E+03 |
| **PC** | **Large** | 4.2E-02 | 6.7E-03 | 9.8E-01 | 1.2E-03 | 1.0E+00 | 1.0E+02 | 3.6E-02 | 0.0E+00 | 9.9E-01 | 1.2E+03 | 2.1E-03 | 1.2E+03 |
| **PC** | **Medium** | 4.2E-02 | 6.7E-03 | 7.8E-01 | 3.6E-04 | 9.6E-01 | 3.0E+01 | 3.6E-02 | 0.0E+00 | 9.9E-01 | 1.2E+03 | 2.1E-03 | 1.2E+03 |
| **PC** | **Small** | 4.2E-02 | 6.7E-03 | 5.6E-01 | 6.0E-05 | 1.0E-01 | 5.0E+00 | 3.6E-02 | 0.0E+00 | 9.9E-01 | 1.2E+03 | 2.1E-03 | 1.2E+03 |
| **PC-ABS** | **Large** | 4.2E-02 | 6.7E-03 | 9.8E-01 | 1.1E-03 | 1.0E+00 | 1.0E+02 | 3.6E-02 | 0.0E+00 | 9.9E-01 | 1.1E+03 | 1.3E-03 | 1.1E+03 |
| **PC-ABS** | **Medium** | 4.2E-02 | 6.7E-03 | 7.6E-01 | 3.4E-04 | 9.6E-01 | 3.0E+01 | 3.6E-02 | 0.0E+00 | 9.9E-01 | 1.1E+03 | 1.3E-03 | 1.1E+03 |
| **PC-ABS** | **Small** | 4.2E-02 | 6.7E-03 | 5.5E-01 | 5.6E-05 | 1.0E-01 | 5.0E+00 | 3.6E-02 | 0.0E+00 | 9.9E-01 | 1.1E+03 | 1.3E-03 | 1.1E+03 |
| **PC-Ferrous** | **Large** | 7.8E-01 | 7.3E-01 | 1.0E+00 | 7.9E-03 | 1.0E+00 | 1.0E+02 | 1.0E-01 | 1.0E+00 | 1.7E-01 | 4.2E+03 | 1.0E+00 | 4.2E+03 |
| **PC-Ferrous** | **Medium** | 7.8E-01 | 7.3E-01 | 1.0E+00 | 2.4E-03 | 9.6E-01 | 3.0E+01 | 1.0E-01 | 1.0E+00 | 1.7E-01 | 4.2E+03 | 1.0E+00 | 4.2E+03 |
| **PC-Ferrous** | **Small** | 7.8E-01 | 7.3E-01 | 8.0E-01 | 3.9E-04 | 1.0E-01 | 5.0E+00 | 1.0E-01 | 1.0E+00 | 1.7E-01 | 4.2E+03 | 1.0E+00 | 4.2E+03 |
| **PE** | **Large** | 4.2E-02 | 6.7E-03 | 9.8E-01 | 1.2E-03 | 1.0E+00 | 1.0E+02 | 3.6E-02 | 0.0E+00 | 9.9E-01 | 1.2E+03 | 1.7E-03 | 1.2E+03 |
| **PE** | **Medium** | 4.2E-02 | 6.7E-03 | 7.7E-01 | 3.5E-04 | 9.6E-01 | 3.0E+01 | 3.6E-02 | 0.0E+00 | 9.9E-01 | 1.2E+03 | 1.7E-03 | 1.2E+03 |
| **PE** | **Small** | 4.2E-02 | 6.7E-03 | 5.5E-01 | 5.8E-05 | 1.0E-01 | 5.0E+00 | 3.6E-02 | 0.0E+00 | 9.9E-01 | 1.2E+03 | 1.7E-03 | 1.2E+03 |
| **PE-Ferrous** | **Large** | 6.1E-01 | 5.9E-01 | 1.0E+00 | 7.9E-03 | 1.0E+00 | 1.0E+02 | 8.5E-02 | 8.4E-01 | 2.1E-01 | 4.1E+03 | 1.0E+00 | 4.1E+03 |
| **PE-Ferrous** | **Medium** | 6.1E-01 | 5.9E-01 | 1.0E+00 | 2.4E-03 | 9.6E-01 | 3.0E+01 | 8.5E-02 | 8.4E-01 | 2.1E-01 | 4.1E+03 | 1.0E+00 | 4.1E+03 |
| **PE-Ferrous** | **Small** | 6.1E-01 | 5.9E-01 | 8.0E-01 | 3.9E-04 | 1.0E-01 | 5.0E+00 | 8.5E-02 | 8.4E-01 | 2.1E-01 | 4.1E+03 | 1.0E+00 | 4.1E+03 |
| **PET** | **Large** | 4.2E-02 | 6.7E-03 | 9.9E-01 | 1.3E-03 | 1.0E+00 | 1.0E+02 | 3.6E-02 | 0.0E+00 | 9.9E-01 | 1.3E+03 | 3.6E-03 | 1.3E+03 |
| **PET** | **Medium** | 4.2E-02 | 6.7E-03 | 8.0E-01 | 3.9E-04 | 9.6E-01 | 3.0E+01 | 3.6E-02 | 0.0E+00 | 9.9E-01 | 1.3E+03 | 3.6E-03 | 1.3E+03 |
| **PET** | **Small** | 4.2E-02 | 6.7E-03 | 5.6E-01 | 6.5E-05 | 1.0E-01 | 5.0E+00 | 3.6E-02 | 0.0E+00 | 9.9E-01 | 1.3E+03 | 3.6E-03 | 1.3E+03 |
| **PET-Ferrous** | **Large** | 7.5E-01 | 7.0E-01 | 1.0E+00 | 7.9E-03 | 1.0E+00 | 1.0E+02 | 9.9E-02 | 9.9E-01 | 2.3E-01 | 4.1E+03 | 1.0E+00 | 4.1E+03 |
| **PET-Ferrous** | **Medium** | 7.5E-01 | 7.0E-01 | 1.0E+00 | 2.4E-03 | 9.6E-01 | 3.0E+01 | 9.9E-02 | 9.9E-01 | 2.3E-01 | 4.1E+03 | 1.0E+00 | 4.1E+03 |
| **PET-Ferrous** | **Small** | 7.5E-01 | 7.0E-01 | 8.0E-01 | 3.9E-04 | 1.0E-01 | 5.0E+00 | 9.9E-02 | 9.9E-01 | 2.3E-01 | 4.1E+03 | 1.0E+00 | 4.1E+03 |
| **PP** | **Large** | 4.2E-02 | 6.7E-03 | 9.6E-01 | 9.4E-04 | 1.0E+00 | 1.0E+02 | 3.6E-02 | 0.0E+00 | 1.0E+00 | 9.4E+02 | 4.9E-04 | 9.4E+02 |
| **PP** | **Medium** | 4.2E-02 | 6.7E-03 | 7.3E-01 | 2.8E-04 | 9.6E-01 | 3.0E+01 | 3.6E-02 | 0.0E+00 | 1.0E+00 | 9.4E+02 | 4.9E-04 | 9.4E+02 |
| **PP** | **Small** | 4.2E-02 | 6.7E-03 | 5.4E-01 | 4.7E-05 | 1.0E-01 | 5.0E+00 | 3.6E-02 | 0.0E+00 | 1.0E+00 | 9.4E+02 | 4.9E-04 | 9.4E+02 |
| **PP-Ferrous** | **Large** | 7.7E-01 | 7.1E-01 | 1.0E+00 | 7.9E-03 | 1.0E+00 | 1.0E+02 | 1.0E-01 | 1.0E+00 | 1.4E-01 | 4.4E+03 | 1.0E+00 | 4.4E+03 |
| **PP-Ferrous** | **Medium** | 7.7E-01 | 7.1E-01 | 1.0E+00 | 2.4E-03 | 9.6E-01 | 3.0E+01 | 1.0E-01 | 1.0E+00 | 1.4E-01 | 4.4E+03 | 1.0E+00 | 4.4E+03 |
| **PP-Ferrous** | **Small** | 7.7E-01 | 7.1E-01 | 8.0E-01 | 3.9E-04 | 1.0E-01 | 5.0E+00 | 1.0E-01 | 1.0E+00 | 1.4E-01 | 4.4E+03 | 1.0E+00 | 4.4E+03 |
| **PP-SKOP** | **Large** | 4.2E-02 | 6.7E-03 | 9.8E-01 | 1.2E-03 | 1.0E+00 | 1.0E+02 | 3.6E-02 | 0.0E+00 | 1.0E+00 | 9.6E+02 | 5.6E-04 | 9.6E+02 |
| **PP-SKOP** | **Medium** | 4.2E-02 | 6.7E-03 | 7.7E-01 | 3.5E-04 | 9.6E-01 | 3.0E+01 | 3.6E-02 | 0.0E+00 | 1.0E+00 | 9.6E+02 | 5.6E-04 | 9.6E+02 |
| **PP-SKOP** | **Small** | 4.2E-02 | 6.7E-03 | 5.5E-01 | 5.9E-05 | 1.0E-01 | 5.0E+00 | 3.6E-02 | 0.0E+00 | 1.0E+00 | 9.6E+02 | 5.6E-04 | 9.6E+02 |
| **PUR** | **Large** | 4.2E-02 | 6.7E-03 | 8.3E-01 | 4.5E-04 | 1.0E+00 | 1.0E+02 | 3.6E-02 | 0.0E+00 | 1.0E+00 | 4.5E+02 | 3.4E-05 | 4.5E+02 |

| | | | | | | | | | | | | | |
|---|---|---|---|---|---|---|---|---|---|---|---|---|---|
| **PUR** | **Medium** | 4.2E-02 | 6.7E-03 | 6.2E-01 | 1.4E-04 | 9.6E-01 | 3.0E+01 | 3.6E-02 | 0.0E+00 | 1.0E+00 | 4.5E+02 | 3.4E-05 | 4.5E+02 |
| **PUR** | **Small** | 4.2E-02 | 6.7E-03 | 5.2E-01 | 2.3E-05 | 1.0E-01 | 5.0E+00 | 3.6E-02 | 0.0E+00 | 1.0E+00 | 4.5E+02 | 3.4E-05 | 4.5E+02 |
| **PUR-Ferrous** | **Large** | 9.5E-01 | 9.9E-01 | 1.0E+00 | 7.9E-03 | 1.0E+00 | 1.0E+02 | 1.5E-01 | 1.4E+00 | 1.3E-04 | 7.6E+03 | 1.0E+00 | 7.6E+03 |
| **PUR-Ferrous** | **Medium** | 9.5E-01 | 9.9E-01 | 1.0E+00 | 2.4E-03 | 9.6E-01 | 3.0E+01 | 1.5E-01 | 1.4E+00 | 1.3E-04 | 7.6E+03 | 1.0E+00 | 7.6E+03 |
| **PUR-Ferrous** | **Small** | 9.5E-01 | 9.9E-01 | 8.0E-01 | 3.9E-04 | 1.0E-01 | 5.0E+00 | 1.5E-01 | 1.4E+00 | 1.3E-04 | 7.6E+03 | 1.0E+00 | 7.6E+03 |
| **SKOP** | **Large** | 4.2E-02 | 6.7E-03 | 9.8E-01 | 1.2E-03 | 1.0E+00 | 1.0E+02 | 3.6E-02 | 0.0E+00 | 9.9E-01 | 1.2E+03 | 1.8E-03 | 1.2E+03 |
| **SKOP** | **Medium** | 4.2E-02 | 6.7E-03 | 7.7E-01 | 3.5E-04 | 9.6E-01 | 3.0E+01 | 3.6E-02 | 0.0E+00 | 9.9E-01 | 1.2E+03 | 1.8E-03 | 1.2E+03 |
| **SKOP** | **Small** | 4.2E-02 | 6.7E-03 | 5.5E-01 | 5.9E-05 | 1.0E-01 | 5.0E+00 | 3.6E-02 | 0.0E+00 | 9.9E-01 | 1.2E+03 | 1.8E-03 | 1.2E+03 |
| **SKOP-Copper** | **Large** | 4.2E-02 | 6.7E-03 | 1.0E+00 | 9.0E-03 | 1.0E+00 | 1.0E+02 | 9.7E-01 | 6.2E+00 | 2.3E-02 | 5.2E+03 | 1.0E+00 | 5.2E+03 |
| **SKOP-Copper** | **Medium** | 4.2E-02 | 6.7E-03 | 1.0E+00 | 2.7E-03 | 9.6E-01 | 3.0E+01 | 9.7E-01 | 6.2E+00 | 2.3E-02 | 5.2E+03 | 1.0E+00 | 5.2E+03 |
| **SKOP-Copper** | **Small** | 4.2E-02 | 6.7E-03 | 8.3E-01 | 4.5E-04 | 1.0E-01 | 5.0E+00 | 9.7E-01 | 6.2E+00 | 2.3E-02 | 5.2E+03 | 1.0E+00 | 5.2E+03 |
| **SKOP-Ferrous** | **Large** | 6.6E-01 | 6.3E-01 | 1.0E+00 | 7.9E-03 | 1.0E+00 | 1.0E+02 | 9.0E-02 | 9.0E-01 | 1.2E-01 | 4.4E+03 | 1.0E+00 | 4.4E+03 |
| **SKOP-Ferrous** | **Medium** | 6.6E-01 | 6.3E-01 | 1.0E+00 | 2.4E-03 | 9.6E-01 | 3.0E+01 | 9.0E-02 | 9.0E-01 | 1.2E-01 | 4.4E+03 | 1.0E+00 | 4.4E+03 |
| **SKOP-Ferrous** | **Small** | 6.6E-01 | 6.3E-01 | 8.0E-01 | 3.9E-04 | 1.0E-01 | 5.0E+00 | 9.0E-02 | 9.0E-01 | 1.2E-01 | 4.4E+03 | 1.0E+00 | 4.4E+03 |
| **SKOS** | **Large** | 5.7E-02 | 5.9E-02 | 1.0E+00 | 2.5E-03 | 1.0E+00 | 1.0E+02 | 3.9E-01 | 2.6E+00 | 1.2E-03 | 6.6E+03 | 1.0E+00 | 6.6E+03 |
| **SKOS** | **Medium** | 5.7E-02 | 5.9E-02 | 9.3E-01 | 7.5E-04 | 9.6E-01 | 3.0E+01 | 3.9E-01 | 2.6E+00 | 1.2E-03 | 6.6E+03 | 1.0E+00 | 6.6E+03 |
| **SKOS** | **Small** | 5.7E-02 | 5.9E-02 | 6.1E-01 | 1.3E-04 | 1.0E-01 | 5.0E+00 | 3.9E-01 | 2.6E+00 | 1.2E-03 | 6.6E+03 | 1.0E+00 | 6.6E+03 |
| **SKOS-Ferrous** | **Large** | 4.2E-01 | 4.7E-01 | 1.0E+00 | 7.9E-03 | 1.0E+00 | 1.0E+02 | 2.7E-01 | 2.1E+00 | 5.2E-04 | 7.0E+03 | 1.0E+00 | 7.0E+03 |
| **SKOS-Ferrous** | **Medium** | 4.2E-01 | 4.7E-01 | 1.0E+00 | 2.4E-03 | 9.6E-01 | 3.0E+01 | 2.7E-01 | 2.1E+00 | 5.2E-04 | 7.0E+03 | 1.0E+00 | 7.0E+03 |
| **SKOS-Ferrous** | **Small** | 4.2E-01 | 4.7E-01 | 8.0E-01 | 3.9E-04 | 1.0E-01 | 5.0E+00 | 2.7E-01 | 2.1E+00 | 5.2E-04 | 7.0E+03 | 1.0E+00 | 7.0E+03 |
| **TPO** | **Large** | 4.2E-02 | 6.7E-03 | 9.9E-01 | 1.3E-03 | 1.0E+00 | 1.0E+02 | 3.6E-02 | 0.0E+00 | 9.9E-01 | 1.3E+03 | 2.7E-03 | 1.3E+03 |
| **TPO** | **Medium** | 4.2E-02 | 6.7E-03 | 7.9E-01 | 3.8E-04 | 9.6E-01 | 3.0E+01 | 3.6E-02 | 0.0E+00 | 9.9E-01 | 1.3E+03 | 2.7E-03 | 1.3E+03 |
| **TPO** | **Small** | 4.2E-02 | 6.7E-03 | 5.6E-01 | 6.3E-05 | 1.0E-01 | 5.0E+00 | 3.6E-02 | 0.0E+00 | 9.9E-01 | 1.3E+03 | 2.7E-03 | 1.3E+03 |
| **TPO-Ferrous** | **Large** | 4.6E-01 | 4.9E-01 | 1.0E+00 | 7.9E-03 | 1.0E+00 | 1.0E+02 | 7.4E-02 | 7.0E-01 | 1.0E-01 | 4.5E+03 | 1.0E+00 | 4.5E+03 |
| **TPO-Ferrous** | **Medium** | 4.6E-01 | 4.9E-01 | 1.0E+00 | 2.4E-03 | 9.6E-01 | 3.0E+01 | 7.4E-02 | 7.0E-01 | 1.0E-01 | 4.5E+03 | 1.0E+00 | 4.5E+03 |
| **TPO-Ferrous** | **Small** | 4.6E-01 | 4.9E-01 | 8.0E-01 | 3.9E-04 | 1.0E-01 | 5.0E+00 | 7.4E-02 | 7.0E-01 | 1.0E-01 | 4.5E+03 | 1.0E+00 | 4.5E+03 |
| **Xenoy** | **Large** | 4.2E-02 | 6.7E-03 | 9.9E-01 | 1.2E-03 | 1.0E+00 | 1.0E+02 | 3.6E-02 | 0.0E+00 | 9.9E-01 | 1.2E+03 | 2.4E-03 | 1.2E+03 |
| **Xenoy** | **Medium** | 4.2E-02 | 6.7E-03 | 7.8E-01 | 3.7E-04 | 9.6E-01 | 3.0E+01 | 3.6E-02 | 0.0E+00 | 9.9E-01 | 1.2E+03 | 2.4E-03 | 1.2E+03 |
| **Xenoy** | **Small** | 4.2E-02 | 6.7E-03 | 5.6E-01 | 6.2E-05 | 1.0E-01 | 5.0E+00 | 3.6E-02 | 0.0E+00 | 9.9E-01 | 1.2E+03 | 2.4E-03 | 1.2E+03 |
| **Xenoy-Ferrous** | **Large** | 7.8E-01 | 7.2E-01 | 1.0E+00 | 7.9E-03 | 1.0E+00 | 1.0E+02 | 1.0E-01 | 1.0E+00 | 1.7E-01 | 4.2E+03 | 1.0E+00 | 4.2E+03 |
| **Xenoy-Ferrous** | **Medium** | 7.8E-01 | 7.2E-01 | 1.0E+00 | 2.4E-03 | 9.6E-01 | 3.0E+01 | 1.0E-01 | 1.0E+00 | 1.7E-01 | 4.2E+03 | 1.0E+00 | 4.2E+03 |
| **Xenoy-Ferrous** | **Small** | 7.8E-01 | 7.2E-01 | 8.0E-01 | 3.9E-04 | 1.0E-01 | 5.0E+00 | 1.0E-01 | 1.0E+00 | 1.7E-01 | 4.2E+03 | 1.0E+00 | 4.2E+03 |
| **Zinc** | **Large** | 4.2E-02 | 6.7E-03 | 1.0E+00 | 7.0E-03 | 1.0E+00 | 1.0E+02 | 3.2E-01 | 2.3E+00 | 4.8E-04 | 7.0E+03 | 1.0E+00 | 7.0E+03 |
| **Zinc** | **Medium** | 4.2E-02 | 6.7E-03 | 1.0E+00 | 2.1E-03 | 9.6E-01 | 3.0E+01 | 3.2E-01 | 2.3E+00 | 4.8E-04 | 7.0E+03 | 1.0E+00 | 7.0E+03 |
| **Zinc** | **Small** | 4.2E-02 | 6.7E-03 | 7.7E-01 | 3.5E-04 | 1.0E-01 | 5.0E+00 | 3.2E-01 | 2.3E+00 | 4.8E-04 | 7.0E+03 | 1.0E+00 | 7.0E+03 |

*Table A-4 Calculated separation efficiencies for the separation units used using their corresponding material property values used to generate them using the Napier Partition Curves*

| MATERIAL | SIZE | Mass(kg) | SIZE | Mass(kg) | SIZE | Mass(kg) |
|---|---|---|---|---|---|---|
| **PP** | Large | 1.79 | Medium | 6.25 | Small | 0.89 |
| **Aluminum** | Large | 19.24 | Medium | 67.35 | Small | 9.62 |
| **Ferrous** | Large | 208.71 | Medium | 730.49 | Small | 104.36 |
| **Glass** | Large | 4.10 | Medium | 14.37 | Small | 2.05 |
| **Carpet** | Large | 5.97 | Medium | 20.90 | Small | 2.99 |
| **ABS** | Large | 1.94 | Medium | 6.80 | Small | 0.97 |
| **TPO** | Large | 0.53 | Medium | 1.87 | Small | 0.27 |
| **Lead** | Large | 0.02 | Medium | 0.06 | Small | 0.01 |
| **SKOS** | Large | 1.29 | Medium | 4.52 | Small | 0.65 |
| **Magnesium** | Large | 0.35 | Medium | 1.21 | Small | 0.17 |
| **Copper** | Large | 3.55 | Medium | 12.44 | Small | 1.78 |
| **SKOP** | Large | 11.65 | Medium | 40.78 | Small | 5.83 |
| **Elastomer** | Large | 10.21 | Medium | 35.72 | Small | 5.10 |
| **PUR** | Large | 2.52 | Medium | 8.82 | Small | 1.26 |
| **Xenoy** | Large | 3.63 | Medium | 12.72 | Small | 1.82 |
| **Zinc** | Large | 0.54 | Medium | 1.90 | Small | 0.27 |
| **PC-ABS** | Large | 0.08 | Medium | 0.28 | Small | 0.04 |
| **PC** | Large | 0.12 | Medium | 0.40 | Small | 0.06 |
| **PE** | Large | 0.36 | Medium | 1.27 | Small | 0.18 |
| **PET** | Large | 0.92 | Medium | 3.23 | Small | 0.46 |
| **Elastomer-Ferrous** | Large | 0.81 | Medium | 0.00 | Small | 0.00 |
| **SKOP-Copper** | Large | 2.90 | Medium | 0.00 | Small | 0.00 |
| **Copper-Ferrous** | Large | 0.24 | Medium | 0.00 | Small | 0.00 |
| **PUR-Ferrous** | Large | 0.35 | Medium | 0.00 | Small | 0.00 |
| **PC-Ferrous** | Large | 0.10 | Medium | 0.00 | Small | 0.00 |
| **Carpet-SKOP** | Large | 0.01 | Medium | 0.00 | Small | 0.00 |
| **Aluminum-Ferrous** | Large | 1.02 | Medium | 0.00 | Small | 0.00 |
| **PET-Ferrous** | Large | 0.32 | Medium | 0.00 | Small | 0.00 |
| **Xenoy-Ferrous** | Large | 0.29 | Medium | 0.00 | Small | 0.00 |
| **Carpet-Ferrous** | Large | 0.00 | Medium | 0.00 | Small | 0.00 |
| **ABS-Ferrous** | Large | 0.13 | Medium | 0.00 | Small | 0.00 |
| **ABS-SKOP** | Large | 0.00 | Medium | 0.00 | Small | 0.00 |
| **SKOS-Ferrous** | Large | 0.04 | Medium | 0.00 | Small | 0.00 |
| **Elastomer-SKOP** | Large | 0.03 | Medium | 0.00 | Small | 0.00 |
| **Ferrous-SKOP** | Large | 0.08 | Medium | 0.00 | Small | 0.00 |
| **TPO-Ferrous** | Large | 0.21 | Medium | 0.00 | Small | 0.00 |
| **PP-SKOP** | Large | 0.05 | Medium | 0.00 | Small | 0.00 |
| **Ferrous-Copper** | Large | 9.76 | Medium | 0.00 | Small | 0.00 |
| **PP-Ferrous** | Large | 0.66 | Medium | 0.00 | Small | 0.00 |
| **PE-Ferrous** | Large | 0.13 | Medium | 0.00 | Small | 0.00 |

| | | | | | | |
|---|---|---|---|---|---|---|
| **SKOP-Ferrous** | Large | 2.45 | Medium | 0.00 | Small | 0.00 |
| | TOTAL | 297.11 | TOTAL | 971.38 | TOTAL | 138.77 |

*Table A- 5 Mass of particles (liberated and non-liberated) by material type and size at the end of the shredding process*

*Table A- 6: Particle flows by material class and size class through the network of separation units (Uo-U8) and output collection units (V1-V8) for baseline ELV*

| Material | Size | U0(kg) | U1(kg) | U2(kg) | U3(kg) | U4(kg) | U5(kg) | U6(kg) | U7(kg) | U8(kg) | V1(kg) | V3(kg) | V4(kg) | V5(kg) | V6(kg) | V7(kg) | V8(kg) |
|---|---|---|---|---|---|---|---|---|---|---|---|---|---|---|---|---|---|
| **ABS** | Large | 1.9E+00 | 8.1E-02 | 1.9E+00 | 1.8E+00 | 1.4E-08 | 1.8E+00 | 6.5E-02 | 6.5E-02 | 5.7E-05 | 8.1E-02 | 5.7E-05 | 4.9E-02 | 1.7E+00 | 1.3E-08 | 6.5E-02 | 2.4E-07 |
| **ABS** | Medium | 6.8E+00 | 2.8E-01 | 6.5E+00 | 4.9E+00 | 1.7E-01 | 4.7E+00 | 1.7E-01 | 1.7E-01 | 1.5E-04 | 2.8E-01 | 1.5E-04 | 1.6E+00 | 4.5E+00 | 1.7E-01 | 1.7E-01 | 6.6E-07 |
| **ABS** | Small | 9.7E-01 | 4.1E-02 | 9.3E-01 | 5.1E-01 | 4.6E-01 | 5.1E-02 | 1.8E-03 | 1.8E-02 | 1.6E-05 | 4.1E-02 | 1.6E-05 | 4.2E-01 | 4.9E-02 | 4.4E-01 | 1.8E-02 | 6.9E-08 |
| **ABS-Ferrous** | Large | 1.3E-01 | 5.4E-02 | 7.3E-02 | 7.3E-02 | 5.6E-10 | 7.3E-02 | 5.2E-03 | 5.2E-03 | 5.2E-03 | 5.4E-02 | 9.0E-04 | 3.4E-08 | 6.8E-02 | 5.2E-10 | 1.4E-07 | 4.3E-03 |
| **ABS-SKOP** | Large | 3.2E-03 | 1.3E-04 | 3.0E-03 | 3.0E-03 | 2.3E-11 | 3.0E-03 | 1.1E-04 | 1.1E-04 | 1.0E-07 | 1.3E-04 | 1.0E-07 | 7.7E-05 | 2.9E-03 | 2.2E-11 | 1.1E-04 | 4.4E-10 |
| **Aluminum** | Large | 1.9E+01 | 8.0E-01 | 1.8E+01 | 1.8E+01 | 1.4E-07 | 1.8E+01 | 1.8E+01 | 1.8E+01 | 1.6E+01 | 8.0E-01 | 1.4E+01 | 1.7E-03 | 1.4E-04 | 1.1E-12 | 2.1E+00 | 2.3E+00 |
| **Aluminum** | Medium | 6.7E+01 | 2.8E+00 | 6.5E+01 | 6.1E+01 | 2.2E+00 | 5.9E+01 | 5.9E+01 | 6.1E+01 | 5.4E+01 | 2.8E+00 | 4.6E+01 | 3.7E+00 | 4.5E-04 | 1.7E-05 | 6.9E+00 | 7.5E+00 |
| **Aluminum** | Small | 9.6E+00 | 4.0E-01 | 9.2E+00 | 5.7E+00 | 5.1E+00 | 5.7E-01 | 5.7E-01 | 5.7E+00 | 5.0E+00 | 4.0E-01 | 4.3E+00 | 3.5E+00 | 4.3E-06 | 3.9E-05 | 6.5E-01 | 7.1E-01 |
| **Aluminum-Ferrous** | Large | 1.0E+00 | 1.8E-01 | 8.4E-01 | 8.4E-01 | 6.4E-09 | 8.4E-01 | 8.4E-01 | 8.4E-01 | 8.4E-01 | 1.8E-01 | 1.9E-01 | 6.9E-07 | 2.3E-04 | 1.8E-12 | 5.6E-05 | 6.4E-01 |
| **Carpet** | Large | 6.0E+00 | 2.5E-01 | 5.7E+00 | 5.7E+00 | 4.4E-08 | 5.7E+00 | 2.0E-01 | 2.0E-01 | 7.8E-04 | 2.5E-01 | 7.7E-04 | 6.1E-02 | 5.5E+00 | 4.2E-08 | 2.0E-01 | 6.0E-06 |
| **Carpet** | Medium | 2.1E+01 | 8.7E-01 | 2.0E+01 | 1.6E+01 | 5.7E-01 | 1.5E+01 | 5.5E-01 | 5.7E-01 | 2.2E-03 | 8.7E-01 | 2.2E-03 | 4.1E+00 | 1.5E+01 | 5.5E-01 | 5.7E-01 | 1.7E-05 |
| **Carpet** | Small | 3.0E+00 | 1.2E-01 | 2.9E+00 | 1.6E+00 | 1.4E+00 | 1.6E-01 | 5.7E-03 | 5.7E-02 | 2.2E-04 | 1.2E-01 | 2.2E-04 | 1.3E+00 | 1.5E-01 | 1.4E+00 | 5.7E-02 | 1.7E-06 |
| **Carpet-Ferrous** | Large | 4.4E-03 | 1.6E-03 | 2.8E-03 | 2.8E-03 | 2.1E-11 | 2.8E-03 | 1.9E-04 | 1.9E-04 | 1.9E-04 | 1.6E-03 | 4.3E-05 | 2.3E-09 | 2.6E-03 | 2.0E-11 | 1.3E-08 | 1.4E-04 |
| **Carpet-SKOP** | Large | 1.1E-02 | 4.5E-04 | 1.0E-02 | 1.0E-02 | 7.9E-11 | 1.0E-02 | 3.7E-04 | 3.7E-04 | 1.3E-06 | 4.5E-04 | 1.3E-06 | 1.2E-04 | 1.0E-02 | 7.7E-11 | 3.7E-04 | 9.9E-09 |
| **Copper** | Large | 3.6E+00 | 1.5E-01 | 3.4E+00 | 3.4E+00 | 2.6E-08 | 3.4E+00 | 3.3E+00 | 3.3E+00 | 3.3E+00 | 1.5E-01 | 2.2E-05 | 1.4E-13 | 6.6E-02 | 5.1E-10 | 7.4E-16 | 3.3E+00 |
| **Copper** | Medium | 1.2E+01 | 5.2E-01 | 1.2E+01 | 1.2E+01 | 4.3E-01 | 1.1E+01 | 1.1E+01 | 1.2E+01 | 1.2E+01 | 5.2E-01 | 7.6E-05 | 1.1E-03 | 2.2E-01 | 8.3E-03 | 2.6E-15 | 1.2E+01 |
| **Copper** | Small | 1.8E+00 | 7.4E-02 | 1.7E+00 | 1.4E+00 | 1.3E+00 | 1.4E-01 | 1.4E-01 | 1.4E+00 | 1.4E+00 | 7.4E-02 | 8.9E-06 | 3.0E-01 | 2.7E-03 | 2.5E-02 | 3.1E-16 | 1.4E+00 |
| **Copper-Ferrous** | Large | 2.4E-01 | 1.8E-02 | 2.3E-01 | 2.3E-01 | 1.7E-09 | 2.3E-01 | 2.2E-01 | 2.2E-01 | 2.2E-01 | 1.8E-02 | 1.8E-06 | 1.4E-14 | 7.6E-03 | 5.8E-11 | 4.8E-17 | 2.2E-01 |
| **Elastomer** | Large | 1.0E+01 | 4.3E-01 | 9.8E+00 | 9.8E+00 | 7.5E-08 | 9.8E+00 | 3.5E-01 | 3.5E-01 | 2.6E-02 | 4.3E-01 | 2.6E-02 | 1.6E-02 | 9.4E+00 | 7.2E-08 | 3.2E-01 | 6.8E-04 |
| **Elastomer** | Medium | 3.6E+01 | 1.5E+00 | 3.4E+01 | 3.0E+01 | 1.1E+00 | 2.9E+01 | 1.0E+00 | 1.1E+00 | 8.1E-02 | 1.5E+00 | 7.9E-02 | 4.3E+00 | 2.8E+01 | 1.0E+00 | 9.9E-01 | 2.1E-03 |
| **Elastomer** | Small | 5.1E+00 | 2.1E-01 | 4.9E+00 | 2.9E+00 | 2.6E+00 | 2.9E-01 | 1.0E-02 | 1.0E-01 | 7.7E-03 | 2.1E-01 | 7.5E-03 | 2.0E+00 | 2.8E-01 | 2.5E+00 | 9.4E-02 | 2.0E-04 |
| **Elastomer-Ferrous** | Large | 8.1E-01 | 5.9E-01 | 2.2E-01 | 2.2E-01 | 1.7E-09 | 2.2E-01 | 2.1E-02 | 2.1E-02 | 2.1E-02 | 5.9E-01 | 1.0E-04 | 2.9E-10 | 2.0E-01 | 1.5E-09 | 4.8E-11 | 2.1E-02 |
| **Elastomer-SKOP** | Large | 2.7E-02 | 1.1E-03 | 2.6E-02 | 2.5E-02 | 2.0E-10 | 2.5E-02 | 9.1E-04 | 9.1E-04 | 3.1E-05 | 1.1E-03 | 3.1E-05 | 6.9E-05 | 2.5E-02 | 1.9E-10 | 8.8E-04 | 5.8E-07 |
| **Ferrous** | Large | 2.1E+02 | 2.0E+02 | 1.1E+01 | 1.1E+01 | 8.1E-08 | 1.1E+01 | 1.6E+00 | 1.6E+00 | 1.6E+00 | 2.0E+02 | 1.1E-04 | 1.9E-11 | 9.0E+00 | 6.9E-08 | 9.3E-14 | 1.6E+00 |
| **Ferrous** | Medium | 7.3E+02 | 6.9E+02 | 3.7E+01 | 3.7E+01 | 1.3E+00 | 3.6E+01 | 5.4E+00 | 5.6E+00 | 5.6E+00 | 6.9E+02 | 4.0E-04 | 1.1E-02 | 3.0E+01 | 1.1E+00 | 3.3E-13 | 5.6E+00 |

| | | | | | | | | | | | | | | | | |
|---|---|---|---|---|---|---|---|---|---|---|---|---|---|---|---|---|
| **Ferrous** | Small | 1.0E+02 | 9.9E+01 | 5.3E+00 | 4.2E+00 | 3.8E+00 | 4.2E-01 | 6.4E-02 | 6.4E-01 | 6.4E-01 | 9.9E+01 | 4.5E-05 | 1.1E+00 | 3.6E-01 | 3.2E+00 | 3.7E-14 | 6.4E-01 |
| **Ferrous-Copper** | Large | 9.8E+00 | 8.8E+00 | 1.0E+00 | 1.0E+00 | 7.7E-09 | 1.0E+00 | 2.6E-01 | 2.6E-01 | 2.6E-01 | 8.8E+00 | 1.4E-05 | 1.1E-12 | 7.3E-01 | 5.6E-09 | 7.3E-15 | 2.6E-01 |
| **Ferrous-SKOP** | Large | 8.2E-02 | 7.7E-02 | 4.5E-03 | 4.5E-03 | 3.5E-11 | 4.5E-03 | 6.7E-04 | 6.7E-04 | 6.7E-04 | 7.7E-02 | 6.0E-08 | 1.2E-14 | 3.9E-03 | 3.0E-11 | 7.1E-17 | 6.7E-04 |
| **Glass** | Large | 4.1E+00 | 1.7E-01 | 3.9E+00 | 3.9E+00 | 3.0E-08 | 3.9E+00 | 1.4E-01 | 1.4E-01 | 1.1E-01 | 1.7E-01 | 1.0E-01 | 5.1E-04 | 3.8E+00 | 2.9E-08 | 2.5E-02 | 1.3E-02 |
| **Glass** | Medium | 1.4E+01 | 6.0E-01 | 1.4E+01 | 1.3E+01 | 4.6E-01 | 1.2E+01 | 4.4E-01 | 4.6E-01 | 3.8E-01 | 6.0E-01 | 3.3E-01 | 8.7E-01 | 1.2E+01 | 4.4E-01 | 8.3E-02 | 4.4E-02 |
| **Glass** | Small | 2.1E+00 | 8.6E-02 | 2.0E+00 | 1.2E+00 | 1.1E+00 | 1.2E-01 | 4.3E-03 | 4.3E-02 | 3.5E-02 | 8.6E-02 | 3.1E-02 | 7.6E-01 | 1.2E-01 | 1.0E+00 | 7.8E-03 | 4.1E-03 |
| **Lead** | Large | 1.6E-02 | 6.8E-04 | 1.6E-02 | 1.6E-02 | 1.2E-10 | 1.6E-02 | 8.8E-04 | 8.8E-04 | 8.8E-04 | 6.8E-04 | 3.0E-11 | 0.0E+00 | 1.5E-02 | 1.1E-10 | 0.0E+00 | 8.8E-04 |
| **Lead** | Medium | 5.7E-02 | 2.4E-03 | 5.5E-02 | 5.5E-02 | 2.0E-03 | 5.3E-02 | 3.0E-03 | 3.1E-03 | 3.1E-03 | 2.4E-03 | 1.1E-10 | 4.6E-07 | 5.0E-02 | 1.9E-03 | 0.0E+00 | 3.1E-03 |
| **Lead** | Small | 8.2E-03 | 3.4E-04 | 7.9E-03 | 6.9E-03 | 6.2E-03 | 6.9E-04 | 3.8E-05 | 3.8E-04 | 3.8E-04 | 3.4E-04 | 1.3E-11 | 9.7E-04 | 6.5E-04 | 5.9E-03 | 0.0E+00 | 3.8E-04 |
| **Magnesium** | Large | 3.5E-01 | 1.4E-02 | 3.3E-01 | 3.3E-01 | 2.6E-09 | 3.3E-01 | 3.3E-01 | 3.3E-01 | 1.3E-02 | 1.4E-02 | 1.3E-02 | 8.3E-04 | 9.8E-06 | 7.5E-14 | 3.2E-01 | 2.5E-04 |
| **Magnesium** | Medium | 1.2E+00 | 5.1E-02 | 1.2E+00 | 1.0E+00 | 3.6E-02 | 9.6E-01 | 9.6E-01 | 1.0E+00 | 3.9E-02 | 5.1E-02 | 3.8E-02 | 1.6E-01 | 2.8E-05 | 1.0E-06 | 9.6E-01 | 7.5E-04 |
| **Magnesium** | Small | 1.7E-01 | 7.2E-03 | 1.7E-01 | 9.6E-02 | 8.7E-02 | 9.6E-03 | 9.6E-03 | 9.6E-02 | 3.7E-03 | 7.2E-03 | 3.6E-03 | 7.0E-02 | 2.8E-07 | 2.5E-06 | 9.2E-02 | 7.2E-05 |
| **PC** | Large | 1.2E-01 | 4.8E-03 | 1.1E-01 | 1.1E-01 | 8.4E-10 | 1.1E-01 | 3.9E-03 | 3.9E-03 | 8.0E-06 | 4.8E-03 | 8.0E-06 | 1.7E-03 | 1.1E-01 | 8.1E-10 | 3.9E-03 | 4.8E-08 |
| **PC** | Medium | 4.0E-01 | 1.7E-02 | 3.9E-01 | 3.0E-01 | 1.1E-02 | 2.9E-01 | 1.0E-02 | 1.1E-02 | 2.2E-05 | 1.7E-02 | 2.2E-05 | 8.6E-02 | 2.8E-01 | 1.0E-02 | 1.1E-02 | 1.3E-07 |
| **PC** | Small | 5.8E-02 | 2.4E-03 | 5.5E-02 | 3.1E-02 | 2.8E-02 | 3.1E-03 | 1.1E-04 | 1.1E-03 | 2.3E-06 | 2.4E-03 | 2.2E-06 | 2.5E-02 | 3.0E-03 | 2.7E-02 | 1.1E-03 | 1.4E-08 |
| **PC-ABS** | Large | 8.0E-02 | 3.3E-03 | 7.7E-02 | 7.5E-02 | 5.8E-10 | 7.5E-02 | 2.7E-03 | 2.7E-03 | 3.6E-06 | 3.3E-03 | 3.6E-06 | 1.6E-03 | 7.2E-02 | 5.6E-10 | 2.7E-03 | 1.8E-08 |
| **PC-ABS** | Medium | 2.8E-01 | 1.2E-02 | 2.7E-01 | 2.0E-01 | 7.3E-03 | 2.0E-01 | 7.0E-03 | 7.3E-03 | 9.9E-06 | 1.2E-02 | 9.8E-06 | 6.3E-02 | 1.9E-01 | 7.0E-03 | 7.3E-03 | 5.0E-08 |
| **PC-ABS** | Small | 4.0E-02 | 1.7E-03 | 3.8E-02 | 2.1E-02 | 1.9E-02 | 2.1E-03 | 7.5E-05 | 7.6E-04 | 1.0E-06 | 1.7E-03 | 1.0E-06 | 1.7E-02 | 2.0E-03 | 1.8E-02 | 7.5E-04 | 5.2E-09 |
| **PC-Ferrous** | Large | 9.6E-02 | 3.9E-02 | 5.7E-02 | 5.7E-02 | 4.4E-10 | 5.7E-02 | 4.0E-03 | 4.0E-03 | 4.0E-03 | 3.9E-02 | 6.9E-04 | 2.7E-08 | 5.3E-02 | 4.1E-10 | 1.1E-07 | 3.3E-03 |
| **PE** | Large | 3.6E-01 | 1.5E-02 | 3.5E-01 | 3.4E-01 | 2.6E-09 | 3.4E-01 | 1.2E-02 | 1.2E-02 | 2.0E-05 | 1.5E-02 | 2.0E-05 | 6.2E-03 | 3.3E-01 | 2.5E-09 | 1.2E-02 | 1.1E-07 |
| **PE** | Medium | 1.3E+00 | 5.3E-02 | 1.2E+00 | 9.4E-01 | 3.3E-02 | 9.0E-01 | 3.2E-02 | 3.3E-02 | 5.6E-05 | 5.3E-02 | 5.6E-05 | 2.8E-01 | 8.7E-01 | 3.2E-02 | 3.3E-02 | 3.1E-07 |
| **PE** | Small | 1.8E-01 | 7.6E-03 | 1.7E-01 | 9.6E-02 | 8.6E-02 | 9.6E-03 | 3.4E-04 | 3.4E-03 | 5.7E-06 | 7.6E-03 | 5.7E-06 | 7.7E-02 | 9.3E-03 | 8.3E-02 | 3.4E-03 | 3.2E-08 |
| **PE-Ferrous** | Large | 1.3E-01 | 4.9E-02 | 7.7E-02 | 7.7E-02 | 5.9E-10 | 7.7E-02 | 5.3E-03 | 5.3E-03 | 5.3E-03 | 4.9E-02 | 1.1E-03 | 5.3E-08 | 7.1E-02 | 5.5E-10 | 2.7E-07 | 4.2E-03 |
| **PET** | Large | 9.2E-01 | 3.8E-02 | 8.8E-01 | 8.7E-01 | 6.7E-09 | 8.7E-01 | 3.1E-02 | 3.1E-02 | 1.1E-04 | 3.8E-02 | 1.1E-04 | 9.9E-03 | 8.4E-01 | 6.5E-09 | 3.1E-02 | 8.3E-07 |
| **PET** | Medium | 3.2E+00 | 1.3E-01 | 3.1E+00 | 2.5E+00 | 8.8E-02 | 2.4E+00 | 8.5E-02 | 8.8E-02 | 3.1E-04 | 1.3E-01 | 3.1E-04 | 6.3E-01 | 2.3E+00 | 8.5E-02 | 8.7E-02 | 2.3E-06 |
| **PET** | Small | 4.6E-01 | 1.9E-02 | 4.4E-01 | 2.5E-01 | 2.2E-01 | 2.5E-02 | 8.8E-04 | 8.8E-03 | 3.1E-05 | 1.9E-02 | 3.1E-05 | 1.9E-01 | 2.4E-02 | 2.1E-01 | 8.8E-03 | 2.3E-07 |
| **PET-Ferrous** | Large | 3.2E-01 | 1.2E-01 | 2.1E-01 | 2.1E-01 | 1.6E-09 | 2.1E-01 | 1.4E-02 | 1.4E-02 | 1.4E-02 | 1.2E-01 | 3.2E-03 | 1.8E-07 | 1.9E-01 | 1.5E-09 | 9.7E-07 | 1.1E-02 |
| **PP** | Large | 1.8E+00 | 7.5E-02 | 1.7E+00 | 1.6E+00 | 1.3E-08 | 1.6E+00 | 5.9E-02 | 5.9E-02 | 2.9E-05 | 7.5E-02 | 2.9E-05 | 6.5E-02 | 1.6E+00 | 1.2E-08 | 5.9E-02 | 9.7E-08 |
| **PP** | Medium | 6.3E+00 | 2.6E-01 | 6.0E+00 | 4.4E+00 | 1.6E-01 | 4.2E+00 | 1.5E-01 | 1.6E-01 | 7.6E-05 | 2.6E-01 | 7.5E-05 | 1.6E+00 | 4.1E+00 | 1.5E-01 | 1.6E-01 | 2.6E-07 |

| | | | | | | | | | | | | | | | | |
|---|---|---|---|---|---|---|---|---|---|---|---|---|---|---|---|---|
| **PP** | Small | 8.9E-01 | 3.7E-02 | 8.6E-01 | 4.7E-01 | 4.2E-01 | 4.7E-02 | 1.7E-03 | 1.7E-02 | 8.1E-06 | 3.7E-02 | 8.1E-06 | 3.9E-01 | 4.5E-02 | 4.0E-01 | 1.7E-02 | 2.7E-08 |
| **PP-Ferrous** | Large | 6.6E-01 | 3.1E-01 | 3.5E-01 | 3.5E-01 | 2.7E-09 | 3.5E-01 | 2.6E-02 | 2.6E-02 | 2.6E-02 | 3.1E-01 | 3.7E-03 | 1.1E-07 | 3.3E-01 | 2.5E-09 | 3.8E-07 | 2.3E-02 |
| **PP-SKOP** | Large | 4.8E-02 | 2.0E-03 | 4.6E-02 | 4.4E-02 | 3.4E-10 | 4.4E-02 | 1.6E-03 | 1.6E-03 | 8.8E-07 | 2.0E-03 | 8.8E-07 | 1.6E-03 | 4.2E-02 | 3.3E-10 | 1.6E-03 | 3.2E-09 |
| **PUR** | Large | 2.5E+00 | 1.1E-01 | 2.4E+00 | 2.0E+00 | 1.5E-08 | 2.0E+00 | 7.1E-02 | 7.1E-02 | 2.4E-06 | 1.1E-01 | 2.4E-06 | 4.1E-01 | 1.9E+00 | 1.5E-08 | 7.1E-02 | 2.9E-09 |
| **PUR** | Medium | 8.8E+00 | 3.7E-01 | 8.5E+00 | 5.2E+00 | 1.9E-01 | 5.0E+00 | 1.8E-01 | 1.9E-01 | 6.4E-06 | 3.7E-01 | 6.4E-06 | 3.2E+00 | 4.9E+00 | 1.8E-01 | 1.9E-01 | 7.5E-09 |
| **PUR** | Small | 1.3E+00 | 5.3E-02 | 1.2E+00 | 6.3E-01 | 5.7E-01 | 6.3E-02 | 2.3E-03 | 2.3E-02 | 7.7E-07 | 5.3E-02 | 7.7E-07 | 5.8E-01 | 6.1E-02 | 5.5E-01 | 2.3E-02 | 9.0E-10 |
| **PUR-Ferrous** | Large | 3.5E-01 | 3.3E-01 | 2.2E-02 | 2.2E-02 | 1.7E-10 | 2.2E-02 | 3.2E-03 | 3.2E-03 | 3.2E-03 | 3.3E-01 | 3.9E-07 | 9.4E-14 | 1.9E-02 | 1.4E-10 | 7.5E-16 | 3.2E-03 |
| **SKOP** | Large | 1.2E+01 | 4.9E-01 | 1.1E+01 | 1.1E+01 | 8.4E-08 | 1.1E+01 | 3.9E-01 | 3.9E-01 | 6.9E-04 | 4.9E-01 | 6.9E-04 | 1.9E-01 | 1.1E+01 | 8.1E-08 | 3.9E-01 | 3.9E-06 |
| **SKOP** | Medium | 4.1E+01 | 1.7E+00 | 3.9E+01 | 3.0E+01 | 1.1E+00 | 2.9E+01 | 1.0E+00 | 1.1E+00 | 1.9E-03 | 1.7E+00 | 1.9E-03 | 8.9E+00 | 2.8E+01 | 1.0E+00 | 1.1E+00 | 1.1E-05 |
| **SKOP** | Small | 5.8E+00 | 2.4E-01 | 5.6E+00 | 3.1E+00 | 2.8E+00 | 3.1E-01 | 1.1E-02 | 1.1E-01 | 1.9E-04 | 2.4E-01 | 1.9E-04 | 2.5E+00 | 3.0E-01 | 2.7E+00 | 1.1E-01 | 1.1E-06 |
| **SKOP-Copper** | Large | 2.9E+00 | 1.2E-01 | 2.8E+00 | 2.8E+00 | 2.1E-08 | 2.8E+00 | 1.7E+00 | 1.7E+00 | 1.7E+00 | 1.2E-01 | 3.9E-02 | 4.4E-08 | 1.1E+00 | 8.3E-09 | 2.0E-07 | 1.7E+00 |
| **SKOP-Ferrous** | Large | 2.5E+00 | 1.1E+00 | 1.3E+00 | 1.3E+00 | 1.0E-08 | 1.3E+00 | 9.8E-02 | 9.8E-02 | 9.8E-02 | 1.1E+00 | 1.2E-02 | 3.1E-07 | 1.2E+00 | 9.5E-09 | 8.7E-07 | 8.7E-02 |
| **SKOS** | Large | 1.3E+00 | 1.4E-01 | 1.2E+00 | 1.2E+00 | 8.9E-09 | 1.2E+00 | 1.1E+00 | 1.1E+00 | 1.1E+00 | 1.4E-01 | 1.3E-03 | 1.6E-10 | 3.5E-02 | 2.7E-10 | 7.0E-11 | 1.1E+00 |
| **SKOS** | Medium | 4.5E+00 | 4.8E-01 | 4.0E+00 | 4.0E+00 | 1.4E-01 | 3.9E+00 | 3.8E+00 | 3.9E+00 | 3.9E+00 | 4.8E-01 | 4.5E-03 | 4.4E-03 | 1.2E-01 | 4.3E-03 | 2.4E-10 | 3.9E+00 |
| **SKOS** | Small | 6.5E-01 | 6.9E-02 | 5.8E-01 | 4.4E-01 | 3.9E-01 | 4.4E-02 | 4.2E-02 | 4.2E-01 | 4.2E-01 | 6.9E-02 | 4.9E-04 | 1.4E-01 | 1.3E-03 | 1.2E-02 | 2.6E-11 | 4.2E-01 |
| **SKOS-Ferrous** | Large | 3.7E-02 | 1.3E-02 | 2.5E-02 | 2.5E-02 | 1.9E-10 | 2.5E-02 | 2.2E-02 | 2.2E-02 | 2.2E-02 | 1.3E-02 | 1.1E-05 | 1.0E-12 | 3.0E-03 | 2.3E-11 | 1.9E-13 | 2.2E-02 |
| **TPO** | Large | 5.3E-01 | 2.2E-02 | 5.1E-01 | 5.0E-01 | 3.9E-09 | 5.0E-01 | 1.8E-02 | 1.8E-02 | 4.9E-05 | 2.2E-02 | 4.8E-05 | 6.8E-03 | 4.9E-01 | 3.7E-09 | 1.8E-02 | 3.3E-07 |
| **TPO** | Medium | 1.9E+00 | 7.8E-02 | 1.8E+00 | 1.4E+00 | 5.0E-02 | 1.4E+00 | 4.8E-02 | 5.0E-02 | 1.4E-04 | 7.8E-02 | 1.4E-04 | 3.8E-01 | 1.3E+00 | 4.8E-02 | 5.0E-02 | 9.1E-07 |
| **TPO** | Small | 2.7E-01 | 1.1E-02 | 2.6E-01 | 1.4E-01 | 1.3E-01 | 1.4E-02 | 5.1E-04 | 5.1E-03 | 1.4E-05 | 1.1E-02 | 1.4E-05 | 1.1E-01 | 1.4E-02 | 1.2E-01 | 5.1E-03 | 9.2E-08 |
| **TPO-Ferrous** | Large | 2.1E-01 | 9.7E-02 | 1.1E-01 | 1.1E-01 | 8.7E-10 | 1.1E-01 | 8.4E-03 | 8.4E-03 | 8.4E-03 | 9.7E-02 | 8.6E-04 | 2.1E-08 | 1.0E-01 | 8.0E-10 | 5.0E-08 | 7.5E-03 |
| **Xenoy** | Large | 3.6E+00 | 1.5E-01 | 3.5E+00 | 3.4E+00 | 2.6E-08 | 3.4E+00 | 1.2E-01 | 1.2E-01 | 3.0E-04 | 1.5E-01 | 3.0E-04 | 4.9E-02 | 3.3E+00 | 2.5E-08 | 1.2E-01 | 1.9E-06 |
| **Xenoy** | Medium | 1.3E+01 | 5.3E-01 | 1.2E+01 | 9.5E+00 | 3.4E-01 | 9.2E+00 | 3.3E-01 | 3.4E-01 | 8.3E-04 | 5.3E-01 | 8.2E-04 | 2.6E+00 | 8.9E+00 | 3.3E-01 | 3.4E-01 | 5.3E-06 |
| **Xenoy** | Small | 1.8E+00 | 7.6E-02 | 1.7E+00 | 9.7E-01 | 8.7E-01 | 9.7E-02 | 3.5E-03 | 3.5E-02 | 8.4E-05 | 7.6E-02 | 8.4E-05 | 7.7E-01 | 9.3E-02 | 8.4E-01 | 3.5E-02 | 5.4E-07 |
| **Xenoy-Ferrous** | Large | 2.9E-01 | 1.2E-01 | 1.7E-01 | 1.7E-01 | 1.3E-09 | 1.7E-01 | 1.2E-02 | 1.2E-02 | 1.2E-02 | 1.2E-01 | 2.1E-03 | 8.3E-08 | 1.6E-01 | 1.2E-09 | 3.4E-07 | 1.0E-02 |
| **Zinc** | Large | 5.4E-01 | 2.3E-02 | 5.2E-01 | 5.2E-01 | 4.0E-09 | 5.2E-01 | 1.6E-01 | 1.6E-01 | 1.6E-01 | 2.3E-02 | 7.9E-05 | 1.8E-11 | 3.5E-01 | 2.7E-09 | 1.1E-12 | 1.6E-01 |
| **Zinc** | Medium | 1.9E+00 | 7.9E-02 | 1.8E+00 | 1.8E+00 | 6.5E-02 | 1.7E+00 | 5.6E-01 | 5.8E-01 | 5.8E-01 | 7.9E-02 | 2.8E-04 | 1.3E-03 | 1.2E+00 | 4.4E-02 | 4.0E-12 | 5.8E-01 |
| **Zinc** | Small | 2.7E-01 | 1.1E-02 | 2.6E-01 | 2.0E-01 | 1.8E-01 | 2.0E-02 | 6.4E-03 | 6.4E-02 | 6.4E-02 | 1.1E-02 | 3.1E-05 | 5.9E-02 | 1.4E-02 | 1.2E-01 | 4.4E-13 | 6.4E-02 |
| **all** | all | 1.4E+03 | 1.0E+03 | 3.9E+02 | 3.4E+02 | 3.0E+01 | 3.1E+02 | 1.2E+02 | 1.3E+02 | 1.1E+02 | | | | | | | |

*Table A-7 Input material flow to the shredder, for lightweight aluminum-intensive vehicle*

| MATERIAL | SIZE | Mass(kg) | Difference with baseline ELV (kg) |
|---|---|---|---|
| **ABS** | Large | 9.69 | 0.0 |
| **ABS-Ferrous** | Large | 0.25 | 0.0 |
| **ABS-SKOP** | Large | 0.01 | 0.0 |
| **Aluminum** | Large | 470.51 | 374.7 |
| **Aluminum-Copper** | Large | 1.38 | 1.4 |
| **Aluminum-Ferrous** | Large | 7.30 | 5.3 |
| **Carpet** | Large | 29.85 | 0.0 |
| **Carpet-Ferrous** | Large | 0.01 | 0.0 |
| **Carpet-SKOP** | Large | 0.02 | 0.0 |
| **Copper** | Large | 11.70 | 0.0 |
| **Copper-Ferrous** | Large | 0.49 | 0.0 |
| **Elastomer** | Large | 50.93 | 0.0 |
| **Elastomer-Ferrous** | Large | 1.61 | 0.0 |
| **Elastomer-SKOP** | Large | 0.05 | 0.0 |
| **Ferrous** | Large | 285.42 | -746.7 |
| **Ferrous-Copper** | Large | 17.15 | -2.4 |
| **Ferrous-SKOP** | Large | 0.16 | 0.0 |
| **Glass** | Large | 20.53 | 0.0 |
| **Lead** | Large | 0.08 | 0.0 |
| **Magnesium** | Large | 1.73 | 0.0 |
| **PC** | Large | 0.56 | 0.0 |
| **PC-ABS** | Large | 0.40 | 0.0 |

| | | | |
|---|---|---|---|
| **PC-Ferrous** | Large | 0.19 | 0.0 |
| **PE** | Large | 1.78 | 0.0 |
| **PE-Ferrous** | Large | 0.25 | 0.0 |
| **PET** | Large | 4.52 | 0.0 |
| **PET-Ferrous** | Large | 0.65 | 0.0 |
| **PP** | Large | 8.77 | 0.0 |
| **PP-Ferrous** | Large | 1.32 | 0.0 |
| **PP-SKOP** | Large | 0.10 | 0.0 |
| **PUR** | Large | 12.60 | 0.0 |
| **PUR-Ferrous** | Large | 0.71 | 0.0 |
| **SKOP** | Large | 57.16 | 0.0 |
| **SKOP-Copper** | Large | 5.81 | 0.0 |
| **SKOP-Ferrous** | Large | 4.91 | 0.0 |
| **SKOS** | Large | 6.44 | 0.0 |
| **SKOS-Ferrous** | Large | 0.07 | 0.0 |
| **TPO** | Large | 2.62 | 0.0 |
| **TPO-Ferrous** | Large | 0.42 | 0.0 |
| **Xenoy** | Large | 18.11 | 0.0 |
| **Xenoy-Ferrous** | Large | 0.58 | 0.0 |
| **Zinc** | Large | 2.71 | 0.0 |

# Appendix B Disassembly optimization data

*Table B- 1 Reduced 2-level hierarchy end-of-life vehicle part data used for disassembly optimization, including part values and removal times, and component types (1. assembly, 2. sub-assembly, 3. Stand-alone component), adapted from [22], [27]*

| Part ID | Name | Part Value ($) | Removal Time (s) | Weight (kg) | Material | Component Type |
|---|---|---|---|---|---|---|
| 1 | DoorFrontRight | 450 | 33 | 33.34 | Mixed | 1 Assembly |
| 2 | DoorFrontRight.Panel | 0 | 95 | 2.96 | Mixed | 2 Sub-assembly |
| 13 | DoorFrontRight.MirrorPanel | 0 | 5 | 0.02 | ABS | 2 Sub-assembly |
| 14 | DoorFrontRight.Shoddy | 0 | 14 | 0.12 | SKOS | 2 Sub-assembly |
| 15 | DoorFrontRight.Structure | 0 | 0 | 31.7 | Mixed | 2 Sub-assembly |
| 28 | DoorFrontLeft | 450 | 33 | 33.34 | Mixed | 1 Assembly |
| 29 | DoorFrontLeft.Panel | 0 | 95 | 2.96 | Mixed | 2 Sub-assembly |
| 40 | DoorFrontLeft.MirrorPanel | 0 | 5 | 0.02 | ABS | 2 Sub-assembly |
| 41 | DoorFrontLeft.Shoddy | 0 | 14 | 0.12 | SKOS | 2 Sub-assembly |
| 42 | DoorFrontLeft.Structure | 0 | 0 | 31.7 | Mixed | 2 Sub-assembly |
| 56 | DoorRearRight | 425 | 21 | 25.5 | Mixed | 1 Assembly |
| 57 | DoorRearRight.Panel | 0 | 80 | 2.2 | Mixed | 2 Sub-assembly |
| 70 | DoorRearRight.Structure | 0 | 0 | 23.28 | Mixed | 2 Sub-assembly |
| 74 | DoorRearLeft | 425 | 21 | 25.5 | Mixed | 1 Assembly |
| 75 | DoorRearLeft.Panel | 0 | 80 | 2.2 | Mixed | 2 Sub-assembly |
| 88 | DoorRearLeft.Structure | 0 | 0 | 23.28 | Mixed | 2 Sub-assembly |
| 92 | SeatFrontRight | 50 | 91 | 21.72 | Mixed | 1 Assembly |
| 93 | SeatFrontRight.HeadRest | 0 | 4 | 0.88 | Mixed | 2 Sub-assembly |
| 98 | SeatFrontRight.LateralCover | 0 | 20 | 0.22 | SKOP | 2 Sub-assembly |
| 99 | SeatFrontRight.BackFoam | 0 | 85 | 0.68 | PUR | 2 Sub-assembly |
| 100 | SeatFrontRight.BackCover | 0 | 2 | 0.8 | Carpet | 2 Sub-assembly |
| 101 | SeatFrontRight.ArmRestCovers | 0 | 2 | 0.04 | SKOP | 2 Sub-assembly |
| 102 | SeatFrontRight.ArmRest | 0 | 240 | 0.7 | Mixed | 2 Sub-assembly |
| 103 | SeatFrontRight.ArmRestBigCover | 0 | 1 | 0.08 | SKOP | 2 Sub-assembly |
| 108 | SeatFrontRight.BottomCover | 0 | 100 | 0.58 | Carpet | 2 Sub-assembly |
| 109 | SeatFrontRight.BottomFoam | 0 | 82 | 0.88 | PUR | 2 Sub-assembly |
| 110 | SeatFrontRight.BottomBase | 0 | 0 | 16.36 | Mixed | 2 Sub-assembly |
| 113 | SeatFrontRight.SeatBeltFrontMid | 0 | 0 | 0.22 | Mixed | 2 Sub-assembly |
| 117 | SeatFrontLeft | 50 | 91 | 21.72 | Mixed | 1 Assembly |
| 118 | SeatFrontLeft.HeadRest | 0 | 4 | 0.88 | Mixed | 2 Sub-assembly |
| 123 | SeatFrontLeft.LateralCover | 0 | 20 | 0.22 | SKOP | 2 Sub-assembly |

| | | | | | | |
|---|---|---|---|---|---|---|
| **124** | SeatFrontLeft.BackFoam | 0 | 85 | 0.68 | PUR | 2 Sub-assembly |
| **125** | SeatFrontLeft.BackCover | 0 | 2 | 0.8 | Carpet | 2 Sub-assembly |
| **126** | SeatFrontLeft.ArmRestCovers | 0 | 2 | 0.04 | SKOP | 2 Sub-assembly |
| **127** | SeatFrontLeft.ArmRest | 0 | 240 | 0.7 | Mixed | 2 Sub-assembly |
| **128** | SeatFrontLeft.ArmRestBigCover | 0 | 1 | 0.08 | SKOP | 2 Sub-assembly |
| **133** | SeatFrontLeft.BottomCover | 0 | 100 | 0.58 | Carpet | 2 Sub-assembly |
| **134** | SeatFrontLeft.BottomFoam | 0 | 82 | 0.88 | PUR | 2 Sub-assembly |
| **135** | SeatFrontLeft.BottomBase | 0 | 0 | 16.36 | Mixed | 2 Sub-assembly |
| **138** | SeatFrontLeft.SeatBeltFrontMid | 0 | 0 | 0.22 | Mixed | 2 Sub-assembly |
| **142** | RearViewMirror | 0 | 10 | 0.3 | SKOS | 3 Part |
| **143** | SeatRearBottom | 25 | 43 | 6.64 | Mixed | 1 Assembly |
| **144** | SeatRearBottom.Cover | 0 | 30 | 1 | Carpet | 2 Sub-assembly |
| **145** | SeatRearBottom.Base | 0 | 0 | 5.58 | Mixed | 2 Sub-assembly |
| **150** | SeatRearBack | 25 | 16 | 7.2 | Mixed | 1 Assembly |
| **151** | SeatRearBack.Base | 0 | 0 | 6.02 | Mixed | 2 Sub-assembly |
| **158** | SeatRearBack.Cover | 0 | 34 | 1.14 | Carpet | 2 Sub-assembly |
| **159** | APillarTrimLeft | 0 | 3 | 0.2 | Mixed | 1 Assembly |
| **160** | APillarTrimLeft.Clips | 0 | 20 | 0.01 | Ferrous | 2 Sub-assembly |
| **161** | APillarTrimLeft.ABS | 0 | 0 | 0.19 | ABS | 2 Sub-assembly |
| **162** | APillarTrimRight | 0 | 5 | 0.2 | Mixed | 1 Assembly |
| **163** | APillarTrimRight.Clips | 0 | 20 | 0.01 | Ferrous | 2 Sub-assembly |
| **165** | SunvisorRight | 0 | 9 | 0.52 | SKOS | 3 Part |
| **166** | SunvisorLeft | 0 | 9 | 0.8 | SKOS | 3 Part |
| **167** | Handles | 0 | 37 | 0.32 | SKOP | 3 Part |
| **168** | DomeLight | 0 | 13 | 0.2 | SKOS | 3 Part |
| **173** | SeatbeltFrontLeftCover | 0 | 2 | 0.01 | SKOP | 3 Part |
| **174** | CPillarLeft | 0 | 7 | 0.4 | PP | 3 Part |
| **175** | CPillarRight | 0 | 7 | 0.4 | PP | 3 Part |
| **176** | SeatbeltFrontRightCover | 0 | 7 | 0.01 | SKOP | 3 Part |
| **177** | BPillarUpperRight | 0 | 13 | 0.1 | PP | 3 Part |
| **179** | BPillarUpperLeft | 0 | 10 | 0.1 | PP | 3 Part |
| **180** | Headliner | 0 | 8 | 2 | SKOS | 3 Part |
| **181** | BPillarLowerRight | 0 | 65 | 0.71 | TPO | 3 Part |
| **182** | BPillarLowerLeft | 0 | 43 | 0.71 | TPO | 3 Part |
| **183** | SeatBeltFrontRight | 40 | 12 | 1.4 | Mixed | 1 Assembly |
| **184** | SeatBeltFrontRight.Steelcase | 0 | 0 | 0.86 | Mixed | 2 Sub-assembly |
| **187** | SeatBeltFrontRight.Strap | 0 | 20 | 0.16 | PE | 2 Sub-assembly |
| **188** | SeatBeltFrontRight.Other | 0 | 12 | 0.1 | Mixed | 2 Sub-assembly |
| **191** | SeatBeltFrontRight.Lead | 0 | 45 | 0.02 | Lead | 2 Sub-assembly |
| **192** | SeatBeltFrontLeft | 40 | 12 | 1.4 | Mixed | 1 Assembly |
| **193** | SeatBeltFrontLeft.Steelcase | 0 | 0 | 0.86 | Mixed | 2 Sub-assembly |
| **196** | SeatBeltFrontLeft.Strap | 0 | 20 | 0.16 | PE | 2 Sub-assembly |

| | | | | | | |
|---|---|---|---|---|---|---|
| **197** | SeatBeltFrontLeft.Other | 0 | 12 | 0.1 | Mixed | 2 Sub-assembly |
| **200** | SeatBeltFrontLeft.Lead | 0 | 45 | 0.02 | Lead | 2 Sub-assembly |
| **201** | BPillarShoddyRight | 0 | 2 | 0.1 | Mixed | 1 Assembly |
| **202** | BPillarShoddyRight.Shoddy | 0 | 23 | 0.04 | Carpet | 2 Sub-assembly |
| **203** | BPillarShoddyRight.SKOP | 0 | 0 | 0.06 | SKOP | 2 Sub-assembly |
| **204** | BPillarShoddyLeft | 0 | 2 | 0.1 | Mixed | 1 Assembly |
| **205** | BPillarShoddyLeft.Shoddy | 0 | 23 | 0.04 | Carpet | 2 Sub-assembly |
| **206** | BPillarShoddyLeft.SKOP | 0 | 0 | 0.06 | SKOP | 2 Sub-assembly |
| **207** | QuartertrimRight | 0 | 15 | 0.18 | Mixed | 1 Assembly |
| **208** | QuartertrimRight.Shoddy | 0 | 3 | 0.08 | Carpet | 2 Sub-assembly |
| **209** | QuartertrimRight.PP | 0 | 0 | 0.1 | PP | 2 Sub-assembly |
| **210** | QuartertrimLeft | 0 | 15 | 0.18 | Mixed | 1 Assembly |
| **211** | QuartertrimLeft.Shoddy | 0 | 3 | 0.08 | Carpet | 2 Sub-assembly |
| **212** | QuartertrimLeft.PP | 0 | 0 | 0.1 | PP | 2 Sub-assembly |
| **213** | KickPanelRight | 0 | 17 | 0.06 | PP | 3 Part |
| **214** | KickPanelLeft | 0 | 17 | 0.06 | PP | 3 Part |
| **215** | ThirdBrakeLight | 0 | 60 | 0.34 | Mixed | 1 Assembly |
| **216** | ThirdBrakeLight.Lens | 0 | 2 | 0.01 | SKOP | 2 Sub-assembly |
| **217** | ThirdBrakeLight.Reflector | 0 | 5 | 0.04 | PC | 2 Sub-assembly |
| **218** | ThirdBrakeLight.Case | 0 | 0 | 0.26 | Mixed | 2 Sub-assembly |
| **221** | SpeakerCovers | 0 | 3 | 0.22 | Ferrous | 3 Part |
| **222** | ParcelTray | 0 | 23 | 1.58 | SKOS | 3 Part |
| **223** | SpeakerRearLeft | 0 | 27 | 0.7 | Mixed | 1 Assembly |
| **224** | SpeakerRearLeft.Steel | 0 | 1.00E+09 | 0.67 | Ferrous | 2 Sub-assembly |
| **225** | SpeakerRearLeft.SKOP | 0 | 1.00E+09 | 0.03 | SKOP | 2 Sub-assembly |
| **226** | SpeakerRearRight | 0 | 27 | 0.7 | Mixed | 1 Assembly |
| **227** | SpeakerRearRight.Steel | 0 | 1.00E+09 | 0.67 | Ferrous | 2 Sub-assembly |
| **228** | SpeakerRearRight.SKOP | 0 | 1.00E+09 | 0.03 | SKOP | 2 Sub-assembly |
| **229** | ParcelTrayShoddy | 0 | 31 | 0.68 | Carpet | 3 Part |
| **230** | BackSeatShoddy | 0 | 10 | 2.18 | Carpet | 3 Part |
| **231** | SeatBeltRearRight | 40 | 47 | 0.96 | Mixed | 1 Assembly |
| **232** | SeatBeltRearRight.Steelcase | 0 | 0 | 0.62 | Mixed | 2 Sub-assembly |
| **235** | SeatBeltRearRight.Strap | 0 | 5 | 0.14 | PE | 2 Sub-assembly |
| **236** | SeatBeltRearRight.PlasticCase | 0 | 8 | 0.02 | SKOP | 2 Sub-assembly |
| **237** | SeatBeltRearRight.Other | 0 | 4 | 0.1 | Mixed | 2 Sub-assembly |
| **240** | SeatBeltRearRight.Lead | 0 | 25 | 0.02 | Lead | 2 Sub-assembly |
| **241** | SeatBeltRearLeft | 40 | 47 | 0.96 | Mixed | 1 Assembly |
| **242** | SeatBeltRearLeft.Steelcase | 0 | 0 | 0.62 | Mixed | 2 Sub-assembly |
| **245** | SeatBeltRearLeft.Strap | 0 | 5 | 0.14 | PE | 2 Sub-assembly |
| **246** | SeatBeltRearLeft.PlasticCase | 0 | 8 | 0.02 | SKOP | 2 Sub-assembly |
| **247** | SeatBeltRearLeft.Other | 0 | 4 | 0.1 | Mixed | 2 Sub-assembly |
| **250** | SeatBeltRearLeft.Lead | 0 | 25 | 0.02 | Lead | 2 Sub-assembly |
| **251** | SeatbeltRearRightLower | 0 | 12 | 0.36 | Mixed | 1 Assembly |

| | | | | | | |
|---|---|---|---|---|---|---|
| 252 | SeatbeltRearRightLower.Other | 0 | 15 | 0.1 | Mixed | 2 Sub-assembly |
| 255 | SeatbeltRearRightLower.Strap | 0 | 15 | 0.08 | PE | 2 Sub-assembly |
| 256 | SeatbeltRearRightLower.Buckle | 0 | 0 | 0.08 | SKOS | 2 Sub-assembly |
| 257 | SeatbeltRearRightLower.Latch | 0 | 0 | 0.1 | Ferrous | 2 Sub-assembly |
| 258 | SeatbeltRearRightLower.PlasticCase | 0 | 2 | 0.02 | SKOP | 2 Sub-assembly |
| 259 | SeatbeltRearLeftLower | 40 | 8 | 0.26 | Mixed | 1 Assembly |
| 260 | SeatbeltRearLeftLower.Strap | 0 | 0 | 0.04 | PE | 2 Sub-assembly |
| 261 | SeatbeltRearLeftLower.PlasticCase | 0 | 1.00E+09 | 0.02 | SKOP | 2 Sub-assembly |
| 262 | SeatbeltRearLeftLower.Steel | 0 | 1.00E+09 | 0.1 | Ferrous | 2 Sub-assembly |
| 263 | SeatbeltRearLeftLower.Buckles | 0 | 20 | 0.14 | SKOS | 2 Sub-assembly |
| 264 | LowerIP | 0 | 60 | 1.12 | Mixed | 1 Assembly |
| 265 | LowerIP.Steel | 0 | 0 | 1.09 | Ferrous | 2 Sub-assembly |
| 266 | LowerIP.SKOP | 0 | 5 | 0.03 | SKOP | 2 Sub-assembly |
| 267 | LowerIPReinforcement | 0 | 8 | 0.18 | Ferrous | 3 Part |
| 268 | LowerIPReinforcement2 | 0 | 44 | 1.22 | Ferrous | 3 Part |
| 289 | TrunkSpareTireCover.Carpet | 0 | 45 | 0.19 | Carpet | 2 Sub-assembly |
| 271 | SteeringColumnSupport | 0 | 120 | 2.26 | Mixed | 1 Assembly |
| 272 | SteeringColumnSupport.Electrical | 0 | 20 | 0.28 | SKOS | 2 Sub-assembly |
| 273 | SteeringColumnSupport.Case | 0 | 0 | 1.8 | Aluminum | 2 Sub-assembly |
| 274 | SteeringColumnSupport.Bracket | 0 | 5 | 0.14 | Ferrous | 2 Sub-assembly |
| 275 | SteeringColumnTurnSignal | 0 | 25 | 0.22 | SKOS | 3 Part |
| 276 | SteeringColumnLowerPanel | 0 | 125 | 0.08 | SKOP | 3 Part |
| 277 | SteeringColumnAssembly | 200 | 140 | 10.06 | Mixed | 1 Assembly |
| 278 | SteeringColumnAssembly.AirBag | 0 | 60 | 1.7 | Mixed | 2 Sub-assembly |
| 281 | SteeringColumnAssembly.Base | 50 | 0 | 8.36 | Mixed | 2 Sub-assembly |
| 284 | TrunkCloseOut | 0 | 7 | 0.84 | Mixed | 1 Assembly |
| 285 | TrunkCloseOut.Shoddy | 0 | 0 | 0.26 | Carpet | 2 Sub-assembly |
| 286 | TrunkCloseOut.SKOS | 0 | 50 | 0.58 | SKOS | 2 Sub-assembly |
| 287 | TrunkScuffPlateRear | 0 | 2 | 0.12 | PP | 3 Part |
| 288 | TrunkSpareTireCover | 0 | 2 | 1.8 | Mixed | 1 Assembly |
| 290 | TrunkSpareTireCover.Carboard | 0 | 0 | 1.61 | SKOS | 2 Sub-assembly |
| 291 | SpareTire | 0 | 3 | 11.3 | Mixed | 1 Assembly |
| 292 | SpareTire.Rim | 0 | 126 | 6.55 | Ferrous | 2 Sub-assembly |
| 293 | SpareTire.Rubber | 0 | 0 | 4.73 | Elastomer | 2 Sub-assembly |
| 294 | Jack | 0 | 22 | 2.44 | Ferrous | 3 Part |
| 295 | TrunkLiner | 0 | 33 | 3.56 | Mixed | 1 Assembly |
| 296 | TrunkLiner.Shoddy | 0 | 245 | 0.24 | Carpet | 2 Sub-assembly |
| 297 | TrunkLiner.Carpet | 0 | 0 | 3.32 | Carpet | 2 Sub-assembly |
| 298 | WeatherStripping | 0 | 66 | 6.78 | Elastomer | 3 Part |
| 299 | TailLightCoverRight | 65 | 91 | 0.54 | SKOP | 1 Assembly |
| 300 | TailLightCoverRight.Red | 0 | 100 | 0.16 | SKOP | 2 Sub-assembly |
| 301 | TailLightCoverRight.Black | 0 | 0 | 0.38 | ABS | 2 Sub-assembly |
| 302 | TailLightCoverLeft | 65 | 91 | 0.54 | SKOP | 1 Assembly |

| | | | | | | |
|---|---|---|---|---|---|---|
| **303** | TailLightCoverLeft.Red | 0 | 100 | 0.16 | SKOP | 2 Sub-assembly |
| **304** | TailLightCoverLeft.Black | 0 | 0 | 0.38 | ABS | 2 Sub-assembly |
| **305** | TailLightCoverCenter | 50 | 59 | 1.28 | SKOS | 3 Part |
| **306** | FasciaRearUpper | 0 | 61 | 1.73 | PUR | 3 Part |
| **307** | FasciaRearlower | 200 | 117 | 8.56 | Xenoy | 3 Part |
| **308** | EnergyAbsorberRearLeft | 40 | 25 | 2.46 | Ferrous | 3 Part |
| **309** | EnergyAbsorberRearRight | 40 | 35 | 2.46 | Ferrous | 3 Part |
| **310** | DeckLid | 163 | 110 | 13.26 | Mixed | 1 Assembly |
| **311** | DeckLid.Lid | 0 | 1.00E+09 | 10.88 | Ferrous | 2 Sub-assembly |
| **312** | DeckLid.SKOS | 0 | 1.00E+09 | 0.13 | SKOS | 2 Sub-assembly |
| **313** | WiringHarnessCloseOut | 0 | 7 | 0.3 | SKOP | 3 Part |
| **314** | WiperAssemblies | 0 | 14 | 0.92 | Mixed | 1 Assembly |
| **315** | WiperAssemblies.Steel | 0 | 100 | 0.86 | Ferrous | 2 Sub-assembly |
| **316** | WiperAssemblies.Blade | 0 | 0 | 0.06 | Mixed | 2 Sub-assembly |
| **319** | CowlVent | 0 | 73 | 0.54 | ABS | 3 Part |
| **320** | Battery | 20 | 48 | 20 | Lead | 3 Part |
| **321** | AirCleanerAssembly | 113 | 21 | 1.7 | Mixed | 1 Assembly |
| **322** | AirCleanerAssembly.Hose | 0 | 10 | 0.4 | Mixed | 2 Sub-assembly |
| **325** | AirCleanerAssembly.Top | 0 | 60 | 0.4 | PP | 2 Sub-assembly |
| **326** | AirCleanerAssembly.Bottom | 0 | 0 | 0.88 | PP | 2 Sub-assembly |
| **327** | AirCleanerAssembly.Filter | 0 | 0 | 0.18 | SKOS | 2 Sub-assembly |
| **328** | WasherCoolantBottleAssembly | 0 | 18 | 0.9 | Mixed | 1 Assembly |
| **329** | WasherCoolantBottleAssembly.Bottles | 0 | 0 | 0.82 | PP | 2 Sub-assembly |
| **330** | WasherCoolantBottleAssembly.Rubber | 0 | 20 | 0.08 | Elastomer | 2 Sub-assembly |
| **331** | HeatBoxAssemblyBase | 0 | 45 | 2.24 | PET | 3 Part |
| **332** | HeatBoxAssembly | 20 | 780 | 8.64 | Mixed | 1 Assembly |
| **333** | HeatBoxAssembly.EC | 0 | 37 | 0.24 | SKOS | 2 Sub-assembly |
| **334** | HeatBoxAssembly.LateralCover | 0 | 49 | 0.05 | PP | 2 Sub-assembly |
| **335** | HeatBoxAssembly.Elastomer | 0 | 5 | 0.05 | Elastomer | 2 Sub-assembly |
| **336** | HeatBoxAssembly.Filter1 | 0 | 5 | 0.81 | Aluminum | 2 Sub-assembly |
| **337** | HeatBoxAssembly.SpringHeater | 0 | 25 | 0.04 | SKOS | 2 Sub-assembly |
| **338** | HeatBoxAssembly.Panel1 | 0 | 10 | 0.23 | Mixed | 2 Sub-assembly |
| **341** | HeatBoxAssembly.Duct1 | 0 | 60 | 0.77 | Mixed | 2 Sub-assembly |
| **349** | HeatBoxAssembly.Elastomer2 | 0 | 5 | 0.13 | Elastomer | 2 Sub-assembly |
| **350** | HeatBoxAssembly.Fan | 0 | 30 | 0.12 | PP | 2 Sub-assembly |
| **351** | HeatBoxAssembly.Motor | 28 | 60 | 1.6 | Mixed | 2 Sub-assembly |
| **355** | HeatBoxAssembly.Duct2 | 0 | 45 | 0.5 | Mixed | 2 Sub-assembly |
| **358** | HeatBoxAssembly.Box | 0 | 0 | 3.85 | Mixed | 2 Sub-assembly |
| **362** | GasPedalAssembly | 0 | 41 | 0.52 | Mixed | 1 Assembly |
| **363** | GasPedalAssembly.Steel | 0 | 45 | 0.48 | Ferrous | 2 Sub-assembly |
| **364** | GasPedalAssembly.SKOP | 0 | 0 | 0.04 | SKOP | 2 Sub-assembly |

| | | | | | | |
|---|---|---|---|---|---|---|
| **365** | BreakPedalAssembly | 0 | 77 | 2.23 | Mixed | 1 Assembly |
| **366** | BreakPedalAssembly.Bracket | 0 | 5 | 0.26 | Ferrous | 2 Sub-assembly |
| **367** | BreakPedalAssembly.Rubber | 0 | 10 | 0.07 | Elastomer | 2 Sub-assembly |
| **368** | BreakPedalAssembly.Base | 0 | 0 | 1.9 | Ferrous | 2 Sub-assembly |
| **369** | SteeringColumnSupport2 | 0 | 12 | 0.62 | SKOS | 3 Part |
| **370** | TrunkReleaseCase | 0 | 10 | 0.04 | ABS | 3 Part |
| **371** | carpet | 0 | 40 | 15.88 | Mixed | 1 Assembly |
| **372** | carpet.Shoddy | 0 | 73 | 6.38 | Carpet | 2 Sub-assembly |
| **373** | carpet.Carpet | 0 | 0 | 9.5 | Carpet | 2 Sub-assembly |
| **374** | RearHeaterDuct | 0 | 7 | 0.78 | PP | 3 Part |
| **375** | ECU | 0 | 47 | 1.08 | Mixed | 1 Assembly |
| **376** | ECU.Steel | 0 | 1.00E+09 | 0.11 | Ferrous | 2 Sub-assembly |
| **377** | ECU.AIuminum | 0 | 1.00E+09 | 0.22 | Aluminum | 2 Sub-assembly |
| **378** | ECU.SKOS | 0 | 1.00E+09 | 0.76 | SKOS | 2 Sub-assembly |
| **379** | EmergencyBrake | 0 | 35 | 1.62 | Ferrous | 3 Part |
| **380** | FrontInsulator | 0 | 76 | 6.34 | Mixed | 1 Assembly |
| **381** | FrontInsulator.Shoddy | 0 | 120 | 0.98 | Carpet | 2 Sub-assembly |
| **382** | FrontInsulator.SKOS | 0 | 0 | 5.36 | SKOS | 2 Sub-assembly |
| **383** | BatteryCase | 0 | 20 | 0.76 | SKOP | 3 Part |
| **384** | BrakeBooster | 45 | 100 | 4.14 | Mixed | 1 Assembly |
| **385** | BrakeBooster.Steel | 0 | 1.00E+09 | 2.28 | Ferrous | 2 Sub-assembly |
| **386** | BrakeBooster.Aluminum | 0 | 1.00E+09 | 1.24 | Aluminum | 2 Sub-assembly |
| **387** | BrakeBooster.SKOP | 0 | 1.00E+09 | 0.62 | SKOP | 2 Sub-assembly |
| **388** | FirewallInsulation | 0 | 9 | 0.44 | SKOS | 3 Part |
| **389** | CoolingFanShroudAssembly | 70 | 17 | 3.68 | Mixed | 1 Assembly |
| **390** | CoolingFanShroudAssembly.Steel | 0 | 1.00E+09 | 1.47 | Ferrous | 2 Sub-assembly |
| **391** | CoolingFanShroudAssembly.SKOS | 0 | 1.00E+09 | 2.21 | SKOS | 2 Sub-assembly |
| **392** | CoolingFanModule | 0 | 6 | 0.72 | Mixed | 1 Assembly |
| **393** | CoolingFanModule.Steel | 0 | 1.00E+09 | 0.5 | Ferrous | 2 Sub-assembly |
| **394** | CoolingFanModule.SKOS | 0 | 1.00E+09 | 0.22 | SKOS | 2 Sub-assembly |
| **395** | AirBagSensor | 0 | 7 | 0.34 | Mixed | 1 Assembly |
| **396** | AirBagSensor.Steel | 0 | 1.00E+09 | 0.27 | Ferrous | 2 Sub-assembly |
| **397** | AirBagSensor.SKOS | 0 | 1.00E+09 | 0.07 | SKOS | 2 Sub-assembly |
| **398** | CruiseServo | 48 | 11 | 1.08 | Mixed | 1 Assembly |
| **399** | CruiseServo.Steel | 0 | 1.00E+09 | 0.22 | Ferrous | 2 Sub-assembly |
| **400** | CruiseServo.SKOS | 0 | 1.00E+09 | 0.86 | SKOS | 2 Sub-assembly |
| **401** | EngineHarness | 0 | 60 | 3.16 | Mixed | 1 Assembly |
| **402** | EngineHarness.Steel | 0 | 1.00E+09 | 0.63 | Ferrous | 2 Sub-assembly |
| **403** | EngineHarness.Copper | 0 | 1.00E+09 | 0.03 | Copper | 2 Sub-assembly |
| **404** | EngineHarness.SKOS | 0 | 1.00E+09 | 2.05 | SKOS | 2 Sub-assembly |
| **405** | ACManifold | 0 | 15 | 3.9 | Mixed | 1 Assembly |
| **406** | ACManifold.Steel | 0 | 1.00E+09 | 3.32 | Ferrous | 2 Sub-assembly |
| **407** | ACManifold.SKOS | 0 | 1.00E+09 | 0.59 | SKOS | 2 Sub-assembly |

| | | | | | | |
|---|---|---|---|---|---|---|
| **408** | AirBagSensor2 | 0 | 45 | 0.26 | Mixed | 1 Assembly |
| **409** | AirBagSensor2.Steel | 0 | 1.00E+09 | 0.21 | Ferrous | 2 Sub-assembly |
| **410** | AirBagSensor2.SKOS | 0 | 1.00E+09 | 0.05 | SKOS | 2 Sub-assembly |
| **412** | AirDam | 0 | 15 | 0.34 | Elastomer | 3 Part |
| **413** | WheelHouseLinerFrontRight | 0 | 45 | 1.22 | Mixed | 1 Assembly |
| **414** | WheelHouseLinerFrontRight.SKOS | 0 | 3 | 1.13 | SKOS | 2 Sub-assembly |
| **415** | WheelHouseLinerFrontRight.PP | 0 | 0 | 0.09 | PP | 2 Sub-assembly |
| **416** | WheelHouseLinerFrontLeft | 0 | 45 | 1.22 | Mixed | 1 Assembly |
| **417** | WheelHouseLinerFrontLeft.SKOS | 0 | 3 | 1.13 | SKOS | 2 Sub-assembly |
| **418** | WheelHouseLinerFrontLeft.PP | 0 | 0 | 0.09 | PP | 2 Sub-assembly |
| **419** | CharcoalCanister | 0 | 8 | 0.82 | SKOS | 3 Part |
| **420** | VacuumTank | 0 | 7 | 0.74 | SKOP | 3 Part |
| **421** | HornAssembly | 0 | 2 | 0.6 | Mixed | 1 Assembly |
| **422** | HornAssembly.Steel | 0 | 1.00E+09 | 0.48 | Ferrous | 2 Sub-assembly |
| **423** | HornAssembly.SKOP | 0 | 1.00E+09 | 0.12 | SKOP | 2 Sub-assembly |
| **424** | RockerMoldingRight | 0 | 75 | 1.44 | Elastomer | 3 Part |
| **425** | RockerMoldingLeft | 0 | 42 | 1.4 | Elastomer | 3 Part |
| **426** | WheelRearRight | 0 | 15 | 16.28 | Mixed | 1 Assembly |
| **427** | WheelRearRight.Cover | 33 | 1 | 0.18 | PC | 2 Sub-assembly |
| **428** | WheelRearRight.Rim | 45 | 126 | 7.18 | Aluminum | 2 Sub-assembly |
| **429** | WheelRearRight.Rubber | 0 | 1 | 8.84 | Elastomer | 2 Sub-assembly |
| **430** | WheelRearLeft | 0 | 15 | 16.28 | Mixed | 1 Assembly |
| **431** | WheelRearLeft.Cover | 33 | 1 | 0.18 | PC | 2 Sub-assembly |
| **432** | WheelRearLeft.Rim | 45 | 126 | 7.18 | Aluminum | 2 Sub-assembly |
| **433** | WheelRearLeft.Rubber | 0 | 1 | 8.84 | Elastomer | 2 Sub-assembly |
| **434** | WireHarnessCover | 0 | 115 | 0.48 | PP | 3 Part |
| **435** | TrunkRelease | 0 | 58 | 0.42 | Mixed | 1 Assembly |
| **436** | TrunkRelease.Steel | 0 | 1.00E+09 | 0.38 | Ferrous | 2 Sub-assembly |
| **437** | TrunkRelease.SKOP | 0 | 1.00E+09 | 0.04 | SKOP | 2 Sub-assembly |
| **438** | WireHarness | 0 | 180 | 3.94 | Mixed | 1 Assembly |
| **439** | WireHarness.Steel | 0 | 1.00E+09 | 0.79 | Ferrous | 2 Sub-assembly |
| **440** | WireHarness.Copper | 0 | 1.00E+09 | 0.59 | Copper | 2 Sub-assembly |
| **441** | WireHarness.SKOP | 0 | 1.00E+09 | 2.56 | SKOP | 2 Sub-assembly |
| **442** | WindshieldWiperMotor | 40 | 30 | 1.98 | Mixed | 1 Assembly |
| **443** | WindshieldWiperMotor.Steel | 0 | 1.00E+09 | 1.49 | Ferrous | 2 Sub-assembly |
| **444** | WindshieldWiperMotor.Magnesium | 0 | 1.00E+09 | 0.2 | Magnesium | 2 Sub-assembly |
| **445** | WindshieldWiperMotor.Copper | 0 | 1.00E+09 | 0.3 | Copper | 2 Sub-assembly |
| **446** | WindShieldFront | 50 | 426 | 11.76 | Glass | 3 Part |
| **448** | FrontClip | 2115 | 720 | 175.54 | Mixed | 1 Assembly |
| **449** | FrontClip.RadiatorHeatExchanger | 85 | 164 | 4.76 | Mixed | 2 Sub-assembly |
| **460** | FrontClip.ACCondensor | 135 | 78 | 2.12 | Mixed | 2 Sub-assembly |
| **463** | FrontClip.MarkerLightFrontLeft | 17 | 80 | 0.34 | SKOP | 2 Sub-assembly |

| | | | | | | |
|---|---|---|---|---|---|---|
| **464** | FrontClip.MarkerLightFrontRight | 17 | 40 | 0.34 | SKOP | 2 Sub-assembly |
| **465** | FrontClip.LightFrontAssembly | 0 | 197 | 4.26 | Mixed | 2 Sub-assembly |
| **476** | FrontClip.FasciaFrontLower | 225 | 115 | 9.68 | Xenoy | 2 Sub-assembly |
| **477** | FrontClip.FasciaFrontUpper | 0 | 220 | 1.2 | PUR | 2 Sub-assembly |
| **478** | FrontClip.EnergyAbsorberFrontRight | 45 | 43 | 2.5 | Ferrous | 2 Sub-assembly |
| **479** | FrontClip.EnergyAbsorberFrontLeft | 45 | 44 | 2.5 | Ferrous | 2 Sub-assembly |
| **480** | FrontClip.RadiatorShroud | 0 | 16 | 0.28 | TPO | 2 Sub-assembly |
| **481** | FrontClip.Hood | 200 | 100 | 22.56 | Mixed | 2 Sub-assembly |
| **484** | FrontClip.Frame | 0 | 0 | 125 | Ferrous | 2 Sub-assembly |
| **485** | DriveTrain | 0 | 1750 | 457.85 | Mixed | 1 Assembly |
| **486** | DriveTrain.ACCompressor | 138 | 30 | 6.36 | Mixed | 2 Sub-assembly |
| **489** | DriveTrain.Alternator | 75 | 57 | 6.58 | Mixed | 2 Sub-assembly |
| **493** | DriveTrain.PowerSteering | 230 | 143 | 6.34 | Mixed | 2 Sub-assembly |
| **497** | DriveTrain.Starter | 35 | 95 | 3.5 | Mixed | 2 Sub-assembly |
| **501** | DriveTrain.Engine | 730 | 1519 | 200 | Mixed | 2 Sub-assembly |
| **505** | DriveTrain.Transmission | 478 | 240 | 94.55 | Mixed | 2 Sub-assembly |
| **508** | DriveTrain.CradleSuspension | 459 | 1 | 107.96 | Ferrous | 2 Sub-assembly |
| **509** | WheelFrontRight | 0 | 15 | 16.28 | Mixed | 1 Assembly |
| **510** | WheelFrontRight.Cover | 33 | 5 | 0.2 | PC-ABS | 2 Sub-assembly |
| **511** | WheelFrontRight.Rim | 85 | 126 | 7.18 | Aluminum | 2 Sub-assembly |
| **512** | WheelFrontRight.Tire | 0 | 1 | 8.84 | Elastomer | 2 Sub-assembly |
| **513** | WheelFrontLeft | 0 | 15 | 16.28 | Mixed | 1 Assembly |
| **514** | WheelFrontLeft.Cover | 33 | 5 | 0.2 | PC-ABS | 2 Sub-assembly |
| **515** | WheelFrontLeft.Rim | 85 | 126 | 7.18 | Aluminum | 2 Sub-assembly |
| **516** | WheelFrontLeft.Tire | 0 | 1 | 8.84 | Elastomer | 2 Sub-assembly |
| **517** | InstrumentPanel | 0 | 825 | 35.96 | Mixed | 1 Assembly |
| **518** | InstrumentPanel.DuctWork | 0 | 60 | 0.52 | PE | 2 Sub-assembly |
| **519** | InstrumentPanel.EvapDuct | 0 | 46 | 1.14 | SKOP | 2 Sub-assembly |
| **520** | InstrumentPanel.DuctWork2 | 0 | 45 | 0.44 | PE | 2 Sub-assembly |
| **521** | InstrumentPanel.Hoses | 0 | 15 | 0.26 | SKOP | 2 Sub-assembly |
| **522** | InstrumentPanel.WireHarness | 0 | 874 | 5.62 | Mixed | 2 Sub-assembly |
| **526** | InstrumentPanel.DashBrain | 0 | 10 | 0.2 | SKOS | 2 Sub-assembly |
| **527** | InstrumentPanel.Dimmer | 0 | 120 | 0.26 | Mixed | 2 Sub-assembly |
| **530** | InstrumentPanel.Radio | 125 | 232 | 1.48 | Mixed | 2 Sub-assembly |
| **533** | InstrumentPanel.TrayAssembly | 0 | 177 | 0.5 | TPO | 2 Sub-assembly |
| **534** | InstrumentPanel.ClusterBezel | 0 | 97 | 1.32 | SKOS | 2 Sub-assembly |
| **535** | InstrumentPanel.Cluster | 125 | 15 | 1.54 | SKOS | 2 Sub-assembly |
| **536** | InstrumentPanel.HeaterControl | 0 | 20 | 0.26 | SKOS | 2 Sub-assembly |
| **537** | InstrumentPanel.GloveBox | 0 | 47 | 2.52 | Mixed | 2 Sub-assembly |
| **543** | InstrumentPanel.Ashtray | 0 | 103 | 1.04 | Mixed | 2 Sub-assembly |
| **546** | InstrumentPanel.CenterBezel | 0 | 2 | 0.18 | ABS | 2 Sub-assembly |

| | | | | | | |
|---|---|---|---|---|---|---|
| **547** | InstrumentPanel.Clock | 0 | 9 | 0.1 | SKOS | 2 Sub-assembly |
| **548** | InstrumentPanel.AirBagPassenger | 0 | 107 | 4.86 | Mixed | 2 Sub-assembly |
| **551** | InstrumentPanel.AirBagCover | 0 | 10 | 0.2 | PC | 2 Sub-assembly |
| **552** | InstrumentPanel.Frame | 0 | 76 | 5.94 | Ferrous | 2 Sub-assembly |
| **553** | InstrumentPanel.Skin | 0 | 0 | 6.5 | SKOP | 2 Sub-assembly |
| **600** | RearFrame | 0 | 0 | 279 | Ferrous | 1 Assembly |
| **601** | RearFrame.A | 0 | 1.00E+09 | 178 | Ferrous | 2 Sub-assembly |
| **602** | RearFrame.B | 0 | 1.00E+09 | 101 | Ferrous | 2 Sub-assembly |
| **605** | DeckLid.Hinge | 0 | 120 | 2.25 | Ferrous | 2 Sub-assembly |

*Table B- 2 ELV part precedence constraints used in disassembly optimization, with parts identified by their part IDs, adapted from [22], [27]*

| Source ID | Source Part Name | Target ID | Target Part Name |
|---|---|---|---|
| 13 | DoorFrontRight.MirrorPanel | 2 | DoorFrontRight.Panel |
| 2 | DoorFrontRight.Panel | 14 | DoorFrontRight.Shoddy |
| 1 | DoorFrontRight | 15 | DoorFrontRight.Structure |
| 14 | DoorFrontRight.Shoddy | 15 | DoorFrontRight.Structure |
| 40 | DoorFrontLeft.MirrorPanel | 29 | DoorFrontLeft.Panel |
| 29 | DoorFrontLeft.Panel | 41 | DoorFrontLeft.Shoddy |
| 28 | DoorFrontLeft | 42 | DoorFrontLeft.Structure |
| 41 | DoorFrontLeft.Shoddy | 42 | DoorFrontLeft.Structure |
| 56 | DoorRearRight | 70 | DoorRearRight.Structure |
| 57 | DoorRearRight.Panel | 70 | DoorRearRight.Structure |
| 74 | DoorRearLeft | 88 | DoorRearLeft.Structure |
| 75 | DoorRearLeft.Panel | 88 | DoorRearLeft.Structure |
| 92 | SeatFrontRight | 98 | SeatFrontRight.LateralCover |
| 99 | SeatFrontRight.BackFoam | 100 | SeatFrontRight.BackCover |
| 101 | SeatFrontRight.ArmRestCovers | 102 | SeatFrontRight.ArmRest |
| 102 | SeatFrontRight.ArmRest | 103 | SeatFrontRight.ArmRestBigCover |
| 92 | SeatFrontRight | 108 | SeatFrontRight.BottomCover |
| 92 | SeatFrontRight | 109 | SeatFrontRight.BottomFoam |
| 93 | SeatFrontRight.HeadRest | 110 | SeatFrontRight.BottomBase |
| 98 | SeatFrontRight.LateralCover | 110 | SeatFrontRight.BottomBase |
| 100 | SeatFrontRight.BackCover | 110 | SeatFrontRight.BottomBase |
| 103 | SeatFrontRight.ArmRestBigCover | 110 | SeatFrontRight.BottomBase |
| 108 | SeatFrontRight.BottomCover | 110 | SeatFrontRight.BottomBase |
| 109 | SeatFrontRight.BottomFoam | 110 | SeatFrontRight.BottomBase |
| 113 | SeatFrontRight.SeatBeltFrontMid | 110 | SeatFrontRight.BottomBase |
| 92 | SeatFrontRight | 113 | SeatFrontRight.SeatBeltFrontMid |
| 102 | SeatFrontRight.ArmRest | 113 | SeatFrontRight.SeatBeltFrontMid |
| 117 | SeatFrontLeft | 123 | SeatFrontLeft.LateralCover |
| 124 | SeatFrontLeft.BackFoam | 125 | SeatFrontLeft.BackCover |
| 126 | SeatFrontLeft.ArmRestCovers | 127 | SeatFrontLeft.ArmRest |
| 127 | SeatFrontLeft.ArmRest | 128 | SeatFrontLeft.ArmRestBigCover |
| 117 | SeatFrontLeft | 133 | SeatFrontLeft.BottomCover |
| 117 | SeatFrontLeft | 134 | SeatFrontLeft.BottomFoam |
| 118 | SeatFrontLeft.HeadRest | 135 | SeatFrontLeft.BottomBase |
| 123 | SeatFrontLeft.LateralCover | 135 | SeatFrontLeft.BottomBase |
| 125 | SeatFrontLeft.BackCover | 135 | SeatFrontLeft.BottomBase |
| 128 | SeatFrontLeft.ArmRestBigCover | 135 | SeatFrontLeft.BottomBase |
| 133 | SeatFrontLeft.BottomCover | 135 | SeatFrontLeft.BottomBase |
| 134 | SeatFrontLeft.BottomFoam | 135 | SeatFrontLeft.BottomBase |

| | | | |
|---|---|---|---|
| **138** | SeatFrontLeft.SeatBeltFrontMid | 135 | SeatFrontLeft.BottomBase |
| **117** | SeatFrontLeft | 138 | SeatFrontLeft.SeatBeltFrontMid |
| **127** | SeatFrontLeft.ArmRest | 138 | SeatFrontLeft.SeatBeltFrontMid |
| **143** | SeatRearBottom | 145 | SeatRearBottom.Base |
| **144** | SeatRearBottom.Cover | 145 | SeatRearBottom.Base |
| **143** | SeatRearBottom | 150 | SeatRearBack |
| **150** | SeatRearBack | 151 | SeatRearBack.Base |
| **158** | SeatRearBack.Cover | 151 | SeatRearBack.Base |
| **159** | APillarTrimLeft | 160 | APillarTrimLeft.Clips |
| **160** | APillarTrimLeft.Clips | 161 | APillarTrimLeft.ABS |
| **162** | APillarTrimRight | 163 | APillarTrimRight.Clips |
| **176** | SeatbeltFrontRightCover | 177 | BPillarUpperRight |
| **173** | SeatbeltFrontLeftCover | 179 | BPillarUpperLeft |
| **159** | APillarTrimLeft | 180 | Headliner |
| **162** | APillarTrimRight | 180 | Headliner |
| **165** | SunvisorRight | 180 | Headliner |
| **166** | SunvisorLeft | 180 | Headliner |
| **167** | Handles | 180 | Headliner |
| **174** | CPillarLeft | 180 | Headliner |
| **175** | CPillarRight | 180 | Headliner |
| **177** | BPillarUpperRight | 180 | Headliner |
| **179** | BPillarUpperLeft | 180 | Headliner |
| **177** | BPillarUpperRight | 181 | BPillarLowerRight |
| **179** | BPillarUpperLeft | 182 | BPillarLowerLeft |
| **181** | BPillarLowerRight | 183 | SeatBeltFrontRight |
| **187** | SeatBeltFrontRight.Strap | 184 | SeatBeltFrontRight.Steelcase |
| **191** | SeatBeltFrontRight.Lead | 187 | SeatBeltFrontRight.Strap |
| **183** | SeatBeltFrontRight | 188 | SeatBeltFrontRight.Other |
| **188** | SeatBeltFrontRight.Other | 191 | SeatBeltFrontRight.Lead |
| **182** | BPillarLowerLeft | 192 | SeatBeltFrontLeft |
| **196** | SeatBeltFrontLeft.Strap | 193 | SeatBeltFrontLeft.Steelcase |
| **200** | SeatBeltFrontLeft.Lead | 196 | SeatBeltFrontLeft.Strap |
| **192** | SeatBeltFrontLeft | 197 | SeatBeltFrontLeft.Other |
| **197** | SeatBeltFrontLeft.Other | 200 | SeatBeltFrontLeft.Lead |
| **183** | SeatBeltFrontRight | 201 | BPillarShoddyRight |
| **201** | BPillarShoddyRight | 202 | BPillarShoddyRight.Shoddy |
| **202** | BPillarShoddyRight.Shoddy | 203 | BPillarShoddyRight.SKOP |
| **192** | SeatBeltFrontLeft | 204 | BPillarShoddyLeft |
| **204** | BPillarShoddyLeft | 205 | BPillarShoddyLeft.Shoddy |
| **205** | BPillarShoddyLeft.Shoddy | 206 | BPillarShoddyLeft.SKOP |
| **143** | SeatRearBottom | 207 | QuartertrimRight |
| **150** | SeatRearBack | 207 | QuartertrimRight |
| **181** | BPillarLowerRight | 207 | QuartertrimRight |

| | | | |
|---|---|---|---|
| **207** | QuartertrimRight | 208 | QuartertrimRight.Shoddy |
| **208** | QuartertrimRight.Shoddy | 209 | QuartertrimRight.PP |
| **143** | SeatRearBottom | 210 | QuartertrimLeft |
| **150** | SeatRearBack | 210 | QuartertrimLeft |
| **182** | BPillarLowerLeft | 210 | QuartertrimLeft |
| **210** | QuartertrimLeft | 211 | QuartertrimLeft.Shoddy |
| **211** | QuartertrimLeft.Shoddy | 212 | QuartertrimLeft.PP |
| **162** | APillarTrimRight | 213 | KickPanelRight |
| **181** | BPillarLowerRight | 213 | KickPanelRight |
| **159** | APillarTrimLeft | 214 | KickPanelLeft |
| **182** | BPillarLowerLeft | 214 | KickPanelLeft |
| **215** | ThirdBrakeLight | 216 | ThirdBrakeLight.Lens |
| **216** | ThirdBrakeLight.Lens | 217 | ThirdBrakeLight.Reflector |
| **217** | ThirdBrakeLight.Reflector | 218 | ThirdBrakeLight.Case |
| **150** | SeatRearBack | 222 | ParcelTray |
| **215** | ThirdBrakeLight | 222 | ParcelTray |
| **221** | SpeakerCovers | 222 | ParcelTray |
| **222** | ParcelTray | 223 | SpeakerRearLeft |
| **222** | ParcelTray | 226 | SpeakerRearRight |
| **223** | SpeakerRearLeft | 229 | ParcelTrayShoddy |
| **226** | SpeakerRearRight | 229 | ParcelTrayShoddy |
| **150** | SeatRearBack | 230 | BackSeatShoddy |
| **222** | ParcelTray | 231 | SeatBeltRearRight |
| **235** | SeatBeltRearRight.Strap | 232 | SeatBeltRearRight.Steelcase |
| **236** | SeatBeltRearRight.PlasticCase | 232 | SeatBeltRearRight.Steelcase |
| **240** | SeatBeltRearRight.Lead | 235 | SeatBeltRearRight.Strap |
| **231** | SeatBeltRearRight | 237 | SeatBeltRearRight.Other |
| **237** | SeatBeltRearRight.Other | 240 | SeatBeltRearRight.Lead |
| **222** | ParcelTray | 241 | SeatBeltRearLeft |
| **245** | SeatBeltRearLeft.Strap | 242 | SeatBeltRearLeft.Steelcase |
| **246** | SeatBeltRearLeft.PlasticCase | 242 | SeatBeltRearLeft.Steelcase |
| **250** | SeatBeltRearLeft.Lead | 245 | SeatBeltRearLeft.Strap |
| **241** | SeatBeltRearLeft | 247 | SeatBeltRearLeft.Other |
| **247** | SeatBeltRearLeft.Other | 250 | SeatBeltRearLeft.Lead |
| **143** | SeatRearBottom | 251 | SeatbeltRearRightLower |
| **252** | SeatbeltRearRightLower.Other | 255 | SeatbeltRearRightLower.Strap |
| **258** | SeatbeltRearRightLower.PlasticCase | 256 | SeatbeltRearRightLower.Buckle |
| **258** | SeatbeltRearRightLower.PlasticCase | 257 | SeatbeltRearRightLower.Latch |
| **255** | SeatbeltRearRightLower.Strap | 258 | SeatbeltRearRightLower.PlasticCase |
| **143** | SeatRearBottom | 259 | SeatbeltRearLeftLower |
| **259** | SeatbeltRearLeftLower | 260 | SeatbeltRearLeftLower.Strap |
| **263** | SeatbeltRearLeftLower.Buckles | 260 | SeatbeltRearLeftLower.Strap |
| **261** | SeatbeltRearLeftLower.PlasticCase | 262 | SeatbeltRearLeftLower.Steel |

| | | | |
|---|---|---|---|
| 262 | SeatbeltRearLeftLower.Steel | 263 | SeatbeltRearLeftLower.Buckles |
| 264 | LowerIP | 265 | LowerIP.Steel |
| 266 | LowerIP.SKOP | 265 | LowerIP.Steel |
| 264 | LowerIP | 267 | LowerIPReinforcement |
| 267 | LowerIPReinforcement | 268 | LowerIPReinforcement2 |
| 517 | InstrumentPanel | 271 | SteeringColumnSupport |
| 271 | SteeringColumnSupport | 272 | SteeringColumnSupport.Electrical |
| 272 | SteeringColumnSupport.Electrical | 273 | SteeringColumnSupport.Case |
| 274 | SteeringColumnSupport.Bracket | 273 | SteeringColumnSupport.Case |
| 271 | SteeringColumnSupport | 274 | SteeringColumnSupport.Bracket |
| 276 | SteeringColumnLowerPanel | 275 | SteeringColumnTurnSignal |
| 268 | LowerIPReinforcement2 | 276 | SteeringColumnLowerPanel |
| 275 | SteeringColumnTurnSignal | 277 | SteeringColumnAssembly |
| 277 | SteeringColumnAssembly | 281 | SteeringColumnAssembly.Base |
| 278 | SteeringColumnAssembly.AirBag | 281 | SteeringColumnAssembly.Base |
| 284 | TrunkCloseOut | 285 | TrunkCloseOut.Shoddy |
| 286 | TrunkCloseOut.SKOS | 285 | TrunkCloseOut.Shoddy |
| 284 | TrunkCloseOut | 286 | TrunkCloseOut.SKOS |
| 288 | TrunkSpareTireCover | 289 | TrunkSpareTireCover.Carpet |
| 289 | TrunkSpareTireCover.Carpet | 290 | TrunkSpareTireCover.Carboard |
| 294 | Jack | 291 | SpareTire |
| 291 | SpareTire | 292 | SpareTire.Rim |
| 292 | SpareTire.Rim | 293 | SpareTire.Rubber |
| 288 | TrunkSpareTireCover | 294 | Jack |
| 287 | TrunkScuffPlateRear | 295 | TrunkLiner |
| 291 | SpareTire | 295 | TrunkLiner |
| 295 | TrunkLiner | 296 | TrunkLiner.Shoddy |
| 296 | TrunkLiner.Shoddy | 297 | TrunkLiner.Carpet |
| 299 | TailLightCoverRight | 300 | TailLightCoverRight.Red |
| 300 | TailLightCoverRight.Red | 301 | TailLightCoverRight.Black |
| 302 | TailLightCoverLeft | 303 | TailLightCoverLeft.Red |
| 303 | TailLightCoverLeft.Red | 304 | TailLightCoverLeft.Black |
| 307 | FasciaRearlower | 308 | EnergyAbsorberRearLeft |
| 307 | FasciaRearlower | 309 | EnergyAbsorberRearRight |
| 314 | WiperAssemblies | 315 | WiperAssemblies.Steel |
| 315 | WiperAssemblies.Steel | 316 | WiperAssemblies.Blade |
| 314 | WiperAssemblies | 319 | CowlVent |
| 320 | Battery | 321 | AirCleanerAssembly |
| 321 | AirCleanerAssembly | 322 | AirCleanerAssembly.Hose |
| 322 | AirCleanerAssembly.Hose | 325 | AirCleanerAssembly.Top |
| 325 | AirCleanerAssembly.Top | 326 | AirCleanerAssembly.Bottom |
| 325 | AirCleanerAssembly.Top | 327 | AirCleanerAssembly.Filter |
| 330 | WasherCoolantBottleAssembly.Rubber | 329 | WasherCoolantBottleAssembly.Bottles |

| | | | |
|---|---|---|---|
| **328** | WasherCoolantBottleAssembly | 330 | WasherCoolantBottleAssembly.Rubber |
| **517** | InstrumentPanel | 332 | HeatBoxAssembly |
| **332** | HeatBoxAssembly | 333 | HeatBoxAssembly.EC |
| **333** | HeatBoxAssembly.EC | 334 | HeatBoxAssembly.LateralCover |
| **334** | HeatBoxAssembly.LateralCover | 335 | HeatBoxAssembly.Elastomer |
| **335** | HeatBoxAssembly.Elastomer | 336 | HeatBoxAssembly.Filter1 |
| **332** | HeatBoxAssembly | 337 | HeatBoxAssembly.SpringHeater |
| **332** | HeatBoxAssembly | 338 | HeatBoxAssembly.Panel1 |
| **338** | HeatBoxAssembly.Panel1 | 341 | HeatBoxAssembly.Duct1 |
| **332** | HeatBoxAssembly | 349 | HeatBoxAssembly.Elastomer2 |
| **341** | HeatBoxAssembly.Duct1 | 350 | HeatBoxAssembly.Fan |
| **350** | HeatBoxAssembly.Fan | 351 | HeatBoxAssembly.Motor |
| **338** | HeatBoxAssembly.Panel1 | 355 | HeatBoxAssembly.Duct2 |
| **336** | HeatBoxAssembly.Filter1 | 358 | HeatBoxAssembly.Box |
| **337** | HeatBoxAssembly.SpringHeater | 358 | HeatBoxAssembly.Box |
| **349** | HeatBoxAssembly.Elastomer2 | 358 | HeatBoxAssembly.Box |
| **351** | HeatBoxAssembly.Motor | 358 | HeatBoxAssembly.Box |
| **355** | HeatBoxAssembly.Duct2 | 358 | HeatBoxAssembly.Box |
| **362** | GasPedalAssembly | 363 | GasPedalAssembly.Steel |
| **363** | GasPedalAssembly.Steel | 364 | GasPedalAssembly.SKOP |
| **517** | InstrumentPanel | 365 | BreakPedalAssembly |
| **365** | BreakPedalAssembly | 366 | BreakPedalAssembly.Bracket |
| **366** | BreakPedalAssembly.Bracket | 367 | BreakPedalAssembly.Rubber |
| **367** | BreakPedalAssembly.Rubber | 368 | BreakPedalAssembly.Base |
| **517** | InstrumentPanel | 369 | SteeringColumnSupport2 |
| **92** | SeatFrontRight | 371 | carpet |
| **117** | SeatFrontLeft | 371 | carpet |
| **159** | APillarTrimLeft | 371 | carpet |
| **162** | APillarTrimRight | 371 | carpet |
| **174** | CPillarLeft | 371 | carpet |
| **175** | CPillarRight | 371 | carpet |
| **181** | BPillarLowerRight | 371 | carpet |
| **182** | BPillarLowerLeft | 371 | carpet |
| **371** | carpet | 372 | carpet.Shoddy |
| **372** | carpet.Shoddy | 373 | carpet.Carpet |
| **371** | carpet | 374 | RearHeaterDuct |
| **537** | InstrumentPanel.GloveBox | 375 | ECU |
| **268** | LowerIPReinforcement2 | 379 | EmergencyBrake |
| **362** | GasPedalAssembly | 380 | FrontInsulator |
| **365** | BreakPedalAssembly | 380 | FrontInsulator |
| **379** | EmergencyBrake | 380 | FrontInsulator |
| **517** | InstrumentPanel | 380 | FrontInsulator |
| **382** | FrontInsulator.SKOS | 381 | FrontInsulator.Shoddy |

| | | | |
|---|---|---|---|
| **380** | FrontInsulator | 382 | FrontInsulator.SKOS |
| **320** | Battery | 383 | BatteryCase |
| **384** | BrakeBooster | 388 | FirewallInsulation |
| **485** | DriveTrain | 388 | FirewallInsulation |
| **392** | CoolingFanModule | 401 | EngineHarness |
| **395** | AirBagSensor | 401 | EngineHarness |
| **485** | DriveTrain | 401 | EngineHarness |
| **485** | DriveTrain | 405 | ACManifold |
| **413** | WheelHouseLinerFrontRight | 414 | WheelHouseLinerFrontRight.SKOS |
| **414** | WheelHouseLinerFrontRight.SKOS | 415 | WheelHouseLinerFrontRight.PP |
| **416** | WheelHouseLinerFrontLeft | 417 | WheelHouseLinerFrontLeft.SKOS |
| **417** | WheelHouseLinerFrontLeft.SKOS | 418 | WheelHouseLinerFrontLeft.PP |
| **416** | WheelHouseLinerFrontLeft | 420 | VacuumTank |
| **426** | WheelRearRight | 428 | WheelRearRight.Rim |
| **428** | WheelRearRight.Rim | 429 | WheelRearRight.Rubber |
| **430** | WheelRearLeft | 432 | WheelRearLeft.Rim |
| **432** | WheelRearLeft.Rim | 433 | WheelRearLeft.Rubber |
| **371** | carpet | 434 | WireHarnessCover |
| **370** | TrunkReleaseCase | 435 | TrunkRelease |
| **434** | WireHarnessCover | 435 | TrunkRelease |
| **434** | WireHarnessCover | 438 | WireHarness |
| **319** | CowlVent | 442 | WindshieldWiperMotor |
| **142** | RearViewMirror | 448 | FrontClip |
| **180** | Headliner | 448 | FrontClip |
| **213** | KickPanelRight | 448 | FrontClip |
| **214** | KickPanelLeft | 448 | FrontClip |
| **277** | SteeringColumnAssembly | 448 | FrontClip |
| **298** | WeatherStripping | 448 | FrontClip |
| **313** | WiringHarnessCloseOut | 448 | FrontClip |
| **321** | AirCleanerAssembly | 448 | FrontClip |
| **328** | WasherCoolantBottleAssembly | 448 | FrontClip |
| **331** | HeatBoxAssemblyBase | 448 | FrontClip |
| **332** | HeatBoxAssembly | 448 | FrontClip |
| **369** | SteeringColumnSupport2 | 448 | FrontClip |
| **371** | carpet | 448 | FrontClip |
| **389** | CoolingFanShroudAssembly | 449 | FrontClip.RadiatorHeatExchanger |
| **392** | CoolingFanModule | 449 | FrontClip.RadiatorHeatExchanger |
| **449** | FrontClip.RadiatorHeatExchanger | 460 | FrontClip.ACCondensor |
| **476** | FrontClip.FasciaFrontLower | 465 | FrontClip.LightFrontAssembly |
| **477** | FrontClip.FasciaFrontUpper | 465 | FrontClip.LightFrontAssembly |
| **476** | FrontClip.FasciaFrontLower | 477 | FrontClip.FasciaFrontUpper |
| **476** | FrontClip.FasciaFrontLower | 478 | FrontClip.EnergyAbsorberFrontRight |
| **476** | FrontClip.FasciaFrontLower | 479 | FrontClip.EnergyAbsorberFrontLeft |

| | | | |
|---|---|---|---|
| 448 | FrontClip | 484 | FrontClip.Frame |
| 449 | FrontClip.RadiatorHeatExchanger | 484 | FrontClip.Frame |
| 460 | FrontClip.ACCondensor | 484 | FrontClip.Frame |
| 463 | FrontClip.MarkerLightFrontLeft | 484 | FrontClip.Frame |
| 464 | FrontClip.MarkerLightFrontRight | 484 | FrontClip.Frame |
| 465 | FrontClip.LightFrontAssembly | 484 | FrontClip.Frame |
| 477 | FrontClip.FasciaFrontUpper | 484 | FrontClip.Frame |
| 478 | FrontClip.EnergyAbsorberFrontRight | 484 | FrontClip.Frame |
| 485 | DriveTrain | 486 | DriveTrain.ACCompressor |
| 485 | DriveTrain | 497 | DriveTrain.Starter |
| 485 | DriveTrain | 501 | DriveTrain.Engine |
| 501 | DriveTrain.Engine | 505 | DriveTrain.Transmission |
| 505 | DriveTrain.Transmission | 508 | DriveTrain.CradleSuspension |
| 509 | WheelFrontRight | 508 | DriveTrain.CradleSuspension |
| 512 | WheelFrontRight.Tire | 508 | DriveTrain.CradleSuspension |
| 509 | WheelFrontRight | 511 | WheelFrontRight.Rim |
| 511 | WheelFrontRight.Rim | 512 | WheelFrontRight.Tire |
| 513 | WheelFrontLeft | 515 | WheelFrontLeft.Rim |
| 515 | WheelFrontLeft.Rim | 516 | WheelFrontLeft.Tire |
| 264 | LowerIP | 517 | InstrumentPanel |
| 277 | SteeringColumnAssembly | 517 | InstrumentPanel |
| 313 | WiringHarnessCloseOut | 517 | InstrumentPanel |
| 517 | InstrumentPanel | 518 | InstrumentPanel.DuctWork |
| 518 | InstrumentPanel.DuctWork | 519 | InstrumentPanel.EvapDuct |
| 519 | InstrumentPanel.EvapDuct | 520 | InstrumentPanel.DuctWork2 |
| 520 | InstrumentPanel.DuctWork2 | 521 | InstrumentPanel.Hoses |
| 521 | InstrumentPanel.Hoses | 522 | InstrumentPanel.WireHarness |
| 520 | InstrumentPanel.DuctWork2 | 526 | InstrumentPanel.DashBrain |
| 520 | InstrumentPanel.DuctWork2 | 527 | InstrumentPanel.Dimmer |
| 530 | InstrumentPanel.Radio | 533 | InstrumentPanel.TrayAssembly |
| 534 | InstrumentPanel.ClusterBezel | 535 | InstrumentPanel.Cluster |
| 534 | InstrumentPanel.ClusterBezel | 536 | InstrumentPanel.HeaterControl |
| 522 | InstrumentPanel.WireHarness | 543 | InstrumentPanel.Ashtray |
| 533 | InstrumentPanel.TrayAssembly | 543 | InstrumentPanel.Ashtray |
| 543 | InstrumentPanel.Ashtray | 546 | InstrumentPanel.CenterBezel |
| 522 | InstrumentPanel.WireHarness | 547 | InstrumentPanel.Clock |
| 522 | InstrumentPanel.WireHarness | 548 | InstrumentPanel.AirBagPassenger |
| 551 | InstrumentPanel.AirBagCover | 548 | InstrumentPanel.AirBagPassenger |
| 517 | InstrumentPanel | 552 | InstrumentPanel.Frame |
| 526 | InstrumentPanel.DashBrain | 552 | InstrumentPanel.Frame |
| 527 | InstrumentPanel.Dimmer | 552 | InstrumentPanel.Frame |
| 535 | InstrumentPanel.Cluster | 552 | InstrumentPanel.Frame |
| 536 | InstrumentPanel.HeaterControl | 552 | InstrumentPanel.Frame |

| | | | |
|---|---|---|---|
| **537** | InstrumentPanel.GloveBox | 552 | InstrumentPanel.Frame |
| **546** | InstrumentPanel.CenterBezel | 552 | InstrumentPanel.Frame |
| **547** | InstrumentPanel.Clock | 552 | InstrumentPanel.Frame |
| **548** | InstrumentPanel.AirBagPassenger | 552 | InstrumentPanel.Frame |
| **552** | InstrumentPanel.Frame | 553 | InstrumentPanel.Skin |
| **1** | DoorFrontRight | 600 | RearFrame |
| **28** | DoorFrontLeft | 600 | RearFrame |
| **56** | DoorRearRight | 600 | RearFrame |
| **74** | DoorRearLeft | 600 | RearFrame |
| **180** | Headliner | 600 | RearFrame |
| **201** | BPillarShoddyRight | 600 | RearFrame |
| **204** | BPillarShoddyLeft | 600 | RearFrame |
| **207** | QuartertrimRight | 600 | RearFrame |
| **210** | QuartertrimLeft | 600 | RearFrame |
| **213** | KickPanelRight | 600 | RearFrame |
| **214** | KickPanelLeft | 600 | RearFrame |
| **229** | ParcelTrayShoddy | 600 | RearFrame |
| **230** | BackSeatShoddy | 600 | RearFrame |
| **448** | FrontClip | 600 | RearFrame |
| **600** | RearFrame | 601 | RearFrame.A |
| **601** | RearFrame.A | 602 | RearFrame.B |
| **310** | DeckLid | 605 | DeckLid.Hinge |

*Table B- 3 Optimization results (list of parts removed, their resale values and removal costs)*

| Part ID | Part Name | Resale Value ($) | Removal Time (s) | Removal Cost($) |
|---|---|---|---|---|
| **501** | DriveTrain.Engine | 730 | 1519 | 3.80 |
| **505** | DriveTrain.Transmission | 478 | 240 | 0.60 |
| **508** | DriveTrain.CradleSuspension | 459 | 1 | 0.0025 |
| **28** | DoorFrontLeft | 450 | 33 | 0.08 |
| **1** | DoorFrontRight | 450 | 33 | 0.08 |
| **56** | DoorRearRight | 425 | 21 | 0.05 |
| **74** | DoorRearLeft | 425 | 21 | 0.05 |
| **476** | FrontClip.FasciaFrontLower | 225 | 115 | 0.29 |
| **481** | FrontClip.Hood | 200 | 100 | 0.25 |
| **277** | SteeringColumnAssembly | 200 | 140 | 0.35 |
| **307** | FasciaRearlower | 200 | 117 | 0.29 |
| **310** | DeckLid | 163 | 110 | 0.27 |
| **535** | InstrumentPanel.Cluster | 125 | 15 | 0.04 |
| **530** | InstrumentPanel.Radio | 125 | 232 | 0.58 |
| **321** | AirCleanerAssembly | 113 | 21 | 0.05 |
| **449** | FrontClip.RadiatorHeatExchanger | 85 | 164 | 0.41 |

| | | | | |
|---|---|---|---|---|
| **515** | WheelFrontLeft.Rim | 85 | 126 | 0.32 |
| **389** | CoolingFanShroudAssembly | 70 | 17 | 0.04 |
| **302** | TailLightCoverLeft | 65 | 91 | 0.23 |
| **299** | TailLightCoverRight | 65 | 91 | 0.23 |
| **117** | SeatFrontLeft | 50 | 91 | 0.23 |
| **92** | SeatFrontRight | 50 | 91 | 0.23 |
| **281** | SteeringColumnAssembly.Base | 50 | 0 | 0.00 |
| **479** | FrontClip.EnergyAbsorberFrontLeft | 45 | 44 | 0.11 |
| **432** | WheelRearLeft.Rim | 45 | 126 | 0.32 |
| **384** | BrakeBooster | 45 | 100 | 0.25 |
| **428** | WheelRearRight.Rim | 45 | 126 | 0.32 |
| **241** | SeatBeltRearLeft | 40 | 47 | 0.12 |
| **192** | SeatBeltFrontLeft | 40 | 12 | 0.03 |
| **183** | SeatBeltFrontRight | 40 | 12 | 0.03 |
| **259** | SeatbeltRearLeftLower | 40 | 8 | 0.02 |
| **442** | WindshieldWiperMotor | 40 | 30 | 0.08 |
| **308** | EnergyAbsorberRearLeft | 40 | 25 | 0.06 |
| **309** | EnergyAbsorberRearRight | 40 | 35 | 0.09 |
| **351** | HeatBoxAssembly.Motor | 28 | 60 | 0.15 |
| **143** | SeatRearBottom | 25 | 43 | 0.11 |
| **320** | Battery | 20 | 48 | 0.12 |
| **332** | HeatBoxAssembly | 20 | 780 | 1.95 |
| **463** | FrontClip.MarkerLightFrontLeft | 17 | 80 | 0.20 |
| **464** | FrontClip.MarkerLightFrontRight | 17 | 40 | 0.10 |
| **429** | WheelRearRight.Rubber | 0 | 1 | 0.00 |
| **430** | WheelRearLeft | 0 | 15 | 0.04 |
| **433** | WheelRearLeft.Rubber | 0 | 1 | 0.00 |
| **485** | DriveTrain | 0 | 1750 | 4.38 |
| **426** | WheelRearRight | 0 | 15 | 0.04 |
| **513** | WheelFrontLeft | 0 | 15 | 0.04 |
| **516** | WheelFrontLeft.Tire | 0 | 1 | 0.00 |
| **517** | InstrumentPanel | 0 | 825 | 2.06 |
| **534** | InstrumentPanel.ClusterBezel | 0 | 97 | 0.24 |
| **552** | InstrumentPanel.Frame | 0 | 76 | 0.19 |
| **361** | HeatBoxAssembly.Box.PP | 0 | 0 | 0.00 |
| **360** | HeatBoxAssembly.Box.Filter2 | 0 | 600 | 1.50 |
| **358** | HeatBoxAssembly.Box | 0 | 0 | 0.00 |
| **313** | WiringHarnessCloseOut | 0 | 7 | 0.02 |
| **350** | HeatBoxAssembly.Fan | 0 | 30 | 0.08 |
| **222** | ParcelTray | 0 | 23 | 0.06 |
| **173** | SeatbeltFrontLeftCover | 0 | 2 | 0.01 |
| **176** | SeatbeltFrontRightCover | 0 | 7 | 0.02 |

| | | | | |
|---|---|---|---|---|
| **177** | BPillarUpperRight | 0 | 13 | 0.03 |
| **179** | BPillarUpperLeft | 0 | 10 | 0.03 |
| **181** | BPillarLowerRight | 0 | 65 | 0.16 |
| **182** | BPillarLowerLeft | 0 | 43 | 0.11 |
| **201** | BPillarShoddyRight | 0 | 2 | 0.01 |
| **202** | BPillarShoddyRight.Shoddy | 0 | 23 | 0.06 |
| **203** | BPillarShoddyRight.SKOP | 0 | 0 | 0.00 |
| **204** | BPillarShoddyLeft | 0 | 2 | 0.01 |
| **205** | BPillarShoddyLeft.Shoddy | 0 | 23 | 0.06 |
| **206** | BPillarShoddyLeft.SKOP | 0 | 0 | 0.00 |
| **221** | SpeakerCovers | 0 | 3 | 0.01 |
| **242** | SeatBeltRearLeft.Steelcase | 0 | 0 | 0.00 |
| **341** | HeatBoxAssembly.Duct1 | 0 | 60 | 0.15 |
| **245** | SeatBeltRearLeft.Strap | 0 | 5 | 0.01 |
| **247** | SeatBeltRearLeft.Other | 0 | 4 | 0.01 |
| **250** | SeatBeltRearLeft.Lead | 0 | 25 | 0.06 |
| **260** | SeatbeltRearLeftLower.Strap | 0 | 0 | 0.00 |
| **264** | LowerIP | 0 | 60 | 0.15 |
| **267** | LowerIPReinforcement | 0 | 8 | 0.02 |
| **268** | LowerIPReinforcement2 | 0 | 44 | 0.11 |
| **275** | SteeringColumnTurnSignal | 0 | 25 | 0.06 |
| **276** | SteeringColumnLowerPanel | 0 | 125 | 0.31 |
| **314** | WiperAssemblies | 0 | 14 | 0.03 |
| **319** | CowlVent | 0 | 73 | 0.18 |
| **322** | AirCleanerAssembly.Hose | 0 | 10 | 0.03 |
| **338** | HeatBoxAssembly.Panel1 | 0 | 10 | 0.03 |
| **553** | InstrumentPanel.Skin | 0 | 0 | 0.00 |

# Appendix C Markov-Chain formulation for separation networks

We consider the passage of a material particle throughout a separation network configuration of $m$ units (sorting and output units, including landfill) as a Markov Chain with $m$ states. This Markov Chain is described in terms of its transition probabilities $p_{ij}$ from unit $i$ to unit $j$. The Markov Chain consists of the sorting units as transient states and of output collection units as absorbing states, i.e. these states are infinitely repeated once they are reached. We are interested in the short-term behavior of the Markov Chain, i.e. the absorption probability $a_i$ that a target material eventually reaches the target output stream V0, given that it enters the system from unit $i$, i.e its initial state $X$ at time step $t$=0 is unit $i$ or $X_0 = i$. $a_i$ is defined as follows:

$$a_i = P(X_n \; eventually \; becomes \; equal \; to \; absorbing \; state \; s | X_0 = i)$$

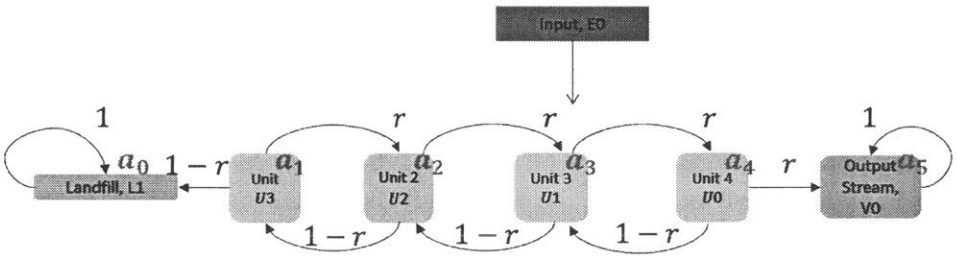


*Figure C- 1 Design 1 (random-walk) of separation network with 4 sorting units*

We have the following absorption probability equations for the configuration of Figure C- 1, with absorbing state $s$ being Outputstream V0 :

$a_5 = 1$, for the target absorbing state at V0

$a_0 = 0$, for absorbing state at the landfill

$a_i = \sum_{j=1}^{5} p_{ij} a_j$ for transient states units U3-U0.

For the 4 unknowns we can solve the above system of equations easily by putting in matrix form :

$$a = Qa + b \rightarrow (I - Q)a = b \rightarrow a = (I - Q)^{-1} b$$

Where

$$Q = \begin{array}{c} \\ a_0 \\ a_1 \\ a_2 \\ a_3 \\ a_4 \\ a_5 \end{array} \begin{array}{c} \begin{array}{cccccc} a_0 & a_1 & a_2 & a_3 & a_4 & a_5 \end{array} \\ \begin{bmatrix} 0 & 0 & 0 & 0 & 0 & 0 \\ 1-r & 0 & r & 0 & 0 & 0 \\ 0 & 1-r & 0 & r & 0 & 0 \\ 0 & 0 & 1-r & 0 & r & 0 \\ 0 & 0 & 0 & 1-r & 0 & r \\ 0 & 0 & 0 & 0 & 0 & 0 \end{bmatrix} \end{array}; \; b = \begin{pmatrix} 0 \\ 0 \\ 0 \\ 0 \\ 0 \\ 1 \end{pmatrix}$$

For the configuration in Figure C- 1, where recirculation occurs to the prior unit and all units have the same separation efficiency $r$, an analytical solution for $a$ can be obtained as follows:

Using $\delta_i = a_{i+1} - a_i$ and $\rho = \frac{1-r}{r}$:

$$\delta_i = \rho\delta_{i-1}$$

Since $\delta_0 + \cdots + \delta_4 = a_5 - a_0 = 1 - 0$,

$$\delta_0(1 + \rho + \rho^2 + \cdots + \rho^4) = 1$$

$$\delta_0 = \frac{1}{(1 + \rho + \rho^2 + \cdots + \rho^4)}$$

Since $a_i = \delta_0 + \cdots + \delta_{i-1}$,

$$a_i = \delta_0(1 + \rho + \cdots + \rho^{i-1}) = \frac{\delta_0(1 + \rho + \cdots + \rho^{i-1})}{(1 + \rho + \rho^2 + \cdots + \rho^4)}$$

Since $\sum_{j=0}^{i} \rho^j = \frac{1-\rho^{i-1}}{1-\rho}$,

$$a_i = \frac{1 - \rho^{i-1}}{1 - \rho^m} \; if \; \rho \neq 1$$

$$= \frac{i}{m} \qquad if \; \rho = 1$$

The absorption probability $a_i$ gives the recovery rate if the input stream is connected to unit $i$:

$$recovery = a_{input\ i}$$

For $i$ as the unit with the input stream, we can calculate the grade in target output stream as:

$$grade = \frac{a_i \gamma_{target}}{a_i \gamma_{target} + \beta_i \gamma_{non-target}}$$

Where $\gamma_{target}$, $\gamma_{non-target}$ are the input mass of the target and non-target material respectively, $\beta_i$ is the absorption probability of the non-target material wrongly into the target stream for the same input stream connection to unit $i$.

$\beta_i$ can be obtained by considering a same Markov Chain and absorbing state V0 as the target material's, except that $r$ is now replaced with $1 - q = 1 - r$ (see Figure C- 2) assuming $q = r$, i.e. same separation efficiency for the target and non-target material.

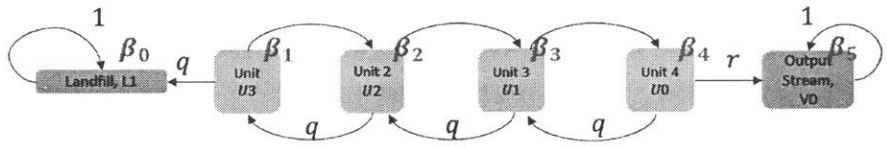


*Figure C- 2 Markov Chain for non-target material, for which the units have separation efficiency q, for same separation configuration as in Figure C- 1*

By solving the system of linear equations $a = (I - Q)^{-1}b$, we can calculate the recovery rate and grade of the output stream for the different scenarios of where the input stream connects. Thus, we can build the Pareto curve of Figure 6.2(right).

We now consider alternative designs: design 2 where recirculation is upstream towards landfill, and design 3 where recirculation is downstream towards the output stream. The transition probabilities are different, with the new $Q$ matrix given by:

$$Q_{\text{design 2}} = \begin{array}{c} \\ a_0 \\ a_1 \\ a_2 \\ a_3 \\ a_4 \\ a_5 \end{array} \begin{array}{c} \begin{array}{cccccc} a_0 & a_1 & a_2 & a_3 & a_4 & a_5 \end{array} \\ \begin{bmatrix} 0 & 0 & 0 & 0 & 0 & 0 \\ 1-r & 0 & r & 0 & 0 & 0 \\ 0 & 1-r & 0 & r & 0 & 0 \\ 0 & 1-r & 0 & 0 & r & 0 \\ 0 & 1-r & 0 & 0 & 0 & r \\ 0 & 0 & 0 & 0 & 0 & 0 \end{bmatrix} \end{array} ; \quad Q_{design\ 3} = \begin{array}{c} \\ a_0 \\ a_1 \\ a_2 \\ a_3 \\ a_4 \\ a_5 \end{array} \begin{array}{c} \begin{array}{cccccc} a_0 & a_1 & a_2 & a_3 & a_4 & a_5 \end{array} \\ \begin{bmatrix} 0 & 0 & 0 & 0 & 0 & 0 \\ 1-r & 0 & 0 & 0 & r & 0 \\ 0 & 1-r & 0 & 0 & r & 0 \\ 0 & 0 & 1-r & 0 & r & 0 \\ 0 & 0 & 0 & 1-r & 0 & r \\ 0 & 0 & 0 & 0 & 0 & 0 \end{bmatrix} \end{array}$$

The new system of linear equations can be solved to obtain the other 2 Pareto curves of Figure 6.2(right).

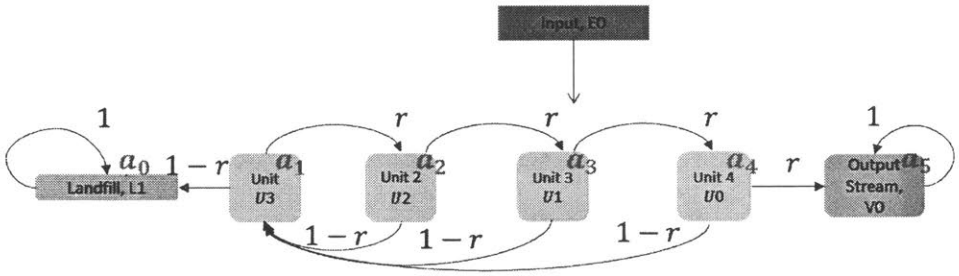


*Figure C- 3 Design 2 (recirculation upstream towards landfill) of separation network with 4 sorting units*

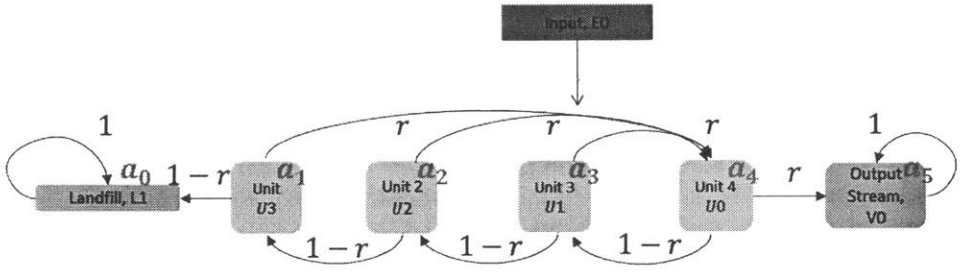


*Figure C- 4 Design 3 (recirculation downstream towards output stream) of separation network with 4 sorting units*

# Bibliography


[1] S. Sakai *et al.*, "An international comparative study of end-of-life vehicle (ELV) recycling systems," *J. Mater. Cycles Waste Manag.*, vol. 16, no. 1, pp. 1–20, Feb. 2014.

[2] H. C. Kim and T. J. Wallington, "Life-Cycle Energy and Greenhouse Gas Emission Benefits of Lightweighting in Automobiles: Review and Harmonization," *Environ. Sci. Technol.*, vol. 47, no. 12, pp. 6089–6097, Jun. 2013.

[3] J. L. Sullivan and J. Hu, "Life Cycle Energy Analysis for Automobiles," presented at the 1995 Total Life Cycle Conference and Exposition, 1995, p. 951829.

[4] J. B. Dahmus and T. G. Gutowski, "What Gets Recycled: An Information Theory Based Model for Product Recycling," *Environ. Sci. Technol.*, vol. 41, no. 21, pp. 7543–7550, Nov. 2007.

[5] E. Brahmst, "Copper in end-of-life vehicle recycling," *Cent. Automot. Res. Ann Arbor Mich.*, 2006.

[6] S. Keeler and M. Kimchi, *Advanced high-strength steels application guidelines V5*. WorldAutoSteel, 2015.

[7] S. S. Sawyer-Beaulieu, "Gate-to-gate life cycle inventory assessment of North American end-of-life vehicle management processes.," PhD Thesis, University of Windsor, Ottawa, 2009.

[8] S. A. H. Scottish Government, "Remanufacture, refurbishment, reuse and recycling of vehicles: Trends and Opportunities," Scottish Government, St. Andrew's House, Regent Road, Edinburgh EH1 3DG Tel:0131 556 8400 ceu@scotland.gsi.gov.uk, Report, Dec. 2013.

[9] F. Cucchiella, I. D'Adamo, P. Rosa, and S. Terzi, "Scrap automotive electronics: A mini-review of current management practices," *Waste Manag. Res.*, vol. 34, no. 1, pp. 3–10, 2016.

[10] S. Belboom, G. Lewis, P.-F. Bareel, and A. Léonard, "Life cycle assessment of hybrid vehicles recycling: Comparison of three business lines of dismantling," *Waste Manag.*, vol. 50, pp. 184–193, Apr. 2016.

[11] R. Cossu and T. Lai, "Automotive shredder residue (ASR) management: An overview," *Waste Manag.*, vol. 45, pp. 143–151, Nov. 2015.

[12] L. Miller, K. Soulliere, S. Sawyer-Beaulieu, S. Tseng, and E. Tam, "Challenges and Alternatives to Plastics Recycling in the Automotive Sector," *Materials*, vol. 7, no. 8, pp. 5883–5902, Aug. 2014.

[13] European Commission - DG Environment, "Ex-post evaluation of certain waste stream Directives," Apr. 2014.

[14] M. Andersson, M. Ljunggren Söderman, and B. A. Sandén, "Lessons from a century of innovating car recycling value chains," *Environ. Innov. Soç. Transit.*, vol. 25, pp. 142–157, Dec. 2017.

[15] S. Cassells, J. Holland, and A. Meister, "End-of-life vehicle disposal: Policy proposals to resolve an environmental issue in New Zealand," *J. Environ. Policy Plan.*, vol. 7, no. 2, pp. 107–124, Jun. 2005.

[16] G. Coates and S. Rahimifard, "Cost models for increased value recovery from end-of-life vehicles," in *Proceedings of CIRP Life Cycle Engineering Conference*, 2006, vol. 2006, pp. 347–352.

[17] G. Coates and S. Rahimifard, "Assessing the economics of pre-fragmentation material recovery within the UK," *Resour. Conserv. Recycl.*, vol. 52, no. 2, pp. 286–302, Dec. 2007.

[18] Coulter, S., Bras, B., G. Winslow, and Yester, S., "Designing for material separation: lessons from automotive recycling," 1998.

[19] J. de Aguiar, L. de Oliveira, J. O. da Silva, D. Bond, R. K. Scalice, and D. Becker, "A design tool to diagnose product recyclability during product design phase," *J. Clean. Prod.*, vol. 141, pp. 219–229, Jan. 2017.

[20] G. Dini, F. Failli, and M. Santochi, "A disassembly planning software system for the optimization of recycling processes," *Prod. Plan. Control*, vol. 12, no. 1, pp. 2–12, Jan. 2001.

[21] Richard T. Paul, Dennis Chung, and David W. Raney, "Actual Recylability of Selected Honda Vehicles," *SAE Tech. Pap.*, no. No. 2004-01-0246, 2004.

[22] Zamudio-Ramirez, Pavel, "Economics of automobile recycling," SM Thesis, Massachusetts Institute of Technology, 1996.
[23] Spicer, Andrew James, "Disassembly modeling and analysis," SM Thesis, University of Windsor, 1996.
[24] C. Duranceau and T. Lindell, "Automotive recycling as reuse: investigation to establish the contribution of reuse on recyclability," SAE Technical Paper, 1999.
[25] A. Santini, L. Morselli, F. Passarini, I. Vassura, S. Di Carlo, and F. Bonino, "End-of-Life Vehicles management: Italian material and energy recovery efficiency," *Waste Manag.*, vol. 31, no. 3, pp. 489–494, Mar. 2011.
[26] E. El Halabi, M. Third, and M. Doolan, "Machine-based dismantling of end of life vehicles: A life cycle perspective," *Procedia Cirp*, vol. 29, pp. 651–655, 2015.
[27] R. Kirchain, "Modeling methods for complex manufacturing systems studying the effects of materials substitution on the automobile recycling infrastructure," Doctoral Dissertation, Massachusetts Institute of Technology, 1999.
[28] C. M. Duranceau and J. S. Spangenberger, "All auto shredding: evaluation of automotive shredder residue generated by shredding only vehicles.," Argonne National Lab.(ANL), Argonne, IL (United States), 2011.
[29] L. Aboussouan, P. Russo, M. N. Pons, D. Thomas, J. P. Birat, and D. Leclerc, "Steel scrap fragmentation by shredders," *Powder Technol.*, vol. 105, no. 1–3, pp. 288–294, 1999.
[30] Edwin K.L. Tam and Lawrence J. Jekel, "Separation and Liberation Factors in Designing for Automotive Materials Recovery," no. 2004-1–471, 2004.
[31] J. A. Stagner, B. Sagan, and E. K. Tam, "Using sieving and pretreatment to separate plastics during end-of-life vehicle recycling," *Waste Manag. Res.*, vol. 31, no. 9, pp. 920–924, 2013.
[32] D. Bruyère, S. Simon, H. Haas, T. Conte, and N.-E. Menad, "Cryogenic ball milling: A key for elemental analysis of plastic-rich automotive shedder residue," *Powder Technol.*, vol. 294, pp. 454–462, Jun. 2016.
[33] J. Kirchner, G. Timmer, and G. Schubert, "Comminution of metals in shredders with horizonally and vertically mounted rotors- microprecesses and parameters," *Powder Technol.*, vol. 105.1-3, pp. 274–281, 1999.
[34] J. Lee, K. Kim, H. Cho, J. Ok, and S. Kim, "Shredding and liberation characteristics of refrigerators and small appliances," *Waste Manag.*, vol. 59, pp. 409–421, Jan. 2017.
[35] L. Jianxiong, P. Juntao, Y. Bangcheng, and H. Jie, "The Research on Shredding Models of Light Metal Scrap of End-of-life Vehicles and Household Appliances," *IERI Procedia*, vol. 1, pp. 146–154, 2012.
[36] S. Luo, B. Xiao, Z. Hu, S. Liu, and X. Guo, "An experimental study on a novel shredder for municipal solid waste (MSW)," *Int. J. Hydrog. Energy*, vol. 34, no. 3, pp. 1270–1274, Feb. 2009.
[37] J. Oberteuffer, "Magnetic separation: A review of principles, devices, and applications," *IEEE Trans. Magn.*, vol. 10, no. 2, pp. 223–238, 1974.
[38] Steinert, "Shredder scrap." [Online]. Available: https://steinertglobal.com/au/metal-recycling/shredder-scrap/. [Accessed: 06-Oct-2018].
[39] S. Zhang, E. Forssberg, B. Arvidson, and W. Moss, "Separation mechanisms and criteria of a rotating eddy-current separator operation," *Resour. Conserv. Recycl.*, vol. 25, no. 3, pp. 215–232, 1999.
[40] S. C. Koermer, "The Application of Mineral Processing Techniques to the Scrap Recycling Industry," Virginia Tech, 2015.
[41] U.S. Environmental Protection Agency, "AP-42 Compilation of air pollutant emission factors Volume I: Stationary point and area sources," Jan. 1995.
[42] G. Gaustad, E. Olivetti, and R. Kirchain, "Improving aluminum recycling: A survey of sorting and impurity removal technologies," *Resour. Conserv. Recycl.*, vol. 58, pp. 79–87, Jan. 2012.
[43] S. M. Kelly, "Recycling of Passenger Vehicles: A framework for upcycling and required enabling technologies," PhD Thesis, Worchester Polytechnic Institute, 2018.

[44] I. Vermeulen, J. Van Caneghem, C. Block, J. Baeyens, and C. Vandecasteele, "Automotive shredder residue (ASR): Reviewing its production from end-of-life vehicles (ELVs) and its recycling, energy or chemicals' valorisation," *J. Hazard. Mater.*, vol. 190, no. 1–3, pp. 8–27, Jun. 2011.
[45] L. Muchová, P. Eder, and Institute for Prospective Technological Studies, *End-of-waste criteria for aluminium and aluminium alloy scrap: technical proposals.* Luxembourg: Publications Office, 2010.
[46] ISRI, "Scrap Specifications Circular 2016." 2016.
[47] Metal Bulletin, "Ferrous scrap indices- Methodology and price specifications - January 2019," 2019.
[48] B. J. Jody and E. J. Daniels, "End-of-life vehicle recycling state of the art of resource recovery from shredder residue," Argonne National Laboratory (ANL), No. ANL/ESD/07-8, 2007.
[49] Y. W. Huang, M. Q. Chen, Q. H. Li, and W. Xing, "A critical evaluation on chemical exergy and its correlation with high heating value for single and multi-component typical plastic wastes," *Energy*, vol. 156, pp. 548–554, Aug. 2018.
[50] E. Sandberg, "Energy and scrap optimisation of electric arc furnaces by statistical analysis of process data," PhD Thesis, Lule\a a tekniska universitet, 2005.
[51] R. D. Peterson, "Recycling of Automotive Wrought Alloys," in *Light Metals 2015*, Springer, 2015, pp. 1023–1028.
[52] R. Modaresi, A. N. Løvik, and D. B. Müller, "Component- and Alloy-Specific Modeling for Evaluating Aluminum Recycling Strategies for Vehicles," *JOM*, vol. 66, no. 11, pp. 2262–2271, Nov. 2014.
[53] A. Rong and R. Lahdelma, "Fuzzy chance constrained linear programming model for optimizing the scrap charge in steel production," *Eur. J. Oper. Res.*, vol. 186, no. 3, pp. 953–964, May 2008.
[54] S. Nakamura, Y. Kondo, K. Matsubae, K. Nakajima, T. Tasaki, and T. Nagasaka, "Quality- and Dilution Losses in the Recycling of Ferrous Materials from End-of-Life Passenger Cars: Input-Output Analysis under Explicit Consideration of Scrap Quality," *Environ. Sci. Technol.*, vol. 46, no. 17, pp. 9266–9273, Sep. 2012.
[55] George C. Wang, *The utilization of slag in civil infrastructure constructionmetal production and ferrous slags*. Woodhead Publishing, 2016.
[56] K. Nakajima, O. Takeda, T. Miki, K. Matsubae, S. Nakamura, and T. Nagasaka, "Thermodynamic analysis of contamination by alloying elements in aluminum recycling," *Environ. Sci. Technol.*, vol. 44, no. 14, pp. 5594–5600, 2010.
[57] M. B. G. Castro, J. A. M. Remmerswaal, M. A. Reuter, and U. J. M. Boin, "A thermodynamic approach to the compatibility of materials combinations for recycling," *Resour. Conserv. Recycl.*, vol. 43, no. 1, pp. 1–19, Dec. 2004.
[58] K. Nakajima, O. Takeda, T. Miki, K. Matsubae, and T. Nagasaka, "Thermodynamic Analysis for the Controllability of Elements in the Recycling Process of Metals," *Environ. Sci. Technol.*, vol. 45, no. 11, pp. 4929–4936, Jun. 2011.
[59] K. Nakajima *et al.*, "Simultaneous Material Flow Analysis of Nickel, Chromium, and Molybdenum Used in Alloy Steel by Means of Input–Output Analysis," *Environ. Sci. Technol.*, vol. 47, no. 9, pp. 4653–4660, May 2013.
[60] B. L. Bramfitt and A. O. Benscoter, *Metallographer's guide: practice and procedures for irons and steels*. Asm International, 2001.
[61] A. Gesing and R. Wolanski, "Recycling light metals from end-of-life vehicle," *JOM*, vol. 53, no. 11, pp. 21–23.
[62] A. Xanthopoulos and E. Iakovou, "On the optimal design of the disassembly and recovery processes," *Waste Manag.*, vol. 29, no. 5, pp. 1702–1711, May 2009.
[63] R. H. Teunter, "Determining optimal disassembly and recovery strategies," *Omega*, vol. 34, no. 6, pp. 533–537, 2006.
[64] K. Feldmann, S. Trautner, and O. Meedt, "Innovative disassembly strategies based on flexible partial destructive tools," *Annu. Rev. Control*, vol. 23, pp. 159–164, 1999.

[65] J. Reap and B. Bras, "Design for disassembly and the value of robotic semi-destructive disassembly," in *ASME 2002 International Design Engineering Technical Conferences and Computers and Information in Engineering Conference*, 2002, pp. 275–281.
[66] H. Klindworth, C. Otto, and A. Scholl, "On a learning precedence graph concept for the automotive industry," *Eur. J. Oper. Res.*, vol. 217, no. 2, pp. 259–269, Mar. 2012.
[67] N. S. Ong and Y. C. Wong, "Automatic subassembly detection from a product model for disassembly sequence generation," *Int. J. Adv. Manuf. Technol.*, vol. 15, no. 6, pp. 425–431, 1999.
[68] M. L. Bentaha, A. Dolgui, O. Battaïa, R. J. Riggs, and J. Hu, "Profit-oriented partial disassembly line design: dealing with hazardous parts and task processing times uncertainty," *Int. J. Prod. Res.*, pp. 1–23, Jan. 2018.
[69] L. Cong, F. Zhao, and J. W. Sutherland, "Value recovery from end-of-use products facilitated by automated dismantling planning," *Clean Technol. Environ. Policy*, vol. 19, no. 7, pp. 1867–1882, Sep. 2017.
[70] A. J. D. Lambert, "Disassembly sequencing: A survey," *Int. J. Prod. Res.*, vol. 41, no. 16, pp. 3721–3759, Jan. 2003.
[71] M.E. Salveson, "The assembly-line balancing problem," *Trans. ASME*, vol. 77, pp. 939–948, 1955.
[72] N. Boysen, M. Fliedner, and A. Scholl, "A classification of assembly line balancing problems," *Eur. J. Oper. Res.*, vol. 183, no. 2, pp. 674–693, Dec. 2007.
[73] K. E. Moore, A. Gungor, and S. M. Gupta, "Disassembly process planning using Petri nets," in *Electronics and the Environment, 1998. ISEE-1998. Proceedings of the 1998 IEEE International Symposium on*, 1998, pp. 88–93.
[74] S. Gupta and Askiner Gungor, "Disassembly Line Balancing," in *Proceedings of the 1999 Annual Meeting of the Northeast Decision Sciences Insititute*, Newport, Rhode Island, 1999, pp. 193–195.
[75] Surendra M. Gupta and Askiner Gungor, "Product recovery using a disassembly line: challenges and solution," in *IEEE Proceedings of the 2001 IEEE International Symposium on*, 2001.
[76] R. J. Riggs, O. Battaïa, and S. J. Hu, "Disassembly line balancing under high variety of end of life states using a joint precedence graph approach," *J. Manuf. Syst.*, vol. 37, pp. 638–648, Oct. 2015.
[77] K. E. Moore, A. Güngör, and S. M. Gupta, "Petri net approach to disassembly process planning for products with complex AND/OR precedence relationships," *Eur. J. Oper. Res.*, vol. 135, no. 2, pp. 428–449, 2001.
[78] C. M. Kang, M. J. Kwak, N. W. Cho, and Y. S. Hong, "Automatic derivation of transition matrix for end-of-life decision making," *Int. J. Prod. Res.*, vol. 48, no. 11, pp. 3269–3298, Jun. 2010.
[79] A. J. D. Lambert, "Automatic determination of transition matrices in optimal disassembly sequence generation," in *Assembly and Task Planning, 2001, Proceedings of the IEEE International Symposium on*, 2001, pp. 220–225.
[80] S. Behdad, M. Kwak, H. Kim, and D. Thurston, "Simultaneous Selective Disassembly and End-of-Life Decision Making for Multiple Products That Share Disassembly Operations," *J. Mech. Des.*, vol. 132, no. 4, p. 041002, 2010.
[81] E. Zussman and M. Zhou, "A methodology for modeling and adaptive planning of disassembly processes," *IEEE Trans. Robot. Autom.*, vol. 15, no. 1, pp. 190–194, 1999.
[82] X. Guo, S. Liu, M. Zhou, and G. Tian, "Disassembly Sequence Optimization for Large-Scale Products With Multiresource Constraints Using Scatter Search and Petri Nets," *IEEE Trans. Cybern.*, vol. 46, no. 11, pp. 2435–2446, Nov. 2016.
[83] D. Navtn-Chandra, "The Recovery Problem in Product Design," *J. Eng. Des.*, vol. 5, no. 1, pp. 65–86, Jan. 1994.
[84] Michael Roger Johnson, "A methodology for planning of product disassembly for recycling, remanufacturing and reuse," University of Windsor, 1994.
[85] M. R. Johnson and M. H. Wang, "Economical evaluation of disassembly operations for recycling, remanufacturing and reuse," *Int. J. Prod. Res.*, vol. 36, no. 12, pp. 3227–3252, Dec. 1998.
[86] W. Hui, X. Dong, and D. Guanghong, "A genetic algorithm for product disassembly sequence planning," *Neurocomputing*, vol. 71, no. 13–15, pp. 2720–2726, Aug. 2008.

[87] H.H.T. Huang, M.H. Wang, and M.R. Johnson, "Disassembly sequence generation using a neural network approach," *J. Manuf. Syst.*, vol. 19.2, pp. 73–82, 2000.
[88] K. Meng, P. Lou, X. Peng, and V. Prybutok, "An improved co-evolutionary algorithm for green manufacturing by integration of recovery option selection and disassembly planning for end-of-life products," *Int. J. Prod. Res.*, vol. 54, no. 18, pp. 5567–5593, Sep. 2016.
[89] A. van Schaik, M. A. Reuter, and K. Heiskanen, "The influence of particle size reduction and liberation on the recycling rate of end-of-life vehicles," *Miner. Eng.*, vol. 17, no. 2, pp. 331–347, Feb. 2004.
[90] M. B. Castro, J. A. M. Remmerswaal, J. C. Brezet, A. van Schaik, and M. A. Reuter, "A simulation model of the comminution–liberation of recycling streams," *Int. J. Miner. Process.*, vol. 75, no. 3–4, pp. 255–281, Feb. 2005.
[91] A. van Schaik and M. A. Reuter, "The time-varying factors influencing the recycling rate of products," *Resour. Conserv. Recycl.*, vol. 40, no. 4, pp. 301–328, Mar. 2004.
[92] K. Heiskanen, "Chapter 5 - Theory and Tools of Physical Separation/Recycling," in *Handbook of Recycling*, Boston: Elsevier, 2014, pp. 39–61.
[93] S. L. Gay, "A liberation model for comminution based on probability theory," *Miner. Eng.*, vol. 17, no. 4, pp. 525–534, 2004.
[94] M. Colledani and T. Tolio, "Integrated process and system modelling for the design of material recycling systems," *CIRP Ann. - Manuf. Technol.*, vol. 62, no. 1, pp. 447–452, 2013.
[95] L. J. Jekel and E. K. Tam, "Plastics waste processing: comminution size distribution and prediction," *J. Environ. Eng.*, vol. 133, no. 2, pp. 245–254, 2007.
[96] R. P. King, *Modeling and Simulation of Mineral Processing Systems*. Elsevier, 2012.
[97] G. Coates and S. Rahimifard, "Modelling of post-fragmentation waste stream processing within UK shredder facilities," *Waste Manag.*, vol. 29, no. 1, pp. 44–53, Jan. 2009.
[98] M. A. Reuter, A. van Schaik, O. Ignatenko, and G. J. de Haan, "Fundamental limits for the recycling of end-of-life vehicles," *Miner. Eng.*, vol. 19, no. 5, pp. 433–449, Apr. 2006.
[99] A. van Schaik and M. A. Reuter, "The time-varying factors influencing the recycling rate of products," *Resour. Conserv. Recycl.*, vol. 40, no. 4, pp. 301–328, Mar. 2004.
[100] M. I. Wolf, "Modeling and design of material separation systems with applications to recycling," Citeseer, 2011.
[101] M. Testa, "Modeling and design of material recovery facilities: genetic algorithm approach," Masters Thesis, Massachusetts Institute of Technology, 2015.
[102] Karine Ip, Maripaola Testa, Anne Raymond, Stephen Graves, and Timothy Gutowski, "Performance evaluation of material separation in a material recovery facility using a network flow model," *Resour. Conserv. Recycl.*, 2017.
[103] M. Testa, "Modeling and Design of Material Recovery Facilities : Genetic Algorithm Approach (SM Thesis)," Massachusetts Institute of Technology, 2015.
[104] S. H. Amini and A. Noble, "Application of linear circuit analysis in the evaluation of mineral processing circuit design under uncertainty," *Miner. Eng.*, vol. 102, pp. 18–29, Mar. 2017.
[105] A. Noble and G. H. Luttrell, "Value-based objective functions applied to circuit analysis.," *Miner. Metall. Process.*, vol. 32, no. 1, 2015.
[106] A. Noble and G. H. Luttrell, "The matrix reduction algorithm for solving separation circuits," *Miner. Eng.*, vol. 64, pp. 97–108, 2014.
[107] "Downloads | SMART - Sustainable Manufacturing & Recycling Technologies - Post-fragmentation modeller." [Online]. Available: http://www.centreforsmart.co.uk/downloads. [Accessed: 12-Apr-2017].
[108] T. J. Napier-Munn, "Modelling and simulating dense medium separation processes—A progress report," *Miner. Eng.*, vol. 4, no. 3–4, pp. 329–346, 1991.
[109] V. K. Soo, P. Compston, and M. Doolan, "The influence of joint technologies on ELV recyclability," *Waste Manag.*, vol. 68, pp. 421–433, Oct. 2017.

[110] O. Forsén, J. Aromaa, and M. Lundström, "Primary Copper Smelter and Refinery as a Recycling Plant—A System Integrated Approach to Estimate Secondary Raw Material Tolerance," *Recycling*, vol. 2, no. 4, p. 19, Oct. 2017.
[111] U. M. J. Boin and M. Bertram, "Melting standardized aluminum scrap: a mass balance model for Europe," *JOM*, vol. 57, no. 8, pp. 26–33, 2005.
[112] I. Miletic, R. Garbaty, S. Waterfall, and M. Mathewson, "Model-based optimization of scrap steel pruchasing," *IFAC Proc. Vol.*, vol. 40, no. 11, pp. 263–266, 2007.
[113] A. Noshadravan, G. Gaustad, R. Kirchain, and E. Olivetti, "Operational Strategies for Increasing Secondary Materials in Metals Production Under Uncertainty," *J. Sustain. Metall.*, vol. 3, no. 2, pp. 350–361, Jun. 2017.
[114] S. H. Amini, J. A. M. Remmerswaal, M. B. Castro, and M. A. Reuter, "Quantifying the quality loss and resource efficiency of recycling by means of exergy analysis," *J. Clean. Prod.*, vol. 15, no. 10, pp. 907–913, Jan. 2007.
[115] "Import analysis and trends of of aluminium scrap twitch under HS Code 76020010 | Zauba." [Online]. Available: https://www.zauba.com/importanalysis-aluminium+scrap+twitch/hs-code-76020010-report.html. [Accessed: 02-Jun-2019].
[116] M. I. Wolf, M. Colledani, S. B. Gershwin, and T. G. Gutowski, "Modeling and design of multi-stage separation systems," in *Proceedings of the 2010 IEEE International Symposium on Sustainable Systems and Technology*, Arlington, VA, USA, 2010, pp. 1–6.
[117] K. Ip, M. Testa, A. Raymond, S. C. Graves, and T. Gutowski, "Performance evaluation of material separation in a material recovery facility using a network flow model," *Resour. Conserv. Recycl.*, vol. 131, pp. 192–205, Apr. 2018.
[118] T. G. Gutowski and J. B. Dahmus, "Mixing entropy and product recycling," in *Proceedings of the 2005 IEEE International Symposium on Electronics and the Environment, 2005.*, 2005, pp. 72–76.
[119] T. G. Gutowski, "Thermodynamics and recycling, a review," in *2008 Ieee International Symposium on Electronics and the Environment*, 2008, pp. 1–5.
[120] Y. Xu, J. Fernandez Sanchez, and J. Njuguna, "Cost modelling to support optimised selection of End-of-Life options for automotive components," *Int. J. Adv. Manuf. Technol.*, vol. 73, no. 1–4, pp. 399–407, Jul. 2014.
[121] G. Villalba, M. Segarra, A. . Fernández, J. . Chimenos, and F. Espiell, "A proposal for quantifying the recyclability of materials," *Resour. Conserv. Recycl.*, vol. 37, no. 1, pp. 39–53, Dec. 2002.
[122] J. Gregory, J. Atlee, and R. Kirchain, "A process-based model of end-of-life electronics recycling driving eco-efficiency-informed decisions," in *Proceedings of the 2006 IEEE International Symposium on Electronics and the Environment, 2006.*, 2006, pp. 138–143.
[123] J. Atlee and R. Kirchain, "Operational Sustainability Metrics Assessing Metric Effectiveness in the Context of Electronics-Recycling Systems," *Environ. Sci. Technol.*, vol. 40, no. 14, pp. 4506–4513, Jul. 2006.
[124] P. Li, J. Dahmus, S. Guldberg, H. O. Riddervold, and R. Kirchain, "How Much Sorting Is Enough: Identifying Economic and Scrap-Reuse Benefits of Sorting Technologies," *J. Ind. Ecol.*, vol. 15, no. 5, pp. 743–759, 2011.
[125] H. Ohno, K. Matsubae, K. Nakajima, S. Nakamura, and T. Nagasaka, "Unintentional Flow of Alloying Elements in Steel during Recycling of End-of-Life Vehicles: Unintentional Flow of Alloying Elements in Steel during ELV Recycling," *J. Ind. Ecol.*, vol. 18, no. 2, pp. 242–253, Apr. 2014.
[126] T. Gutowski and M. I. Wolf, "Separation and energy use performance of material recycling systems," presented at the Proceedings of the 2009 NSF CMMI Engineering Research and Innovation Conference, Hawaii : Research and Education in a Flat World, Honolulu, Hawaii, 2009.
[127] A. Stevels, J. Huisman, F. Wang, J. Li, B. Li, and H. Duan, "Take back and treatment of discarded electronics: a scientific update," *Front. Environ. Sci. Eng.*, vol. 7, no. 4, pp. 475–482, Aug. 2013.

[128] J. Huisman, A. L. N. Stevels, and I. Stobbe, "Eco-efficiency considerations on the end-of-life of consumer electronic products," *IEEE Trans. Electron. Packag. Manuf.*, vol. 27, no. 1, pp. 9–25, Jan. 2004.
[129] V. K. Soo, J. Peeters, D. Paraskevas, P. Compston, M. Doolan, and J. R. Duflou, "Sustainable aluminium recycling of end-of-life products: A joining techniques perspective," *J. Clean. Prod.*, vol. 178, pp. 119–132, Mar. 2018.
[130] Y. A. Cengel and M. Boles, *Thermodynamics: an engineering approach*, 4th ed. McGraw-Hill, 2002.
[131] A. Valero Capilla and A. Valero Delgado, *Thanatia: the destiny of the Earth's mineral resources: a cradle-to-cradle thermodynamic assessment*. New Jersey: World Scientific, 2015.
[132] L. Stougie and M. P. C. Weijnen, "Exergy and sustainability: insights into the value of exergy analysis in sustainability assessment of technological systems," [Uitgever niet vastgesteld], Nederland, 2014.
[133] J. Dewulf *et al.*, "Cumulative Exergy Extraction from the Natural Environment (CEENE): a comprehensive Life Cycle Impact Assessment method for resource accounting," *Environ. Sci. Technol.*, vol. 41, no. 24, pp. 8477–8483, Dec. 2007.
[134] J. Dewulf *et al.*, "Exergy: Its Potential and Limitations in Environmental Science and Technology," *Environ. Sci. Technol.*, vol. 42, no. 7, pp. 2221–2232, Apr. 2008.
[135] G. Finnveden and P. Östlund, "Exergies of natural resources in life-cycle assessment and other applications," *Energy*, vol. 22, no. 9, pp. 923–931, 1997.
[136] G. Finnveden, Y. Arushanyan, and M. Brandão, "Exergy as a Measure of Resource Use in Life Cycle Assessment and Other Sustainability Assessment Tools," *Resources*, vol. 5, no. 3, p. 23, Jun. 2016.
[137] M. E. Bösch, S. Hellweg, M. A. Huijbregts, and R. Frischknecht, "Applying cumulative exergy demand (CExD) indicators to the ecoinvent database," *Int. J. Life Cycle Assess.*, vol. 12, no. 3, p. 181, 2007.
[138] J. Szargut, *Exergy method: technical and ecological applications*. Southampton ; Boston: WIT Press, 2005.
[139] A. Ortego, A. Valero, A. Valero, and M. Iglesias, "Downcycling in automobile recycling process: A thermodynamic assessment," *Resour. Conserv. Recycl.*, vol. 136, pp. 24–32, 2018.
[140] A. Ortego, A. Valero, A. Valero, and E. Restrepo, "Vehicles and Critical Raw Materials: A Sustainability Assessment Using Thermodynamic Rarity: Vehicles and Critical Raw Materials," *J. Ind. Ecol.*, vol. 22, no. 5, pp. 1005–1015, Oct. 2018.
[141] H. Ohno, K. Matsubae, K. Nakajima, Y. Kondo, S. Nakamura, and T. Nagasaka, "Toward the efficient recycling of alloying elements from end of life vehicle steel scrap," *Resour. Conserv. Recycl.*, vol. 100, pp. 11–20, Jul. 2015.
[142] J. L. Sullivan *et al.*, "Life cycle inventory of a generic US family sedan overview of results USCAR AMP project," SAE Technical paper, 1998.
[143] J. Sprovieri, "Wire Harness Recycling," *Assembly Mag*, 01-Jul-2014. [Online]. Available: https://www.assemblymag.com/articles/92263-wire-harness-recycling. [Accessed: 11-Jun-2019].
[144] K. Chi, "The Impact Analysis of Automobile Weight Reduction Polivies on Automotive Fastener Development in Advanced Countries," *Fastener World*, 2015. [Online]. Available: http://www.fastener-world.com.tw/0_magazine/ebook/pdf_download/FW_154_E_405.pdf. [Accessed: 11-Jun-2019].
[145] C. Westerberg, "Finite element simulation of crash testing of self-piercing rivet joints, peel specimen," 2002.
[146] A. Schmid, M. Batton-Hubert, P. Naquin, and R. Gourdon, "Multi-Criteria Evaluation of End-of-Life Vehicles' Dismantling Scenarios with Respect to Technical Performance and Sustainability Issues," *Resources*, vol. 5, no. 4, p. 42, Dec. 2016.
[147] Semblex, "Flow Drill Screw hor High-Strength Sheet Joints."

[148] C. Herrmann, W. Dewulf, M. Hauschild, A. Kaluza, S. Kara, and S. Skerlos, "Life cycle engineering of lightweight structures," *CIRP Ann.*, vol. 67, no. 2, pp. 651–672, 2018.
[149] P. K. Mallick, Ed., *Materials, design and manufacturing for lightweight vehicles*. Boca Raton, Fla. : Oxford: CRC Press ; Woodhead, 2010.
[150] S. Das, D. Graziano, V. K. K. Upadhyayula, E. Masanet, M. Riddle, and J. Cresko, "Vehicle lightweighting energy use impacts in U.S. light-duty vehicle fleet," *Sustain. Mater. Technol.*, vol. 8, pp. 5–13, Jul. 2016.
[151] A. Mascarin, T. Hannibal, A. Raghunathan, Z. Ivanic, and J. Francfort, "Vehicle Lightweighting: 40% and 45% Weight Savings Analysis: Technical Cost Modeling for Vehicle Lightweighting (No. INL/EXT-14-33863)," Idaho National Lab (INL), Idaho Falls, ID (United States), 2015.
[152] N. P. Lutsey, "Review of technical literature and trends related to automobile mass-reduction technology," 2010.
[153] J. C. Kelly, J. L. Sullivan, A. Burnham, and A. Elgowainy, "Impacts of Vehicle Weight Reduction via Material Substitution on Life-Cycle Greenhouse Gas Emissions," *Environ. Sci. Technol.*, vol. 49, no. 20, pp. 12535–12542, Oct. 2015.
[154] A. T. Mayyas, A. Qattawi, A. R. Mayyas, and M. A. Omar, "Life cycle assessment-based selection for a sustainable lightweight body-in-white design," *Energy*, vol. 39, no. 1, pp. 412–425, 2012.
[155] A. M. Lewis, J. C. Kelly, and G. A. Keoleian, "Vehicle lightweighting vs. electrification: life cycle energy and GHG emissions results for diverse powertrain vehicles," *Appl. Energy*, vol. 126, pp. 13–20, 2014.
[156] R. A. Witik, J. Payet, V. Michaud, C. Ludwig, and J.-A. E. M\a anson, "Assessing the life cycle costs and environmental performance of lightweight materials in automobile applications," *Compos. Part Appl. Sci. Manuf.*, vol. 42, no. 11, pp. 1694–1709, 2011.
[157] Q. Dai, J. Kelly, and A. Elgowainy, "Material efficiencies and recycling of aluminum and carbon fiber reinforced plastics for automotive applications," Argonne National Lab.(ANL), Argonne, IL (United States), 2016.
[158] J. Hirsch, "Aluminium in innovative light-weight car design," *Mater. Trans.*, vol. 52, no. 5, pp. 818–824, 2011.
[159] Ducker Worldwide, "2015 North American Light Vehicle Aluminum Content Study," Jun. 2014.
[160] V. K. Soo, P. Compston, and M. Doolan, "Interaction between New Car Design and Recycling Impact on Life Cycle Assessment," *Procedia CIRP*, vol. 29, pp. 426–431, 2015.
[161] A. Burnham, "Updated Vehicle Specifications in the GREET Vehicle-Cycle Model," Argonne National Lab.(ANL), Argonne, IL (United States), 2012.
[162] A. Elgowainy *et al.*, "Cradle-to-Grave Lifecycle Analysis of US Light Duty Vehicle-Fuel Pathways: A Greenhouse Gas Emissions and Economic Assessment of Current (2015) and Future (2025-2030) Technologies," Argonne National Lab.(ANL), Argonne, IL (United States), 2016.
[163] F. Stodolsky, A. Vyas, R. Cuenca, and L. Gaines, "Life-cycle energy savings potential from aluminum-intensive vehicles," Argonne National Lab., IL (United States), 1995.
[164] "The Aluminium Automotive Manual," European Aluminium Association, Düsseldorf, 2013.
[165] K. Martinsen, S. J. Hu, and B. E. Carlson, "Joining of dissimilar materials," *CIRP Ann.*, vol. 64, no. 2, pp. 679–699, Jan. 2015.
[166] autonews, "As Ford spends big, GM joins aluminum with simple welds," *Automotive News*, 24-Nov-2014.
[167] M. Mirdamadi and G. Korchnak, "Great automotive designs enabled by advances in adhesive bonding," *Gt. Des. Steel*, 2006.
[168] D. Li, A. Chrysanthou, I. Patel, and G. Williams, "Self-piercing riveting-a review," *Int. J. Adv. Manuf. Technol.*, vol. 92, no. 5–8, pp. 1777–1824, 2017.
[169] N.-H. Hoang, R. Porcaro, M. Langseth, and A.-G. Hanssen, "Self-piercing riveting connections using aluminium rivets," *Int. J. Solids Struct.*, vol. 47, no. 3–4, pp. 427–439, 2010.
[170] L. Claus and S. Weitzel, "Self-Tapping Fasteners for Lightweight Designs," SAE Technical Paper, 2014.

[171] J. Conklin, R. Beals, and Z. Brown, "BIW Design and CAE," presented at the SAE 2015 World Congress & Exhibition, 2015, pp. 2015-01–0408.
[172] UNEP, Ed., *Metal recycling: opportunities, limits, infrastructure: this is report 2b of the Global Metal Flows Working Group of the International Resource Panel of UNEP*. Nairobi, Kenya: United Nations Environment Programme, 2013.
[173] C. Fitzpatrick, E. Olivetti, T. R. Miller, R. Roth, and R. Kirchain, "Conflict Minerals in the Compute Sector: Estimating Extent of Tin, Tantalum, Tungsten, and Gold Use in ICT Products," *Environ. Sci. Technol.*, vol. 49, no. 2, pp. 974–981, Jan. 2015.
[174] A. Kumar, M. Holuszko, and D. C. R. Espinosa, "E-waste: An overview on generation, collection, legislation and recycling practices," *Resour. Conserv. Recycl.*, vol. 122, pp. 32–42, Jul. 2017.
[175] Ford, "Ford Sustainability Report 2018/19," Ford, 2019.